The development of low-activation, multi-principal element alloys for nuclear fusion applications

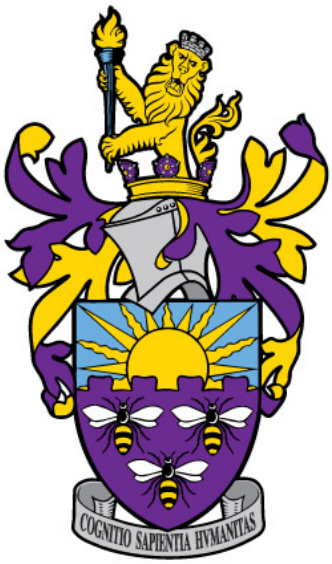

A thesis submitted to The University of Manchester for the degree of Doctor of Philosophy in the Faculty of Science & Engineering.

2021

Paul J. Barron

Department of Materials

Contents

List of Figures

List of Tables

Abbreviations

BCC body centred cubic. 11, 97

CBED convergent beam electron diffraction. 11, 99

D-T deuterium-tritium. 11, 22

DBTT ductile-brittle transition temperature. 11, 39

DFT density functional theory. 11, 36

dpa displacements per atom. 11, 33

EB electron beam. 11, 44

EBSD electron backscatter diffraction. 11, 98

EDX energy dispersive X-ray. 11, 98, 166

ELMs edge-localised modes. 11, 28

EPMA electron probe microanalyser. 11

FCC face centred cubic. 11, 46

FIB focused ion beam. 11, 99

FPs Frenkel pairs. 11, 32

GTA gas tungsten arc. 11, 44

HAZ heat affected zone. 11, 44

HEAs high entropy alloys. 11, 19, 34, 164

HIP hot isostatic pressing. 11, 45

ICF inertial confinement fusion. 11, 23

LLW low-level waste. 11, 29

LOCA loss-of-coolant accident. 11, 32, 162

MCF magnetic confinement fusion. 11, 23

MD molecular dynamics. 11, 40, 69

MPEAs multi-principal element alloys. 11, 19

ODS oxide dispersion strengthened. 11, 48

OPS oxide polishing suspension. 11, 95

PFM plasma-facing material. 11, 58, 72

PKA primary knock-on atom. 11, 32

PWHT post-weld heat treatment. 11, 44

RAFM reduced activaton ferritic-martensitic. 11, 47, 163

SEBM selected electron beam melting. 11, 66

SEM secondary electron microscopy. 11, 38, 97, 98, 166

STEM scanning transmission electron microscopy. 11, 99

TBM test blanket module. 11, 54

TEM transmission electron microscopy. 11, 35, 99

WDS wavelength dispersive spectroscopy. 11, 98, 166, 190

wppm weight parts per million. 11, 37

XRD X-ray diffraction. 11, 97

Word count

The length of this thesis is 49,159 words (not including references).

Abstract

Nuclear fusion offers an attractive future prospect for energy production with no carbon emissions. However, a viable nuclear fusion reactor has yet to be demonstrated. One of the factors limiting the development of such a device is the hostile environment that reactor materials will be exposed to. A combination of high-energy neutron fluxes, high temperatures, large temperature gradients, thermal shocks, transient loading events, and corrosion from coolants/tritium breeding materials creates a set of conditions that will be detrimental to materials performance. Several candidate materials for various reactor components exist, but they are all limited in some capacity. The aim of this project was to use a novel alloy development approach to produce a material that may be better suited for certain fusion applications, or otherwise may be able to inform the future development of such an alloy.

One potential advantage of nuclear fusion power is its relative lack of radioactive waste products compared to nuclear fission. However, this imposes a restriction on the elements used in reactor materials: they must not produce radioactive waste that is long-lived. By using elements with favourable nuclear activation properties and adopting a similar development rationale used in high entropy alloys, a set of low-activation, multi-principal component alloys were produced. The alloy systems investigated, Ti-V-Cr-Mn and V-Cr-Mn, produced a microstructure that would be favourable for fusion applications after a homogenisation treatment, in contrast to some other, highly-concentrated alloys. Furthermore, the alloys generally showed no or limited microstructural evolution after ageing at fusion relevant temperatures. This kind of behaviour is essential for any candidate fusion material. The high temperature oxidation properties of the alloys were also assessed and were found to be improved relative to other fusion candidate alloys. Resistance to oxidation has important implications for the safety case of using a given material and may also aid in manufacturing.

This work has examined two virtually unexplored alloy systems and found that they may hold promise for fusion applications. Further characterisation will be required to assess whether they are truly viable candidate materials. Regardless, this work will aid in the exploration of new alloy systems and may inspire further fusion alloy development.

Declaration & copyright statement

i The author declares that no portion of the work referred to in the thesis has been submitted in support of an application for another degree or qualification of this or any other university or other institute of learning.

ii The author of this thesis (including any appendices and/or schedules to this thesis) owns certain copyright or related rights in it (the "Copyright") and s/he has given The University of Manchester certain rights to use such Copyright, including for administrative purposes.

iii Copies of this thesis, either in full or in extracts and whether in hard or electronic copy, may be made **only** in accordance with the Copyright, Designs and Patents Act 1988 (as amended) and regulations issued under it or, where appropriate, in accordance with licensing agreements which the University has from time to time. This page must form part of any such copies made.

iv The ownership of certain Copyright, patents, designs, trademarks and other intellectual property (the "Intellectual Property") and any reproductions of copyright works in the thesis, for example graphs and tables ("Reproductions"), which may be described in this thesis, may not be owned by the author and may be owned by third parties. Such Intellectual Property and Reproductions cannot and must not be made available for use without the prior written permission of the owner(s) of the relevant Intellectual Property and/or Reproductions.

v Further information on the conditions under which disclosure, publication and commercialisation of this thesis, the Copyright and any Intellectual Property and/or Reproductions described in it may take place is available in the University IP Policy (see `http://documents.manchester.ac.uk/DocuInfo.aspx?DocID=24420`), in any relevant Thesis restriction declarations deposited in the University Library, The University Library's regulations (see `http://www.library.manchester.ac.uk/about/regulations/`) and in The University's policy on Presentation of Theses.

Acknowledgements

First and foremost, I would like to convey my deepest gratitude and love to Lorna and Richard, my mum and dad. I am eternally grateful for all your hard work and for continually supporting the decisions I have made (even when those decisions led to me pursuing four years of postgraduate education...). The same goes to my sister, Steph. Thank you for being a generally wonderful person and always being there for me. I must also extend my love to and thank the rest of my family, who have all supported me in some way throughout these last few years of work (and the many more preceding those!).

To all my friends, wherever they may be: If I were to fully express the ways you have all filled the time I have spent pursuing this degree with joy, laughter, and wisdom, there is a good chance it would put me well over my allowed 80,000 words. Instead, this paragraph will have to suffice. You have all helped in some way, large or small, and I am truly glad to have met all of you. A special mention must go to my year group in the Fusion CDT. It has been a pleasure learning about the wonderful world of fusion with you for the last four years. Most of you have contributed in some way to my knowledge of the field and I can only hope I have imparted some of my knowledge to you in return. And to Nick: Congratulations on beating me by two weeks, I hope you're happy.

I am also extremely grateful to all the academic and technical staff and colleagues at the University of Manchester (and beyond) who have directly helped with my work. In particular, I would like to thank Alex Carruthers and Max Rigby for their mastery of microscopy, Ken Gyves for running such a tight ship in the Morton lab, and Huw Dawson for his assistance in all matters fusion. I am also indebted to Dr Brian Connolly for his supervision and assistance, both academic and practical, related to preparing and running the oxidation experiments. I am also grateful to all members of the steel and fusion research groups for providing (usually) fruitful discussion, especially during lockdown.

Finally, I must extend my sincere thanks and admiration to my supervisor, Ed Pickering, without whom this work would not have been possible. I feel lucky to have had the honour of being your first PhD student, hopefully the feeling is mutual! Your hard work and willingness to help myself and others, especially in these last few months, are an inspiration.

Chapter 1

Introduction

1.1 Fusion energy

Atmospheric carbon dioxide levels continue to rise across the world with disastrous and far-reaching effects, which will only get worse as concentrations increase[1]. Energy production resulted in the release 33.1 Gt of carbon dioxide into the atmosphere in 2018[2]. Decarbonising energy generation has been identified as a key objective in the fight against climate change[3]. Coal- and gas-fired power plants are the power sources with the highest carbon emissions, so phasing these plants out is a necessity for any long-term climate plan. The United Nation's Paris Agreement to reduce greenhouse gas emissions came into effect in late 2016, so there is now additional legislative pressure to reduce carbon emissions[4].

However, global energy demand is also growing, necessitating the construction of new power sources to cope with this increased requirement. Furthermore, electrical energy will make up an increasing share of the energy demand as industries like transportation move towards increased electrification[2]. Renewable sources such as solar and wind have had significant technological improvements in recent years and are more cost-effective than ever, but they are still beset by problems with supply reliability, which can leave electrical grids short of power if there is less sunshine or wind than expected[5].

Due to these problems, nuclear fission power is touted as an alternative to augment the fluctuating supply of renewables with a constant, baseline load. Despite large capital costs, fission power can provide very large amounts of power with excellent reliability. However, the issue of potentially dangerous radioactive waste and other issues relating to decommissioning still tarnish public perception of nuclear power, especially with the question of waste disposal remaining unanswered in the UK[6, 7]. This negative perception is compounded by incidents such as Fukushima and Chernobyl in living memory. The steps required to enrich the uranium fuel needed for fission power

can also be used in the proliferation of nuclear weapons, an outcome that many object to.

Although still in the research stages of its development, nuclear fusion should be considered as a long-term alternative to fission power. Nuclear fusion offers a low-carbon energy source that minimises long-lived radioactive waste and cannot be weaponised. By fusing deuterium and tritium, an extremely large amount of energy in the process is released in the form of a helium ion and a neutron. The energy from these particles can be captured by a reactor, where it will then be used to drive a turbine to provide electricity. Deuterium is abundant in nature and can be easily separated from its natural mixture with protium. Tritium, although not naturally occurring, can be generated inside a fusion reactor using lithium, another readily available element.

1.2 Fusion materials

Before sustainable and economically viable fusion power can be achieved, there are many challenges that need to be addressed, especially in the field of materials science. High temperatures, large doses of energetic neutrons, cyclic heating, cyclic loading, extreme transient thermal loads, corrosion and plasma erosion are amongst some of the challenging conditions that a material inside a fusion reactor will be subject to. Such a unique environment necessitates the use of unique materials. Many new materials have been developed specifically for fusion applications, and many more will continue to be developed as the requirements for materials become clearer as fusion research progresses.

One of the constraints imposed on fusion materials is a restriction based on the neutron activation properties of their constituent elements. Transmutation of elements used in the reactor structure will cause previously inert materials to become radioactive. As a functional fusion reactor could be constructed while ignoring activation properties, it is not an engineering requirement. However, due to the desire of the fusion research community to offer an alternative to fission with no (or reduced) long-lived radioactive waste, new fusion materials should conform to these low-activation requirements.

Some of these new materials will be modifications of existing alloys, as is the case for EUROFER-97 and F82H, ferritic-martensitic steels that are candidates for structural materials in the reactor. Their compositions are based on existing steels, with elements that produce long-lived activation products replaced with other less activating elements that can produce similar metallurgical effects. In other cases, new materials, such as tungsten and vanadium alloys, have been developed. These alloy systems have not been used for any practical applications to date. *Each of these materials have limitations, which will be discussed in more detail later. It is clear that there is scope for new materials to be developed for fusion applications.*

1.3 High entropy alloys

In 2004, Jian-Wei Yeh and Brian Cantor, independently of each other, had the idea of producing alloys with equal (or near-equal) proportions of several elements[8, 9]. The rationale behind this previously untested idea was that the entropy of mixing many elements would be high enough to stabilise a single solid solution.

Despite being a relatively recent development in materials science, the field of high entropy alloys (HEAs) has exploded in popularity, with more than 7,500 articles published on the topic since the idea was first conceived[10]. Part of the reason behind this popularity will no doubt be the variety of interesting properties that HEAs have exhibited since their discovery. These properties include remarkable ductility at cryogenic temperatures, extreme wear resistance and resistance to neutron irradiation[11, 12].

There are virtually endless combinations of possible high entropy alloys (Cantor created a 20 component alloy in his 2004 paper!), with the possibility of more unique properties yet to be discovered. Relatively little work has been done on exploring the use of HEAs for nuclear applications, and even less on fusion specifically, so there are still many potentially attractive alloy systems that have been hitherto unexplored.

1.4 Thesis aims

With so little of the HEA phase space explored, it is entirely possible that there exists HEAs (or multi-principal component alloys) that are comprised entirely of low activation alloys and have the requisite properties to be suitable for use inside a fusion reactor. Therefore, the aim of this thesis is to map out a small segment of the phase space of a few selected elements that may offer a pathway to the development of HEAs for nuclear fusion applications. It should be noted that this work does not, strictly speaking, focus on HEAs as they are commonly defined (i.e. alloys with $\geq$5 elements). Instead, the alloys under investigation will be referred to as multi-principal element alloys (MPEAs). During this exploration, key features such as phase thermal stability in fusion relevant conditions, mechanical properties, and oxidation properties will be investigated.

Specifically, the aims of the work are to:

- Perform design and preliminary experimental studies working towards a fusion HEA, comprising of elements with low-activation properties and using existing vanadium alloys as a starting point to begin investigation.
- Assess phase stability of a suite of appropriate alloy compositions by exposing the alloys to fusion relevant temperatures for long periods of time.

- Assess mechanical/oxidation performance to determine suitability of the alloys for engineering applications.

1.5 Thesis structure

Chapter 2 of this thesis consists of a review of the relevant literature broadly separated into two parts. Firstly, the requirements of contemporary and future fusion reactors are detailed. Secondly, some of the candidate materials developed to deal with these challenges are assessed by examining their advantages and drawbacks. The second part of the literature review also covers HEAs, some of their properties, and the limited work that has been done on assessing their candidacy for nuclear applications.

The three results chapters, which are presented in the form of papers following the alternative format, address each of the aims stated above, starting with Chapter 3, which presents the experimental methods used in this work alongside a brief description of the theory underlying each technique. This chapter complements the methodology sections of the subsequent experimental chapters.

Chapter 4 contains an initial phase stability assessment of the system of alloys to be investigated. The rationale behind the elements chosen is presented. Phase stability is assessed with a variety of techniques alongside investigation of the microstructure.

A more detailed evaluation of the alloys' stability in fusion environments is presented in Chapter 5. A series of heat treatments are performed on the alloys and the resulting microstructure and properties are assessed.

The final body of experimental work is contained with in Chapter 6. This chapter focuses on the oxidation behaviour of the alloys with a view to determining their accident tolerance and processability.

Finally, Chapters 7 and 8 present the final conclusions of this work and possible directions for future work, respectively.

1.6 Publications

The experimental chapters of this thesis will be provided in the format of journal articles, including Chapter 4 which is presented as published in:
P.J. Barron et al. "Towards V-based high-entropy alloys for nuclear fusion applications". *Scripta Materialia* 176 (Feb. 2020).

References

[1] Samer Fawzy et al. *Strategies for mitigation of climate change: a review*. Nov. 2020. DOI: 10.1007/s10311-020-01059-w.

[2] International Energy Agency (IEA). *Global Energy & CO2 Status Report 2019 – Analysis*. 2020.

[3] Paul Ekins. "Step changes for decarbonising the energy system: Research needs for renewables, energy efficiency and nuclear power". In: *Energy Policy* 32.17 (Nov. 2004), pp. 1891–1904. ISSN: 03014215. DOI: 10.1016/j.enpol.2004.03.009.

[4] United Nations. *The Paris Agreement*. 2016.

[5] B.P. Heard et al. *Burden of proof: A comprehensive review of the feasibility of 100% renewable-electricity systems*. Tech. rep. Sept. 2017, pp. 1122–1133. DOI: 10.1016/j.rser.2017.03.114.

[6] W. F. Lawless et al. "Public consent for the geologic disposal of highly radioactive wastes and spent nuclear fuel". In: *International Journal of Environmental Studies* 71.1 (Jan. 2014), pp. 41–62. ISSN: 00207233. DOI: 10.1080/00207233.2014.881165.

[7] F. M. McEvoy et al. "Tectonic and climatic considerations for deep geological disposal of radioactive waste: A UK perspective". In: *Science of the Total Environment* 571 (Nov. 2016), pp. 507–521. ISSN: 18791026. DOI: 10.1016/j.scitotenv.2016.07.018.

[8] J.-W. Yeh et al. "Nanostructured High-Entropy Alloys with Multiple Principal Elements: Novel Alloy Design Concepts and Outcomes". In: *Advanced Engineering Materials* 6.5 (May 2004), pp. 299–303. ISSN: 1438-1656. DOI: 10.1002/adem.200300567.

[9] B. Cantor et al. "Microstructural development in equiatomic multicomponent alloys". In: *Materials Science and Engineering A* 375-377.1-2 SPEC. ISS. (2004), pp. 213–218. ISSN: 09215093. DOI: 10.1016/j.msea.2003.10.257.

[10] *Web of Science search for "high entropy alloys"*. Available at https://apps.webofknowledge.com/.

[11] D. B. Miracle and O. N. Senkov. "A critical review of high entropy alloys and related concepts". In: *Acta Materialia* 122 (2017), pp. 448–511. ISSN: 13596454. DOI: 10.1016/j.actamat.2016.08.081.

[12] E. J. Pickering and N. G. Jones. "High-entropy alloys: a critical assessment of their founding principles and future prospects". In: *International Materials Reviews* 6608.May (2016), pp. 1–20. ISSN: 0950-6608. DOI: 10.1080/09506608.2016.1180020.

Chapter 2

Literature review

2.1 Fusion energy

2.1.1 The fusion reaction

The process of nuclear fusion is defined as a "process by which nuclear reactions between light elements form heavier elements, [in which] substantial amounts of energy are released."[1]. From inspection of the nucleon binding energies presented in Fig. 2.1, fusing two hydrogen nuclei together will release large amounts of energy, as the ^{4}He nucleon is considerably more tightly bound than the ^{2}H and ^{3}H nucleons. The most viable fusion reaction for energy generation is the deuterium-tritium (D-T) reaction, shown below:

$$ {}^{2}_{1}\mathrm{H}^{+} \; + \; {}^{3}_{1}\mathrm{H}^{+} \; \rightarrow \; {}^{4}_{2}\mathrm{He}^{+} \, (3.5\,\mathrm{MeV}) \; + \; {}^{1}_{0}\mathrm{n} \, (14.1\ \mathrm{MeV}) $$

The D-T reaction is the most viable as it has the largest maximum reactivity of any fusion reaction by an order of magnitude, seen in Fig. 2.2a. It also has the lowest reaction triple product condition of any reaction, again by over an order of magnitude (see Fig. 2.2b). The fusion triple product is a figure of merit that indicates the conditions required for ignition, which is when a fusion reaction produces more energy than it loses to the environment. The triple product consists of a plasma's density (n_e), temperature (T), and confinement time (τ_E) multiplied together. When this value is greater than a reaction- and temperature-dependent value (a condition known as the Lawson criterion[3]), ignition is said to have occurred.

Fig. 2.2b also shows that the temperatures required to meet the triple product condition at its minimum are enormous, with a temperature of around 100 million Kelvin for the D-T reaction. Despite the massive temperatures required for ignition, the D-T reaction still represents the easiest path to fusion as it has the lowest requirements for ignition and the greatest reactivity of any reaction. All of the following discussion of fusion power is based on using a D-T fuel mixture.

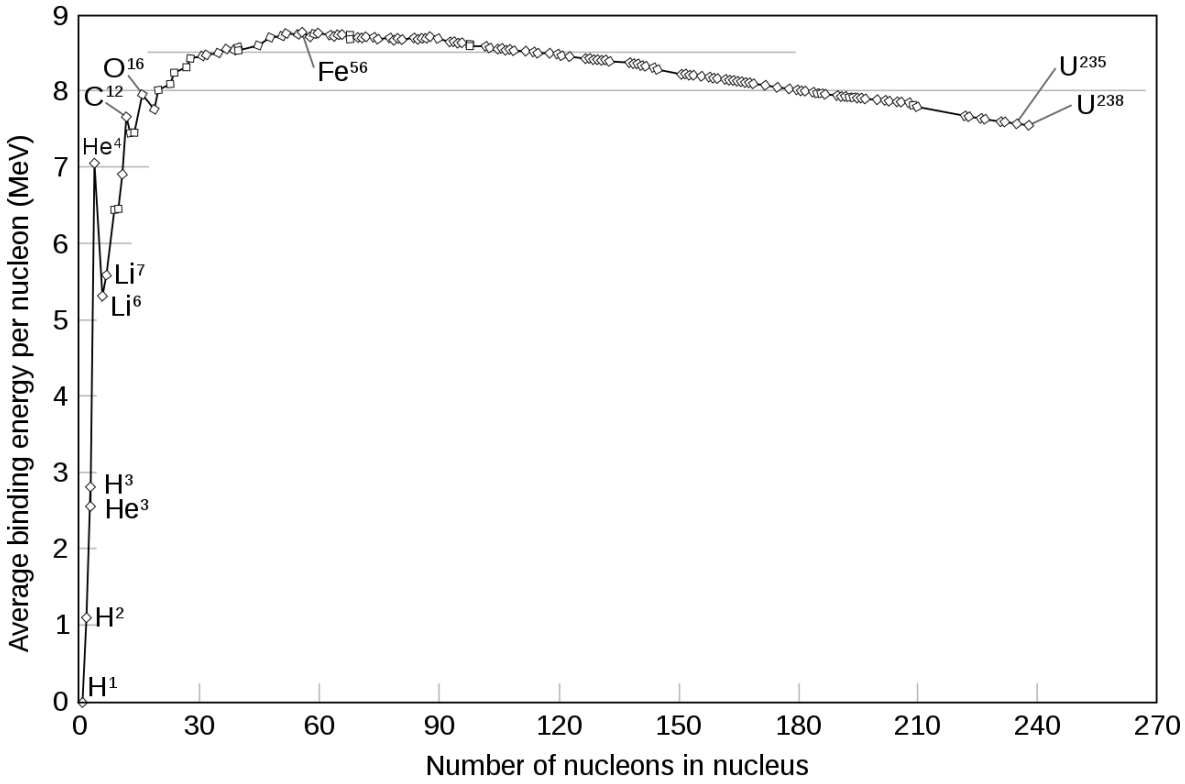

Figure 2.1: Binding energy of nucleons. Taken from [2].

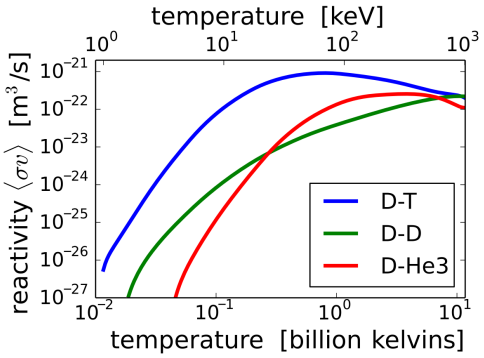

(a) Fusion reaction reactivity for selected reactions. Taken from [4].

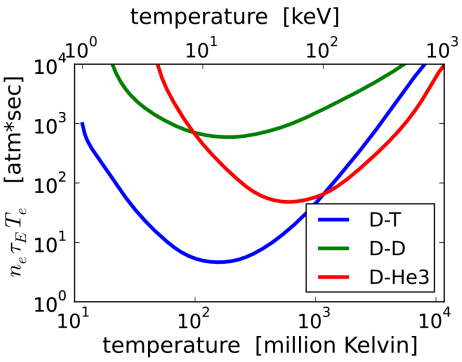

(b) Fusion reaction triple product required for ignition in selected reactions. Taken from [5].

Figure 2.2: Properties of selected nuclear fusion reactions.

2.1.2 Fusion reactors

In order to confine plasmas at such high temperatures, fusion reactors generally utilise one of two methods: magnetic confinement fusion (MCF) and inertial confinement fusion (ICF). Other types of device do exist but these two are the most common. Although the fusion reactions in both cases are the same, the methods are differentiated by how the plasmas are confined. MCF utilises large magnets to keep the plasma in a toroidal loop (also known as a tokamak), leading to relatively large confinement times

with moderate plasma densities. ICF uses a large array of high powered lasers fired simultaneously to compress and heat a small pellet of fuel, with much greater plasma densities at the expense of comparatively short confinement times.

This thesis will focus on alloys for use in a future MCF reactor. As the more technologically developed of the two primary types of fusion device, the conditions that components will be subjected to are more clearly known. ITER[1], a tokamak currently under construction in France, will be the largest (in terms of both physical size and power output) and most advanced fusion reactor built to date when complete. As the materials that will be used in ITER have already been chosen and, in some cases, manufactured, the alloys presented here are being investigated to further the range of potential materials which could be used in fusion reactors in the far future. This may be DEMO, the power-generating demonstration reactor scheduled for construction in the 2040s[6], or some other device.

A depiction of a functional tokamak reactor is shown in Fig. 2.3, which shows a 3D model of ITER. This figure is presented simply to indicate the scale and complexity of a large fusion device. A more useful representation is provided in Fig. 2.4, which shows a schematic of a tokamak reactor cross-section. While the exact nature of the components will depend on the design of the individual reactor, all of the components and systems shown in the diagram are essential for the operation of a power generating fusion reactor. Out of these components, the vacuum vessel, cryostat and biological shield can all perform to an acceptable level with current engineering materials[7][2], and the magnet coils require specialised superconducting materials that are outside the scope of this work. Therefore, it is arguably the blanket, first wall, and divertor components that have the greatest scope for new material developments, and will be the focus of this work.

2.1.2.1 Fusion blankets

The deuterium-tritium reaction generates neutrons with 14.1 MeV of kinetic energy, which are then captured by the reactor structure and their kinetic energy converted into heat. Fig. 2.4 shows where the blanket lies in relation to other components in tokamak reactors. In addition to absorbing energy, the blanket also contains the tritium breeding systems. As tritium is not a naturally occurring isotope, a fusion reactor must breed its own supply in order to operate continuously and in an economically feasible manner. Breeder systems work by generating additional neutrons with a multiplier material (beryllium or lead) to bombard a supply of lithium-6, which in turn generates

[1]Which originally stood for International Thermonuclear Experimental Reactor but has since been changed to represent "the way" in Latin

[2]That is not to say the materials used for these components cannot be further improved with research (e.g. a cheaper steel or more environmentally friendly concrete), but merely that these components can be manufactured using currently available materials, irrespective of reactor conditions.

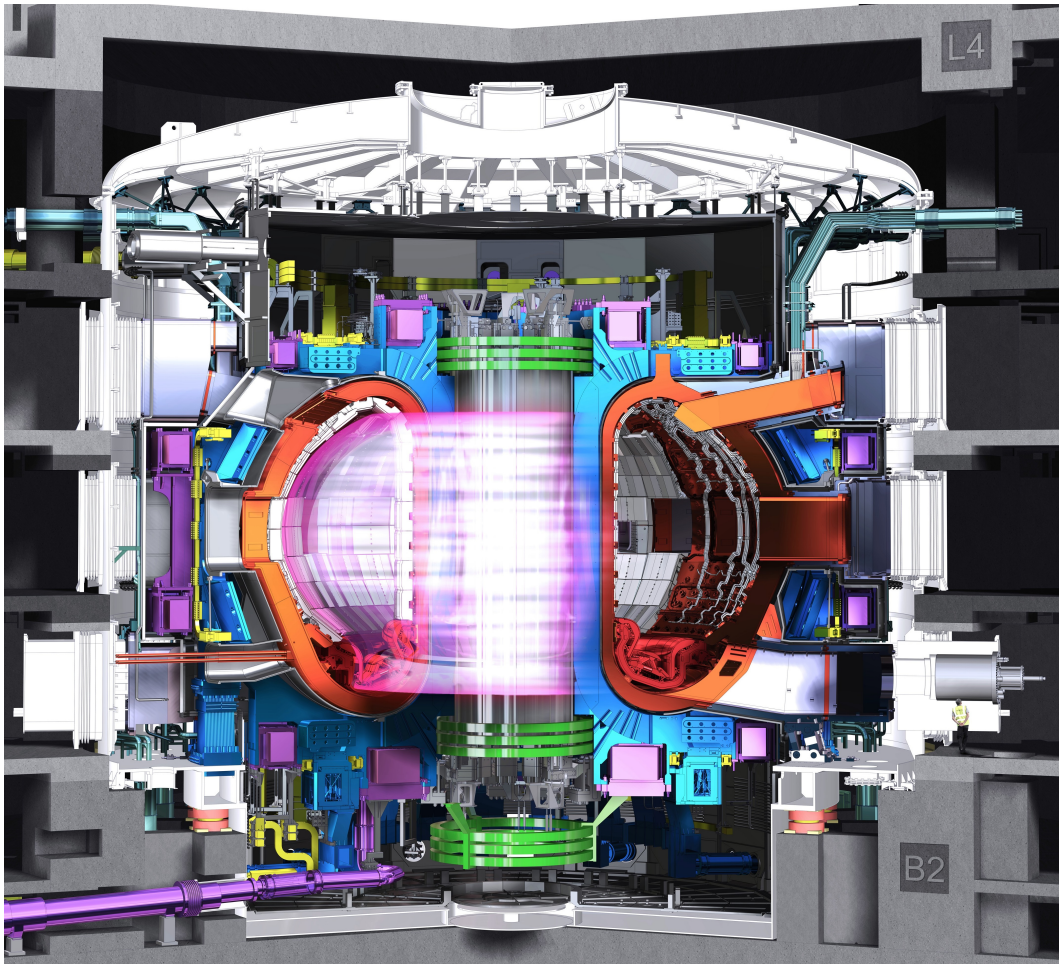

Figure 2.3: A cross-sectional 3D model of the ITER reactor. Note the worker provided for scale in the bottom right of the image. Taken from [8].

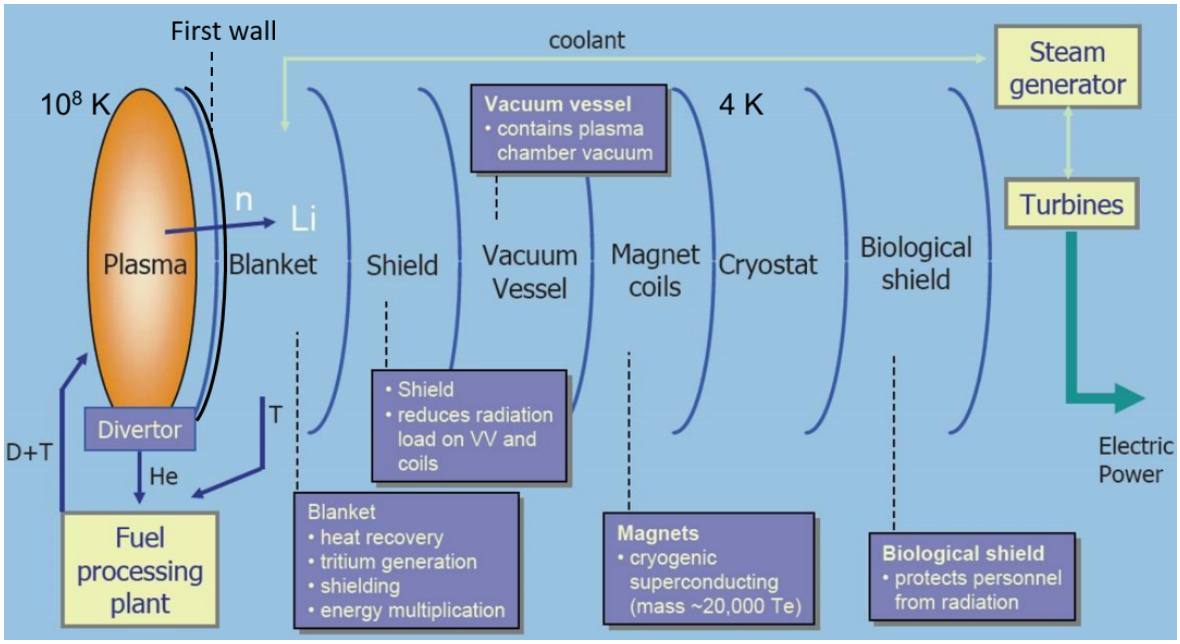

Figure 2.4: Schematic showing the role of the blanket and other components within a Tokamak. Taken from the Culham Centre for Fusion Energy.

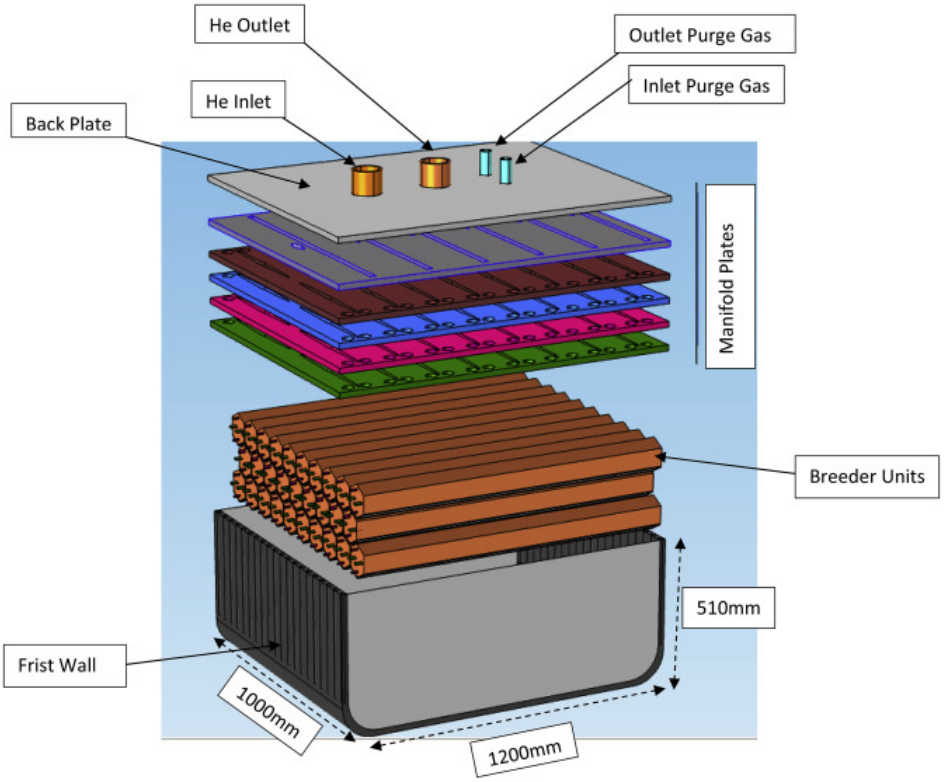

Figure 2.5: The design of a helium-cooled pebble bed tritium test blanket module that may be used in DEMO. The breeder units in this design will be filled with lithium orthosilicate and beryllium in solid pebble form. The structural material is a ferritic steel. Taken from [14].

more tritium to be extracted and used as fuel.

Behind the first wall of an MCF device blanket lies the structural support material and corresponding breeding materials. This structure will absorb many of the neutrons emitted from the reactor core in addition supporting the tritium breeding and coolant systems. As such it will need to retain good mechanical properties under irradiation at high temperatures. It must also be compatible with the tritium breeding and coolant systems.

The exact nature of the design of the blanket for DEMO and its corresponding systems has yet to be decided. A variety of blanket designs that utilise different structural materials, tritium breeding materials and coolants will be tested in modules installed in ITER. These test blanket modules will allow the performance of the various proposed blanket designs to be tested in a fusion environment[9, 10, 11, 12, 13]. One prospective blanket module design is shown in Fig. 2.5, but this is only provided for illustrative purposes and is not necessarily indicative of what will actually be chosen to be used in DEMO or any future reactor.

Thermal performance and stability is a key aspect of blanket material selection. The efficiency of a fusion reactor will increase with operating temperatures, so it is desirable that a reactor be operated as hot as possible[15]. Fig. 2.6 shows the predicted operating

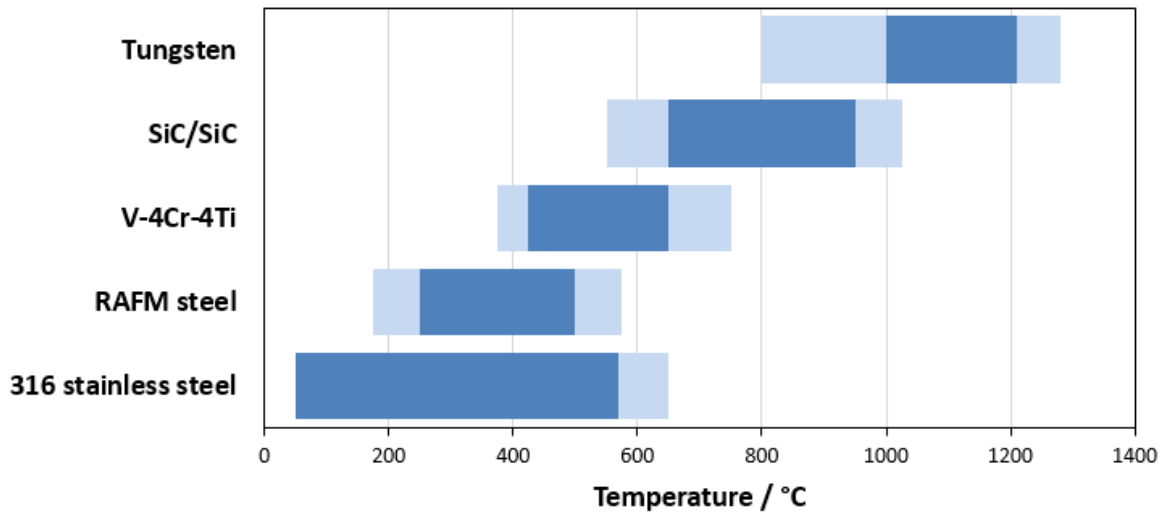

Figure 2.6: Operating temperatures of blanket candidate materials. Adapted from [16].

temperature ranges for some candidate blanket materials in a fusion environment[16]. These materials will be discussed in more detail in the following sections.

This thermal performance must be maintained in the presence of neutron irradiation. Neutrons can cause extensive microstructural changes in materials, which will be discussed in Section 2.2. All of these changes will lead to a degradation of materials' properties. Embrittlement and hardening caused by radiation will determine the lower operating temperature limit of blanket materials (see Sections 2.4 and 2.5). As reactor blankets will be operated for extended periods of time (up to several years)[17], the materials used must also be resistant to thermal creep. Creep properties are one of the key factors that determine the upper temperature limits in fusion structural materials, alongside microstructural stability[16].

The coolant used in the blanket will impose additional material requirements. A variety of different coolant systems are being explored across a number of devices: helium, water, molten Li-Pb alloys, molten Li salt, and dual coolant systems[9, 10, 11, 12, 13]. Corrosion from the coolant itself or its impurities may necessitate the use of a protective coating on the blanket material. Uptake and retention of the tritium that is bred inside the blanket may also require some form of barrier coating to minimise this effect (see Section 2.4.1.6).

The blanket's multifunctionality will require a complex geometry of parts joined together. A variety of joining methods are available to combine both similar and dissimilar materials. However, materials must be designed with these joining requirements in mind, as such processes can degrade material performance (see Sections 2.4.1.7 and 2.5.1.5).

2.1.2.2 First wall

Between the plasma core and the rest of the reactor structure lies the first wall of armour material. In addition to intense neutron irradiation, the armour material will interact with the plasma ions and neutral particles. The plasma-wall interactions will result in a thermal load of up to 4.6 $\mathrm{MW\,m^{-2}}$ (for a worst-case scenario in ITER [18]) in addition to much more intense transient events in the core, known as edge-localised modes (ELMs). ELMs can lead to fluxes in excess of gigawatts per square meter[19]. The steady state heat loads can cause microstructural changes and failure of component joints, even in extremely high melting point materials such as tungsten[20]. The more extreme transient events can lead to melting, cracking and the formation of dust particles[19].

Exposure to highly energetic ions in the plasma can cause sputtering of the wall material. This will lead to erosion of the first wall and deposition in other less exposed parts of the reactor interior. Furthermore, implantation of deuterium and tritium results in embrittlement of the plasma facing material[21]. This embrittlement will have a negative effect on the wall's ability to withstand transient thermal loads. In the case of tungsten, one of the leading plasma-facing candidate materials, helium implantation causes morphological changes in the form of microscale tendrils growing out of the surface, leading to the formation of tungsten "fuzz". This fuzz will lead to a deterioration in the thermal transport properties of the tungsten, which could make localised melting more likely[22].

Finally, the wall material will be exposed to the highest neutron fluxes in the reactor, as it is situated directly adjacent to the plasma core, unlike the blanket which will be partially shielded from neutrons by the first wall. This will lead to similar damage effects mentioned in the above section and discussed in more detail in Section 2.2.

2.1.2.3 Divertor

The divertor of a fusion device functions as the exhaust system of the reactor. The ionised fusion products (i.e. He^+ and minor amounts of other species) are carried by the magnetic fields in the plasma core to the surface of the divertor at specific strike points, shown schematically in Fig. 2.7. The exhaust products are extremely hot and the strike points are concentrated to a relatively small area, only $3.5\,\mathrm{m^2}$ in ITER, which has a plasma radius of 6.2 m[23]. This means that the divertor will be subject to enormous thermal loads of around $10\,\mathrm{MW\,m^{-2}}$ in ITER, or even higher for future reactor designs[24].

As a result, the divertor materials will be exposed to all of the hostile conditions listed above for the first wall, with the added constraint of an even higher baseline thermal load. Such conditions necessitate the use of extremely high melting point tem-

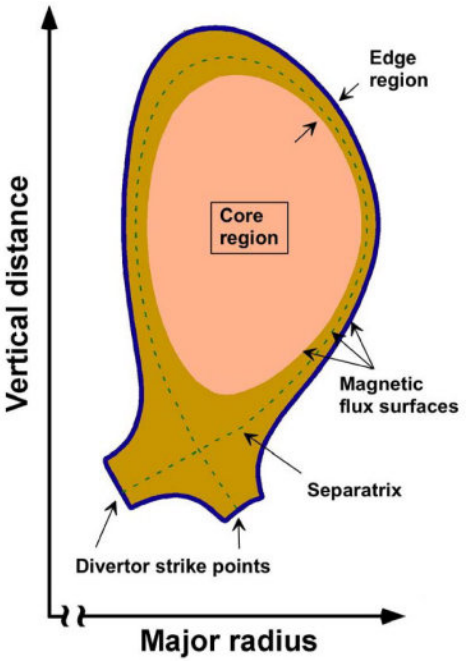

Figure 2.7: Schematic of the location of the divertor strike points in a fusion reactor. Taken from [24].

peratures, with tungsten and tungsten-based alloys as the currently preferred option (see Section 2.6).

2.1.3 Low-activation materials

One of the most significant differences between the environmental impact of a fission reactor versus a fusion one is the radioactive waste products that are generated. Fission reactors produce significant quantities of long-lived waste consisting of fission products from the spent uranium fuel. If one considers the D-T reaction, no radioactive waste is produced *directly* from the fusion process. Only when the fusion neutrons interact with the materials inside the reactor are radioactive byproducts produced.[3]

Unlike their fission counterparts, the materials used in a fusion reactor will be the sole source of any radioactive waste produced. Therefore, it is desirable that the waste produced in a fusion reactor be as short-lived as possible in order to provide a compelling environmental and safety argument for fusion over fission (and other energy sources). Indeed, the fusion community is in broad agreement that so called low-activation elements should be used. Although there is no set definition for what constitutes a low-activation element, it is sometimes defined as an element that takes a period of less than 100 years to reach low-level waste (LLW)[25, 26]. In this instance, the UK government's definition of LLW will be used. This is defined as waste with a

[3]Analogous processes occur with fission neutrons. However, they are not main sources of radioactive waste for fission reactors.

radioactivity of <4 MBq/kg of alpha radiation and <12 MBq/kg of combined beta and gamma radiation. LLW in the UK is able to be recycled or incinerated in some cases, or otherwise directly disposed of in special repositories[27]. Other classifications of waste not based on legal limits also exist. One such example is the remote handling limit, which is based solely on gamma emissions that can damage the electronics of robotic handling equipment. As this is a limit based on technology and not on legislation, it does not have a fixed value. 2 mSv/hr is a value that has been used in literature[28] as a conservative limit, but electronics may well become tolerant of higher doses as technology improves.

The nuclear reactions undergone by most elements when exposed to neutron radiation are well characterised, which means that it is possible to predict the activation behaviour of materials after use in a fusion reactor. Work by Gilbert et al. (shown in Fig. 2.8) shows how long elements will take to reach LLW criteria after 12 years of pulsed operation in a hypothetical DEMO reactor design[29]. Materials will be exposed to different neutron irradiation fluxes depending on their position in the reactor and their activities will change correspondingly. Although the data in Fig. 2.8 is specific to the divertor, comparisons between elements can be made for any component exposed to significant amounts of neutron irradiation. If fusion reactors are to limit the amount of radioactive waste produced during and after operation, it is clear that some restrictions on materials selection will be imposed. For example: it can be seen that nickel, which is extremely common in a variety of steels, often in large weight fractions, would remain radioactive for 66,000 years if used in a fusion divertor.

2.1.4 Accident tolerance

When designing materials for a fusion reactor, it is important to consider both the environment that materials will exist in during normal operation but also the conditions that may be faced during an accident or some other unexpected event. Such events could include: plasma disruption, magnetic discharge; water, air or helium ingress into the vacuum chamber; dust or hydrogen explosions, fires, earthquakes and loss of power/coolant[30, 31, 32].

Materials should be chosen to mitigate the hazards that will arise, if possible. A paper examining the safety case with respect to the nuclear activation of elements identified four figures of merit for elements:

1. Prompt dose rating
2. Latent dose rating
3. Time before damage (from decay heat)
4. Maximum temperature rise[33]

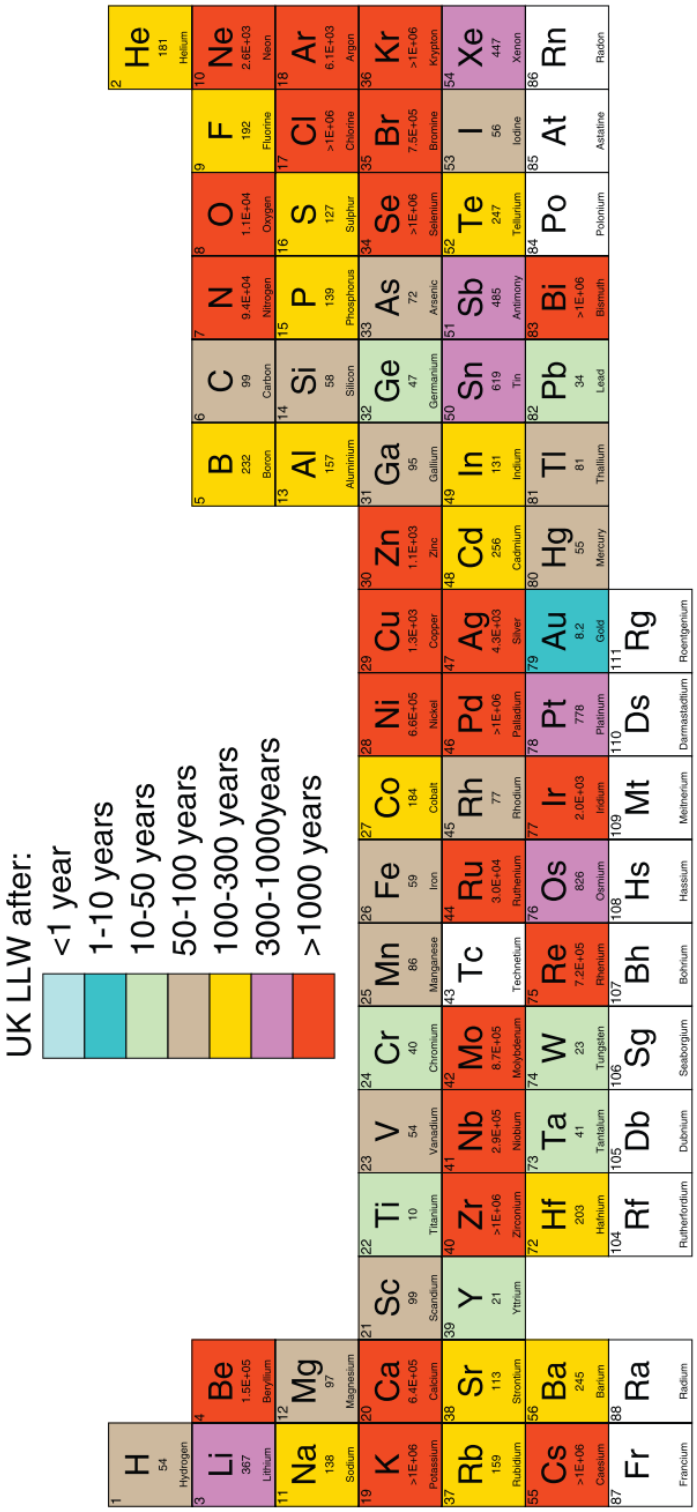

Figure 2.8: Time taken to reach low-level waste after 14 years of pulsed operation in the DEMO divertor. From Gilbert et al[29].

A follow-up study by the same authors outlined the criteria a material should ideally fulfil to be considered "low-activation":

1. Prompt dose rate of <2 Sv from 100% release of inventory
2. Possible cancer risk of <0.1%/yr to local residents in realistic release scenarios
3. Decay heat should be limited to ensure the design is passively safe
4. Used materials could be recycled or disposed of as near-surface waste
5. Hands-on maintenance should be possible in coolant systems
6. Effluents of activation products should not pose significant extra risk c.f. tritium effluents[34]

Radioactivity concerns are not the only safety issues that have been considered in the literature. If air ingress is accompanied by a loss-of-coolant accident (LOCA), then the first wall material could be exposed to oxygen at high temperatures for a period of weeks in a DEMO-type reactor[35]. Significant oxidation for this length of time would have severe safety implications. Therefore, some recent work has been devoted to developing oxidation-resistance first wall materials[36, 37, 38].

If these assessments are taken into consideration, it is clear that a holistic view of material safety should be adopted, not just one that focuses only on the long-term activation properties of an alloy.

2.2 Irradiation damage

As mentioned in previous sections, irradiation can have profound effects on the properties of materials. This section only aims to summarise the basics of radiation damage as described by Was[39], whose work offers a far more complete summary than can be presented here. When a neutron (or some other particle) with sufficient energy collides with an atom, the neutron imparts some of its energy to the atom, which is then displaced from its lattice site with a portion of this energy. This atom, known as the primary knock-on atom (PKA), will then go onto collide with other atoms, which in turn collide with more atoms, creating a displacement cascade. In this cascade region, many Frenkel pairs (FPs), consisting of an atomic vacancy and corresponding interstitial atom, are created. FPs are the primary mechanism behind the formation of other microstructural features that form as a result of irradiation. At lower homologous temperatures ($T/T_m < 0.2$), only the interstitials are sufficiently mobile to form clusters and larger defects such as dislocation loops. When the homologous temperature is higher ($T/T_m > 0.2$), the vacancies will be mobile enough to form large clusters known as voids. When both vacancies and interstitials are mobile, other radiation damage mechanisms such as elemental segregation, phase transformations, and precipitation can occur. These microstructural features can significantly degrade the

mechanical properties of materials, leading to them becoming potentially unsuitable for their original application, if these changes are not taken into account or some how mitigated. The exact nature of radiation damage can vary widely depending on irradiation temperature, fluence, flux, material composition and thermomechanical history.

The most common method of quantifying the amount of damage in a material is to use the number of displacements per atom (dpa). It is a measure of how many times, on average, each atom in a material has been displaced from its original lattice point within a crystal. This number is defined by how much energy is transferred from the incident radiation particle to the PKA, and by how many other atomic displacements the PKA will go on to make. This means that is not just the particle fluence (i.e. the number of incident particles) that is important in determining damage, but the energy spectrum of these particles too. A larger fluence of less energetic particles may be less damaging to a given material than a smaller fluence of more energetic ones, as the more energetic particles can displace more atoms from a given cascade event.

Alongside activation and safety concerns (see Section 2.1.3), nuclear transmutation will also be strongly detrimental to materials' properties when considered alongside displacive damage. As mentioned in Section 2.1.2.2, tungsten transmutes into rhenium and, subsequently, osmium. When this "new" alloy is exposed to neutron radiation, it will also undergo elemental clustering, further deteriorating its properties[40]. Another transmutative effect that is significant in fusion materials is the production of He and H from certain nuclear reactions. These atoms are highly mobile in materials due to their small size, and can contribute further to damage by diffusing to defects and grain boundaries. He and H can also be introduced into the first wall materials via bombardment from the plasma, which itself can be considered a form of radiation damage.

2.3 Candidate fusion materials

It is clear that the field of nuclear fusion poses a number of materials challenges that are unique even when the challenges are faced individually, let alone in conjunction with other problems. The development of new materials has been a cornerstone of fusion research for many decades, which has resulted in numerous new materials being researched and developed with varying degrees of success and technological readiness.

The following sections will provide an overview of some of the research that has been done on candidate fusion materials. As the alloys studied in this work contain vanadium as the major element (or one of the major elements), the focus of this section of the review will primarily be on vanadium-based alloys. The secondary focus will be on low-activation steels, which are the primary competitors to vanadium alloys in the role of a blanket structural material. Other materials will also be covered, but in

limited depth as they are either intended to fulfil a different role to vanadium alloys and steels (in the case of tungsten and beryllium), or they represent a departure from the metallurgical focus of this work (in the case of silicon carbide). This is by no means an exhaustive list of every material to have been considered for use in fusion applications, it is merely meant to highlight some of the main classes of materials and their relative advantages and limitations.

Following these sections, an introduction will be given to the field high entropy alloys (HEAs), accompanied by some discussion of the properties that may render them useful as fusion materials, especially when compared to some of the deficiencies of vanadium alloys and steels.

2.4 Vanadium alloys

Although vanadium-based alloys have been in development for fission applications since the 1960s[41, 42], they have remained purely experimental materials and have not been put to any practical use in the nuclear industry. Chromium and titanium are the most common alloying elements, both often present in concentrations of several wt%. They both have good solubility with V and offer improved mechanical properties when added. However, adding more Cr and Ti has diminishing returns when it comes to strength and irradiation resistance and can decrease ductility[43]. As these elements are some of the least activating transition metals (see Fig. 5.1), they are attractive candidate materials for blanket applications.

Many different vanadium alloy compositions containing various elements such as Al, Cr, Ti, Ni, Si, Mo and W have all been tested to varying degrees, V-4Cr-4Ti has been decided as the most favourable reference alloy for future development[44], however more recent results have cast doubt on this long-held assumption[45]. It has good resistance irradiation swelling and embrittlement, good mechanical properties[46, 47, 48], as well as favourable creep properties, in both irradiated and unirradiated states[49]. More generally, solute additions of a larger size relative to V, such as Ti, inhibit irradiation swelling[50].

2.4.1 Properties

2.4.1.1 Strength & hardness

As a structural component, the blanket must be able to withstand the loads required to support the enormous reactor structure. Additionally, less material can be used if it is stronger, so high strength may confer economic benefits. As with any other alloy, the strength of a vanadium alloy is highly dependent on its composition and thermomechanical processing. Fig. 2.9 shows the ultimate tensile strength of V-4Cr-

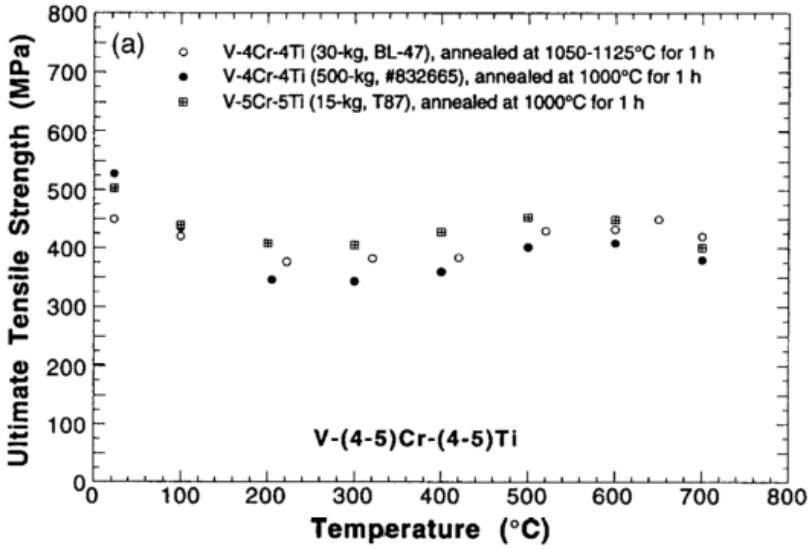

Figure 2.9: Strength of V-(4-5)Cr-(4-5)Ti alloys at varying temperatures. Taken from [44].

4Ti as ranging from approximately 350 to 525 MPa at temperatures between 20 and 700 °C.

Chen et al.[51] investigated the effects of thermomechanical processing on V-4Cr-4Ti and found that with appropriate annealing and cold working, large increases in hardness and tensile strength can be achieved compared to a solution annealed sample. Highest hardness was found to occur after annealing for 10 hours at 600 °C. Earlier transmission electron microscopy (TEM) work performed to characterise the strengthening mechanisms of V-4Cr-4Ti found that Ti-C-O precipitates were the cause of strengthening from annealing[52, 53].

Hardness is positively correlated with both O and N content in both unalloyed vanadium and V-4Cr-4Ti. N is contained in large precipitates which are stable at 1373 K. O was found to be present in both small and large precipitates. However, the smaller precipitates dissolved into the matrix at 1373 K, leading to a solid solution strengthening effect from the O released[52]. Notably, this study also found that repeated annealing during rolling may produce less pronounced high temperature hardening behaviour due to the formation of large precipitates which reduce the matrix impurity concentration. This leads to the important suggestion that chemically similar vanadium alloys may be sensitive to thermomechanical processing history. Findings from Muroga et al.[54] also highlighted the importance of precipitate control when producing vanadium alloys, shown in Fig. 2.10.

Recent work by Zhang and Han[55] has also emphasised the significant and variable effect that oxygen content has on pure vanadium. At high O concentrations (>1 at%), the presence of oxygen greatly strengthens the alloy through a combination of solid solution hardening and a contribution from the dynamic formation of oxygen-

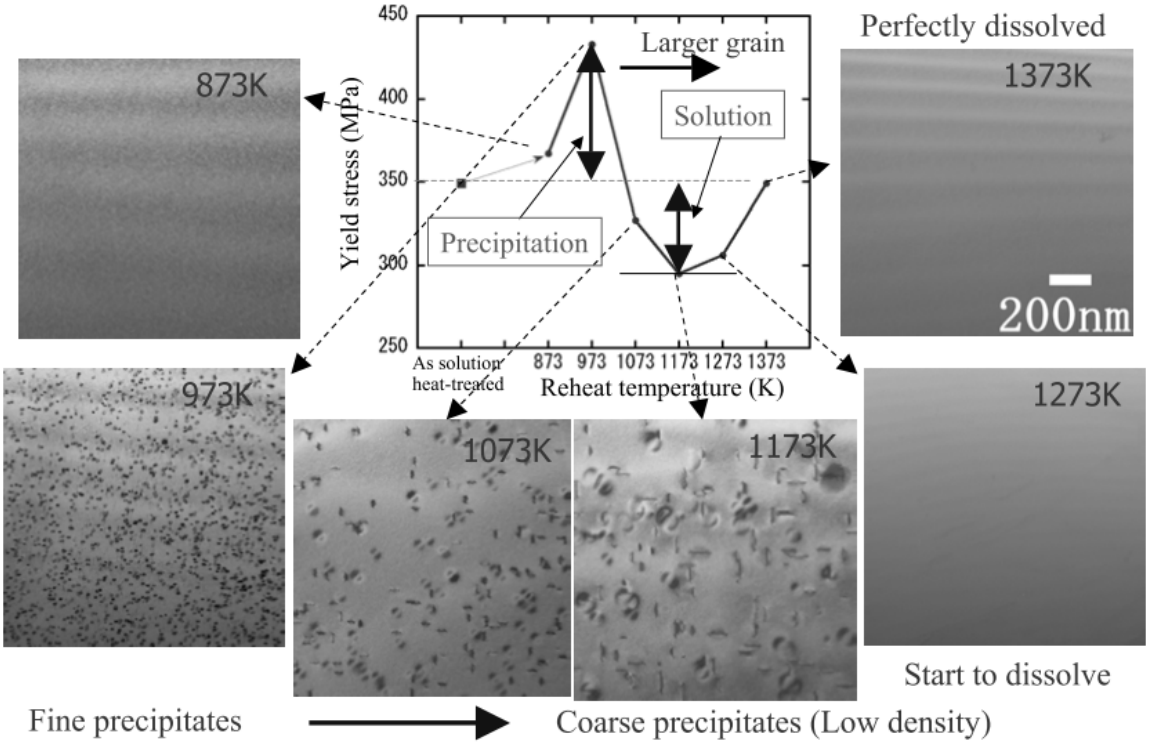

Figure 2.10: Microstructure and yield stress for V-4Cr-4Ti after heating at various temperatures. Taken from [54].

vacancy complexes. In the case of alloys with intermediate O content (≈ 1 at%), these oxygen-vacancy complexes also induce strain hardening, which causes the alloys to retain significant ductility. However, as O content increases beyond this, the density of oxygen-vacancy complexes is too high and dislocation glide is inhibited, leading to brittle fracture. Although this work was performed on pure V metal, it signifies the importance of forming interstitial-vacancy complexes in BCC alloys. These effects are in addition to those posited in an earlier density functional theory (DFT) work by Zhang et al.[56]. This study found that the presence of 1 at% C, N or O is enough to significantly increase the energy required to activate slip systems in pure V, causing the normally ductile metal to become brittle.

Chen et al.[57] investigated the effects of alloy composition on strengthening. By comparing V-4Cr-4Ti to V-6W-4Ti and V-4Ti, it was found that the precipitation hardening effect was much stronger in V-4Cr-4Ti than in V-6W-4Ti and V-4Ti, suggesting that although the precipitates are formed from Ti, it is the addition of Cr that changes the behaviour of these precipitates and results in improved strength. The addition of W on its own resulted in no significant increase in hardness, exhibiting similar hardness to V-4Ti[58]. The mechanical properties of vanadium alloys, particularly at high temperatures, seem well-suited to a fusion environment.

2.4.1.2 Creep behaviour

As the blanket structure will be operating at high temperatures, it is vital that the material used is able to resist creep. In this section, thermal creep will be discussed separately from irradiation induced creep as the operating mechanisms differ in each case.

Thermal creep data shows that V-4Cr-4Ti at higher temperatures (650-800 °C or approximately 0.4 - 0.5 T_m) and normalised stresses greater than 0.002, has a creep rate with a power law dependence, given by:

$$\dot{\varepsilon} = A\sigma^n \exp\left(-Q/RT\right) \tag{2.1}$$

where σ is the applied stress, n is the stress exponent, Q is the activation energy for the creep mechanism, R is the universal gas constant and T is the temperature. Both uniaxial[59] and biaxial[60] tests in vacuum found that the stress exponent is approximately 4, and the activation energy for creep was around 300 kJ/mol. This is similar to the activation energy of pure vanadium self-diffusion, which indicates that climb-assisted dislocation glide is the dominant creep mechanism.

Creep tests performed in a liquid Li environment showed creep rates that were generally consistent with results obtained under vacuum. Certain tests did show an increased creep rate in the lithium environment, but the author acknowledged that longer exposure times would be necessary for further investigation[61, 62]. An explanation for the differing creep behaviour in liquid Li may be offered by the effect of O interstitial levels. Biaxial tests performed with an O concentration of 699 weight parts per million (wppm)[60] exhibited greatly decreased creep rates compared to uniaxial tests with an O concentration of 310 wppm[59]. Kurtz[60] asserts that the difference is due to O interstitials and not texture differences that may be present between uniaxial tensile and biaxial tube specimens. However, a highly purified ingot of V-4Cr-4Ti with ∼180 wppm O, was found to have comparable creep properties to other less pure alloys, suggesting that O concentrations of this level are still enough to impede dislocation motion and consequently, creep behaviour[63].

Thermomechanical processing also effects creep performance. Creep tests on various thermomechanical treatments of another high purity V-4Cr-4Ti alloy found that the specimen that had been heat treated and cold rolled by 20% had reduced creep rates above a certain stress level between 700 and 800 °C, compared to a sample with the same heat treatment and no rolling[64]. Below this stress level, creep rates were similar in both rolled and unrolled specimens. The critical stress decreased with increasing temperature. Increases in yield strength from cold rolling found in the same study can partially explain this improved creep performance. However, the activation energies for both samples were much higher than those determined by Natesan et al.[59], suggesting

that climb assisted dislocation glide is not the mechanism responsible for creep in these heat treated alloys. Secondary electron microscopy (SEM) examination showed grain structure on the deformed regions of the test specimen, suggesting that Coble creep, grain boundary motion governed by diffusion, was the mechanism at play.

This is in contrast with results from Zheng et al.[65] which found that STD[4] or SAACW[5] specimens both exhibited dislocation glide-assisted climb above 180 MPa. Below 180 MPa, dislocation climb was the only mechanism observed. SACWA[6] specimens have a higher threshold stress of 280 MPa for dislocation glide to become active. This is thought to be caused by the high density of fine precipitates pinning dislocations and suppressing glide. However, the same increased density allows for easier climb, leading to higher creep rates at stresses below 180 MPa. Diffusion based creep is not offered as a possible mechanism for any regime. This suggests that the diffusion-based Coble creep only starts to operate at around 800 °C.

Muroga et al.[66, 67] suggested that sessile $\boldsymbol{a}\langle 100\rangle$ type dislocations prevent precipitates from coarsening, allowing vanadium alloys to maintain their strength and creep resistance at high temperatures. However, the authors offer no mechanistic explanation for this process. Cold rolling produced a mixture of $\boldsymbol{a}\langle 100\rangle$ and $\boldsymbol{a}/2\langle 111\rangle$ dislocations, which explains the improved creep performance of cold worked alloys previously found. The authors state that operating temperatures and loads should be kept within a range where these dislocations cannot recover. SACWA treated alloys have much lower creep rates at high stresses compared to STD and SAACW treatments, but at lower stresses the reverse is true (see Fig. 2.11)[68]. This is because grain boundary creep is dominant at low stresses, whereas dislocation creep dominates at higher stresses. leading to improved creep performance for SACWA alloys with greater dislocation densities.

Grain size also has a strong effect on creep resistance. V-1.6Y-8W-0.8TiC tested at various grain sizes at 800 °C and 250 MPa showed that creep rate decreased with increasing grain sizes, up to around 1000 µm[69]. This was attributed to the fact that creep occurs via grain boundary sliding in this alloy, as opposed to the dislocation glide that occurs for V-4Cr-4Ti under the same conditions. The solute W and dispersoids of Y_2O_3, YN and TiC were able to suppress dislocation glide, leading to a grain boundary mechanism dominating.

Recent results have revealed a stress dependence on the effects of interstitials on creep properties. At lower stresses (<100 MPa), no difference in creep behaviour was observed between the highly-purified (339 wppm of C + N + O) Japanese NH2 ingot and the less pure US ingot (600 wppm). However, at higher stresses, the alloy with increased interstitial content has a higher time to rupture and reduced creep rate[70] due

[4]Standard annealing at 1000 °C for 2hrs
[5]Solid solution annealing at 1100 °C for 1hr + aging at 600 °C for 20hrs + 20% cold working
[6]Solid solution annealing at 1100 °C for 1hr + 20% cold working + aging at 600 °C for 20hrs

to purification softening in the NH2 alloy. The design stress for fusion blanket materials is expected to be under 100 MPa (based on existing design codes for nuclear structural materials), so the benefits afforded by reduced interstitial content, such as improved weldability (see Section 2.4.1.7) and neutron activation properties (see Section 2.5.1.4), mean that reduced interstitial content is a desirable property for vanadium alloys.

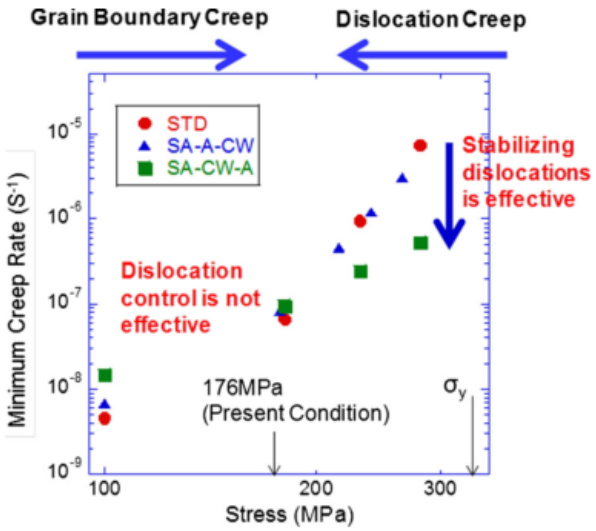

Figure 2.11: Stress against creep rate for different heats of V-4Cr-4Ti, with arrows to indicate the two creep mechanisms at play. Taken from [68].

Thermal creep behaviour is a key factor in determining the upper limit of the a material's operating temperature in a fusion reactor[16]. Both mechanical alloying and appropriate thermomechanical treatments have shown to be effective in improving creep performance and are promising avenues for further investigation.

2.4.1.3 Irradiation resistance

Early work discovered that when unirradiated, various vanadium alloys (pure V and V-Cr-Ti alloys with <10wt.% combined Cr + Ti and various additions of Si and Nb) have a very low (<77 K) ductile-brittle transition temperature (DBTT)[71, 72], although this can rise to room temperature with annealing at 1100 °C[73]. However, when irradiated at moderately low temperatures (200-300 °C), DBTT increased dramatically to 300 °C[73]. Shear punch tests on vanadium alloys irradiated at the same temperature range also found a loss of ductility[74]. From 90-200 °C, both the density of dislocation loops and hardness increased with increasing irradiation temperature, suggesting that the irradiation hardening is caused by these loops. V-5Ti and V-5Nb were the exceptions, with loop density remaining the same and decreasing respectively. Additionally, at higher irradiation temperatures (350-400 °C), no voids were observed in these two alloys. This behaviour is thought to be caused by larger atomic radii of Ti and Nb compared to V, with vacancies being trapped by the oversized solute atoms[75].

Recovery of irradiation damage incurred at 228 °C was possible through annealing at 600-700 °C and for some alloys, complete disappearance of irradiation hardening was observed[76].

Alloy composition is also known to strongly effect irradiation swelling behaviour. Addition of Cr to V leads to greatly increased swelling when compared to pure V, a behaviour that becomes more prominent at higher temperatures. The addition of Si also increases swelling in V, but with an inverted temperature dependence. Adding 1 wt% Zr does not lead to high rates of swelling at any temperature[77]. However, the increased swelling from the addition of Cr between 420 and 600 °C can be counteracted by introducing Ti in quantities over 3 wt% as long as Cr concentrations remain below 15 wt%[78]. Although atomic size effects have been implicated in the swelling behaviour of V binary alloys[79], more recent DFT studies suggest that the swelling suppressing effects of Ti are due to the chemical nature of the Ti-vacancy complexes formed during irradiation[80]. A molecular dynamics (MD) study comparing pure V to V-4Ti found that the addition of Ti does not effect the number of Frenkel pairs generated during atomic displacement cascades of 0.5-20 keV[81]. However, the Ti-containing alloy did have a larger proportion of small-sized clusters (mainly monovacancies) compared to pure V.

The formation of vacancy complexes is not exclusive to metal alloying additions. Another DFT study showed that He atoms will bind less strongly to O- or N- vacancy complexes compared to lone vacancies in pure vanadium[82]. As He is less tightly bound to interstitial-vacancy complexes, dissolution of He becomes easier, resulting in less growth and swelling of the trapping He clusters.

Tailoring the grain structure of vanadium alloys may also be beneficial for resisting radiation damage. MD studies of grain boundaries in vanadium alloys show that self-healing of radiation damage can occur at some symmetrical tilt boundaries via a interstitial emission mechanism[83]. The addition of Cr and Ti also appear to reduce the activation energy of this process, indicating that maximising grain boundaries may be an effective method of lessening radiation damage in V-Cr-Ti alloys.

At higher irradiation temperatures, creep behaviour is the mechanical property of primary concern. As many components in the blanket structure will be operating in this high temperature regime, possibly involving thermal cycles, it is important that the creep behaviour under irradiation is understood. Fukumoto et al.[73] performed creep irradiation experiments at a variety of temperatures on V-Cr-Ti and V-Fe-Ti alloys, and found that there was no significant acceleration of creep below 300 °C. Tsai et al.[84] showed that strain rate linearly increased with stress for V-4Cr-4Ti for temperatures up to 500 °C. This is in contrast to the behaviour seen by Troyanov et al.[85] who observed a bilinear creep regime, with strain rate rapidly increasing at stresses above 120 MPa. Li et al.[86] performed experiments on the higher temperature

creep performance of V-4Cr-4Ti. Linear creep behaviour was observed below 110 MPa and 600 °C. For stresses above 110 MPa, the creep behaviour became non-linear, which could not be fully accounted for by consideration of thermal creep alone. More recent irradiation creep results from vanadium alloys in liquid lithium environments have found that at temperatures below 500 °C, creep rate is proportional to the square root of the neutron dose. Above these temperatures, creep strain is much larger but the dependence on irradiation dose is unclear due to insufficient data[87].

Overall, the behaviour of irradiated vanadium alloys are reasonably well characterised and understood. However, some questions remain about the irradiated creep behaviour of otherwise well-characterised alloys like V-4Cr-4Ti, which may limit safe operating temperature ranges.

2.4.1.4 Oxidation

As alluded to in Section 2.1.4, the oxidation resistance will be an important part of the safety case for a material, even if it is not expected to be exposed to oxygen during normal operation. Additionally, the uptake of oxygen into vanadium alloys in its interstitial form is detrimental to the alloys' mechanical properties (see section 2.4.1.1). The prevention of interstitial-related degradation is the motivation for much of the literature on vanadium alloy oxidation[88, 89, 90, 91, 92, 93, 94].

An early study of the V-Cr system found that oxidation rates could be reduced by increasing Cr content[95]. The formation of V_2O_5 at high temperatures was observed in a later work on pure vanadium[96]. This oxide melted at 670 °C and resulted in reaction rates that were too rapid to measure when oxidation was performed above this temperature at high oxygen partial pressures (>0.1 atm). It is worth noting that V_2O_5 is highly toxic, so the formation of this chemical (especially in its liquid state) has the potential to be highly hazardous[97].

The first work performed on a V-Cr-Ti alloy (using He gas with H_2O impurities) found that the addition of Ti to the V-Cr binary improved oxide scale adherence to the alloy and led to reduced spallation[98]. However, the elevated oxygen content in the alloy matrix after oxidation (5 wt%) would result in such severe embrittlement that the use of a He cooled design would be incompatible with a V alloy blanket (in the absence of corrosion barriers). Indeed, much of the work that followed this served to confirm the embrittling effects that oxidation had on V-Cr-Ti alloys[89, 99, 59].

Doping elements such as Al, Si and Y were added to V-Cr-Ti alloys and all three were able to reduce oxidation rates at 500 and 600 °C. Y doping resulted in the smallest decrease in ductility after oxidation[100], caused by Y inhibiting the depth to which O was able to diffuse. This led to a more shallow brittle region and greater ductility overall[91].

Altering the Cr and Ti content of the alloys was also effective at mitigating the

effects of oxidation in air. Increasing Cr content from 4 wt% was effective in reducing weight gain at temperatures ranging from 500 - 900 °C. Increasing Ti content resulted in smaller changes (both positive and negative) in weight gain. However, increasing the Cr content came at the cost of reducing their ductility[92], as discussed above. Increasing Cr content was also effective in inhibiting corrosion from pressured water, and also lead to losses of ductility after corrosion. This could be mitigated by degassing the H dissolved in the matrix after exposure or by doping with Y[101].

In the last decade there has been limited work on the oxidation performance of vanadium alloys, with the exception of a few interesting developments. Silicide diffusion coatings have been successfully applied to V-4Cr-4Ti alloys. Ostensibly designed for sodium-cooled fast fission reactors, these coatings were found to resist oxidation in air (approximately an order of magnitude decrease in weight gain compared with uncoated V-4Cr-4Ti) and corrosion in liquid Na[102]. V-Ti-Ta alloys have better oxidation properties across a wide range of fusion relevant temperatures[103], but this alloy is in very preliminary stages of research, with only basic results available for other properties of interest[104, 105].

The high temperature oxidation behaviour of vanadium alloys is somewhat underexplored, given the potential safety implications that a toxic, low-melting point oxide might have in the event of a fusion reactor accident. However, the use of coating materials may mitigate some of these risks.

2.4.1.5 Coolant compatibility

Although the plasma chamber of a fusion reactor will be under vacuum, the blanket structure will still be exposed to liquids capable of corroding the materials used and gases that may become embedded in the structure. These substances may come from both the coolants and the breeder materials used, and some designs use a material that can perform both functions. Liquid Li, Li-Pb eutectic, and FLiBe molten salt, all of which can breed tritium, have been considered as coolants.

Studies featuring liquid lithium at 700 °C flowing round a thermal convection loop of V-4Cr-4Ti for 2355 hours found a maximum mass loss of approximately 2.5 mg m^{-2} hr^{-1}, occurring on the hot leg of the loop. Mass gain was observed elsewhere on the sample[106]. Furthermore, the areas that gained mass also had slightly higher yield stresses and lower ductility. This was consistent with increased N and C content in the mass gain regions.

Further work using the same apparatus found negligible decreases in ductility for samples exposed to lithium. The increase in yield stress was higher at lower lithium exposure temperatures[107]. More detailed hardness studies by Zheng et al[108] showed that increases in surface hardness after flowing lithium exposure corresponded to the approximate diffusion distance of N in V-4Cr-4Ti, and that the hardening effect was

absent in pure V. This suggests the conclusion that Ti(C,O,N) precipitates, caused by mass transfer of N and C from the Li, are responsible for the hardening effect. Hardness is further increased closer to the surface. This is caused by N-rich precipitates, due to the slower diffusion rate of N in V compared to C and O. This precipitate hardening is also able to counteract the loss of O atoms, which offer solid solution hardening, into Li.

Water and helium have not been seriously investigated due to excessive corrosion rates from either the bulk water, or the water present in small quantities in commercial grade helium[109, 98]. This limits the blanket design options available to vanadium alloys.

2.4.1.6 Tritium uptake

A review by Muroga et al.[110] calculated the expected levels of tritium uptake into 700 tons of V-4Cr-4Ti from FLiBe and Li, as well as upper and lower bounds for Li-Pb, are shown in Fig. 2.12. Nuclear regulators in France have legislated a limit of 1 kg on the amount of tritium that may be present on-site at ITER[111]. This implies that at reasonable tritium concentrations, retention in V-4Cr-4Ti will be well over the limit for FLiBe and possibly Li-Pb coolants[31]. This limit has been imposed due to safety concerns. Given the radioactivity of tritium, the amount present on a nuclear site must be kept to a minimum in case of a catastrophic accident involving release of the entire inventory. There is also an economic argument for minimising tritium retention, as any tritium contained in the reactor materials cannot be burnt in the plasma core.

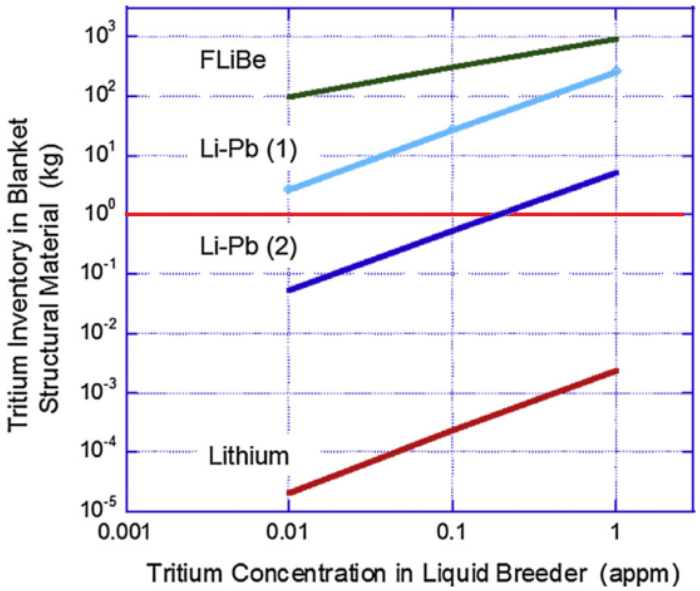

Figure 2.12: Calculated equilibrium tritium inventory in V-4Cr-4Ti at 1000 K. The ITER reactor retained tritium inventory limit of 1 kg is marked (taken from [110]).

In order to prevent corrosion and tritium uptake, as well as reduce the magnetohy-

drodynamic pressure drop with a liquid Li coolant, it may be necessary to use a thin barrier coating to protect the vanadium alloys. Er_2O_3 has been suggested for use in this application[112].

2.4.1.7 Primary production & welding

Although a final design has not been decided, the blanket of DEMO will be an extremely complex structure weighing thousands of tons. In order to be a viable blanket material, vanadium alloys must be capable of being manufactured in large quantities and welded together while maintaining structural integrity.

V-4Cr-4Ti ingots with masses ranging from tens to hundreds of kg and consistent material properties have been developed in the US, Japan, China, Russia, and France[113, 114, 115, 116, 117]. Although the exact nature of the fabrication techniques vary, most of the steps are broadly similar. For instance, all procedures involve the use of electron beam melting to initially join the constituent metals combined with either vacuum degassing or remelting. These steps are necessary to reduce interstitial impurity content to acceptable levels. In order to avoid interstitial pickup during hot forging, the billets were either coated with stainless steel or canned. Finally, samples were worked and annealed to give the desired microstructure. Fig. 2.13 shows the fabrication steps for CEA-J57, the French V-4Cr-4Ti alloy grade, as an example[117].

These techniques are suitable for producing plates, but the more complex geometries involved in a fusion blanket structure will require joining techniques. Initial efforts to weld V-4Cr-4Ti used gas tungsten arc (GTA) welding. With an appropriate post-weld heat treatment (PWHT) and a sufficiently pure atmosphere, a DBTT of 50 °C was achieved[118]. Further improvements to purity of the bulk and fillet resulted in an even lower DBTT. A good correlation between O concentration in the fusion zone and DBTT was observed. Laser welding increases hardness of the heat affected zone (HAZ), caused by increased impurity levels from the dissolution of precipitates. Impact absorption energy was the same in both the base and the weld metal[119]. Precipitate dissolution may negatively affect irradiation resistance as the precipitates act as sinks for radiation-induced defects. This causes increased irradiation hardening and a higher DBTT in the weld metal compared to the base metal. These property changes can be reversed with appropriate post-irradiation annealing[120, 121]. Investigation into optimal PWHTs for laser welds found that annealing at 800 °C for an hour was optimal for forming Ti precipitates and purifying the matrix from oxygen impurities. Higher temperatures resulted in partial precipitate dissolution[122].

More recent investigation of electron beam (EB) welding found that weld metal had superior impact properties to the base metal, thought to be caused by a narrow fusion zone and/or remaining thermal stresses. Despite dissolution of fine Ti precipitates, there was no shift in DBTT as one might expect from the O solid solution hardening

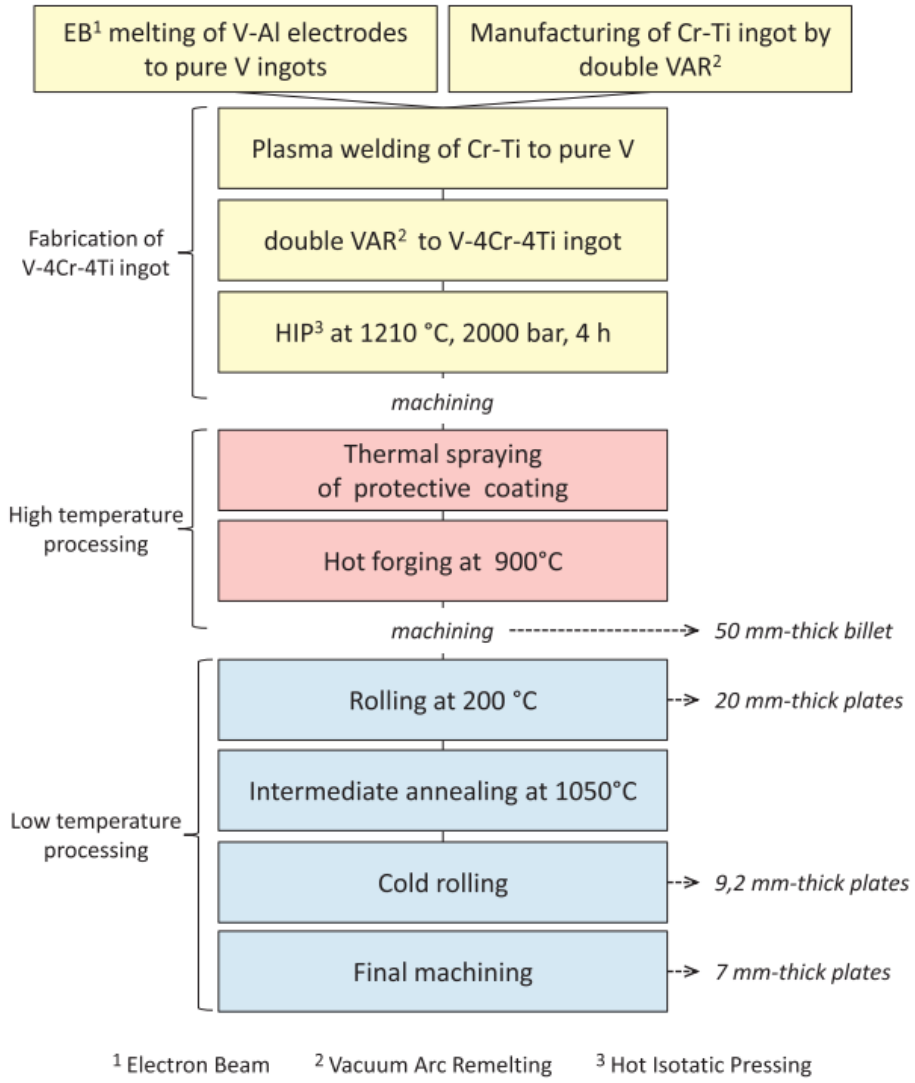

Figure 2.13: Fabrication steps of CEA-J57. Taken from [117]).

effects[123]. EB weld joints showed poorer Charpy impact properties, after a PWHT and after exposure to liquid Li, caused by precipitation hardening[124]. In order to avoid embrittlement at fusion reactor operating temperatures (∼700 °C), a PWHT at 800 °C should be performed even though the weld metal prior to PWHT has superior impact properties to the base metal[125].

In addition to joining V-4Cr-4Ti to itself, there is also the possibility of joining it to dissimilar metals. Diffusion bonding by hot isostatic pressing (HIP) between V-4Cr-4Ti and a carbide dispersion strengthened V alloy resulted in a join with good strength and ductility with no PWHT required, although grain growth was a problem at the temperature used[126].

Hastelloy X, a corrosion resistant nickel-based alloy, has been suggested as a material for use in the heat exchanger of a lithium molten salt blanket design. Both EB and explosive welding techniques have been investigated for joining Hastelloy to

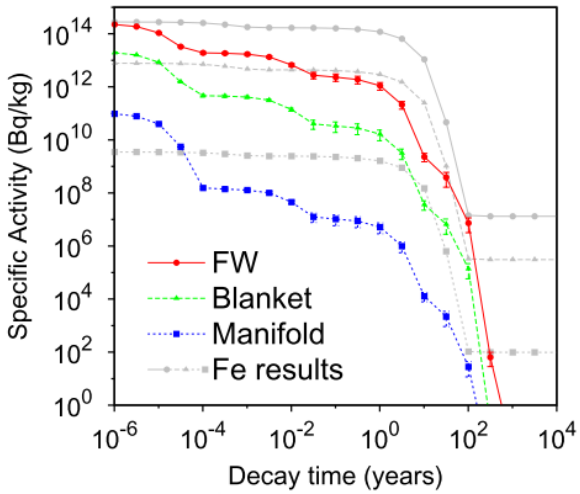

Figure 2.14: Specific activity of vanadium c.f. iron in various reactor components after 2 full power years of service in DEMO-like conditions. Taken from [131].

vanadium alloys[127, 128]. EB welding required the use of a Cu interlayer to avoid the formation of embrittling intermetallic phases, at the expense of a softer weld region. Explosive welding avoided the formation of intermetallic phases, instead producing an face centred cubic (FCC) phase in the weld region. Curiously, this FCC phase is compositionally complex and would fit most definitions of a HEA, making it one of the few HEAs that has appeared so far in fusion research (see Section 2.9.3).

Although fabrication of high quality vanadium alloys has been performed in large quantities across various countries, the joining technology required to make the larger, more complex components used in fusion blankets is still at a relatively early stage. EB welding shows promise as an effective technique for joining vanadium alloys when combined with an appropriate PWHT. However, the effects of irradiation on these welds has not been well-investigated nor has how to mitigate these potential effects with PWHTs.

2.4.1.8 Activation properties

Fig. 2.14 shows that vanadium itself has relatively favourable long-term activation properties compared to iron, the majority component of the steels that are the other main competitor blanket material to vanadium alloys. Of course, minor alloying and also impurity elements must also be included in an activation analysis. A recent study investigating prospective vacuum vessel materials for the ARC (affordable, robust, compact) reactor (a proposed spherical tokamak design) found that V-15Cr-5Ti was the preferred choice from an activation perspective, when likely impurity elements were taken into account[129]. An earlier analysis performed for impure V-4Cr-4Ti that included 66 different elements found that impurities, particularly Mo and Nb, from the source metal had a large impact on activation properties[130].

As mentioned in section 2.1.4, it is not merely the long term activation properties of a material that must be considered, but also the potential for prompt release of radiation. Piet et al. gives an average safety grade of C (grades range from A to G) for vanadium, and D and B for titanium and chromium respectively. Although these grades indicate intermediate levels of safety, they are the three lowest of all the transition metals (alongside iron, which also scores D).

2.4.2 New alloy development

In terms of alloy development, V-4Cr-4Ti is not necessarily the only composition that should be investigated, despite it being the most well-characterised alloy. By utilising mechanical alloying techniques, such as using yttrium as an impurity getter and carbide nanoparticles as strengtheners, researchers may be able to push the operating limits of vanadium alloys beyond what is currently possible. Various vanadium-based alloys utilising yttrium and nanocarbides have already shown improved strength and creep properties[69, 132, 133, 134, 135, 136]. Focusing on V-4Cr-4Ti in particular, Zheng et al.[137] have investigated a range of mechanically alloyed carbide particles and found that Ti_3SiC_2 had the best thermal stability and offers the most promising precipitate strengthening.

However, these are only relatively preliminary investigations into the mechanical properties of these new alloys. Production of samples is performed by hot isostatic pressing and it is unclear if this process is appropriate for manufacturing components on the scale of a fusion blanket. Furthermore, there has been no investigation of many other properties discussed in this review which are vital for fusion blanket applications.

2.5 Steels

A review of relevant fusion materials would not be complete without examining the progress made in developing new steels for fusion applications. A significant amount of work has been devoted to the investigation of reduced activaton ferritic-martensitic (RAFM) steels. RAFM steels also aim to utilise the low activation elements highlighted in Fig. 2.8. Their compositions are based on those of stainless steels designed for use in fast breeder fission reactors[7] but with highly-activating elements such as Co and Nb taken out and replaced with other, less-activating elements[139]. A review identified the four RAFM steels that have been the most widely researched, shown in Table 2.1[140].

Of these four, F82H and EUROFER-97 have the largest selection of data available

[7]These steels have, somewhat ironically, been used in high temperature fossil fuel applications instead[138].

	wt%							
Steel	**Fe**	**Cr**	**W**	**Mn**	**V**	**Si**	**C**	**Ta**
F82H	balance	7.46	1.96	0.21	0.15	0.1	0.09	0.023
JLF-1	balance	9.0	2.0	0.45	0.25	0.2	0.1	0.07
EUROFER 97	balance	8.9	1.1	0.47	0.2	-	0.11	0.14
CLAM	balance	8.98	1.55	0.4	0.21	-	0.11	0.15

Table 2.1: Compositions of common RAFM steels. Taken from [140].

and have demonstrated the greatest promise for preparing the shapes required in a fusion blanket[141]. As such, the rest of this section will primarily focus on the recent advances in these steels and their derivatives.

2.5.1 Properties

The properties required of a steel used in a fusion blanket are much the same as those required by vanadium alloys. Fusion reactors will inherently entail large fluxes of neutrons and high temperatures, so being able to maintain their properties in these conditions is essential for both types of materials, even the mechanisms underlying their properties is different. The similarities end for properties like corrosion resistance, where the requirements will be dependent on the choice of coolant and blanket system, which themselves will be selected based on the structural material used.

2.5.1.1 Mechanical properties

The mechanical properties of EUROFER steels have been well characterised, seen in Fig. 2.15[142]. A maximum operating temperature of around 575 °C (based on an assessment of high temperature creep properties) has been suggested for RAFM steels in fusion applications[16], which corresponds to a tensile strength of approximately 400 MPa in EUROFER97.

Although EUROFER97 is stronger than V-4Cr-4Ti for temperatures up to about 500 °C (see Figs. 2.9 and 2.15), it is difficult to draw any meaningful conclusions from this fact since blanket design, and therefore applied loads, will be heavily dependent on the structural material used. Other considerations, such as weldability and coolant compatibility, will influence blanket design far more than strength considerations alone.

As previously mentioned, creep behaviour is the determining factor in the upper temperature limit for RAFM steels[16]. At 550 °C, the creep stress exponent for EUROFER97 is around 14[143]. This is greater than the exponent of vanadium alloys, indicating a greater dependence on stress.

Of perhaps greater interest, however, is the creep behaviour of oxide dispersion strengthened (ODS) EUROFER97, created by mechanically alloying Y_2O_3 particles in a steel matrix. Creep exponents for this material were in the range 3.9-5.5 for tests

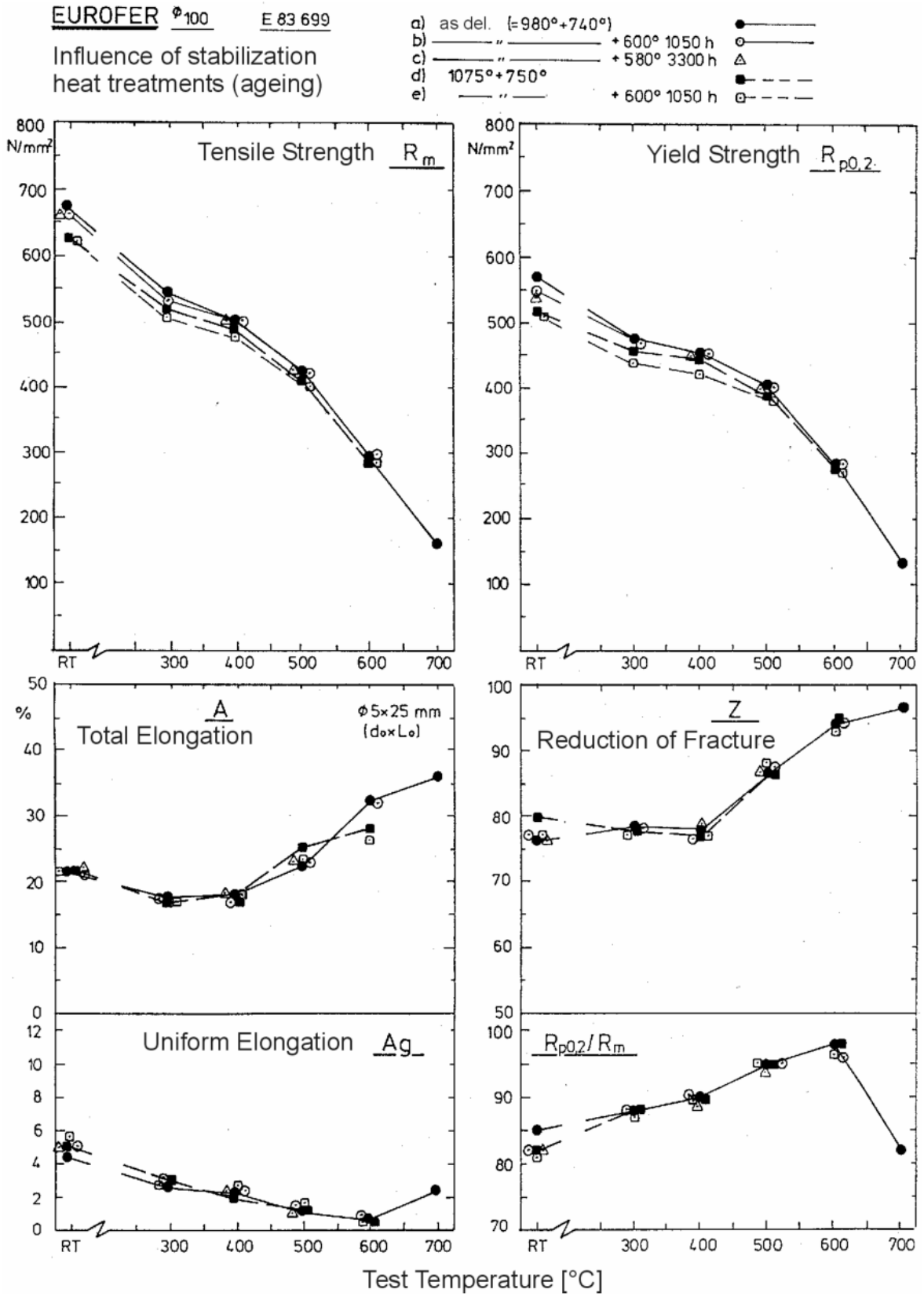

Figure 2.15: Influence of ageing on mechanical properties of EUROFER97. Taken from [142].

performed between 500 and 700 °C[143]. Values in this range are indicative of creep occurring via dislocation movement in the ferrite matrix[144]. These exponents are in contrast to the much greater values of 9-15[144, 145] and 50[146] found in similar ODS steels published in earlier studies. These anomalous values are explained by the much larger grain sizes in the earlier works, which is known to have a large effect on creep exponent in dispersion strengthened alloys[147]. The concept of a threshold stress, below which creep rate is negligible, can also explain the large variations in n values. This improved creep performance suggests that ODS-RAFM steels could have a higher operating temperature for fusion applications.

Other grades of ODS steels are also being considered, such as reduced activation ferritic steels[148]. These steels contain higher proportions of Cr (12-16 wt%), which yields a fully ferritic matrix and may allow operating temperatures to be pushed as high as 800 °C. However, they also suffer from embrittlement at intermediate temperatures, due to the precipitation of a brittle Cr-rich α' phase[149, 150]. It has been suggested that the two grades of steel be used in conjunction with each other inside a fusion reactor, with ODS ferritic steel utilised in areas exposed to higher temperatures and ferritic-martensitic steels used in the intermediate temperature regions[139].

2.5.1.2 Irradiation resistance

As in vanadium alloys, irradiation of RAFM steels results in significant property changes which will have serious impacts on their performance in a fusion environment.

The microstructure of highly irradiated EUROFER97 has been well-characterised. Irradiation causes dislocation loops, defect clusters, precipitates, and voids in RAFM steels[151, 152]. Dislocation loop analysis in TEM found a loop density of 4.9×10^{21} m^{-3} for $\boldsymbol{a}\langle100\rangle$ type dislocations and 6.3×10^{21} m^{-3} for $\boldsymbol{a}/2\langle111\rangle$ type after irradiation to 15 dpa at 300 °C. Void density was 6.3×10^{21} m^{-3} with an average diameter of 2.3 nm. Loop density increases with dose and dose rate, whereas average loop size increases with dose. Precipitates took the form of Ta and V enriched MX types, and Cr and W enriched $M_{23}C_6$ types. A breakdown of precipitate size and number is presented in Fig 2.16. Precipitate volume fraction grows with increased neutron dose[152].

Void formation was found to be heavily dependent on the neutron spectrum, with the thermal neutron flux of the High Flux Reactor (HFR) generating a void density a factor of 20 higher than what was generated by the fast neutron flux from the BOR-60 reactor, shown in Fig 2.17[151, 153]. This is thought to be due to the increased amounts of helium generated in the HFR compared to the BOR-60. As helium is known to stabilise and enhance void formation, this explains the increased number density of voids[154]. Large uncertainties in the measurements of void size mean that it is difficult to draw conclusions regarding the effects of neutron dose on void diameter.

These microstructural changes have large effects on the steel properties. Fig. 2.18

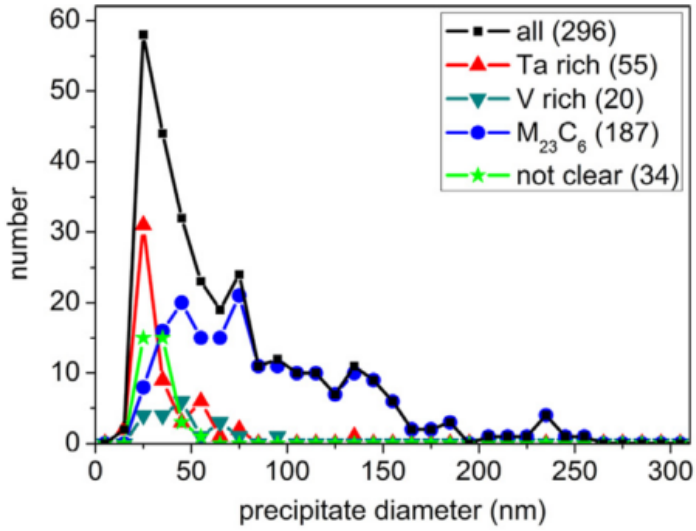

Figure 2.16: Precipitate distribution in a 23 µm^2 sample of EUROFER97 irradiated to 15 dpa. Taken from [152].

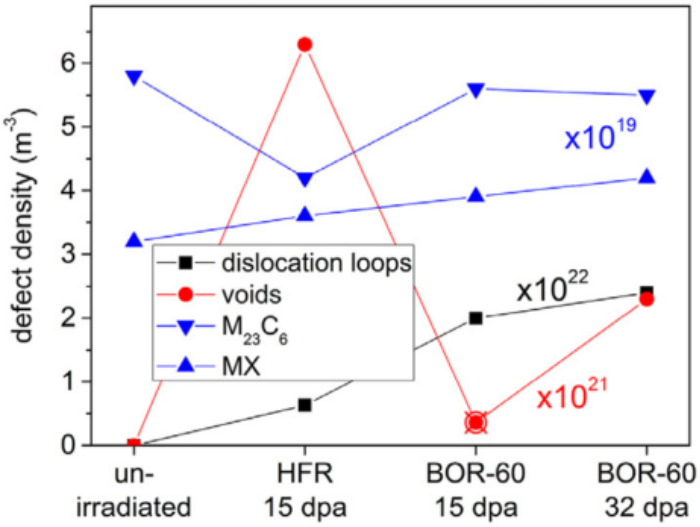

Figure 2.17: Density of various microstructural features of EUROFER97 irradiated under various conditions. Taken from [152]

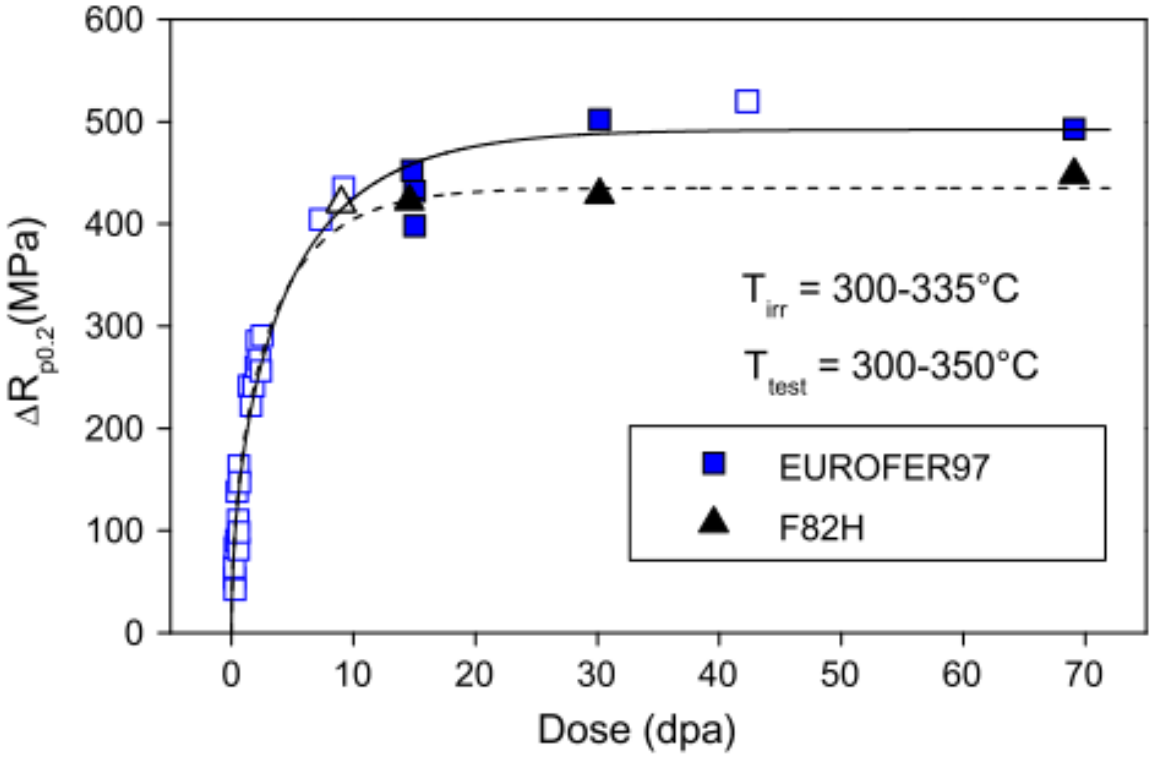

Figure 2.18: Irradiation hardening vs. irradiation dose for EUROFER97 and F82H. Taken from [155].

shows the dependence of RAFM steel hardness on neutron dose, saturating at approximately 30 dpa. This increase in hardness is believed to be caused by the dislocation loops generated from neutron irradiation[155]. Another cause of hardening and strengthening effects are α' precipitates in ferritic steels[156] and, to a lesser extent, He bubbles[157]. These loops and precipitates also embrittle the steels by impeding dislocation motion, raising the DBTT significantly from around -100 °C, saturating at 70 dpa, as seen in Fig 2.19.

Partial recovery of mechanical properties is possible with post-irradiation annealing at 550 °C for 3 hours. This treatment leads to the DBTT of heat-treated EUROFER dropping from 135 to -43 °C, for a ΔDBTT of 48 °C relative to the unirradiated state. F82H displays slightly poorer performance, with a less pronounced drop in DBTT after annealing. This recovery is caused by the dissolution of dislocation loops and α' precipitates that occurs in samples irradiated or annealed at high temperatures[157].

Recent results on the irradiation resistance of ODS-EUORFER97 are promising. The Y_2O_3 strengthening particles lead to an extremely fine grain structure, with grain sizes of several microns, resulting in improved strength for both irradiated and unirradiated samples. Moreover, the particles act as sinks for defects introduced by irradiation and He that is produced by transmutation. Unirradiated OSD-EUROFER97 had a yield strength 220 MPa higher than EUROFER97, but with sightly reduced strain to failure. When irradiated to 16.3 dpa, the ODS steel showed no increase in

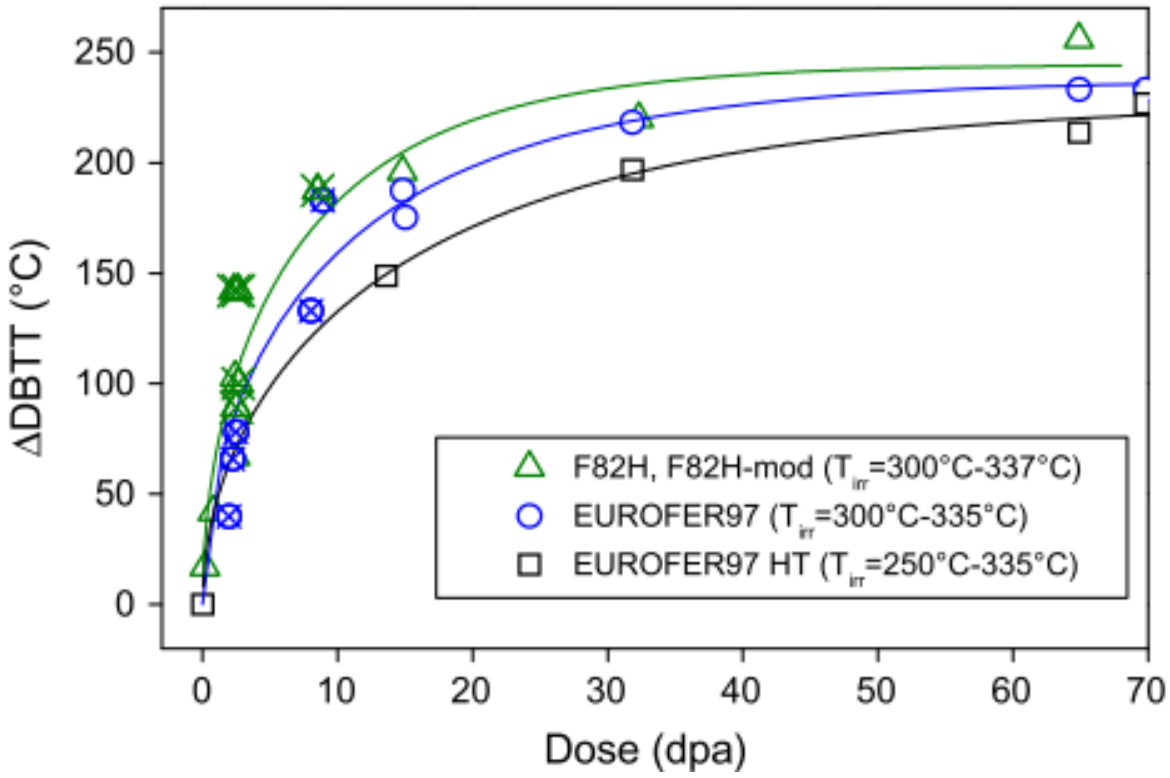

Figure 2.19: Dependence of DBTT on neutron dose for various EUROFER97, heat treated EUROFER97, and F82H. Taken from [155].

yield strength and no strain localisation. Macroscopic strain localisation (or plastic instability) is a behaviour found in irradiated RAFM steels which is manifested as a stress drop after yielding, caused by irradiation induced embrittlement[158, 159]. Further microstructural study confirmed that irradiated ODS-EUROFER97 had a number density of dislocation loops an order of magnitude less than EUROFER97 irradiated under the same conditions (16 dpa, 250 °C). Furthermore, areas of material with a higher number density of fine (<10nm) ODS nanoclusters had much lower concentrations of dislocation loops and voids compared to coarser areas of microstructure across all temperatures tested. However, it was not possible to determine the effects of irradiation on the Y_2O_3 particles beyond the fact they were in an amorphous state after irradiation[160]. Higher temperature irradiations (>450 °C) have no effect on tensile behaviour[161].

The DBTT shift of ODS-EUROFER97 increases with increasing neutron dose, with ΔDBTT values of 56 and 151 °C at 1 and 3 dpa respectively. Like with strength, this shift is only observed for irradiations at 300 °C, at higher temperatures the shifts are negligible[161]. ODS steels are the better performers for lower temperature irradiations, but at higher temperatures many of the microstructural features that cause hardness and embrittlement disappear due to thermal effects.

The void swelling levels of ODS steels are less than half of those found in conven-

tional ferritic steels, for both ion and neutron irradiation of several hundred dpa[162, 163]. This resistance to swelling is thought to arise from a combination of the fine grain structure, leading to increased grain boundary areas where defects can be trapped and annihilated, and the fine nanoprecipitates which also trap defects[162].

One significant caveat to the work presented in this section is that the response to these materials in a true fusion neutron environment (i.e. a highly energetic neutron spectra combined with H and He production from transmutation) remains untested. However, dual- and triple- ion beam (self ion irradiation combined with H and He) have shown ODS steels to be more resistant to irradiation damage than their non-ODS counterparts[139].

2.5.1.3 Coolant compatibility

The current European designs for a test blanket module (TBM) to be used in ITER will utilise either a Pb-16Li eutectic as a tritium breeder and neutron multiplier, or lithiated ceramic pebbles as a tritium breeder with beryllium pebbles as neutron multiplier. Both designs utilise EUROFER97 as the structural material and liquid He as the coolant[164]. There are also designs that utilise water cooling with RAFM as the structural material[165].

Recent results on the corrosion behaviour of EUROFER97 in a flowing Pb-17Li loop (flow rate of 0.22 m/s at 550 °C) found a corrosion rate of 400 µm/year. Additionally, the rapid corrosion rates led to line blockages after 3000 hours of operation at cooler portions of the loop, caused by precipitation of dissolved material[166]. These findings indicate the need for a coating layer to be used to protect the steel structure, or for the coolant to be run in at a lower temperature with reduced corrosion rates. ODS particles in the steel are found to have no visible impact on corrosion rate[167].

Water is also detrimental to RAFM steels, by way of promoting stress corrosion cracking. However, chloride content in the water was found to be dominating factor in the cracking behaviour, suggesting that these effects can be suppressed with appropriate water chemistry control[168].

Hydrogen uptake also poses a significant problem for RAFM steels, be it in the form of embrittling the steel itself, or trapped tritium that creates a radioactive inventory issue. Hydrogen and deuterium uptake of EUROFER97 compared favourably to other RAFM steels, but was still about an order of magnitude higher than austenitic stainless steels[169]. Embrittlement was found to occur in EUROFER97 in wppm quantities[170]. Again, barrier coatings have been suggested as a potential solution to this problem[171]. Helium uptake of upto 1000 appm does not have any significant effect on the creep properties of RAFM steels[172]. However, it does produce a non-hardening embrittlement effect, starting at He concentrations of around 400-600 appm[173].

2.5.1.4 Activation properties

Despite efforts to make fusion steels low-activation through careful selection of elements, a recent study by Gilbert et al.[29] has cast doubts on the prospect of leading fusion candidate steels (namely EUROFER and SS316) actually being classified as low-activation after use in DEMO, when certain minor alloying elements are taken into account. In EUROFER, one of the two main culprits responsible for the long-lived waste products is ^{14}C, produced from the hundreds of wppm of ^{14}N that is present in the alloy to form nitride precipitates for high temperature strength. The other is ^{94}Nb, produced in small quantities from the tens of wppm of ^{93}Nb present in EUROFER. Unlike N, which is an intentional microalloying addition, Nb is present only as an impurity from the raw metal that is difficult to remove.

The specific activity produced by ^{14}C in the most radioactive region of the DEMO blanket would be too high for it to be considered LLW in the UK (which uses a combination of beta and gamma emissions from all sources to determine limits) for thousands of years. However, in France, limits are defined on a per isotope basis and the levels and the activity of ^{14}C would be acceptable for disposal in Centre Stockage de l'Aube, a LLW facility that will handle the waste produced by ITER. ^{94}Nb is what would make EUROFER unacceptable for LLW disposal in France, as the activity of this isotope would remain well over the French disposal limit for thousands of years.

It is currently unclear how these issues, which are in clear opposition to nuclear fusion's assumed goal of exclusively producing short-lived level waste, can be resolved. The authors of the work suggest possible mitigation approaches:

1. Change the DEMO operation schedule so that materials are exposed to smaller neutron doses
2. Alter material composition to remove the parent elements of the problematic radionuclides
3. Create a DEMO-specific waste repository with different disposal requirements to account for the extremely small concentrations of long-lived radionuclides
4. Process waste material to remove the problematic nuclides

1 would not solve the problem inherent to the materials and cannot be regarded as a solution for a viable fusion reactor. 2 may be possible but it is unclear how these adjustments would effect the behaviour of the alloys in question. 3 would require enormous legislative effort, but may be the best potential solution, an idea echoed in another review[174]. 4 has not been shown to be technically or economically feasible.

2.5.1.5 Primary production & welding

A 2011 review claims that "the status of RAFM manufacturing technology indicates that there is enough experience for F82H and EUROFER to be manufactured for use

as the structural material for TBM". However, more sophisticated fabrication techniques such as vacuum arc remelting and careful selection of raw materials used to control impurities will be required for DEMO readiness[175]. Despite the advantages that ODS-RAFM steels possess, they are held back by manufacturing technology and methods. Another review has identified that a lack of industrial-scale fabrication and heat treatment methodologies are a current issue for the use of ODS-RAFM steels for fusion applications[139]. A more recent study has shown that casting large ingots of ODS ferritic martensitic steels with relatively homogeneous microstructures is possible[55].

Four EUROFER97 joining methods have been identified for use in the European TBM[164]:

- TIG fusion welding
- YAG laser + HIP - diffusion welding (DW)
- two step HIP
- drilling + spark erosion + bending

HIP has proven itself to be a viable RAFM steel joining method. A full scale mockup of a breeding blanket structure made from F82H was produced in 2008[176]. A study into the welding of EUROFER97 plates found that below a certain size (5 mm for EB or laser welds, 12 mm for TIG welds), welds require no or only one PWHT. An EB weld below the maximum size has a DBTT very close to the base material. Laser welds have a slightly raised DBTT, which can be restored to near-base levels with a 700 °C heat treatment. TIG welds are much more brittle and require at least one PWHT. Creep strength is decreased in all welds and requires a two-step PWHT to restore it. However, creep strength may be sufficient if operation temperature is near the limits of the material (550 °C for EUROFER97)[177].

Welding of ODS-RAFM steels is possible, but results in a reduction in mechanical performance. EB welds of similar ODS-EUROFER97 joints had a higher DBTT and worse tensile properties, with little improvement after a PWHT, caused by agglomeration of the the strengthening nanoparticles[178]. However, creep strength and DBTT in dissimilar ODS-EUROFER97 to EUROFER97 joins can be improved with a suitable PWHT. This improvement is brought about by grain structure modification and carbide re-precipitation in the fusion zone[179]. Diffusion bonding and solid-state welding may allow for ODS steels to be joined without coarsening the oxide dispersion[180, 181, 182].

2.5.2 Future work

2.5.2.1 Existing alloy development

In terms of near-future applications, EUROFER97 is sufficiently understood for it to be used as the structural material for some ITER TBM designs[164, 165]. Mockup blanket components have been manufactured, clearly demonstrating the capability of producing future blanket structures. However, for more advanced long-term applications, such as the DEMO reactor, more work is required. Although current joining technology is sufficient for ITER, DEMO components will require larger and stronger joints, possibly to dissimilar materials. Fission neutron irradiation data are still being accumulated, but testing with a fusion-relevant neutron spectra is highly desirable to determine the effects of transmutation products such as H and He.

ODS-RAFM steels offer confer many advantages over standard RAFM steels, especially in irradiation resistance. However, difficulties in fabrication and joining on a large scale mean that it is currently unsuitable for use in fusion blanket components. However, promising results with dissimilar joining to RAFM steels give rise to the possibility of using ODS steels in areas of the blanket nearer the first wall or even being used *as* the first wall (in the case of high Cr ODS-ferritic steels [141, 183]), where temperatures and radiation doses are higher. Again, prediction of the effects of fusion irradiation conditions is challenging and data from real fusion neutrons would be ideal.

2.5.2.2 New alloy development

It is clear that existing RAFM steels such as EUROFER97 and F82H have been well-characterised and researched. However, FM steels developed for fossil fuel applications (i.e. without the reduced activation requirement) have shown long term creep performance well in excess of what current RAFM steels can achieve[142, 184]. If the high activation elements present in the fossil fuel steels (namely Co, Nb and Ni) can be replaced with reduced-activation equivalents, then there is a large potential for increased creep performance in RAFM steels. However, developing and characterising new steels, especially those with several alloying components, is a time consuming process.

Fortunately, advances in computational thermodynamic calculations and improvements in phase equilibrium databases mean that rapid and accurate predictions of equilibrium phases are now possible. Such calculations have been used to create high-strength FM and RAFM steels with improved properties, comparable to ODS steels[185, 186, 187]. By optimising composition and thermomechanical treatment, it is possible to promote microstructural features, such as disperse nanoscale precipitates, that strengthen the steels and improve resistance to radiation damage. Nevertheless, since these computationally designed alloys are relatively new, there are many gaps in the knowledge compared to more mature RAFM steels. Many of the issues that have

been examined in EUROFER97 and F82H, such as creep behaviour, coolant compatibility, joining, and in particular, radiation resistance, are almost completely unexplored for the new alloys and will need to be investigated thoroughly.

2.6 Tungsten

As the element with the highest melting point, tungsten would seem like an obvious choice for the areas of the reactor subject to the most severe thermal loads: the divertor and first wall regions. Possessing decent thermal conductivity and low sputter yield (to prevent poisoning the plasma with high Z atoms), tungsten has been described as an "almost perfect plasma-facing material (PFM)"[19]. It has also demonstrated that it meets the requirements of ITER and will be used as the divertor material[188].

However, despite the advantages that tungsten offers, it still falls short when considered for use in a DEMO-type reactor. A review of the materials requirements of the plasma-facing components in DEMO identified the following key issues that need to be addressed[21]:

Operating temperature window Transient events such as unmitigated ELMs can cause large fluctuations in temperature. Such a disruption could lead to a temperature rise of 1500 K in the top 1 mm of material[189], leading to thermal cracking or even localised melting if the operating temperature is not low enough.

Thermal properties Although pure tungsten has good thermal conductivity in its initial state, exposure to fusion neutrons will rapidly deteriorate this property. Even a small amount of irradiation damage (0.1 dpa) can lead to a significant drop in thermal conductivity, caused by defects generated in the lattice and also transmutation of W into Re and Os.

Embrittlement The DBTT of unirradiated tungsten is around 50 °C, which is unlikely to be a problem for plasma-facing tungsten components in normal operation. However, the DBTT of unirradiated tungsten increases significantly with neutron fluence as shown in Fig. 2.20. This embrittlement will be compounded by the grain growth of tungsten that occurs at temperatures over 1200 °C.

Activation and transmutation The long-term activation properties of a fusion material are important from an environmental and safety perspective as outlined in section 2.1.3. Tungsten has acceptable activation properties, and will be less active than iron after a year of cooling following DEMO-like operation[131]. However, the grade of tungsten that will be used in ITER has been shown to contain sufficient impurity

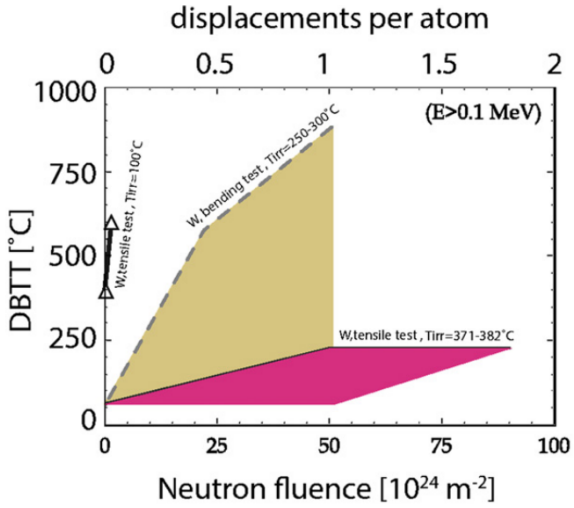

Figure 2.20: DBTT dependence on neutron fluence for pure tungsten. Taken from [21].

content to significantly extend its lifespan as ILW according to UK regulations[29]. The risks of latent radiological dose in an accident scenario are higher in tungsten than many other common fusion elements, owing to its relatively high short-term specific activity. However, as there is no way to reduce radioactivity while retaining the properties that make tungsten one of the most (if not only) attractive options for PFMs, it must be instead managed to ensure that risks are minimised.

Tritium retention and permeation The uptake of radioactive tritium into the PFMs of a fusion reactor is a critical safety issue. Due to the proximity of the PFMs to the plasma core, exposure to tritium is an inevitability. In order to ensure a safe and economical operation of a reactor, the retention and permeation of tritium into the PFMs must be kept to a minimum (see section 2.4.1.6).

Oxidation Although not mentioned in the review, the oxidation performance of tungsten and its alloys has also been the subject of investigation. In the event of a LOCA occurring in conjunction with a vacuum leak, the sublimation of the oxide formed, WO_3, could result in an evaporation rate of up to $300\,\mathrm{kg\,hr^{-1}}$ at 1450 K, the highest predicted temperature for this scenario[190]. This would lead to large amounts of radioactive material being released into the atmosphere.

2.6.1 New developments

With the exception of transmutation properties, which are inherent to tungsten in any form, these issues can be mitigated with the development of new materials and processing methods.

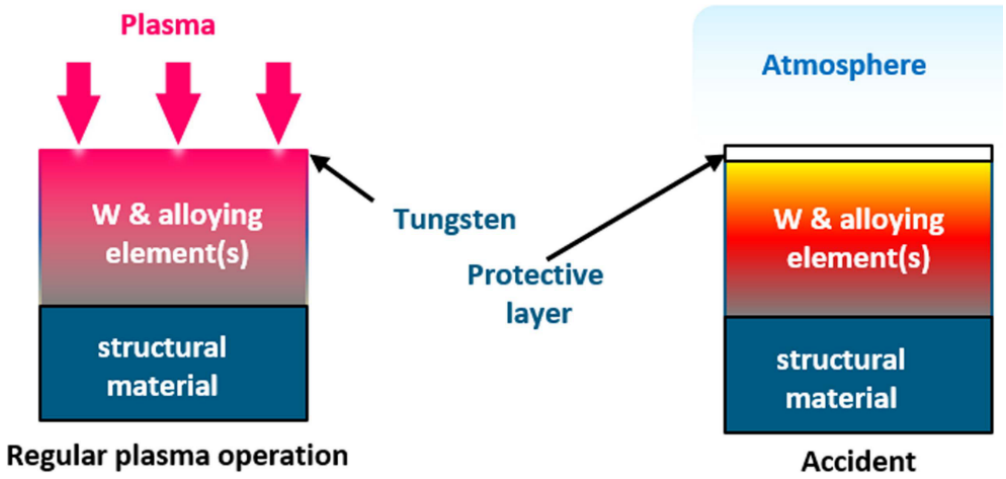

Figure 2.21: Schematic showing the response of smart tungsten to regular operation and to an accident scenario. Taken from [196].

Ultrafine-grained tungsten Ultrafine-grained or nanostructured tungsten alloys can be prepared through a variety of methods such as powder metallurgical processes like sintering[191] or mechanical processes like surface mechanical attrition treatment[192]. Both methods lead to microstructures with average grain size of the order of 100 nm. Not only does this lend the alloys extra strength from the Hall-Petch effect, but also lowers the DBTT[193].

Tungsten composites Another method for improving toughness is to use composite materials. Tungsten fibre/tungsten composites have been successfully produced, leading to greatly increased toughness and resistance to local overloads or fabrication flaws compared to a monolithic sample[194]. Tungsten laminates, using thin layers of tungsten sandwiched between layers of a different metal, have also been proposed as a method for increasing ductility while retaining tungsten's useful physical properties[195].

Smart tungsten alloys So-called "smart" tungsten alloys (so named for their apparent ability to react to changes in local environment) may offer a solution to the serious safety concerns raised about the high oxidation and subsequent sublimation rates of tungsten during a LOCA and vacuum leak. During normal operation, the plasma will preferentially sputter the lighter alloying elements such as Cr and Ti. This will leave a W-enriched surface layer (approx. 10 nm thick) that is more resistant to sputtering and less harmful to plasma performance. In the event of an accident, this thin layer will volatilise, releasing a relatively small amount of material. The bulk alloy will then produce a passivating layer of Cr_2O_3, which greatly slows oxidation rates compared to pure tungsten[36]. A schematic of this behaviour is shown in Fig. 2.21.

Functionally graded materials Due to the aforementioned embrittlement issues associated with irradiated tungsten, using it outside of the high temperature regions of a reactor is unlikely to be feasible. Instead, bonding tungsten to another structural material such as steel or vanadium alloys with a functionally graded material is a more promising route[21]. By introducing interlayers of material that have a more gradual change in coefficient of thermal expansion between the two parent metals, thermal mismatch stresses and strains can be minimised, thereby reducing the chance of failure during thermal cycling[197].

2.7 Beryllium

The first wall of ITER will be lined with tiles made of beryllium[20]. As fusion plasmas have a low tolerance to the presence of heavy element impurities, the low Z number of beryllium is the primary reason for this selection. Conversely, its low atomic mass also means that it has a high sputtering yield compared to heavier elements, leading to accelerated erosion. Given the toxic nature of beryllium, redeposition of sputtered material is a serious safety issue. Co-deposition of hydrogen isotopes is also an issue for the tritium inventory of a reactor. Co-deposition rates can be nearly as high as carbon fibre composites[198], another candidate material that has been discounted an account of its tritium uptake behaviour. However, in the case of beryllium, baking at 350 °C will cause degassing of the tritium, which will allow for mitigation of the inventory issue.

Despite its advantages, beryllium is unlikely to be used in any plasma facing component in a reactor after ITER, such as DEMO, with tungsten being the favoured material[199]. However, beryllium may still see usage in fusion reactors as a functional material used for neutron multiplication to aid with tritium breeding[200].

Beryllium can also suffer from activation issues, as identified by Gilbert et al[29]. If a Be pebble bed blanket design is used in DEMO, then uranium impurities in the beryllium can produce highly radioactive actinides, in particular ^{239}Pu. However, these impurities are strongly dependent on the geological source of the beryllium and specific activity can be brought down to acceptable levels for UK LLW disposal by using beryllium from a particular region.

2.8 Silicon carbide

Of all the structural materials considered for fusion applications, only one ceramic has emerged as a candidate so far: silicon carbide (in the form of a SiC fibre/SiC matrix composite). Although a relatively immature option, silicon carbide possesses good activation properties, high temperature strength and resistance to radiation damage[201,

202]. It is viewed as a long-term option for use in DEMO-like reactors or beyond.

A review by Koyanagi et al. claims that SiC/SiC composites are now engineering materials (rather than being simply confined to the laboratory), and that future research on their use in fusion reactors should be focussed on engineering issues such as material codes and lifetime assessments[202]. In particular, it has been suggested as a flow channel insert (components that act as thermal and electrical insulation between flowing liquid metal and structural steel) material in the EU blanket design[203], with PbLi corrosion remaining a critical issue.

2.9 High entropy alloys

As mentioned in the previous chapter, the field of HEAs is still in its infancy. Having undergone less than two decades of development, it is still unclear what niche HEAs can fill. However, meeting the demanding materials requirements of a fusion reactor will necessitate the consideration and exploration of a wide range of materials, and HEAs are no exception. By their very nature, the properties and components of HEAs are nearly infinitely variable, so the following sections will aim only to give a brief overview of some of the underlying theory of HEAs and some examples of properties that may hold some promise for future fusion applications.

2.9.1 HEA theory

High entropy alloys (HEAs) are defined by their composition, consisting of several principle alloying elements often at equiatomic or near-equiatomic ratios. The rationale behind these mixtures of elements is that the high entropy of mixing will stabilise the formation of solid solution phases, instead of stoichiometric intermetallic phases.

Jien-Wei Yeh, the researcher who first brought attention to HEAs[204], has suggested four core principles which underpin the properties of HEAs[205]:

- High configurational entropy of mixing
- Lattice distortion caused by atomic radii mismatch between elements
- Sluggish diffusion kinetics
- The “cocktail effect”, a blanket term for interactions between elements producing unusual behaviours

All four of these claims have either had serious doubt cast upon their validity by experimental studies, or describe effects that are found in many other conventional alloys and as such cannot be taken as a “core principle” of HEAs[206, 207]. Despite

the nebulousness of these claims, briefly covering them will help to elucidate what *are* the unique properties of HEAs and why they arise.

2.9.1.1 High configurational entropy

By maximising the entropy term of the Gibbs free energy equation of mixing various alloying elements in to a disordered solid solution (shown in equation 2.2), it appears that it should be possible to minimise free energy of this phase and render it more stable. As the entropic term is proportional to temperature, it suggests that this stabilising effect will be even more effective at higher temperatures.

$$\Delta G_{\text{mix}} = \Delta H_{\text{mix}} - T\Delta S_{\text{mix}} \tag{2.2}$$

However, the disordered phase will be in competition with ordered intermetallic phases, which will have equivalent equations for the free energy of their formation. As more elements are added, the likelihood of a thermodynamically stable intermetallic phase arising will increase as more phases are able to coexist.

The entropy of a completely randomly mixed solid solution is given in equation 2.3. This equation suggests that entropy can be increased by maximising the number of components, N, and maintaining an equiatomic composition. However, this equation merely provides an upper bound to the entropy term, as it does not consider short range order effects or contributions arising from electronic, phononic and magnetic sources, which are not directly related to atomic configuration.

$$\Delta S_{\text{mix}} = -k_B \Sigma_i^N x_i \ln x_i \tag{2.3}$$

The so-called "entropy hypothesis" posits that HEAs with a large number of constituent elements in equiatomic compositions will result in a single stable disordered phase due to these entropic stabilisation effects. However, this is not often seen in practice and many different quinary alloy systems decompose into multiple phases when heat treated. One of the earliest and most-studied HEAs, CrMnFeCoNi (or Cantor alloy after it's discoverer) was long believed to form a single FCC phase, as initially reported[208]. Despite its position as HEA par excellence, Cantor alloy was later found to also compose of multiple phases after extended annealing[209, 210]. A systematic investigation of five Cantor-like alloys, with one of the elements being replaced with a similar one for each alloy, found that none of these produced a stable single-phase microstructure (with the unmodified Cantor alloy still being presumed stable).

Three reviews of the field all conclude that the entropy hypothesis is, at best, of limited usefulness[207, 206, 211]. Entropy of solid solution should not be considered the thermodynamically dominant factor over the entropy of other phases, or over the enthalpies of both the disordered solution and intermetallics.

Recent computational results also cast serious doubts on the validity of the entropy hypothesis. A paper by Schön et al. suggests that configurational frustration caused by conflicting interactions and correlations in the solid solution is the main driver for the stabilisation of a disordered phase in both an idealised equinteracting system, and in a model HEA (VNbTaMoW)[212]. The same work also showed that configurational entropy only exerted a minor influence on disordered phase stability.

As mentioned earlier, other entropic terms aside from the configurational entropy also contribute to free energy. Ab initio studies found that magnetic and electronic entropy terms can contribute up to 50% of the configurational entropy in Cantor alloy[213]. Vibrational entropy was also considered, but as all phases investigated had S_{vib} values of similar magnitudes, these contributions will partially cancel each other, meaning only the spread in values is relevant.

2.9.1.2 Lattice distortion

Another core effect originally posited by Yeh is the severe lattice distortion experienced by atoms in HEAs[214]. The combination of many different atoms of varying atomic radii, all in high concentrations, was thought to introduce significant strains into the lattice as atoms are highly displaced from their ideal lattice positions.

Both experimental[215] and computational[216] results show that a strain effect clearly exists, although this effect is no more pronounced than in other less concentrated and less compositionally complex alloys[207].

However, this is not to say that the effects of the strain are unimportant. The internal strain in these alloys produces solid solution strengthening effects, and a strength scaling factor based on the mean squared atomic displacement has been introduced by Okamoto et al.[217].

2.9.1.3 Sluggish diffusion

Another one of the core effects that may be said to arise from the distorted lattice is the apparent phenomena of relatively sluggish diffusion observed in HEAs[214]. The rationale behind this is that the large amount of variation in atomic sizes and displacement from lattice sites will result in an uneven energy landscape with local minima acting as traps for diffusing atoms, shown schematically in Fig. 2.22.

Two review papers have concluded that the apparent sluggish diffusion in HEAs arises from misinterpretation of results (such as recrystallisation resistance being evidence of slow diffusion, ignoring other factors like dislocations, grain size and other inomogenities[207]) or is simply not found in practice (with HEA diffusion being comparable to other conventional alloys[206]). A comprehensive review focused on the topic also found no experimental evidence to suggest that sluggish diffusion exists in

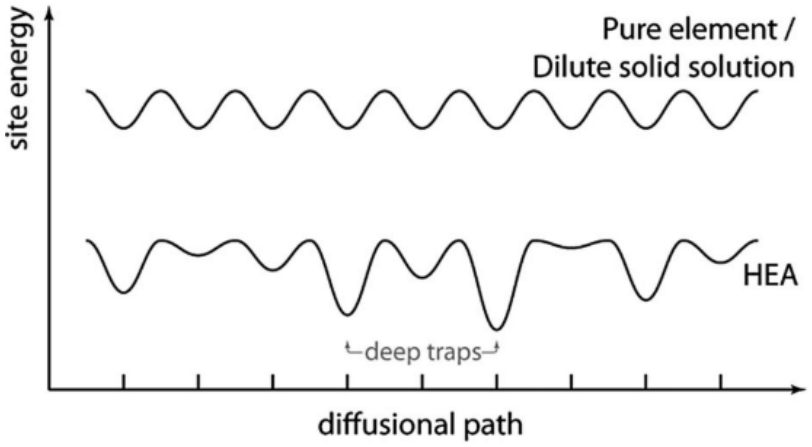

Figure 2.22: Schematic representation of differences in energy profile for diffusion in a pure element compared with an HEA. Taken from [207].

known HEAs, although did concede that the evidence was mostly based on FCC metals and that the relatively unexplored class of BCC HEAs could yield new results[218].

Despite the lack of evidence for sluggish diffusion, there is a compelling case that diffusion in HEAs may be more complex than in less compositionally varied alloys. Recent computational results using DICTRA codes have shown considerable complexity (such as non-linear diffusion paths) in the diffusion behaviour of multicomponent alloys[219]. An *ab initio* study of the entropy hypothesis also yielded some intriguing diffusion results, suggesting that diffusion behaviour in the VNbTaMoW system is highly complex (e.g. the diffusion direction of some species is inverted below a certain temperature)[212]. The authors suggest that the quasi-binary approached adopted by Tsai et al.[220] should be criticised. However, this approach has been utilised in a more recent study[221] that has elucidated some of the diffusion behaviour in "medium entropy" CrFeCoNi alloys.

2.9.1.4 Cocktail effect

This is the most nebulous of the four proposed core effects, even the origins of the term "cocktail effect" are hard to define: two different explanations[222, 223] are offered. Etymology aside, no consistent definition of the term has been agreed upon. It has been suggested that the term is merely an artistic flourish used to refer to the varied and often unpredictable nature of HEAs[206], or that it should be dismissed entirely[207]. In any case, the term is not particularly useful for a critical review of the field, and can be substituted for more specific examples of potentially useful HEA effects and properties.

2.9.1.5 Summary

Although it can be seen that the originally proposed core effects for HEAs are somewhat unclear and dissatisfying, closer examination of each of the effects reveals underlying complexity that does make a difference to material behaviour. Some of the more specific effects and features will be outlined in the following sections.

2.9.2 Mechanical properties & microstructure

It is difficult to discuss the mechanical properties (or indeed, any other type of property) of HEAs in general terms due to the varied nature of materials that are defined by the term HEA. However, certain HEAs have shown promising mechanical properties at fusion relevant conditions. The underlying microstructure that gives rise to these properties can be used a basis for the development of fusion HEAs.

Several HEAs have exhibited promising mechanical behaviour at high temperatures. $Al_xCoCrFeNi$ ($0 < x < 1.8$) displays a wide array of microstructures depending on the x value of the composition and temperature[224]. All compositions of this alloy show better higher-temperature softening resistance than similar commercial multicomponent alloys (T-800, In718, and In718H). The $Al_{0.9}$ and $Al_{1.0}$ alloys even exhibited rehardening behaviour between 700 and 800 °C, although they softened the most rapidly above this temperature (see Fig.2.23(a)-(d)). These compositions and temperature ranges correspond to the formation of the Fe-Cr σ phase, which is though to provide the rehardening effect. These results show that it is possible to finely tune the mechanical behaviour of HEAs by forming specific precipitates with relatively small variations in composition. Additionally, the authors suggest that sluggish diffusion at higher temperatures is another factor lending it resistance to softening, as the dominant deformation mechanisms are diffusional in nature at these temperatures. $AlCoCr_xFeMo_{0.5}Ni$ exhibits superior hot-softening properties to $Al_xCoCrFeNi$ (see Fig. 2.23) and is also σ phase strengthened. This class of HEAs has also displayed impressive mechanical properties when tested in tension[225, 226].

However, the microstructures are sensitive to process routes. Selected electron beam melting (SEBM) is an additive manufacturing technique which offers rapid solidification cooling rates, of the order 10^4 K s^{-1}[228]. Using this technique on a AlCoCrFeNi alloy produced an FCC phase not observed during conventional vacuum arc melting[229]. The resulting microstructure also had vastly improved plasticity, with a failure strain four times larger than the cast specimen[230]. The effect of SEBM on the high temperature softening behaviour and the formation of σ phases has not been investigated. Furthermore, homogenised $Al_{0.5}CoCrFeNi$ has improved flow stress behaviour as well as better hot-workability[231]. It is evident that appropriate thermomechanical processing is required to obtain optimum properties from this class of HEAs.

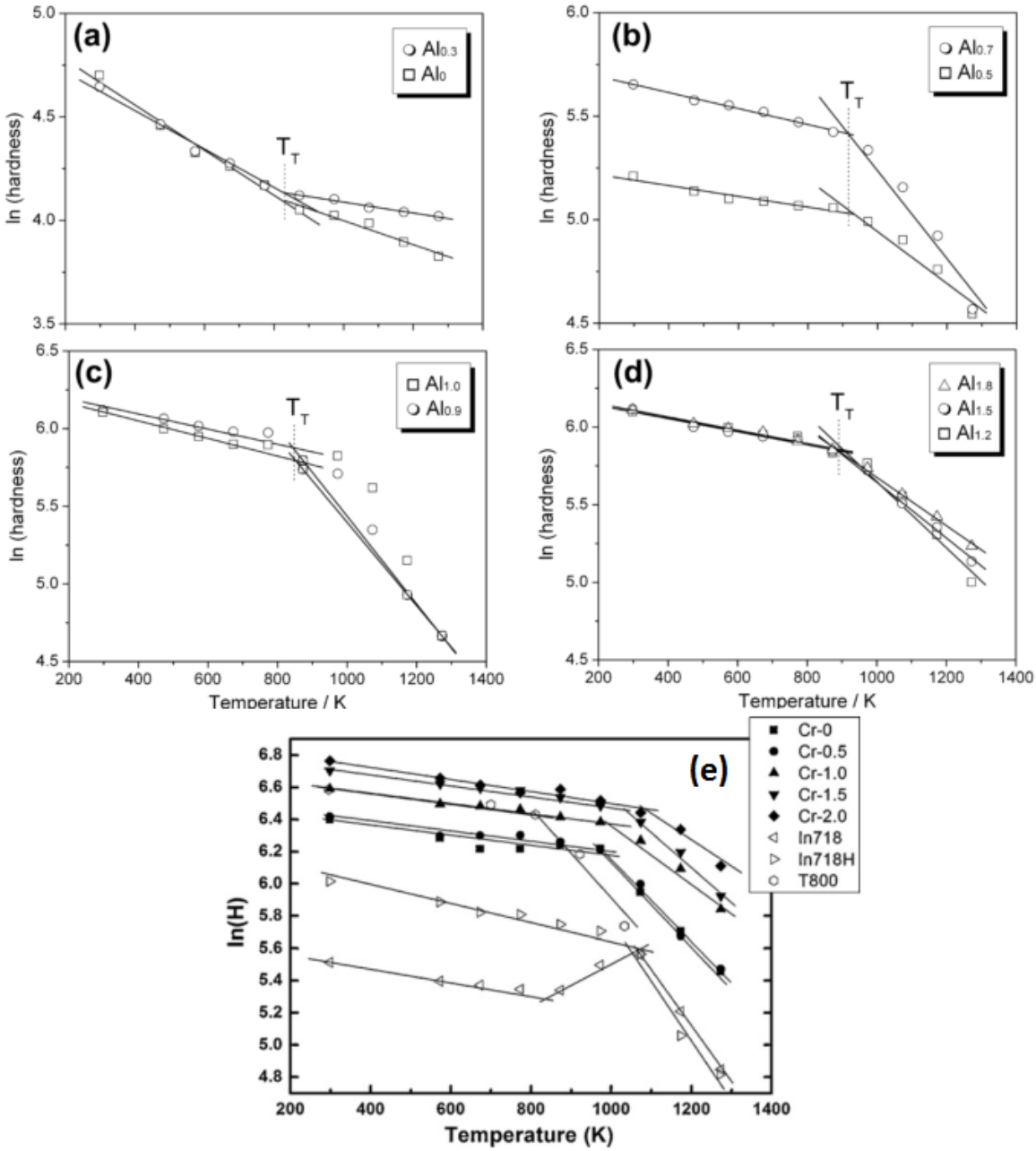

Figure 2.23: Log of hot hardness against temperature for: (a)-(d) $Al_xCoCrFeNi$ alloys[224] (e)$AlCoCr_xFeMo_{0.5}Ni$ alloys[227].

$Al_{0.5}$CoCrCuFeNi exhibits resistance to dynamic recovery after cold working and recrystallisation after cold working, both at 900 °C[232]. The authors propose two factors responsible for this behaviour: the formation of nanotwins, and the corresponding low twin boundary energy which leads to a low driving force for recrystallisation; and the sluggish diffusion of atoms and vacancies. Nanotwinning is seen under TEM and is consistent with the observed behaviour. However, no evidence is offered in favour of the explanation of sluggish diffusion. However, the same alloy, when annealed for several days at high temperatures was found to have a slightly different phase composition than the as-cast microstructure, indicating that the kinetics of reaching equilibrium were indeed slow[233].

Arguably the most impressive mechanical property exhibited by an HEA is the outstanding ductility observed in CoCrFeMnNi at cryogenic temperatures (see Fig. 2.24)[234]. This impressive behaviour is attributed to its low stacking fault energy at low temperatures, which results in significant twinning to accommodate the plastic deformation[235]. A recent study has clarified the exact nature of the difference between the cryogenic and room temperature deformation behaviour[236]. Slip and twinning are parallel processes in the cryogenic regime. There is some uncertainty as to whether both of these processes are active at room temperature, with some studies suggesting that only dislocation glide is the only active mechanism[237, 238].

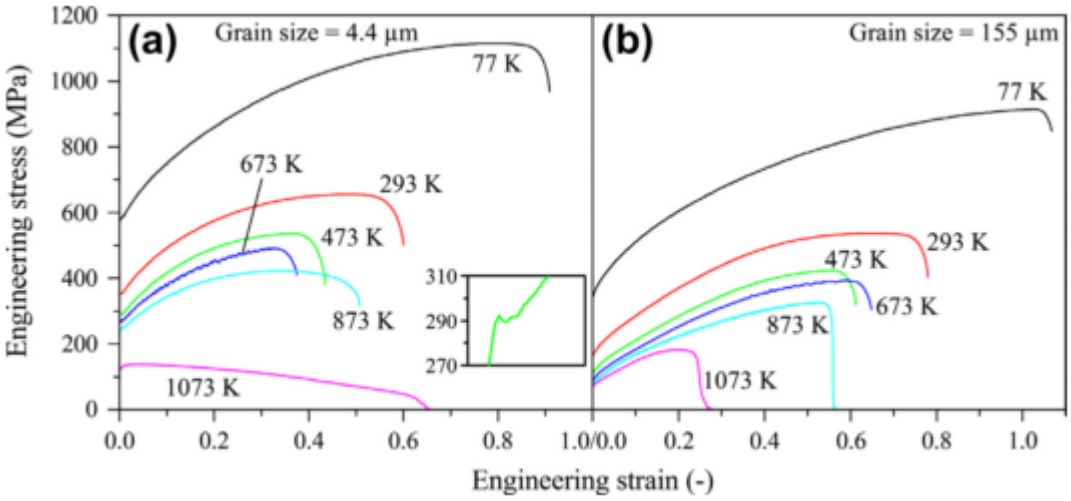

Figure 2.24: Ductility of CoCrFeMnNi at various temperatures for two different grain sizes. Taken from [235]

HEAs have also shown unexpected responses to interstitial doping. In TiZrHfNb doped with 2 at.% oxygen, strength is significantly improved and ductility is almost doubled[239]. This behaviour is caused by the creation of short range, (O,Zr,Ti)-rich, ordered oxygen complexes within the alloy matrix. These complexes alter the dislocation behaviour of the alloy during plastic deformation, by pinning dislocations and promoting cross-slip which leads to dislocation multiplication. This multiplicative

effect produces a greater work hardening rate and consequently, higher ductility.

2.9.3 Irradiation resistance

As research on HEAs has only garnered significant attention in the last decade or so, many aspects of their properties are still unclear. Their behaviour under radiation is no exception and is arguably one of the least characterised features of these alloys. This section will follow the same approach as a review by Pickering et al.[240] in detailing the various claims made about the irradiation resistance in HEAs.

2.9.3.1 Displacement cascade effects

After a displacement cascade has occurred in a crystal, the energy from the incident particle will be dissipated around the cascade site. If the material has good thermal conductivity, the energy will be dissipated over a larger area. Conversely, a lower thermal conductivity means that the energy will remain more localised for a longer period of time, in theory allowing more time for the recombination of FP defects. As HEAs tend to have lower thermal conductivities than single elements[241], it has been posited that this effect leads to a reduced defect concentration after displacement cascades. This hypothesis has been backed up by MD studies comparing irradiated Ni-containing equiatomic alloys to pure Ni, which found fewer irradiation-induced FP defects in the alloys compared with the pure element[241, 242, 243]. Other results showed that this effect is highly dependent on the particular element that is added, with dislocation mobility believed to be the controlling factor[244].

Other studies have offered alternative explanations for the reduced damage. One is that the range of atomic sizes present in HEAs results in higher inter-atom stresses, which in turn leads to easier amorphisation of the cascade region. The amorphised region can immediately recrystallise, leading to the suggestion that HEAs are self-healing[245, 246]. It is unclear how true such claims given the discussion of the lattice strain effects of HEAs in Section 2.9.1.2.

2.9.3.2 Defect mobility

There has been much debate about the general nature of diffusion in HEAs and whether it is abnormally sluggish as early studies claimed (see Section 2.9.1.3). As radiation damage is strongly governed by diffusional processes, it is natural that such discussion will appear here too. As the mobile species for radiation damage (interstitials and vacancies) are different than in conventional thermal diffusion, it would be reasonable to question if the behaviour is the same (i.e. there is no abnormally sluggish diffusion).

Results in this area are limited but suggest that defects in HEAs are no less mobile than in conventional alloys. Chen et al.[247] concluded that sluggish diffusion likely

played little role in the microstructural evolution of FCC HEAs irradiated at 300 °C. However, the authors did acknowledge that this picture may be different at higher temperatures where long-range diffusion of point defects is more prevalent. Again, the full picture appears to be complex and element dependent, as another study concluded that a pair of FCC alloys ($Cr_{18}Fe_{27}Mn_{27}Ni_{28}$ and $Cr_{15}Fe_{35}Mn_{15}Ni_{35}$) had significant differences in vacancy mobility due to differing levels of Mn in the alloys[248].

2.9.3.3 Defect formation

This complex picture is found yet again when considering the energy required to form defects. Differences between the clustering behaviour of pure elements and equiatomic alloys in some of the previous studies referenced has been attributed to changes in the energy required to form extended defects[242, 243]. In the case of interstitials, these changes have been found to be a result of the differing chemical environment in the alloys[249, 250]. Vacancy formation energies tend to be higher in equiatomic alloys compared to pure Ni in DFT studies[250, 247]. However, an experimental study found little difference in vacancy formation energy between CrFeCoNiMn and pure Ni[251].

2.9.3.4 Phase stability

As discussed in Pickering et al.[240], some HEAs have shown good phase stability under irradiation, whereas some have exhibited significant microstructural evolution. This should come as no surprise given the highly varied microstructures that are present in HEAs after thermal ageing without irradiation. Indeed, it is unclear whether the microstructural changes reported in many irradiations would have occurred simply from thermal effects without any irradiation.

However, some studies have compared the microstructural evolution of irradiated samples with equivalently aged unirradiated ones. Irradiating $Al_{0.3}$CoCrFeNi was found to suppress precipitation at low temperatures and enhanced it at higher temperatures[252]. $Al_{0.12}$NiCoFeCr remained as a single FCC phase after long-term ageing at 500 °C, but when irradiated at a similar temperature, an $L1_2$ phase was found to precipitate[253].

2.9.3.5 Mechanical properties

Certain BCC HEAs have shown curious mechanical properties after irradiation, particularly no or limited hardening[254, 255, 256]. For example, TiZrNbHfTa was found to undergo a small increase in nanohardness and strength after He-irradiation without the corresponding loss of ductility found in other BCC alloys[257]. Another alloy, $V_{2.5}Cr_{1.2}WMoCo_{0.04}$, has even exhibited irradiation softening[258].

2.9.4 Oxidation & corrosion

Elements that are capable of forming protective oxides such as Al and Cr are commonplace amongst HEAs that have been developed and studied. $Al_xCo_{1.5}CrFeNi_{1.5}Ti_y$ alloys have been shown to form protective Cr_2O_3 layers, with the Al present promoting the formation of his layer[259]. Soare et al.[260] found that remelted AlCoCrFeNiTi had improved corrosion performance compared to the as-cast alloy, caused by improved distribution of elements and phases within the alloy. Such behaviour indicates the important role of processing in corrosion.

A comprehensive review by Qui et al.[261] details the effects of several common HEA elements on corrosion properties. Addition of Cr in high quantities is not necessarily enough to provide corrosion resistance, as is the case in stainless steels. The impact of other elements on the corrosion and oxide-forming behaviour should be investigated as Cr does not guarantee corrosion resistance. This is the case for AlCoCrFeNi, where the dendritic Al-rich regions and interdendritic Cr-rich regions became anodic and cathodic, respectively. This resulted in dissolution of the Al-rich regions[262]. Qui et al.[261] also suggest that HEAs show promise for applications in industry due to their corrosion properties, but also assert the need for industry-specific corrosion studies.

To this end, a search for literature involving the oxidation properties of nuclear fusion-relevant HEAs was conducted. Only one study was found, which investigated the high temperature oxidation properties of a Ti_xWTaVCr alloy, for the purpose of investigating its suitability for use in a fusion divertor[263]. The oxidation results presented were relatively simple as oxidation was not the main focus of the paper, but nevertheless drew the interesting conclusion that the addition of Ti improved oxidation resistance in that compositional range.

2.9.5 HEAs for fusion

As mentioned above, if the field of HEAs is to be considered a young branch of materials science, the subfield of HEAs for fusion is very much in its infancy. Most of the extant work in this area has been focused on using low-activation elements to create materials for applications in the divertor or blanket region of a fusion reactor. The utilisation of low-activation elements has been suggested as a niche that HEAs may be able to exploit, especially when combined with their promising irradiation resistance and high temperature properties[240].

Table 2.2 shows the range of alloy systems studied for fusion applications. All alloys shown are BCC and most of the elements used are low-activation (after 100 years, see Fig. 2.8), with the exception of Mo, Zr, and Hf. However, the authors studying the Zr and Hf containing alloys mention remote handling of radioactive waste as a motivating factor in their element selection as opposed to legislative limits[255]. All of

the alloys listed have shown promising behaviour in either their mechanical properties or irradiation resistance.

Even within these alloy systems, compositions that deviate from equiatomic compositions may improve properties further still. Furthermore, there are many more potential alloy systems waiting to be characterised. This may involve the use of different elements from the ten listed in Table 2.2, or going beyond five elements in a single system. Irrespective of the approach taken, there is much exploration to be done!

2.10 Summary

This chapter began by giving a short overview of the conditions that are found inside a fusion reactor, why they are problematic for materials, and some of the materials that have been developed to withstand the harsh conditions found across the various components of a fusion reactor. It is apparent that existing materials that are currently favoured for use in fusion reactors are not without their drawbacks. HEAs (or even more broadly: compositionally-complex alloys) may offer an alternative to some of the proposed materials, in particular due to their observed high-temperature and irradiation properties. However, research into HEAs for fusion applications has only begun to scratch the surface of this potentially promising class of materials.

This thesis aims to add to the growing body of research on fusion HEAs. Specifically, a new suite of low-activation alloy systems will be investigated. This will begin with an assessment of the alloys in their solution annealed state and whether the resultant microstructures appear to be suitable for fusion applications. The work will then continue with investigation into their microstructural and mechanical behaviour after various fusion-relevant heat treatments. Finally, the oxidation properties of the alloys will be assessed, with a view to determining their tolerance to accidents and processability.

Alloy System	**Proposed Application**	**Reference**
WTaTiVCr	Divertor	[264, 263]
VTiFeCrZr	Blanket	[265]
TaTiVZrW	Blanket	[266]
TaTiVZrHf	Blanket	[266, 255]
WTaCrV	Divertor/PFM	[254]
TiVZrTa	Blanket	[256]
TiVCrTa	Blanket	[256]
SiFeVCr	PFM	[267]
SiFeVCrMo	PFM	[267]
TiVCrFe	Blanket	[268]

Table 2.2: Fusion alloy systems investigated and their potential applications.

References

[1] "Nuclear fusion". In: *Encyclopaedia Britannica. Available at https://www.britannica.com/science/nuclear-fusion*. 2020.

[2] *Wikimedia Commons: Binding energy curve*. Available at https://commons.wikimedia.org/wiki/File:Binding_energy_curve_-_common_isotopes.svg.

[3] J. D. Lawson. "Some criteria for a power producing thermonuclear reactor". In: *Proceedings of the Physical Society. Section B* 70.1 (Jan. 1957), pp. 6–10. ISSN: 03701301. DOI: 10.1088/0370-1301/70/1/303.

[4] *Wikimedia Commons: Fusion reaction rate*. Available at https://commons.wikimedia.org/wiki/File:Fusion_rxnrate.svg.

[5] *Wikimedia Commons: Fusion triple product*. Available at https://commons.wikimedia.org/wiki/File:Fusion_tripleprod.svg.

[6] EUROfusion. *European Research Roadmap to the Realisation of Fusion Energy*. Tech. rep. 2018, p. 16.

[7] G. Federici et al. "European DEMO design strategy and consequences for materials". In: *Nuclear Fusion* 57.9 (Sept. 2017), p. 092002. ISSN: 0029-5515. DOI: 10.1088/1741-4326/57/9/092002.

[8] *ITER Organisation: What is ITER?* Available at https://www.iter.org/proj/inafewlines.

[9] Y. Wu. "Conceptual design and testing strategy of a dual functional lithium-lead test blanket module in ITER and EAST". In: *Nuclear Fusion* 47.11 (Oct. 2007), pp. 1533–1539. ISSN: 00295515. DOI: 10.1088/0029-5515/47/11/015.

[10] E. Rajendra Kumar et al. "Preliminary design of Indian Test Blanket Module for ITER". In: *Fusion Engineering and Design* 83.7-9 (Dec. 2008), pp. 1169–1172. ISSN: 09203796. DOI: 10.1016/j.fusengdes.2008.07.030.

[11] J. F. Salavy et al. "The HCLL Test Blanket Module system: Present reference design, system integration in ITER and R&D needs". In: *Fusion Engineering and Design* 83.7-9 (Dec. 2008), pp. 1157–1162. ISSN: 09203796. DOI: 10.1016/j.fusengdes.2008.05.017.

[12] L. V. Boccaccini et al. "The European test blanket module systems: Design and integration in ITER". In: *Fusion Engineering and Design*. Vol. 81 A. 1-4. North-Holland, Feb. 2006, pp. 407–414. DOI: 10.1016/j.fusengdes.2005.09.008.

[13] F. Hernandez et al. "A new HCPB breeding blanket for the EU DEMO: Evolution, rationale and preliminary performances". In: *Fusion Engineering and Design* 124 (Nov. 2017), pp. 882–886. ISSN: 09203796. DOI: 10.1016/j.fusengdes.2017.02.008.

[14] H. Sadeghi et al. "Design and simulation of a blanket module with high efficiency cooling system of tokamak focused on DEMO reactor". In: *Nuclear Engineering and Technology* 52.2 (Feb. 2020), pp. 323–327. ISSN: 2234358X. DOI: 10.1016/j.net.2019.07.019.

[15] M Kovari et al. "Converting energy from fusion into useful forms". In: *Proceedings of the Institution of Mechanical Engineers, Part A: Journal of Power and Energy* 228.3 (May 2014), pp. 234–240. ISSN: 0957-6509. DOI: 10.1177/0957650913514230.

[16] S. J. Zinkle and N. M. Ghoniem. "Operating temperature windows for fusion reactor structural materials". In: *Fusion Engineering and Design* 51-52.2000 (2000), pp. 55–71. ISSN: 09203796. DOI: 10.1016/S0920-3796(00)00320-3.

[17] Mohamed Abdou et al. *Blanket/first wall challenges and required R&D on the pathway to DEMO*. Nov. 2015. DOI: 10.1016/j.fusengdes.2015.07.021.

[18] "Heat loads and shape design of the ITER first wall". In: *Fusion Engineering and Design* 85.10-12 (Dec. 2010), pp. 2049–2053. ISSN: 09203796. DOI: 10.1016/j.fusengdes.2010.07.022.

[19] Jochen Linke et al. "Challenges for plasma-facing components in nuclear fusion". In: *Matter and Radiation at Extremes* 4.5 (Sept. 2019), p. 056201. ISSN: 2468080X. DOI: 10.1063/1.5090100.

[20] R. A. Pitts et al. "Physics basis and design of the ITER plasma-facing components". In: *Journal of Nuclear Materials*. Vol. 415. 1 SUPPL. Elsevier B.V., Aug. 2011, S957–S964. DOI: 10.1016/j.jnucmat.2011.01.114.

[21] J. W. Coenen et al. "Materials for DEMO and reactor applications - Boundary conditions and new concepts". In: *Physica Scripta* 2016.T167 (2016). ISSN: 02811847. DOI: 10.1088/0031-8949/2016/T167/014002.

[22] Shin Kajita, Naoaki Yoshida, and Noriyasu Ohno. "Tungsten fuzz: Deposition effects and influence to fusion devices". In: *Nuclear Materials and Energy* 25 (Dec. 2020), p. 100828. ISSN: 23521791. DOI: 10.1016/j.nme.2020.100828.

[23] R. A. Pitts et al. "Status and physics basis of the ITER divertor". In: *Physica Scripta T*. Vol. T138. T138. IOP Publishing, Dec. 2009, p. 10. DOI: 10.1088/0031-8949/2009/T138/014001.

[24] M. S. Tillack et al. "Summary of the ARIES Town Meeting: Edge plasma physics and plasma material interactions in the fusion power plant regime". In: *Nuclear Fusion*. Vol. 53. 2. IOP Publishing, Feb. 2013, p. 027003. DOI: 10.1088/0029-5515/53/2/027003.

[25] M. J. Gorley. "Critical Assessment 12: Prospects for reduced activation steel for fusion plant". In: *Materials Science and Technology* 31.8 (June 2015), pp. 975–980. ISSN: 0267-0836. DOI: 10.1179/1743284714Y.0000000732.

[26] G W Bailey, O V Vilkhivskaya, and M R Gilbert. "Waste expectations of fusion steels under current waste repository criteria". In: (2021). DOI: 10.1088/1741-4326/abc933.

[27] UK Department of Energy and Climate Change. *UK Strategy for the Management of Solid Low Level Waste from the Nuclear Industry*. Tech. rep. 2016.

[28] Mark R Gilbert, M Fleming, and J.-Ch Sublet. "Automated Inventory and Material Science Scoping Calculations under Fission and Fusion Conditions". In: *International Conference on Mathematics & Computational Methods Applied to Nuclear Science & Engineering*. Jeju, Korea, 2017.

[29] M.R. Gilbert et al. "Waste implications from minor impurities in European DEMO materials". In: *Nuclear Fusion* 59.7 (July 2019), p. 076015. ISSN: 0029-5515. DOI: 10.1088/1741-4326/ab154e.

[30] Didier Perrault. "Nuclear safety aspects on the road towards fusion energy". In: *Fusion Engineering and Design* 146.September 2018 (2019), pp. 130–134. ISSN: 09203796. DOI: 10.1016/j.fusengdes.2018.11.053.

[31] Y Wu et al. "Identification of safety gaps for fusion demonstration reactors". In: *Nature Energy* 1 (Oct. 2016), p. 16154. ISSN: 2058-7546. DOI: 10.1038/nenergy.2016.154.

[32] Felix Klein et al. "Sublimation of advanced tungsten alloys under DEMO relevant accidental conditions". In: *Fusion Engineering and Design* 146.February (2019), pp. 1198–1202. ISSN: 09203796. DOI: 10.1016/j.fusengdes.2019.02.039.

[33] Steven J. Piet, Edward T. Cheng, and Lisa J. Porter. "Accident safety comparison of elements to define low-activation materials". In: *Fusion Technology* 17.4 (1990), pp. 636–657. ISSN: 07481896. DOI: 10.13182/FST17-4-636.

[34] Steven J. Piet et al. "Initial integration of accident safety, waste management, recycling, effluent, and maintenance considerations for low-activation materials". In: *Fusion Technology* 19.1 (1991), pp. 146–161. ISSN: 07481896. DOI: 10.13182/FST19-1-146.

[35] D. Maisonnier et al. "The European power plant conceptual study". In: *Fusion Engineering and Design* 75-79.SUPPL. (Nov. 2005), pp. 1173–1179. ISSN: 09203796. DOI: 10.1016/j.fusengdes.2005.06.095.

[36] A. Litnovsky et al. "Smart tungsten alloys as a material for the first wall of a future fusion power plant". In: *Nuclear Fusion* 57.6 (2017). ISSN: 17414326. DOI: 10.1088/1741-4326/aa6816.

[37] Tobias Wegener et al. "Development and analyses of self-passivating tungsten alloys for DEMO accidental conditions". In: *Fusion Engineering and Design* 124 (Nov. 2017), pp. 183–186. ISSN: 09203796. DOI: 10.1016/j.fusengdes.2017.03.072.

[38] F. Klein et al. "Oxidation resistance of bulk plasma-facing tungsten alloys". In: *Nuclear Materials and Energy* 15 (May 2018), pp. 226–231. ISSN: 23521791. DOI: 10.1016/j.nme.2018.05.003.

[39] Gary S. Was. *Fundamentals of Radiation Materials Science*. eng. Berlin, Heidelberg: Springer Berlin Heidelberg, 2007. ISBN: 978-3-540-49471-3. DOI: 10.1007/978-3-540-49472-0.

[40] Alan Xu et al. "Ion-irradiation-induced clustering in W-Re and W-Re-Os alloys: A comparative study using atom probe tomography and nanoindentation measurements". In: *Acta Materialia* 87 (Apr. 2015), pp. 121–127. ISSN: 13596454. DOI: 10.1016/j.actamat.2014.12.049.

[41] H. Bohm et al. "Irradiation Effects on the Mechanical Properties of Vanadium-Base Alloys". In: *Effects of Radiation on Structural Metals*. 100 Barr Harbor Drive, PO Box C700, West Conshohocken, PA 19428-2959: ASTM International, 1967, pp. 95–95–12. DOI: 10.1520/STP41319S.

[42] G Edison and G A Whitlow. "VANADIUM ALLOYS vs STAINLESS STEEL FOR SODIUM-COOLED FAST REACTOR CLADDING". In: *Nuclear Applications & Technology* 7.November (1969), pp. 443–455.

[43] Steven J. Zinkle et al. "Research and development on vanadium alloys for fusion applications". In: *Journal of Nuclear Materials* 258-263.1998 (1998), pp. 205–214. ISSN: 00223115. DOI: 10.1016/S0022-3115(98)00269-4.

[44] D. L. Smith et al. "Reference vanadium alloy V-4Cr-4Ti for fusion application". In: *Journal of Nuclear Materials* 233-237.PART 1 (1996), pp. 356–363. ISSN: 00223115. DOI: 10.1016/S0022-3115(96)00231-0.

[45] Ken-ichi Fukumoto et al. "Irradiation Hardening Behavior of He-Irradiated V–Cr–Ti Alloys with Low Ti Addition". In: *Quantum Beam Science* 5.1 (Dec. 2020), p. 1. ISSN: 2412-382X. DOI: 10.3390/qubs5010001.

[46] H.M. Chung, B.A Loomis, and D.L. Smith. "Effect of irradiation damage and helium on swelling and structure of vanadium-base alloys". In: *Journal of Nuclear Materials* 212-215 (Sept. 1994), pp. 804–812. ISSN: 00223115. DOI: 10.1016/0022-3115(94)90167-8.

[47] B.A. Loomis et al. "Effects of neutron irradiation and hydrogen on ductile-brittle transition temperatures of V-Cr-Ti alloys". In: *Journal of Nuclear Materials* 212-215.94 (Sept. 1994), pp. 799–803. ISSN: 00223115. DOI: 10.1016/0022-3115(94)90166-X.

[48] B.a. Loomis, L.J. Nowicki, and D.L. Smith. "Effect of neutron irradiation on tensile properties of V-Cr-Ti alloys". In: *Journal of Nuclear Materials* 212-215 (Sept. 1994), pp. 790–793. ISSN: 00223115. DOI: 10.1016/0022-3115(94)90164-3.

[49] H.M. Chung, B.A. Loomis, and D.L. Smith. "Creep properties of vanadium-base alloys". In: *Journal of Nuclear Materials* 212-215.PART 1 (Sept. 1994), pp. 772–777. ISSN: 00223115. DOI: 10.1016/0022-3115(94)90161-9.

[50] D.S. Gelles and J.F. Stubbins. "Microstructural development in irradiated vanadium alloys". In: *Journal of Nuclear Materials* 212-215.PART 1 (Sept. 1994), pp. 778–783. ISSN: 00223115. DOI: 10.1016/0022-3115(94)90162-7.

[51] J.M. Chen, T. Muroga, T. Nagasaka, et al. "The mechanical properties of V-4Cr-4Ti in various thermo-mechanical states". In: *Fusion Engineering and Design* 81.23 (2006), pp. 2899–2905. ISSN: 09203796. DOI: 10.1016/j.fusengdes.2006.07.051.

[52] N. J. Heo, T. Nagasaka, T. Muroga, et al. "Effect of impurity levels on precipitation behavior in the low-activation V-4Cr-4Ti alloys". In: *Journal of Nuclear Materials* 307-311.1 SUPPL. (2002), pp. 620–624. ISSN: 00223115. DOI: 10.1016/S0022-3115(02)01040-1.

[53] A. Nishimura, A. Iwahori, N. J. Heo, et al. "Effect of precipitation and solution behavior of impurities on mechanical properties of low activation vanadium alloy". In: *Journal of Nuclear Materials* 329-333.1-3 PART A (2004), pp. 438–441. ISSN: 00223115. DOI: 10.1016/j.jnucmat.2004.04.072.

[54] Takeo Muroga, Takuya Nagasaka, A Nishimura, et al. "Improvement of Vanadium Alloys by Precipitate Control for Structural Components of Fusion Reactors". In: *Materials Science Forum* 475-479 (2005), pp. 1449–1454. ISSN: 1662-9752. DOI: 10.4028/www.scientific.net/MSF.475-479.1449.

[55] Jian Zhang and Wei-Zhong Han. "Oxygen solutes induced anomalous hardening, toughening and embrittlement in body-centered cubic vanadium". In: *Acta Materialia* 196 (Sept. 2020), pp. 122–132. ISSN: 13596454. DOI: 10.1016/j.actamat.2020.06.023.

[56] Xingming Zhang et al. "The effects of interstitial impurities on the mechanical properties of vanadium alloys: A first-principles study". In: *Journal of Alloys and Compounds* 701 (Apr. 2017), pp. 975–980. ISSN: 09258388. DOI: 10.1016/j.jallcom.2017.01.135.

[57] J.M. Chen, T. Muroga, T. Nagasaka, et al. "Precipitation behavior in V-6W-4Ti, V-4Ti and V-4Cr-4Ti alloys". In: *Journal of Nuclear Materials* 334.2 (2004), pp. 159–165. ISSN: 00223115. DOI: 10.1016/j.jnucmat.2004.05.019.

[58] J.M. Chen, T. Muroga, T. Nagasaka, et al. "The recovery and recrystallization of cold rolled V-W-Ti alloys". In: *Journal of Nuclear Materials* 322.1 (Oct. 2003), pp. 73–79. ISSN: 00223115. DOI: 10.1016/S0022-3115(03)00317-9.

[59] K. Natesan, W.K. Soppet, and A. Purohit. "Uniaxial creep behavior of V-4Cr-4Ti alloy". In: *Journal of Nuclear Materials* 307-311 (Dec. 2002), pp. 585–590. ISSN: 00223115. DOI: 10.1016/S0022-3115(02)01014-0.

[60] R.J. Kurtz, A.M. Ermi, and H. Matsui. "An update on biaxial thermal creep of vanadium alloys". In: *Fusion materials semiannual progress report* (2002), pp. 7–17.

[61] M.L Grossbeck. "Creep of V-4Cr-4Ti in a lithium environment". In: *Journal of Nuclear Materials* 307-311 (Dec. 2002), pp. 615–619. ISSN: 00223115. DOI: 10.1016/S0022-3115(02)01017-6.

[62] M.L. Grossbeck. "Thermal creep of V-4Cr-4Ti in a Li environment". In: *Fusion materials semiannual progress report* (2002), pp. 2–5.

[63] K. Fukumoto, T. Yamamoto, N. Nakao, et al. "High temperature performance of highly purified V-4Cr-4Ti alloy, NIFS-Heat1". In: *Journal of Nuclear Materials* 307-311.1 SUPPL. (2002), pp. 610–614. ISSN: 00223115. DOI: 10.1016/S0022-3115(02)01216-3.

[64] J.M. Chen, T Nagasaka, T Muroga, et al. "Mechanical properties of V-4Cr-4Ti strengthened by precipitation and cold rolling". In: *Journal of Nuclear Materials* 374.1-2 (Feb. 2008), pp. 298–303. ISSN: 00223115. DOI: 10.1016/j.jnucmat.2007.08.012.

[65] P F Zheng, T Nagasaka, T Muroga, et al. "Creep properties of V-Cr-4Ti strengthened by cold working and aging". In: *Fusion Engineering and Design* 86 (2011), pp. 2561–2564. DOI: 10.1016/j.fusengdes.2011.01.081.

[66] T Muroga, T Nagasaka, J.M. Chen, et al. "Microstructure of creep-deformed V-4Cr-4Ti strengthened by precipitation and cold rolling". In: *Journal of Nuclear Materials* 386-388 (Apr. 2009), pp. 606–609. ISSN: 00223115. DOI: 10.1016/j.jnucmat.2008.12.188.

[67] T Muroga, T Nagasaka, P.F. Zheng, et al. "Microstructural Control for Improving Properties of V-4Cr-4Ti Alloys". In: *Advances in Science and Technology* 73 (Oct. 2010), pp. 22–26. DOI: 10.4028/www.scientific.net/AST.73.22.

[68] T Muroga, T Nagasaka, P F Zheng, et al. "Dislocation evolution during thermal creep deformation in V-4Cr-4Ti with various thermal and mechanical treatments". In: *Journal of Nuclear Materials* 442 (2013), S354–S359. DOI: 10.1016/j.jnucmat.2013.03.061.

[69] T Furuno, H Kurishita, T Nagasaka, et al. "Effects of grain size on high temperature creep of fine grained, solution and dispersion hardened V-1.6Y-8W-0.8TiC". In: *Journal of Nuclear Materials* 417.1-3 (Oct. 2011), pp. 299–302. ISSN: 00223115. DOI: 10.1016/j.jnucmat.2010.12.105.

[70] T. Nagasaka et al. "High-temperature creep properties of NIFS-HEAT-2 high-purity low-activation vanadium alloy". In: *Nuclear Fusion* 59.9 (Sept. 2019), p. 096046. ISSN: 0029-5515. DOI: 10.1088/1741-4326/ab1c8f.

[71] H. M. Chung, B. A. Loomis, and D. L. Smith. "Development and testing of vanadium alloys for fusion applications". In: *Journal of Nuclear Materials* 239.1-3 (1996), pp. 139–156. ISSN: 00223115. DOI: 10.1016/S0022-3115(96)00676-9.

[72] H. Matsui, K. Fukumoto, D. L. Smith, et al. "Status of vanadium alloys for fusion reactors". In: *Journal of Nuclear Materials* 233-237.PART 1 (1996), pp. 92–99. ISSN: 00223115. DOI: 10.1016/S0022-3115(96)00331-5.

[73] K.-I Fukumoto, H Matsui, H Tsai, et al. "Mechanical behavior and microstructural evolution of vanadium alloys irradiated in ATR-A1". In: *Journal of Nuclear Materials* 283-287 (Dec. 2000), pp. 492–497. ISSN: 00223115. DOI: 10.1016/S0022-3115(00)00310-X.

[74] ML Hamilton and MB Toloczko. "Effect of low temperature irradiation on the mechanical properties of ternary V-Cr-Ti alloys as determined by tensile tests and shear punch tests". In: *Journal of Nuclear Materials* 283-287 (Dec. 2000), pp. 488–491. ISSN: 00223115. DOI: 10.1016/S0022-3115(00)00227-0.

[75] Y Candra, K Fukumoto, A Kimura, et al. "Microstructural evolution and hardening of neutron irradiated vanadium alloys at low temperatures in Japan Material Testing Reactor". In: *Journal of Nuclear Materials* 271-272 (May 1999), pp. 301–305. ISSN: 00223115. DOI: 10.1016/S0022-3115(98)00716-8.

[76] Ken-Ichi Fukumoto, Masanari Sugiyama, and Hideki Matsui. "Features of dislocation channeling in neutron-irradiated V-(Fe, Cr)-Ti alloy". In: *Journal of Nuclear Materials* 367-370 (Aug. 2007), pp. 829–833. ISSN: 00223115. DOI: 10.1016/j.jnucmat.2007.03.075.

[77] F.A. Garner et al. "High swelling rates observed in neutron-irradiated V-Cr and V-Si binary alloys". In: *Journal of Nuclear Materials* 191-194 (Sept. 1992), pp. 948–951. ISSN: 00223115. DOI: 10.1016/0022-3115(92)90613-P.

[78] B.A. Loomis, D.L. Smith, and F.A. Garner. "Swelling of neutron-irradiated vanadium alloys". In: *Journal of Nuclear Materials* 179-181.PART 2 (Mar. 1991), pp. 1166–1167. ISSN: 00223115. DOI: 10.1016/0022-3115(91)90306-R.

[79] H. Matsui, H. Nakajima, and S. Yoshida. "Microstructural evolution in vanadium alloys by fast neutron irradiation". In: *Journal of Nuclear Materials* 205.C (Oct. 1993), pp. 452–459. ISSN: 00223115. DOI: 10.1016/0022-3115(93)90109-C.

[80] A.O. Boev et al. "Interaction of Ti and Cr atoms with point defects in bcc vanadium: A DFT study". In: *Journal of Nuclear Materials* 492 (Aug. 2017), pp. 14–21. ISSN: 00223115. DOI: 10.1016/j.jnucmat.2017.04.046.

[81] A O Boev et al. "Molecular dynamics simulation of primary radiation damage in vanadium and alloy V-4Ti". In: *Journal of Physics: Conference Series* 1147 (Jan. 2019), p. 012087. ISSN: 1742-6588. DOI: 10.1088/1742-6596/1147/1/012087.

[82] Pengbo Zhang et al. "First-principles calculations of vacancy-O-He and vacancy-N-He complexes in vanadium". In: *Computational Materials Science* 160 (Apr. 2019), pp. 180–185. ISSN: 09270256. DOI: 10.1016/j.commatsci.2019.01.005.

[83] Xiao Tong Li et al. "The interstitial emission mechanism in a vanadium-based alloy". In: *Journal of Nuclear Materials* 533 (May 2020), p. 152121. ISSN: 00223115. DOI: 10.1016/j.jnucmat.2020.152121.

[84] H Tsai, T.S Bray, H Matsui, et al. "Effects of low-temperature neutron irradiation on mechanical properties of vanadium-base alloys". In: *Journal of Nuclear Materials* 283-287 (Dec. 2000), pp. 362–366. ISSN: 00223115. DOI: 10.1016/S0022-3115(00)00224-5.

[85] V.M. Troyanov, M.G. Bulkanov, A.S. Kruglov, et al. "Irradiation creep of V-Ti-Cr alloy in BR-10 reactor core instrumented experiments". In: *Journal of Nuclear Materials* 233-237 (Oct. 1996), pp. 381–384. ISSN: 00223115. DOI: 10.1016/S0022-3115(96)00033-5.

[86] Meimei Li, D.T. Hoelzer, M.L. Grossbeck, et al. "Irradiation creep of the US Heat 832665 of V-4Cr-4Ti". In: *Journal of Nuclear Materials* 386 (2009), pp. 618–621. ISSN: 00223115. DOI: 10.1016/j.jnucmat.2008.12.220.

[87] Ken-ichi Fukumoto, Hideki Matsui, and other. "Irradiation creep behavior of V-4Cr-4Ti alloys irradiated in a liquid sodium environment at the JOYO fast reactor". In: *Journal of Nuclear Materials* 437.1 (2013), pp. 341–349. ISSN: 00223115. DOI: 10.1016/j.jnucmat.2013.02.012.

[88] M. Uz, K. Natesan, and V.B. Hang. "Oxidation kinetics and microstructure of V-(4-5) wt% Cr-(4-5) wt% Ti alloys exposed to air at 300–650°C". In: *Journal of Nuclear Materials* 245.2-3 (June 1997), pp. 191–200. ISSN: 00223115. DOI: 10.1016/S0022-3115(97)00008-1.

[89] K Natesan, W.K Soppet, and M Uz. "Effects of oxygen and oxidation on tensile behavior of V-4Cr-4Ti alloy". In: *Journal of Nuclear Materials* 258-263 (Oct. 1998), pp. 1476–1481. ISSN: 00223115. DOI: 10.1016/S0022-3115(98)00399-7.

[90] B.A. Pint and J.R. DiStefano. "Oxygen embrittlement of vanadium alloys with and without surface oxide formation". In: *Journal of Nuclear Materials* 307-311 (Dec. 2002), pp. 560–565. ISSN: 00223115. DOI: 10.1016/S0022-3115(02)01222-9.

[91] Mitsuhiro Fujiwara et al. "Effects of doping elements on oxidation properties of V-Cr-Ti type alloys in several environments". In: *Journal of Nuclear Materials* 307-311 (Dec. 2002), pp. 601–604. ISSN: 00223115. DOI: 10.1016/S0022-3115(02)01101-7.

[92] M Fujiwara et al. "Influence of Cr, Ti concentrations on oxidation and corrosion resistance of V–Cr–Ti type alloys". In: *Journal of Nuclear Materials* 329-333 (Aug. 2004), pp. 452–456. ISSN: 0022-3115. DOI: 10.1016/J.JNUCMAT.2004.04.090.

[93] Zhenyu Yao et al. "Behavior of Oxygen in Fusion Candidate Vanadium Alloys during Oxidation and Annealing". In: *Materials Science Forum* 475-479 (2005), pp. 1445–1448. ISSN: 1662-9752. DOI: 10.4028/www.scientific.net/MSF.475-479.1445.

[94] B. A. Pint and J. R. DiStefano. "The Role of Oxygen Uptake and Scale Formation on the Embrittlement of Vanadium Alloys". In: *Oxidation of Metals* 63.1-2 (Feb. 2005), pp. 33–55. ISSN: 0030-770X. DOI: 10.1007/s11085-005-1950-7.

[95] O. Carlson and A. Eustice. "Vanadium-chromium alloy system". In: *Ames Laboratory Technical Reports* (1959).

[96] A. Mukherjee and S.P. Wach. "Kinetics of the oxidation of vanadium in the temperature range 350-950°C". In: *Journal of the Less Common Metals* 92.2 (Aug. 1983), pp. 289–300. ISSN: 00225088. DOI: 10.1016/0022-5088(83)90495-2.

[97] Sigma-Aldrich. *Vanadium pentoxide safety data sheet*. 2020.

[98] G Busch and A Tobin. "OXIDATION OF VANADIUM AND VANADIUM ALLOYS IN GASEOUS HELIUM COOLANTS CONTAINING WATER VAPOR IMPURITIES". In: *Journal of Nuclear Materials* 141-143 (1986), pp. 599–603.

[99] K Natesan and M Uz. "Oxidation performance of V-Cr-Ti alloys". In: *Fusion Engineering and Design* 51-52.52 (Nov. 2000), pp. 145–152. ISSN: 09203796. DOI: 10.1016/S0920-3796(00)00308-2.

[100] Mitsuhiro Fujiwara et al. "Effects of Doping Elements on Oxidation Properties of Low-Activation Vanadium Alloys". In: *MATERIALS TRANSACTIONS* 42.6 (2001), pp. 1048–1051. ISSN: 1345-9678. DOI: 10.2320/matertrans.42.1048.

[101] Mitsuhiro Fujiwara et al. "Improvement of Corrosion Resistance of Vanadium Alloys in High-Temperature Pressurized Water". In: *MATERIALS TRANSACTIONS* 46.3 (2005), pp. 517–521. ISSN: 1345-9678. DOI: 10.2320/matertrans.46.517.

[102] N. Chaia et al. "An overview of the oxidation performance of silicide diffusion coatings for vanadium-based alloys for generation IV reactors". In: *Corrosion Science* 66 (Jan. 2013), pp. 285–291. ISSN: 0010938X. DOI: 10.1016/j.corsci.2012.09.031.

[103] U. Jain, J. Sonber, and R. Tewari. "High temperature oxidation behaviour of V-Ti-Ta alloys". In: *Fusion Engineering and Design* 144 (July 2019), pp. 125–132. ISSN: 09203796. DOI: 10.1016/j.fusengdes.2019.04.070.

[104] U. Jain, A. Mukherjee, and G. K. Dey. "Thermodynamic properties of Ti in V-Ti-Ta alloys: Effect of Ta addition". In: *Journal of Alloys and Compounds* 686 (Nov. 2016), pp. 946–950. ISSN: 09258388. DOI: 10.1016/j.jallcom.2016.06.200.

[105] U. Jain et al. "Wear Behavior of Vanadium and V-Ti-Ta Alloys under Reciprocating Sliding Conditions". In: *Journal of Materials Engineering and Performance* 28.6 (June 2019), pp. 3372–3380. ISSN: 15441024. DOI: 10.1007/s11665-019-04090-3.

[106] B.A. Pint, S.J. Pawel, M Howell, et al. "Initial characterization of V-4Cr-4Ti and MHD coatings exposed to flowing Li". In: *Journal of Nuclear Materials* 386-388 (Apr. 2009), pp. 712–715. ISSN: 00223115. DOI: 10.1016/j.jnucmat.2008.12.295.

[107] K.A. Unocic, M.J. Lance, and B.A. Pint. "Characterization of specimens exposed in a Li loop". In: *Journal of Nuclear Materials* 442.1-3 (Nov. 2013), S580–S584. ISSN: 00223115. DOI: 10.1016/j.jnucmat.2013.04.055.

[108] Pengfei ZHENG, Takuya NAGASAKA, Takeo MUROGA, et al. "Mechanical Properties of V-4Cr-4Ti after Exposure in Static Lithium at 650 °C". In: *Plasma and Fusion Research* 6 (2011), pp. 2405121–2405121. ISSN: 1880-6821. DOI: 10.1585/pfr.6.2405121.

[109] D. L. Smith, B. A. Loomis, and D. R. Diercks. "Vanadium-base alloys for fusion reactor applications - a review". In: *Journal of Nuclear Materials* 135.2-3 (1985), pp. 125–139. ISSN: 00223115. DOI: 10.1016/0022-3115(85)90070-4.

[110] T. Muroga, J.M. Chen, V.M. Chernov, et al. "Present status of vanadium alloys for fusion applications". In: *Journal of Nuclear Materials* 455.1 (2014), pp. 263–268. ISSN: 00223115. DOI: 10.1016/j.jnucmat.2014.06.025.

[111] G. De Temmerman et al. "Efficiency of thermal outgassing for tritium retention measurement and removal in ITER". In: *Nuclear Materials and Energy* 12 (Aug. 2017), pp. 267–272. ISSN: 23521791. DOI: 10.1016/j.nme.2016.10.016.

[112] Takumi Chikada et al. "Basic study on self-healing of Er2O3 coating for vanadium-lithium blanket system". In: *Fusion Engineering and Design* 82.15-24 (Oct. 2007), pp. 2572–2577. ISSN: 09203796. DOI: 10.1016/j.fusengdes.2007.03.020.

[113] W.R Johnson and J.P Smith. "Fabrication of a 1200 kg ingot of V-4Cr-4Ti alloy for the DIII-D radiative divertor program". In: *Journal of Nuclear Materials* 258-263 (Oct. 1998), pp. 1425–1430. ISSN: 00223115. DOI: 10.1016/S0022-3115(98)00209-8.

[114] T Muroga et al. "NIFS program for large ingot production of a V-Cr-Ti alloy". In: *Journal of Nuclear Materials* 283-287 (Dec. 2000), pp. 711–715. ISSN: 00223115. DOI: 10.1016/S0022-3115(00)00281-6.

[115] H.Y. Fu et al. "Fabrication using electron beam melting of a V-4Cr-4Ti alloy and its thermo-mechanical strengthening study". In: *Journal of Nuclear Materials* 442.1-3 (Nov. 2013), S336–S340. ISSN: 00223115. DOI: 10.1016/j.jnucmat.2013.01.337.

[116] V. Chernov et al. "Low Activation Vanadium Alloys for Fusion Power Reactors - the RF Results". In: *24th IAEA Fusion Energy Conference*. San Diego, USA, 2012.

[117] Vincent Duquesnes, Thomas Guilbert, and Marion Le Flem. "French investigation of a new V-4Cr-4Ti grade: CEA-J57 - Fabrication and microstructure". In: *Journal of Nuclear Materials* 426.1-3 (July 2012), pp. 96–101. ISSN: 00223115. DOI: 10.1016/j.jnucmat.2012.03.029.

[118] M.L. Grossbeck, J.F. King, D.J. Alexander, et al. "Development of techniques for welding V-Cr-Ti alloys". In: *Journal of Nuclear Materials* 258-263 (1998), pp. 1369–1374. ISSN: 00223115. DOI: 10.1016/S0022-3115(98)00205-0.

[119] N.J Heo, T Nagasaka, T Muroga, et al. "Metallurgical and mechanical properties of laser weldment for low activation V-4Cr-4Ti alloy". In: *Fusion Engineering and Design* 61-62 (Nov. 2002), pp. 749–755. ISSN: 09203796. DOI: 10.1016/S0920-3796(02)00181-3.

[120] Takuya Nagasaka, Takeo Muroga, Hideo Watanabe, et al. "Recovery of Hardness, Impact Properties and Microstructure of Neutron-Irradiated Weld Joint of a Fusion Candidate Vanadium Alloy". In: *Materials Transactions* 46.3 (2005), pp. 498–502. ISSN: 1345-9678. DOI: 10.2320/matertrans.46.498.

[121] Takuya Nagasaka, Takeo Muroga, Hideo Watanabe, et al. "Impact property of low-activation vanadium alloy after laser welding and heavy neutron irradiation". In: *Journal of Nuclear Materials* 442.1-3 (Nov. 2013), S364–S369. ISSN: 00223115. DOI: 10.1016/j.jnucmat.2013.05.046.

[122] Takeo Muroga et al. "Heterogeneous Precipitation and Mechanical Property Change by Heat Treatments for the Laser Weldments of V-4Cr-4Ti Alloy". In: *Plasma and Fusion Research* 10 (2015), pp. 1–7. DOI: 10.1585/pfr.10.1405092.

[123] Valentyn Tsisar, Takuya Nagasaka, Marion Le Flem, et al. "Impact properties of electron beam welds of V-4Ti-4Cr alloys NIFS-HEAT-2 and CEA-J57". In: *Fusion Engineering and Design* 89.7-8 (Oct. 2014), pp. 1633–1636. ISSN: 09203796. DOI: 10.1016/j.fusengdes.2014.03.086.

[124] Valentyn Tsisar, Takuya Nagasaka, Takeo Muroga, et al. "Effect of Li on mechanical and corrosion properties of electron beam welds of V-4Ti-4Cr alloy (NIFS-HEAT-2)". In: *Journal of Nuclear Materials* 442.1-3 (Nov. 2013), pp. 528–532. ISSN: 00223115. DOI: 10.1016/j.jnucmat.2013.07.013.

[125] V. Tsisar, T. Nagasaka, M. Le Flem, et al. "Effect of post-weld heat treatment on microstructure, hardness and low-temperature impact toughness of electron beam welds of NIFS-HEAT-2 and CEA-J57 heats of V-4Ti-4Cr alloy". In: *Nuclear Materials and Energy* 0 (2015), pp. 1–5. ISSN: 23521791. DOI: 10.1016/j.nme.2016.04.002.

[126] Li-Wen Zhang et al. "Dissimilar-metal bonding of a carbide-dispersion strengthened vanadium alloy for V/Li fusion blanket application". In: *Tungsten* 2.1 (Mar. 2020), pp. 101–106. ISSN: 2661-8028. DOI: 10.1007/s42864-020-00040-y.

[127] Haiying Fu et al. "Dissimilar-metals bonding between NIFS-HEAT-2 vanadium alloy and Hastelloy X nickel alloy by controlling intermetallics". In: *Fusion Science and Technology* 72.4 (2017), pp. 680–685. ISSN: 15361055. DOI: 10.1080/15361055.2017.1347469.

[128] Shaoning Jiang et al. "Interfacial characterization of dissimilar-metals bonding between vanadium alloy and Hastelloy X alloy by explosive welding". In: *Journal of Nuclear Materials* 539 (June 2020), p. 152322. ISSN: 00223115. DOI: 10.1016/j.jnucmat.2020.152322.

[129] B. Bocci et al. "ARC reactor materials: Activation analysis and optimization". In: *Fusion Engineering and Design* 154 (May 2020), p. 111539. ISSN: 09203796. DOI: 10.1016/j.fusengdes.2020.111539.

[130] M. L. Grossbeck et al. "Analysis of V-Cr-Ti alloys in terms of activation of impurities". In: *Journal of Nuclear Materials* 258-263.PART 2 B (Oct. 1998), pp. 1778–1783. ISSN: 00223115. DOI: 10.1016/S0022-3115(98)00228-1.

[131] M.R. Gilbert, J.-Ch. Sublet, and R. Forrest. "Handbook of activation, transmutation and radiation dmagae properties of the elements simulated using FISPACT-II and TENDL-2014". In: *UK Atomic Energy Authority* CCFE-R(15) (2015).

[132] Tatsuaki Sakamoto, Hiroaki Kurishita, Sengo Kobayashi, et al. "High temperature deformation of V-1.6Y-8.5W-(0.08, 0.15)C alloys". In: *Journal of Nuclear Materials* 386-388 (Apr. 2009), pp. 602–605. ISSN: 00223115. DOI: 10.1016/j.jnucmat.2008.12.187.

[133] T Sakamoto, H Kurishita, T Furuno, et al. "Uniaxial creep behavior of nanostructured, solution and dispersion hardened V-1.4Y-7W-9Mo-0.7TiC with different grain sizes". In: *Materials Science and Engineering: A* 528.27 (Oct. 2011), pp. 7843–7850. ISSN: 09215093. DOI: 10.1016/j.msea.2011.06.033.

[134] H Kurishita, S Oda, S Kobayashi, et al. "Effect of 2wt% Ti addition on high-temperature strength of fine-grained, particle dispersed V-Y alloys". In: *Journal of Nuclear Materials* 367-370 (Aug. 2007), pp. 848–852. ISSN: 00223115. DOI: 10.1016/j.jnucmat.2007.03.071.

[135] Takeshi Miyazawa, Takeo Muroga, and Yoshimitsu Hishinuma. "Effect of Chromium Content on Mechanical Properties of V-xCr-4Ti-0.15Y Alloys". In: *Plasma and Fusion Research* 11 (2015), pp. 89–93.

[136] B.P. Wynne et al. "An analysis of the microstructure of spark plasma sintered and hot isostatically pressed V 4Cr 4Ti 1.8Y 0.4Ti3SiC2 alloy and its thermal stability". In: *Journal of Alloys and Compounds* 680 (Sept. 2016), pp. 506–511. ISSN: 09258388. DOI: 10.1016/j.jallcom.2016.04.159.

[137] P.F. Zheng, J.M. Chen, T. Nagasaka, et al. "Effects of dispersion particle agents on the hardening of V-4Cr-4Ti alloys". In: *Journal of Nuclear Materials* 455.1-3 (Dec. 2014), pp. 669–675. ISSN: 00223115. DOI: 10.1016/j.jnucmat.2014.08.061.

[138] R.P. Chen et al. "Long-term microstructural degradation and creep strength in Gr.91 steel". In: *Materials Science and Engineering: A* 528.13-14 (May 2011), pp. 4390–4394. ISSN: 09215093. DOI: 10.1016/j.msea.2011.02.060.

[139] S.J. Zinkle, J.-L Boutard, D.T. Hoelzer, et al. "Development of next generation tempered and ODS reduced activation ferritic/martensitic steels for fusion energy applications". In: *Nuclear Fusion* 57.9 (Sept. 2017), p. 092005. ISSN: 0029-5515. DOI: 10.1088/1741-4326/57/9/092005.

[140] N Baluc, D.S. Gelles, S Jitsukawa, et al. "Status of reduced activation ferritic/martensitic steel development". In: *Journal of Nuclear Materials* 367-370 (Aug. 2007), pp. 33–41. ISSN: 00223115. DOI: 10.1016/j.jnucmat.2007.03.036.

[141] H. Tanigawa et al. "Development of benchmark reduced activation ferritic/martensitic steels for fusion energy applications". In: *Nuclear Fusion* 57.9 (Sept. 2017), p. 092004. ISSN: 0029-5515. DOI: 10.1088/1741-4326/57/9/092004.

[142] M. Rieth, M. Schirra, A. Falkenstein, et al. *EUROFER 97. Tensile, charpy, creep and structural tests*. Tech. rep. Karlsruhe Institute of Technology, 2003.

[143] G. Yu, N. Nita, and N. Baluc. "Thermal creep behaviour of the EUROFER 97 RAFM steel and two European ODS EUROFER 97 steels". In: *Fusion Engineering and Design* 75-79.SUPPL. (2005), pp. 1037–1041. ISSN: 09203796. DOI: 10.1016/j.fusengdes.2005.06.311.

[144] R.W. Evans, J.A. Preston, B Wilshire, et al. "Creep and creep fracture of an oxide-dispersion-strengthened 13% chromium ferritic steel". In: *Materials Science and Engineering: A* 167.1-2 (Aug. 1993), pp. 65–72. ISSN: 09215093. DOI: 10.1016/0921-5093(93)90338-F.

[145] C. Zakine, C. Prioul, and D. François. "Creep behaviour of ODS steels". In: *Materials Science and Engineering: A* 219.1-2 (Nov. 1996), pp. 102–108. ISSN: 09215093. DOI: 10.1016/S0921-5093(96)10415-9.

[146] A Alamo et al. "Assessment of ODS-14%Cr ferritic alloy for high temperature applications". In: *Journal of Nuclear Materials* 329-333 (Aug. 2004), pp. 333–337. ISSN: 00223115. DOI: 10.1016/j.jnucmat.2004.05.004.

[147] J Rösler, R Joos, and E Arzt. "Microstructure and creep properties of dispersion-strengthened aluminum alloys". In: *Metallurgical Transactions A* 23.5 (May 1992), pp. 1393–1521. ISSN: 1543-1940. DOI: 10.1007/BF02647335.

[148] G. Robert Odette. "On the status and prospects for nanostructured ferritic alloys for nuclear fission and fusion application with emphasis on the underlying science". In: *Scripta Materialia* 143 (Jan. 2018), pp. 142–148. ISSN: 13596462. DOI: 10.1016/j.scriptamat.2017.06.021.

[149] G. Bonny, D. Terentyev, and L. Malerba. "On the α-α' miscibility gap of Fe-Cr alloys". In: *Scripta Materialia* 59.11 (Dec. 2008), pp. 1193–1196. ISSN: 13596462. DOI: 10.1016/j.scriptamat.2008.08.008.

[150] Mukesh Bachhav, G. Robert Odette, and Emmanuelle A. Marquis. "α' precipitation in neutron-irradiated Fe-Cr alloys". In: *Scripta Materialia* 74 (Mar. 2014), pp. 48–51. ISSN: 13596462. DOI: 10.1016/j.scriptamat.2013.10.001.

[151] Oliver J Weiß, Ermile Gaganidze, and Jarir Aktaa. "Quantitative characterization of microstructural defects in up to 32dpa neutron irradiated EUROFER97". In: *Journal of Nuclear Materials* 426.1-3 (July 2012), pp. 52–58. ISSN: 00223115. DOI: 10.1016/j.jnucmat.2012.03.027.

[152] Christian Dethloff, Ermile Gaganidze, and Jarir Aktaa. "Microstructural defects in EUROFER 97 after different neutron irradiation conditions". In: *Nuclear Materials and Energy* 9 (Dec. 2016), pp. 471–475. ISSN: 23521791. DOI: 10.1016/j.nme.2016.05.009.

[153] Christian Dethloff, Ermile Gaganidze, and Jarir Aktaa. "Quantitative TEM analysis of precipitation and grain boundary segregation in neutron irradiated EUROFER97". In: *Journal of Nuclear Materials* 454.1-3 (Nov. 2014), pp. 323–331. ISSN: 00223115. DOI: 10.1016/j.jnucmat.2014.07.078.

[154] S J Zinkle et al. "II. Effect of oxygen and helium on void formation in metals". In: *Philosophical Magazine A* 55.1 (Jan. 1987), pp. 127–140. ISSN: 0141-8610. DOI: 10.1080/01418618708209804.

[155] E Gaganidze et al. "Mechanical properties and TEM examination of RAFM steels irradiated up to 70dpa in BOR-60". In: *Journal of Nuclear Materials* 417.1-3 (Oct. 2011), pp. 93–98. ISSN: 00223115. DOI: 10.1016/j.jnucmat.2010.12.047.

[156] V. Shamanth and K.S. Ravishankar. "Dissolution of alpha-prime precipitates in thermally embrittled S2205-duplex steels during reversion-heat treatment". In: *Results in Physics* 5 (Jan. 2015), pp. 297–303. ISSN: 22113797. DOI: 10.1016/j.rinp.2015.10.004.

[157] E Materna-Morris et al. "Effect of helium on tensile properties and microstructure in 9%Cr-WVTa-steel after neutron irradiation up to 15dpa between 250 and 450°C". In: *Journal of Nuclear Materials* 386-388 (Apr. 2009), pp. 422–425. ISSN: 00223115. DOI: 10.1016/j.jnucmat.2008.12.157.

[158] Thaksang Byun and Naoyuki Hashimoto. "Strain localization in irradiated materials". In: *Nuclear Engineering and Technology* 38.7 (2006).

[159] Edeltraud Materna-Morris et al. "Tensile behavior of EUROFER ODS steel after neutron irradiation up to 16.3dpa between 250 and 450°C". In: *Fusion Engineering and Design* 98-99 (Oct. 2015), pp. 2038–2041. ISSN: 09203796. DOI: 10.1016/j.fusengdes.2015.07.015.

[160] M Klimenkov et al. "Effect of irradiation temperature on microstructure of ferritic-martensitic ODS steel". In: *Journal of Nuclear Materials* 493 (Sept. 2017), pp. 426–435. ISSN: 00223115. DOI: 10.1016/j.jnucmat.2017.06.024.

[161] N.V. Luzginova et al. "Irradiation response of ODS Eurofer97 steel". In: *Journal of Nuclear Materials* 428.1-3 (Sept. 2012), pp. 192–196. ISSN: 00223115. DOI: 10.1016/j.jnucmat.2011.08.030.

[162] Tianyi Chen et al. "Microstructural changes and void swelling of a 12Cr ODS ferritic-martensitic alloy after high-dpa self-ion irradiation". In: *Journal of Nuclear Materials* 467 (Dec. 2015), pp. 42–49. ISSN: 00223115. DOI: 10.1016/j.jnucmat.2015.09.016.

[163] D.S. Gelles. "Microstructural examination of commercial ferritic alloys at 200 dpa". In: *Journal of Nuclear Materials* 233-237 (Oct. 1996), pp. 293–298. ISSN: 00223115. DOI: 10.1016/S0022-3115(96)00222-X.

[164] M Zmitko et al. "The European ITER Test Blanket Modules: EUROFER97 material and TBM's fabrication technologies development and qualification". In: *Fusion Engineering and Design* 9403 (Apr. 2017). ISSN: 09203796. DOI: 10.1016/j.fusengdes.2017.04.051.

[165] S. Malang, A.R. Raffray, and N.B. Morley. "An example pathway to a fusion power plant system based on lead-lithium breeder: Comparison of the dual-coolant lead-lithium (DCLL) blanket with the helium-cooled lead-lithium (HCLL) concept as initial step". In: *Fusion Engineering and Design* 84.12 (Dec. 2009), pp. 2145–2157. ISSN: 09203796. DOI: 10.1016/j.fusengdes.2009.02.049.

[166] J. Konys et al. "Compatibility behavior of EUROFER steel in flowing Pb-17Li". In: *Journal of Nuclear Materials* 386-388 (Apr. 2009), pp. 678–681. ISSN: 00223115. DOI: 10.1016/j.jnucmat.2008.12.271.

[167] W Krauss, S.-E Wulf, and J Konys. "Long-term corrosion behavior of ODS-Eurofer in flowing Pb-15.7Li at 550 °C". In: *Nuclear Materials and Energy* 9 (Dec. 2016), pp. 512–518. ISSN: 23521791. DOI: 10.1016/j.nme.2016.04.011.

[168] Steven Van Dyck and Rik-Wouter Bosch. "Environmentally assisted cracking of Eurofer 97 in water". In: *Fusion Engineering and Design* 75-79 (Nov. 2005), pp. 973–977. ISSN: 09203796. DOI: 10.1016/j.fusengdes.2005.06.261.

[169] A. Aiello et al. "Hydrogen Isotopes Permeability in Eurofer 97 Martensitic Steel". In: *Fusion Science and Technology* 41.3P2 (May 2002), pp. 872–876. ISSN: 1536-1055. DOI: 10.13182/FST41-872.

[170] Karel Splichal et al. "Hydrogen embrittlement and fracture mode of EUROFER 97 ferritic-martensitic steel". In: *International Journal of Pressure Vessels and Piping* 89 (Jan. 2012), pp. 42–47. ISSN: 03080161. DOI: 10.1016/j.ijpvp.2011.09.006.

[171] D. Levchuk et al. "Erbium oxide as a new promising tritium permeation barrier". In: *Journal of Nuclear Materials* 367-370 (Aug. 2007), pp. 1033–1037. ISSN: 00223115. DOI: 10.1016/j.jnucmat.2007.03.183.

[172] N Yamamoto, Y Murase, and J Nagakawa. "An evaluation of helium embrittlement resistance of reduced activation martensitic steels". In: *Fusion Engineering and Design* 81.8-14 (Feb. 2006), pp. 1085–1090. ISSN: 09203796. DOI: 10.1016/j.fusengdes.2005.07.032.

[173] Takuya Yamamoto et al. "On the effects of irradiation and helium on the yield stress changes and hardening and non-hardening embrittlement of 8Cr tempered martensitic steels: Compilation and analysis of existing data". In: *Journal of Nuclear Materials* 356.1-3 (Sept. 2006), pp. 27–49. ISSN: 00223115. DOI: 10.1016/j.jnucmat.2006.05.041.

[174] T.E.G. Nicholas et al. "Re-examining the role of nuclear fusion in a renewables-based energy mix". In: *Energy Policy* 149 (Feb. 2021), p. 112043. ISSN: 03014215. DOI: 10.1016/j.enpol.2020.112043. arXiv: 2101.05727.

[175] H Tanigawa et al. "Status and key issues of reduced activation ferritic/martensitic steels as the structural material for a DEMO blanket". In: *Journal of Nuclear Materials* 417.1-3 (Oct. 2011), pp. 9–15. ISSN: 00223115. DOI: 10.1016/j.jnucmat.2011.05.023.

[176] Takanori Hirose et al. "Structural material properties and dimensional stability of components in first wall components of a breeding blanket module". In: *Fusion Engineering and Design* 83.7-9 (Dec. 2008), pp. 1176–1180. ISSN: 09203796. DOI: 10.1016/j.fusengdes.2008.06.023.

[177] Michael Rieth and Jörg Rey. "Specific welds for test blanket modules". In: *Journal of Nuclear Materials* 386-388 (Apr. 2009), pp. 471–474. ISSN: 00223115. DOI: 10.1016/j.jnucmat.2008.12.142.

[178] R. Lindau et al. "Mechanical and microstructural characterization of electron beam welded reduced activation oxide dispersion strengthened - Eurofer steel". In: *Journal of Nuclear Materials* 416.1-2 (Sept. 2011), pp. 22–29. ISSN: 00223115. DOI: 10.1016/j.jnucmat.2011.01.025.

[179] L. Commin et al. "Characterization of ODS (Oxide Dispersion Strengthened) Eurofer/Eurofer dissimilar electron beam welds". In: *Journal of Nuclear Materials* 442.1-3 (Nov. 2013), S552–S556. ISSN: 00223115. DOI: 10.1016/j.jnucmat.2012.11.019.

[180] Sanghoon Noh et al. "Microstructure and mechanical properties of friction stir processed ODS ferritic steels". In: *Journal of Nuclear Materials*. Vol. 417. 1-3. North-Holland, Oct. 2011, pp. 245–248. DOI: 10.1016/j.jnucmat.2011.01.059.

[181] Sanghoon Noh et al. "Diffusion bonding between ODS ferritic steel and F82H steel for fusion applications". In: *Journal of Nuclear Materials* 426.1-3 (July 2012), pp. 208–213. ISSN: 00223115. DOI: 10.1016/j.jnucmat.2012.02.024.

[182] Sanghoon Noh, Akihiko Kimura, and Tae Kyu Kim. "Diffusion bonding of 9Cr ODS ferritic/martensitic steel with a phase transformation". In: *Fusion Engineering and Design*. Vol. 89. 7-8. Elsevier Ltd, Oct. 2014, pp. 1746–1750. DOI: 10.1016/j.fusengdes.2013.12.023.

[183] S. Heuer et al. "Atmospheric plasma spraying of functionally graded steel/tungsten layers for the first wall of future fusion reactors". In: *Surface and Coatings Technology* 366 (May 2019), pp. 170–178. ISSN: 02578972. DOI: 10.1016/j.surfcoat.2019.03.017.

[184] R Viswanathan, R Purgert, and U Rao. "Materials technology for advanced coal power plants". In: *Advanced materials & processes* 162.8 (2004), pp. 73–76.

[185] L. Tan et al. "Microstructure control for high strength 9Cr ferritic-martensitic steels". In: *Journal of Nuclear Materials* 422.1-3 (Mar. 2012), pp. 45–50. ISSN: 00223115. DOI: 10.1016/j.jnucmat.2011.12.011.

[186] L. Tan et al. "Effect of thermomechanical treatment on 9Cr ferritic-martensitic steels". In: *Journal of Nuclear Materials* 441.1-3 (Oct. 2013), pp. 713–717. ISSN: 00223115. DOI: 10.1016/j.jnucmat.2013.01.323.

[187] L. Tan, Y. Yang, and J.T. Busby. "Effects of alloying elements and thermomechanical treatment on 9Cr Reduced Activation Ferritic-Martensitic (RAFM) steels". In: *Journal of Nuclear Materials* 442.1-3 (Nov. 2013), S13–S17. ISSN: 00223115. DOI: 10.1016/j.jnucmat.2012.10.015.

[188] T. Hirai et al. "Use of tungsten material for the ITER divertor". In: *Nuclear Materials and Energy* 9 (Dec. 2016), pp. 616–622. ISSN: 23521791. DOI: 10.1016/j.nme.2016.07.003.

[189] R. A. Pitts et al. "A full tungsten divertor for ITER: Physics issues and design status". In: *Journal of Nuclear Materials* 438.SUPPL (July 2013), S48–S56. ISSN: 00223115. DOI: 10.1016/j.jnucmat.2013.01.008.

[190] T. Wegener et al. "Development of yttrium-containing self-passivating tungsten alloys for future fusion power plants". In: *Nuclear Materials and Energy* 9 (Dec. 2016), pp. 394–398. ISSN: 23521791. DOI: 10.1016/j.nme.2016.07.011.

[191] Mingyue Zhao et al. "The investigation of Y doping content effect on the microstructure and microhardness of tungsten materials". In: *Materials Science and Engineering A* 618 (2014), pp. 572–577. ISSN: 09215093. DOI: 10.1016/j.msea.2014.09.053.

[192] Hong Yan Guo et al. "Nanostructured laminar tungsten alloy with improved ductility by surface mechanical attrition treatment". In: *Scientific Reports* 7.1 (Dec. 2017), pp. 1–11. ISSN: 20452322. DOI: 10.1038/s41598-017-01458-0.

[193] Yu Cheng Wu et al. *Preparation of ultrafine-grained/nanostructured tungsten materials: An overview*. Mar. 2019. DOI: 10.1016/j.jallcom.2018.11.279.

[194] J. Riesch et al. "Enhanced toughness and stable crack propagation in a novel tungsten fibre-reinforced tungsten composite produced by chemical vapour infiltration". In: *Physica Scripta* T159 (2014). ISSN: 02811847. DOI: 10.1088/0031-8949/2014/T159/014031.

[195] Jens Reiser et al. "Tungsten (W) Laminate Pipes for Innovative High Temperature Energy Conversion Systems". In: *Advanced Engineering Materials* 17.4 (2015), pp. 491–501. DOI: 10.1002/adem.201400204. eprint: https://onlinelibrary.wiley.com/doi/pdf/10.1002/adem.201400204.

[196] A. Litnovsky et al. "Advanced smart tungsten alloys for a future fusion power plant". In: *Plasma Physics and Controlled Fusion* 59.6 (2017). ISSN: 13616587. DOI: 10.1088/1361-6587/aa6948.

[197] J. Aktaa et al. "Manufacturing and joining technologies for helium cooled divertors". In: *Fusion Engineering and Design*. Vol. 89. 7-8. Elsevier Ltd, Oct. 2014, pp. 913–920. DOI: 10.1016/j.fusengdes.2014.01.028.

[198] G. De Temmerman et al. "An empirical scaling for deuterium retention in co-deposited beryllium layers". In: *Nuclear Fusion* 48.7 (July 2008), p. 075008. ISSN: 00295515. DOI: 10.1088/0029-5515/48/7/075008.

[199] Michael Gorley et al. "The EUROfusion materials property handbook for DEMO in-vessel components—Status and the challenge to improve confidence level for engineering data". In: *Fusion Engineering and Design* 158.March (2020), p. 111668. ISSN: 09203796. DOI: 10.1016/j.fusengdes.2020.111668.

[200] S. Konishi et al. "Functional materials for breeding blankets—status and developments". In: *Nuclear Fusion* 57.9 (Sept. 2017), p. 092014. ISSN: 0029-5515. DOI: 10.1088/1741-4326/aa7e4e.

[201] L. L. Snead et al. "Silicon carbide composites as fusion power reactor structural materials". In: *Journal of Nuclear Materials*. Vol. 417. 1-3. North-Holland, Oct. 2011, pp. 330–339. DOI: 10.1016/j.jnucmat.2011.03.005.

[202] T. Koyanagi et al. *Recent progress in the development of SiC composites for nuclear fusion applications*. Dec. 2018. DOI: 10.1016/j.jnucmat.2018.06.017.

[203] P. Norajitra et al. "The EU advanced lead lithium blanket concept using SiCf/SiC flow channel inserts as electrical and thermal insulators". In: *Fusion Engineering and Design* 58-59 (Nov. 2001), pp. 629–634. ISSN: 09203796. DOI: 10.1016/S0920-3796(01)00506-3.

[204] J.-W. Yeh et al. "Nanostructured High-Entropy Alloys with Multiple Principal Elements: Novel Alloy Design Concepts and Outcomes". In: *Advanced Engineering Materials* 6.5 (May 2004), pp. 299–303. ISSN: 1438-1656. DOI: 10.1002/adem.200300567.

[205] Jien-Wei Yeh. "Recent progress in high-entropy alloys". In: *Annales de Chimie Science des Matériaux* 31.6 (Dec. 2006), pp. 633–648. ISSN: 09473580. DOI: 10.3166/acsm.31.633-648. arXiv: 9809069v1 [arXiv:gr-qc].

[206] D. B. Miracle and O. N. Senkov. "A critical review of high entropy alloys and related concepts". In: *Acta Materialia* 122 (2017), pp. 448–511. ISSN: 13596454. DOI: 10.1016/j.actamat.2016.08.081.

[207] E. J. Pickering and N. G. Jones. "High-entropy alloys: a critical assessment of their founding principles and future prospects". In: *International Materials Reviews* 6608.May (2016), pp. 1–20. ISSN: 0950-6608. DOI: 10.1080/09506608.2016.1180020.

[208] B. Cantor et al. "Microstructural development in equiatomic multicomponent alloys". In: *Materials Science and Engineering A* 375-377.1-2 SPEC. ISS. (2004), pp. 213–218. ISSN: 09215093. DOI: 10.1016/j.msea.2003.10.257.

[209] E. J. Pickering et al. "Precipitation in the equiatomic high-entropy alloy CrMnFeCoNi". In: *Scripta Materialia* 113 (2016), pp. 106–109. ISSN: 13596462. DOI: 10.1016/j.scriptamat.2015.10.025.

[210] F. Otto et al. "Decomposition of the single-phase high-entropy alloy CrMnFeCoNi after prolonged anneals at intermediate temperatures". In: *Acta Materialia* 112 (2016), pp. 40–52. ISSN: 13596454. DOI: 10.1016/j.actamat.2016.04.005.

[211] Easo P. George, Dierk Raabe, and Robert O. Ritchie. "High-entropy alloys". In: *Nature Reviews Materials* 4.8 (2019), pp. 515–534. ISSN: 20588437. DOI: 10.1038/s41578-019-0121-4.

[212] Cláudio Geraldo Schön et al. "Probing the entropy hypothesis in highly concentrated alloys". In: *Acta Materialia* 148 (2018), pp. 263–279. ISSN: 13596454. DOI: 10.1016/j.actamat.2018.01.028.

[213] Duancheng Ma et al. "Ab initio thermodynamics of the CoCrFeMnNi high entropy alloy: Importance of entropy contributions beyond the configurational one". In: *Acta Materialia* 100 (2015), pp. 90–97. ISSN: 13596454. DOI: 10.1016/j.actamat.2015.08.050.

[214] Jien Wei Yeh. *Physical Metallurgy of High-Entropy Alloys*. Oct. 2015. DOI: 10.1007/s11837-015-1583-5.

[215] L. R. Owen et al. "An assessment of the lattice strain in the CrMnFeCoNi high-entropy alloy". In: *Acta Materialia* 122 (2017), pp. 11–18. ISSN: 13596454. DOI: 10.1016/j.actamat.2016.09.032.

[216] I. Toda-Caraballo et al. "Interatomic spacing distribution in multicomponent alloys". In: *Acta Materialia* 97 (2015), pp. 156–169. ISSN: 13596454. DOI: 10.1016/j.actamat.2015.07.010.

[217] Norihiko L. Okamoto et al. "Atomic displacement in the CrMnFeCoNi high-entropy alloy - A scaling factor to predict solid solution strengthening". In: *AIP Advances* 6.12 (2016). ISSN: 21583226. DOI: 10.1063/1.4971371.

[218] Juliusz Da browa and Marek Danielewski. "State-of-the-Art Diffusion Studies in the High Entropy Alloys". In: *Metals* 10.3 (Mar. 2020), p. 347. ISSN: 2075-4701. DOI: 10.3390/met10030347.

[219] Cláudio G. Schön et al. "On the complexity of solid-state diffusion in highly concentrated alloys and the sluggish diffusion core-effect". In: *Calphad: Computer Coupling of Phase Diagrams and Thermochemistry* 68.December 2019 (2020). ISSN: 03645916. DOI: 10.1016/j.calphad.2019.101713.

[220] K. Y. Tsai, M. H. Tsai, and J. W. Yeh. "Sluggish diffusion in Co-Cr-Fe-Mn-Ni high-entropy alloys". In: *Acta Materialia* 61.13 (2013), pp. 4887–4897. ISSN: 13596454. DOI: 10.1016/j.actamat.2013.04.058.

[221] A. Durand et al. "Interdiffusion in Cr–Fe–Co–Ni medium-entropy alloys". In: *Intermetallics* 122 (2020), p. 106789. ISSN: 09669795. DOI: 10.1016/j.intermet.2020.106789.

[222] Jien-Wei Yeh. "Alloy Design Strategies and Future Trends in High-Entropy Alloys". In: *JOM* 65.12 (Dec. 2013), pp. 1759–1771. ISSN: 1047-4838. DOI: 10.1007/s11837-013-0761-6.

[223] Yong Zhang et al. "Microstructures and properties of high-entropy alloys". In: *Progress in Materials Science* 61.September 2013 (2014), pp. 1–93. ISSN: 00796425. DOI: 10.1016/j.pmatsci.2013.10.001.

[224] Woei-Ren Wang, Wei-Lin Wang, and Jien-Wei Yeh. "Phases, microstructure and mechanical properties of AlxCoCrFeNi high-entropy alloys at elevated temperatures". In: *Journal of Alloys and Compounds* 589 (Mar. 2014), pp. 143–152. ISSN: 09258388. DOI: 10.1016/j.jallcom.2013.11.084.

[225] Tao Tsung Shun and Yu Chin Du. "Microstructure and tensile behaviors of FCC Al0.3CoCrFeNi high entropy alloy". In: *Journal of Alloys and Compounds* 479.1-2 (June 2009), pp. 157–160. ISSN: 09258388. DOI: 10.1016/j.jallcom.2008.12.088.

[226] Qing Wang et al. "A cuboidal B2 nanoprecipitation-enhanced body-centered-cubic alloy Al0.7CoCrFe2Ni with prominent tensile properties". In: *Scripta Materialia* 120 (July 2016), pp. 85–89. ISSN: 13596462. DOI: 10.1016/j.scriptamat.2016.04.014.

[227] Chin-You Hsu et al. "On the superior hot hardness and softening resistance of AlCoCrxFeMo0.5Ni high-entropy alloys". In: *Materials Science and Engineering: A* 528.10-11 (Apr. 2011), pp. 3581–3588. ISSN: 09215093. DOI: 10.1016/j.msea.2011.01.072.

[228] S. S. Al-Bermani et al. "The Origin of Microstructural Diversity, Texture, and Mechanical Properties in Electron Beam Melted Ti-6Al-4V". In: *Metallurgical and Materials Transactions A* 41.13 (Dec. 2010), pp. 3422–3434. ISSN: 1073-5623. DOI: 10.1007/s11661-010-0397-x.

[229] Tadashi Fujieda et al. "First demonstration of promising selective electron beam melting method for utilizing high-entropy alloys as engineering materials". In: *Materials Letters* 159 (Nov. 2015), pp. 12–15. ISSN: 0167577X. DOI: 10.1016/j.matlet.2015.06.046.

[230] Hiroshi Shiratori et al. "Relationship between the microstructure and mechanical properties of an equiatomic AlCoCrFeNi high-entropy alloy fabricated by selective electron beam melting". In: *Materials Science and Engineering: A* 656 (Feb. 2016), pp. 39–46. ISSN: 09215093. DOI: 10.1016/j.msea.2016.01.019.

[231] Yu Zhang et al. "Hot Deformation Behavior of As-Cast and Homogenized Al0.5CoCrFeNi High Entropy Alloys". In: *Metals* 6.11 (Nov. 2016), p. 277. ISSN: 2075-4701. DOI: 10.3390/met6110277.

[232] Che-Wei Tsai et al. "Deformation and annealing behaviors of high-entropy alloy Al0.5CoCrCuFeNi". In: *Journal of Alloys and Compounds* 486.1-2 (Nov. 2009), pp. 427–435. ISSN: 09258388. DOI: 10.1016/j.jallcom.2009.06.182.

[233] Chun Ng et al. "Entropy-driven phase stability and slow diffusion kinetics in an Al0.5CoCrCuFeNi high entropy alloy". In: *Intermetallics* 31 (Dec. 2012), pp. 165–172. ISSN: 09669795. DOI: 10.1016/j.intermet.2012.07.001.

[234] B. Gludovatz et al. "A fracture-resistant high-entropy alloy for cryogenic applications". In: *Science* 345.6201 (Sept. 2014), pp. 1153–1158. ISSN: 0036-8075. DOI: 10.1126/science.1254581.

[235] F Otto et al. "The influences of temperature and microstructure on the tensile properties of a CoCrFeMnNi high-entropy alloy". In: *Acta Materialia* 61.15 (Sept. 2013), pp. 5743–5755. ISSN: 13596454. DOI: 10.1016/j.actamat.2013.06.018.

[236] Jongun Moon et al. "On the strain rate-dependent deformation mechanism of CoCrFeMnNi high-entropy alloy at liquid nitrogen temperature". In: *Materials Research Letters* 5.7 (Nov. 2017), pp. 472–477. ISSN: 2166-3831. DOI: 10.1080/21663831.2017.1323807.

[237] G Laplanche et al. "Microstructure evolution and critical stress for twinning in the CrMnFeCoNi high-entropy alloy". In: *Acta Materialia* 118 (Oct. 2016), pp. 152–163. ISSN: 13596454. DOI: 10.1016/j.actamat.2016.07.038.

[238] Min Ji Jang et al. "Compressive deformation behavior of CrMnFeCoNi high-entropy alloy". In: *Metals and Materials International* 22.6 (Nov. 2016), pp. 982–986. ISSN: 1598-9623. DOI: 10.1007/s12540-016-6304-2.

[239] Zhifeng Lei et al. "Enhanced strength and ductility in a high-entropy alloy via ordered oxygen complexes". In: (2018). DOI: 10.1038/s41586-018-0685-y.

[240] Ed J. Pickering et al. "High-Entropy Alloys for Advanced Nuclear Applications". In: *Entropy* 23.1 (Jan. 2021), p. 98. ISSN: 1099-4300. DOI: 10.3390/e23010098.

[241] M. Caro et al. "Lattice thermal conductivity of multi-component alloys". In: *Journal of Alloys and Compounds* 648 (July 2015), pp. 408–413. ISSN: 09258388. DOI: 10.1016/j.jallcom.2015.06.035.

[242] Yanwen Zhang et al. "Influence of chemical disorder on energy dissipation and defect evolution in concentrated solid solution alloys". In: *Nature Communications* 6.1 (Oct. 2015), pp. 1–9. ISSN: 20411723. DOI: 10.1038/ncomms9736.

[243] Laurent Karim Béland et al. "Features of primary damage by high energy displacement cascades in concentrated Ni-based alloys". In: *Journal of Applied Physics* 119.8 (Feb. 2016), p. 085901. ISSN: 0021-8979. DOI: 10.1063/1.4942533.

[244] E. Levo et al. "Radiation damage buildup and dislocation evolution in Ni and equiatomic multicomponent Ni-based alloys". In: *Journal of Nuclear Materials* 490 (July 2017), pp. 323–332. ISSN: 00223115. DOI: 10.1016/j.jnucmat.2017.04.023.

[245] T. Egami et al. "Irradiation resistance of multicomponent alloys". In: *Metallurgical and Materials Transactions A: Physical Metallurgy and Materials Science*. Vol. 45. 1. Springer, Jan. 2014, pp. 180–183. DOI: 10.1007/s11661-013-1994-2.

[246] T. Egami et al. "Local Electronic Effects and Irradiation Resistance in High-Entropy Alloys". In: *JOM* 67.10 (Oct. 2015), pp. 2345–2349. ISSN: 15431851. DOI: 10.1007/s11837-015-1579-1.

[247] Wei Ying Chen et al. "Irradiation effects in high entropy alloys and 316H stainless steel at 300 °C". In: *Journal of Nuclear Materials* 510 (Nov. 2018), pp. 421–430. ISSN: 00223115. DOI: 10.1016/j.jnucmat.2018.08.031.

[248] Calvin Parkin et al. "In situ microstructural evolution in face-centered and body-centered cubic complex concentrated solid-solution alloys under heavy ion irradiation". In: *Acta Materialia* 198 (Oct. 2020), pp. 85–99. ISSN: 13596454. DOI: 10.1016/j.actamat.2020.07.066.

[249] Xin Xin Wang, Liang Liang Niu, and Shaoqing Wang. "Interpreting radiation-induced segregation and enhanced radiation tolerance of single-phase concentrated solid-solution alloys from first principles". In: *Materials Letters* 202 (Sept. 2017), pp. 120–122. ISSN: 18734979. DOI: 10.1016/j.matlet.2017.05.051.

[250] Shijun Zhao, G. Malcolm Stocks, and Yanwen Zhang. "Defect energetics of concentrated solid-solution alloys from ab initio calculations: Ni0.5Co0.5, Ni0.5Fe0.5, Ni0.8Fe0.2 and Ni0.8Cr0.2". In: *Physical Chemistry Chemical Physics* 18.34 (Aug. 2016), pp. 24043–24056. ISSN: 14639076. DOI: 10.1039/c6cp05161h.

[251] Kazuki Sugita et al. "Vacancy formation enthalpy in CoCrFeMnNi high-entropy alloy". In: *Scripta Materialia* 176 (Feb. 2020), pp. 32–35. ISSN: 13596462. DOI: 10.1016/j.scriptamat.2019.09.033.

[252] Tengfei Yang et al. "Structural damage and phase stability of Al0.3CoCrFeNi high entropy alloy under high temperature ion irradiation". In: *Acta Materialia* 188 (Apr. 2020), pp. 1–15. ISSN: 13596454. DOI: 10.1016/j.actamat.2020.01.060.

[253] B. Kombaiah et al. "Phase stability of single phase Al0.12CrNiFeCo high entropy alloy upon irradiation". In: *Materials and Design* 160 (Dec. 2018), pp. 1208–1216. ISSN: 18734197. DOI: 10.1016/j.matdes.2018.11.006.

[254] O. El-Atwani et al. "Outstanding radiation resistance of tungsten-based high-entropy alloys". In: *Science Advances* 5.3 (Mar. 2019), eaav2002. ISSN: 23752548. DOI: 10.1126/sciadv.aav2002.

[255] Maryam Sadeghilaridjani et al. "Ion irradiation response and mechanical behavior of reduced activity high entropy alloy". In: *Journal of Nuclear Materials* 529 (Feb. 2020), p. 151955. ISSN: 00223115. DOI: 10.1016/j.jnucmat.2019.151955.

[256] A. Kareer et al. "Short communication: 'Low activation, refractory, high entropy alloys for nuclear applications'". In: *Journal of Nuclear Materials* 526 (Dec. 2019), p. 151744. ISSN: 00223115. DOI: 10.1016/j.jnucmat.2019.151744.

[257] Michael Moschetti et al. "On the Room-Temperature Mechanical Properties of an Ion-Irradiated TiZrNbHfTa Refractory High Entropy Alloy". In: *JOM* 72.1 (Jan. 2020), pp. 130–138. ISSN: 15431851. DOI: 10.1007/s11837-019-03861-6.

[258] Dhinisa Patel et al. "Radiation damage tolerance of a novel metastable refractory high entropy alloy V2.5Cr1.2WMoCo0.04". In: *Journal of Nuclear Materials* 531 (Apr. 2020), p. 152005. ISSN: 00223115. DOI: 10.1016/j.jnucmat.2020.152005.

[259] Yao-Jen Chang and An-Chou Yeh. "The evolution of microstructures and high temperature properties of AlxCo1.5CrFeNi1.5Tiy high entropy alloys". In: *Journal of Alloys and Compounds* 653 (Dec. 2015), pp. 379–385. ISSN: 09258388. DOI: 10.1016/j.jallcom.2015.09.042.

[260] V Soare et al. "Influence of remelting on microstructure, hardness and corrosion behaviour of AlCoCrFeNiTi high entropy alloy". In: *Materials Science and Technology* 31.10 (July 2015), pp. 1194–1200. ISSN: 0267-0836. DOI: 10.1179/1743284715Y.0000000029.

[261] Yao Qiu et al. "Corrosion of high entropy alloys". In: *npj Materials Degradation* 1.1 (Dec. 2017), p. 15. ISSN: 2397-2106. DOI: 10.1038/s41529-017-0009-y.

[262] Q. H. Li et al. "Microstructure and Corrosion Properties of AlCoCrFeNi High Entropy Alloy Coatings Deposited on AISI 1045 Steel by the Electrospark Process". In: *Metallurgical and Materials Transactions A* 44.4 (Apr. 2013), pp. 1767–1778. ISSN: 1073-5623. DOI: 10.1007/s11661-012-1535-4.

[263] Owais Ahmed Waseem et al. "The effect of Ti on the sintering and mechanical properties of refractory high-entropy alloy TixWTaVCr fabricated via spark plasma sintering for fusion plasma-facing materials". In: *Materials Chemistry and Physics* 210 (May 2018), pp. 87–94. ISSN: 02540584. DOI: 10.1016/j.matchemphys.2017.06.054.

[264] Owais Ahmed Waseem and Ho Jin Ryu. "Powder Metallurgy Processing of a WxTaTiVCr High-Entropy Alloy and Its Derivative Alloys for Fusion Material Applications". In: *Scientific Reports* 7.1 (Dec. 2017), p. 1926. ISSN: 2045-2322. DOI: 10.1038/s41598-017-02168-3.

[265] Xin Xian et al. "A high-entropy V35Ti35Fe15Cr10Zr5 alloy with excellent high-temperature strength". In: *Materials and Design* 121 (May 2017), pp. 229–236. ISSN: 18734197. DOI: 10.1016/j.matdes.2017.02.029.

[266] A. Ayyagari et al. "Low activation high entropy alloys for next generation nuclear applications". In: *Materialia* 4 (Dec. 2018), pp. 99–103. ISSN: 2589-1529. DOI: 10.1016/J.MTLA.2018.09.014.

[267] Amy S. Gandy et al. "High Temperature and Ion Implantation-Induced Phase Transformations in Novel Reduced Activation Si-Fe-V-Cr (-Mo) High Entropy Alloys". In: *Frontiers in Materials* 6 (June 2019), p. 146. ISSN: 2296-8016. DOI: 10.3389/fmats.2019.00146.

[268] A. W. Carruthers et al. “Novel reduced-activation TiVCrFe based high entropy alloys”. In: *Journal of Alloys and Compounds* 856 (Mar. 2021), p. 157399. ISSN: 09258388. DOI: 10.1016/j.jallcom.2020.157399.

Chapter 3

Experimental methods

3.1 Introduction

This chapter presents a summary of the experimental techniques used in this work. It is merely intended to outline the basic principles behind the techniques and explain why they were used. It is not meant as an exhaustive description of how each technique functions or of the underlying scientific principles. Nor is it intended to be a detailed description of the experimental parameters utilised, which will instead be presented in the relevant experimental chapters.

3.2 Laboratory techniques

3.2.1 Arc melting

Arc melting is a procedure that uses resistive heating from a high current electric arc to melt solid lumps of material contained in a water-cooled copper crucible, all performed under an inert argon atmosphere. In theory, this liquefaction allows for all the components in the crucible to become mixed together and form a disordered liquid phase, which will then rapidly solidify when the arc is stopped. Due to the short melting time, small amount of material required (typically tens of grams) and the lack of preparation required for the source material, arc melting is a technique well suited to prototyping a variety of alloys in small pieces.

However, the technique is not without its drawbacks. Ideally, all of the pieces will be fully melted and homogeneously mixed. In practice, some pieces can remain unmelted and inhomogeneities will be left in the slug produced. This effect can be particularly prominent when metals with large differences in melting points are mixed. This difficulty can be overcome by physically inverting the slug and remelting several times.

Manganese, a major constituent of the alloys studied in this work, can undergo

severe evaporation when it is used in an arc melter, amounting to several wt.%. This loss can be offset by adding excess manganese (with respect to the intended final composition) to the mixture, and quantified by measuring the weight lost after melting, but obtaining even moderately precise compositions is a challenge.

As metals in their liquid state possess a far greater solubility for gas atoms than in solid state, there is a possibility that impurity gas atoms get introduced to the mixture during melting. This can lead to them being trapped as interstitial impurities upon solidification, either in the metallic solid solution or as new phases.

3.2.1.1 Manganese pickling

Manganese suffers from an additional problem in that it rapidly oxidises in the presence of air, producing a thick brown film. Unfortunately, chemical suppliers tend to supply manganese pieces in this oxidised state, so further treatment is necessary to avoid introducing oxygen impurities into the melt. The oxide can be removed immersing the pieces for several minutes in a 90:10 mixture of ethanol and nitric acid. The pieces can then be washed, dried and quickly placed in the arc melter before any significant oxidation occurs.

3.2.2 Sample preparation

The slugs produced from arc melting were sectioned into smaller pieces using an abrasive cutting wheel. These pieces were heat treated as described in the next section and then further prepared for examination using standard metallurgical techniques. This procedure involves further sectioning (if necessary) and mounting in a hard plastic resin. Samples are then ground flat using abrasive paper of progressively finer grit and polishing with diamond paste. Final preparation for microscopy involved using an oxide polishing suspension (OPS) for several minutes. This process produces a highly polished surface on which microstructural features (such as different phases, precipitates and even grains) are clearly visible under microscopy.

3.2.3 Heat treatment

Care must be taken to avoid any adverse chemical reactions at high temperatures during heat treatment, or to avoid impurity elements from the atmosphere finding their way into the sample. This is particularly true in the case of alloys with significant vanadium content, where there is a possibility of forming vanadium pentoxide. This oxide is not only toxic but also has a low melting point (680 °C), which could lead to extremely rapid oxidation as the oxide melts away if exposed to air at high temperatures.

To counteract this, heat treatments were performed by first encapsulating the samples in quartz tubes which were then backfilled with 0.1 atmospheres of argon (sub atmospheric pressure is used to avoid explosion of tubes when temperature is raised). In order to getter any remaining oxygen impurities, the samples were also wrapped in zirconium foil before encapsulation.

3.2.3.1 Water quenching

In order to ensure the microstructure observed representative of the heat treatment temperature, the samples were quickly water quenched to ensure no microstructural changes could evolve during cooling. When heat treatment was complete, the samples were dumped into a bucket of room temperature water and the encapsulating tubes were cracked open. After quenching, most samples had some degree of oxidation varying from a slight discolouration to a thick black film. It is thought that this oxidation occurred when the tubes were cracked open and the still hot metal was expose to water.

3.2.3.2 Homogenisation times

To ensure an equilibrium microstructure, samples should be homogenised at a high temperature for an extended period of time followed by a quench, to anneal out any metastable microstructures that arise from the rapid heating and cooling of the arc melter. Ideally, this should be performed just below the solidus temperature, but the use of quartz glass imposed a temperature limit of 1200 °C to prevent the glass from softening and potentially rupturing.[1]

Annealing times of the order of 100 hours are common in refractory HEA literature [1, 2, 3, 4]. In order to determine if such a timescale was appropriate for these alloys, diffusion coefficients of various binary pairs were used to find characteristic diffusion distances using equation 3.1. The results of this calculation are shown in table 3.1.

$$d = \sqrt{Dt} \tag{3.1}$$

The shortest diffusion distance was that of chromium in pure vanadium, of the order of 10 µm. No elemental segregation was observed in the alloys in the as-cast state (see Chapter 4), but the microstructural features that were observed (i.e. the precipitates) were also separated by distances of the order of 10 µm. If these precipitates were to dissolve, then 100 hours at 1200 °C would be sufficient to ensure chemical homogeneity, assuming that the most sluggish binary pairing is representative of the minimum diffusion. As seen in Chapter 2, the diffusion behaviour of multi-principal element alloys is complex so these binaries may not be representative. However, in the

[1] Higher temperature anneals were attempted using unencapsulated samples in a vacuum furnace. However, melting of the alloys occurred and this technique was not pursued any further.

absence of more detailed diffusion data and also in the interests of saving experimental time, a 100 hour anneal was deemed sufficient.

System	Temperature / °C	D / m^2 s^{-1}	d / µm	Ref
Ti in V-10%Ti	1200	3.96×10^{-15}	37.8	[5]
V in V-10%Ti	1200	7.47×10^{-13}	519	[5]
Cr in pure V	1170	4.19×10^{-16}	12.3	[6]
Cr in Ti-18%Cr	1178	18.3×10^{-13}	812	[7]
Mn in Ti-14%Mn	1200	5.14×10^{-12}	1360	[8]

Table 3.1: Diffusion parameters for selected element binary systems.

3.2.4 Optical microscopy

Samples were initially inspected optically for ease of examination. However, the magnification and range of information obtainable compared to electron microscopy meant that it was only used for checking that samples were adequately prepared and observation of large features such as hardness testing indents.

3.2.5 X-ray diffraction

X-ray diffraction (XRD) was used to identify phases present in samples and to measure their lattice parameter. Simple 2θ scans were performed to find peaks in intensity, which can be matched with phases present. As the intensity of the lab diffractometers used were relatively low (c.f. synchrotron sources), detection limits are of the order of 1% by volume. This makes laboratory XRD unsuitable for characterising precipitates which only constitute a small proportion of the alloy studied.

Lattice parameters of the body centred cubic (BCC) phase were determined by fitting the diffraction peaks in HiScore XRD analysis software. The positions of the peaks were then used to refine the lattice parameter using a least squares regression.

3.2.6 Secondary electron microscopy

Secondary electron microscopy (SEM) was the primary method of microstructural investigation used in this work. The reason for its prevalence is that it can achieve much finer resolutions than optical microscopes, and that it can also give chemical and microstructural information about the sample investigate using the techniques described below. SEMs also allow for easier investigation of numerous samples, as the relatively large chamber can hold multiple samples that have undergone standard metallographic preparation (described above). This is in contrast to TEM (see section 3.2.7) which can only hold a single sample.

Element	Kα energy / keV	Kβ energy / keV
Ti	4.512	4.933
V	4.953	5.428
Cr	5.415	5.947
Mn	5.900	6.492

Table 3.2: X-ray emission energies of selected elements.

3.2.6.1 Energy dispersive X-ray spectroscopy

Energy dispersive X-ray (EDX) analysis was used to obtain the chemical composition of SEM samples by measuring the energy spectra of the X-rays given off from excited electrons in the atoms. The elements used in this study have characteristic X-ray energies that are very close in value to other elements (see table 3.2). For example, the Kβ energy of Cr is 5.947 keV and the Kα energy of Mn is 5.900 keV, well within the limits of the energy resolution (120 - 130 eV) in commercial EDX systems[9].

3.2.6.2 Wavelength dispersive spectroscopy

Accurate chemical composition was obtained through the use of wavelength dispersive spectroscopy instead. WDS systems are fitted to SEMs (often specialised microscopes with higher beam currents that are more suitable for chemical analysis) . WDS provides a much finer energy resolution (approximately 6 eV for the Fe Kα peak[10]) than EDX and is better suited for quantitatively analysing the compositions of alloys containing elements with overlapping peaks.

It is also able to quantify the concentrations of light elements in samples as it is able to between the Kα peaks of lighter elements that often overlap with the Lα peaks of transition metals. The higher beam current afforded by the SEM which contains the WDS system enables detection of elements present in low concentrations, as it allows for more X-ray counts to be collected in the same time frame.

3.2.6.3 Electron backscatter diffraction

Electron backscatter diffraction (EBSD) is a technique that works in conjunction with SEM to provide crystallographic information. Specialised detectors fitted inside an SEM can pick up diffraction bands present in the backscattered electron signal. By using computer software to fit the band patterns to simulated models, the lattice parameters and crystallographic orientation of the region of interest can be determined.

Although EBSD is a powerful technique, it is often limited by the crystal database used in the fitting software and sensitivity to sample preparation. It is also relatively time intensive; mapping regions of interest can take several hours depending on desired resolution.

3.2.7 Transmission electron microscopy

Transmission electron microscopy (TEM) was also used for investigation of samples. It has a higher resolution to SEM so allows for finer microstructural features to be detected. Although a variety of investigative techniques can be employed using a TEM, this work mostly relied on scanning transmission electron microscopy (STEM) in conjunction with EDX, and convergent beam electron diffraction (CBED). STEM-EDX was used to produce elemental maps of small regions of interest such as fine precipitates and grain boundaries, whereas CBED was used to produce diffraction patterns to aid in phase identification.

3.2.7.1 Sample preparation

Electropolishing As the alloys produced have not been previously, initial TEM sample preparation was done using electropolishing in a perchloric acid-methanol solution. Electropolishing did produce electron transparent samples but suffered from some problems. The precipitates didn't polish at the same rate as the matrix and were too thick for diffraction. Additionally, some precipitates fell out of the matrix, leaving gaps in the sample. Finally, the brittleness of the alloys meant that polished discs were extremely fragile and could be broken by routine handling, necessitating the production of several discs per sample.

Mechanical polishing Mechanical polishing was also trialled as an alternative method for producing TEM discs. However, the brittleness of the alloys meant that samples frequently broke, and their hardness meant that polishing just one sample took much longer than the equivalent electropolishing procedure. Moreover, further treatment using a plasma polisher was required after mechanically polishing. For these reasons, mechanical polishing was avoided for TEM sample preparation.

Plasma polishing In addition to being a finishing procedure for mechanical polishing, plasma polishing was used to improve the quality of electropolished samples by further thinning them. This allowed previously electron opaque areas of discs (in particular precipitates) to produce diffraction patterns.

Focused ion beam Milling out samples using a focused ion beam (FIB) is a technique more suited to fabricating smaller TEM foils from a specific area of a sample. As the target area is selected using an SEM, particular regions of interest could be chosen, such as a particular type of precipitate or phase.

3.2.8 Hardness testing

The main method of mechanical testing performed to samples was a simple Vickers hardness indentation test. Micro and macro scale testing was performed, using loads of 9.8 N and 196 N respectively. Hardness testing offers a simple way of estimating a materials strength. It can also provide a qualitative assessment of a materials ductility based on whether cracking is observed (which is the case for brittle materials). However, more quantitative information requires other forms of mechanical testing to be performed.

3.2.9 Oxidation

Oxidation of samples was performed in air using a tube furnace. A tube furnace was chosen over a conventional muffle furnace as it is able to provide more consistent temperature over long periods of time. As the formation of toxic and potentially volatile vanadium pentoxide was believed to be a risk (see Chapter 6), all oxidation work was carried out with the furnace situated in a fume hood. Temperatures throughout the length of the tube were measured using a thermocouple to determine the position of the hot zone where temperatures were within an acceptable range of values for the experiment.

Samples were placed in porcelain boats before being inserted into the furnace. Ideally, each sample would be placed in an individual pre-weighed boat so that the total weight change of the sample, including any potential spalled oxide films, could be measured. However, due to space constraints inside the tube, several samples were instead placed in one boat so that multiple oxidations could be performed in the limited time that was left for the final section of this work.

3.3 Computational methods

3.3.1 CALPHAD

CALPHAD (or the CALculation of PHAse Diagrams) is a methodology which uses thermodynamic models to compute the equilibrium phase diagrams for a given set of conditions (e.g. an alloy with a specific composition). From this, the equilibrium phases present at different temperatures can be extracted.

As CALPHAD techniques are able to much more quickly assess the properties of alloys than other atomistic techniques such as density functional theory and molecular dynamics, they offer the ability to narrow down the infinitely vast phase space occupied by HEAs. More advanced CALPHAD techniques are also able to predict more than just phase stability, with predictions of diffusion behaviour and properties now possible[11,

12].

However, the speed at which CALPHAD can assess alloys comes at the expense of accuracy. For narrow, well-characterised alloy systems (such as steels and nickel superalloys), CALPHAD can offer excellent predictive power and is regularly used for designing new alloys[13, 14]. Even the most well studied of HEA systems, however, have only been characterised for a comparatively limited range of temperatures and compositions. Not to mention the vast array of exploratory systems to have been barely been characterised, or have only been studied in a metastable state. Analysis of CALPHAD results in multicomponent (i.e. N>3) systems has revealed that a correct description of the relevant ternary systems is generally a requisite for high quality descriptions of the system[15].

Nevertheless, CALPHAD was still used owing to the relatively simplicity and speed at which predictions can be made. The CALPHAD package chosen for this work was Thermocalc, as it has a HEA database (TCHEA) available for use. This database has all the relevant binary systems assessed, and some of the ternary systems[16]. Also of use was the TCPython module, which allowed Python code to interact with the Thermocalc API. Instead of manually entering the compositions to be assessed, a Python script was written to run multiple alloys in succession, then export and plot the phases present.

3.3.2 FISPACT

FISPACT-II[17] is a nuclear inventory code that calculates what nuclides will be present in a material after exposure to a radiation flux or series of fluxes. When used in conjunction with nuclear data libraries, FISPACT-II is able to give a wide variety of information about an irradiated material including: transmutation products, radioactivity, equivalent dose, thermal output power and primary knock-on atom energy spectra. All of this information is calculated at a series of time intervals given by the user, so evolution of all of these properties can be easily observed as a function of time.

A Python module called Pypact was used to generate the input files and parse the output data into a more readable format. As activation properties are a key motivation for this project, the use of FISPACT-II allowed direct calculation of activation properties in response to specific fusion spectra, rather than just extrapolation from already calculated data.

References

[1] Amy S. Gandy et al. “High Temperature and Ion Implantation-Induced Phase Transformations in Novel Reduced Activation Si-Fe-V-Cr (-Mo) High Entropy

Alloys". In: *Frontiers in Materials* 6 (June 2019), p. 146. ISSN: 2296-8016. DOI: 10.3389/fmats.2019.00146.

[2] B. Kombaiah et al. "Phase stability of single phase Al0.12CrNiFeCo high entropy alloy upon irradiation". In: *Materials and Design* 160 (Dec. 2018), pp. 1208–1216. ISSN: 18734197. DOI: 10.1016/j.matdes.2018.11.006.

[3] F Otto et al. "The influences of temperature and microstructure on the tensile properties of a CoCrFeMnNi high-entropy alloy". In: *Acta Materialia* 61.15 (Sept. 2013), pp. 5743–5755. ISSN: 13596454. DOI: 10.1016/j.actamat.2013.06.018.

[4] A. W. Carruthers et al. "Novel reduced-activation TiVCrFe based high entropy alloys". In: *Journal of Alloys and Compounds* 856 (Mar. 2021), p. 157399. ISSN: 09258388. DOI: 10.1016/j.jallcom.2020.157399.

[5] J. F. Murdock and C. J. McHargue. "Self-diffusion in body-centered cubic titanium-vanadium alloys". In: *Acta Metallurgica* 16.4 (1968), pp. 493–500. ISSN: 00016160. DOI: 10.1016/0001-6160(68)90123-5.

[6] J. Pelleg. "The Influence of Interstitial Impurity on Diffusion in Vanadium. Cr Diffusion in Vanadium". In: *Physica Status Solidi (a)* 147.2 (1995), pp. 361–371. ISSN: 1521396X. DOI: 10.1002/pssa.2211470207.

[7] A. J. Mortlocks and D. H. Tomlm. "The atomic diffusion of chromium in the titanium-chromium system". In: *Philosophical Magazine* 4.41 (1959), pp. 628–643. ISSN: 00318086. DOI: 10.1080/14786435908238259.

[8] Xiang Huang et al. "Experimental Diffusion Research on BCC Ti-Mn Binary and Ti-Al-Mn Ternary Alloys". In: *Journal of Phase Equilibria and Diffusion* 39.5 (2018), pp. 702–713. ISSN: 15477037. DOI: 10.1007/s11669-018-0675-7.

[9] Nicolas Brodusch, Karim Zaghib, and Raynald Gauvin. "Improvement of the energy resolution of energy dispersive spectrometers (EDS) using Richardson–Lucy deconvolution". In: *Ultramicroscopy* 209 (Feb. 2020), p. 112886. ISSN: 18792723. DOI: 10.1016/j.ultramic.2019.112886.

[10] Anwar Ul-Hamid et al. "Quantitative WDS analysis using electron probe microanalyzer". In: *Materials Characterization* 56.3 (2006), pp. 192–199. ISSN: 10445803. DOI: 10.1016/j.matchar.2005.11.007.

[11] U. R. Kattner and C. E. Campbell. "Invited review: Modelling of thermodynamics and diffusion in multicomponent systems". In: *Materials Science and Technology* 25.4 (Apr. 2009), pp. 443–459. ISSN: 0267-0836. DOI: 10.1179/174328408X372001.

[12] Renhai Shi and Alan A. Luo. "Applications of CALPHAD modeling and databases in advanced lightweight metallic materials". In: *Calphad: Computer Coupling of Phase Diagrams and Thermochemistry* 62 (Sept. 2018), pp. 1–17. ISSN: 03645916. DOI: 10.1016/j.calphad.2018.04.009.

[13] Trevor Keller et al. "Application of finite element, phase-field, and CALPHAD-based methods to additive manufacturing of Ni-based superalloys". In: *Acta Materialia* 139 (Oct. 2017), pp. 244–253. ISSN: 13596454. DOI: 10.1016/j.actamat.2017.05.003. arXiv: 1705.02016.

[14] Sung Chul Cha et al. "CALPHAD-based alloy design for advanced automotive steels - Part I: Development of bearing steels with enhanced strength and optimized microstructure". In: *Calphad: Computer Coupling of Phase Diagrams and Thermochemistry* 54 (Sept. 2016), pp. 165–171. ISSN: 03645916. DOI: 10.1016/j.calphad.2016.04.007.

[15] Stéphane Gorsse and Oleg Senkov. "About the Reliability of CALPHAD Predictions in Multicomponent Systems". In: *Entropy* 20.12 (Nov. 2018), p. 899. ISSN: 1099-4300. DOI: 10.3390/e20120899.

[16] Thermo-Calc Software. *TCHEA4 Technical Information*. 2021.

[17] UK Atomic Energy Agency. *FISPACT-II*. 2021.

Chapter 4

Towards V-based high-entropy alloys for nuclear fusion applications

P.J. Barron[1], A.W. Carruthers[1], J.W. Fellowes[1], N.G. Jones[2], H. Dawson[3], and E.J. Pickering[1]

[1]Department of Materials, University of Manchester, Oxford Road, Manchester, M13 9PL, UK

[2]Department of Materials Science and Metallurgy, University of Cambridge, 27 Charles Babbage Road, Cambridge, CB3 0FS, UK

[3]Culham Centre for Fusion Energy, Abingdon, OX14 3DB, UK

Foreword

This chapter is presented as published in *Scripta Materialia* Volume 176, February 2020, pages 12-16. Conceptualisation was done by P.J.B. and E.J.P. As-cast alloys were supplied and fabricated by N.G.J. TEM was performed by A.W.C. WDS was performed by J.W.F. All other experimental methods listed were carried out by P.J.B. Manuscript was written by P.J.B with minor revisions from all authors. Supplementary information published alongside the article is presented in Section 4.2. Additional detail is provided in Section 4.3 due to length constraints in the manuscript specified by the publisher and also due to the fact the additional information did not contribute directly to the key conclusions of the paper.

4.1 Manuscript

Abstract

By mixing elements with favourable nuclear activation properties to create high-

entropy alloys, it may be possible to create a material that can withstand a nuclear fusion environment while minimising the radioactive waste produced. Such a material could be used in the extreme thermal and irradiation conditions of a fusion blanket. A suite of previously unexplored V-Cr-Mn and V-Cr-Mn-Ti alloys have been fabricated then homogenised and the resultant microstructures and phases were characterised. Results demonstrate that single-phase body centred cubic solid solution microstructures can be formed in highly-concentrated alloys incorporating low-activation elements, which is promising for a fusion alloy development standpoint.

Nuclear fusion offers an alternative low-carbon energy source with potentially abundant fuel. However, fusion reactors must minimise the amount of harmful radioactive waste they produce in order to be considered a truly green energy source. This criteria necessitates the use of low-activation alloys, made from elements that will not remain radioactive for extended periods of time after exposure to fusion neutrons.

The structural material of a fusion reactor blanket also has to face a variety of hostile conditions, including: extremes of neutron irradiation and temperature, transient loading from plasma instabilities, and corrosion from coolant systems[1]. These conditions necessitate the use of a material that is sufficiently strong, with good irradiation and creep resistance. The blanket will also require thousands of tons of material, precluding the use of extremely costly or scarce elements as significant alloying additions, or alloys that cannot be processed on large scales. Further restrictions are imposed by the aforementioned desire to use low-activation elements. Table 4.1 shows the calculated time taken for selected elements to reach UK low-level waste (LLW) ($<4\,\mathrm{MBq\,kg^{-1}}$ alpha radiation and $<12\,\mathrm{MBq\,kg^{-1}}$ combined gamma and beta radiation) after 5 years of pulsed operation in the DEMO reactor divertor body[2]. Although the divertor will be exposed to a greater fluence of neutrons, these values are still representative of their relative activities when used in a fusion blanket. It is apparent that certain elements such as Ni or Zr which are commonly used for nuclear structural applications would be unacceptable from a waste-management perspective.

Research efforts for fusion structural materials have been primarily focused on reduced activation ferritic-martensitic (RAFM) steels and vanadium alloys[3, 4, 5]. However, RAFM steels have a relatively low maximum operating temperature, limited by creep[6]. Their oxide dispersion strengthened counterparts offer improved high temperature performance but large scale processing is still an issue[4]. V-based alloys containing other elements as minor ($<10\,\mathrm{at.\%}$) additions have been explored as an alternative to steels for fusion blanket applications[3]. However, high-entropy alloys (HEAs) containing multiple low-activation elements have received very little attention. A recent study by Ayyagari et al.[7] examined the Ta-Ti-V-Zr-X system, but here we avoid Zr owing to its activation properties listed in Table 4.1. Investigation of more

Element	Time to LLW / yrs	Element	Time to LLW / yrs	Element	Time to LLW / yrs
C	99	**V**	**54**	Zn	1.1×10^3
N	9.4×10^4	**Cr**	**40**	Y	21
O	1.1×10^4	**Mn**	**86**	Zr	$> 10^6$
Mg	97	Fe	59	Nb	2.9×10^5
Al	157	Co	184	Mo	8.7×10^5
Si	58	Ni	6.6×10^5	Ta	41
Ti	**10**	Cu	1.3×10^3	W	23

Table 4.1: Calculated time taken to reach UK LLW for selected elements after use in a DEMO reactor divertor. Elements used in this study have been highlighted. Data taken from [2].

concentrated alloys covering unexplored compositional space may yield materials that are more processable and have enhanced properties in comparison to the more conventional alloys. Other HEAs have shown surprising toughness[8] and irradiation swelling properties[9], so it is hoped that this work may form the basis for developing fusion alloys with improved properties such as a larger operating temperature window or easier processing.

Due to the favourable activation properties of their constituent elements, alloys in the V-Cr-Mn ternary and V-Cr-Mn-Ti system were investigated. The nominal compositions are shown in Table 4.2. V and Cr were chosen because of their high melting points, which will allow for good creep performance at elevated temperatures in comparison to Fe-based alloys[6]. V and Cr show complete mutual solubility, forming a bcc phase at all compositions below the solidus[10]. A single bcc phase is considered highly desirable for adequate resistance to neutron irradiation swelling[11, 12, 13]. Additionally, Cr provides improved oxidation resistance in the binary system above around 30 wt.%[10]. Such environmental resistance will be useful in limiting corrosion in service as well as in processing.

Mn was chosen as an extra element in working towards a HEA composition because the binary V-Mn and Cr-Mn diagrams show a good solubility of Mn in both Cr and V[14]. The V-Cr-Mn ternary is not well characterized, but the one ternary diagram available in the literature seems to agree that Mn should have good solubility in an alloy containing V and Cr[15]. Although the power of the entropic stabilisation effect in HEAs is disputed [16, 17], the addition of Mn to a mixture of V and Cr will increase the configurational entropy of a solid solution of the elements and, therefore, should increase its high-temperature stability. It was hoped that the stability of the solid solution would be increased sufficiently to allow for the introduction of higher concentration of elements like Ti (see below) with less propensity to form damaging intermetallics, such as Laves phases (which appear in the Ti-Mn and Ti-Cr binary [14]) or secondary

solid solutions. Fe was not considered, despite being bcc and low-activation, as it is known to readily form undesirable sigma phases with Cr[18].

Finally, Ti was added to act as an impurity getter in a similar manner to the behaviour found in V-Cr-Ti alloys[3, 19, 20] and interstitial free steels[21]. A reduction of interstitial solute concentration is desirable as they are known to cause embrittlement in vanadium alloys[22]. However, high quantities of both Cr and Ti are known to embrittle vanadium alloys[23, 24]. Furthermore, observation of the Ti-Mn and Ti-Cr binary phase diagrams suggests that Ti has low solubility in these two elements[14]. For these reasons, the amount of Ti added to the alloys was limited to 8 at.%. Although the alloys studied here contain fewer elements than necessary to be considered HEAs, and may instead be referred to as multi-principle element alloys (MPEAs), it is hoped they will contribute towards the development of true HEAs for fusion applications.

Nominal				Measured (EPMA)			
V	Cr	Mn	Ti	V	Cr	Mn	Ti
60	20	20	-	63.04 ± 0.07	20.58 ± 0.03	16.39 ± 0.09	-
40	20	40	-	39.40 ± 0.24	21.60 ± 0.17	39.01 ± 0.08	-
40	40	20	-	41.08 ± 0.22	43.20 ± 0.35	15.73 ± 0.14	-
33.33	33.33	33.33	-	32.80 ± 0.28	35.53 ± 0.29	31.68 ± 0.04	-
33	33	33	1	42.03 ± 0.03	40.89 ± 0.05	15.69 ± 0.07	1.38 ± 0.01
32.67	32.67	32.67	2	35.82 ± 0.16	36.08 ± 0.15	25.10 ± 0.11	3.00 ± 0.42
32	32	32	4	34.53 ± 0.02	32.09 ± 0.02	27.92 ± 0.02	5.45 ± 0.05
30.67	30.67	30.67	8	35.84 ± 0.18	29.95 ± 0.12	25.52 ± 0.03	8.68 ± 0.32

Table 4.2: Nominal and measured alloy compositions. Values are in at.% with absolute standard errors shown.

Eight alloys were fabricated as ingots weighing approximately 25 g using an arc melting process in an argon atmosphere. The ingots were inverted and remelted three times to ensure homogeneity. Sections of each ingot were cut off, wrapped in tantalum foil, and then encapsulated in a quartz ampoule backfilled with low pressure argon. These samples then underwent a homogenisation heat treatment at 1200 °C for 100 hours, before quenching in water.

Secondary electron microscopy (SEM) specimens were prepared using standard metallographic techniques. The final polish was performed with an 0.06 μm oxide polishing suspension. Back scattered electron (BSE) images were obtained using a Zeiss Ultra55 microscope at 10 kV. Transmission electron microscopy (TEM) foils were produced by electropolishing punched sections of thin foils in a 5% perchloric acid-methanol solution with a temperature of -40 °C using a Tenupol 5 twin jet electropolisher at a voltage of 29 V. Further plasma polishing was performed using a Gatan PIPS II Model 695 polisher with conditions ranging from 1000 V for 20 minutes down to 100 V for two hours. A ThermoScientific Talos TEM with an accelerating voltage of 200 kV was used

to produce annular dark field (ADF) images and energy dispersive X-ray (EDX) maps. Wavelength dispersive spectroscopy (WDS) was performed using a JEOL JXA-8530F FEG electron probe microanalyser (EPMA). Quantification was performed at 20 kV, 10 nA for Ti Kα, V Kα, Cr Kα and Mn Kβ standardised against pure metals. 100 composition measurements were randomly taken from an area 500 μm in radius for each sample. Overlap corrections were applied to the raw X-ray intensities where required (Ti Kβ on V Kα, V Kβ on Cr Kα) and corrected iteratively using the PAP phi-rho-Z matrix correction routine using NIST FFAST mass absorption coefficients. X-ray maps were conducted at 10 kV and 163 nA (V-40Cr-20Mn, Fig. 2) and 46 nA (V-Cr-Mn-8%Ti, Fig. 3). Vickers hardness measurements were taken with a load of 9.8 N and dwell time of 10 s using a Matsuzawa MMT-X indenter. Nine hardness measurements were made spaced 0.5 mm apart in a three by three grid formation.

WDS analysis suggests that there is a difference between the intended alloy composition and what is found in practice (see Table 4.2). In particular, the at.% of Mn is lower than expected in all alloys. This is likely to be caused by the low vapour pressure of Mn, leading to evaporation during the arc melting process.

BSE images (Fig. 4.1) of the alloys show a microstructure consisting of a light grey matrix with darker precipitates. The precipitates found in the ternary alloys (Fig. 4.1 (a) to (d)) are a mixture of larger, more rounded shapes which appear along grain boundaries, and smaller long and thin precipitates that are intragranular. The quaternary alloys have much finer precipitates (Fig. 4.1 (e) to (h)). The matrix appeared as a single phase in all alloys. This was confirmed to be bcc (a = 2.90 - 3.04 Å) through X-ray (see supplementary information) and TEM diffraction. These microstructures and lattice parameters are consistent with observations of a bcc Ti-V-Cr-Mn alloy with differing composition, used for hydrogen storage[25].

WDS was utilised to determine the composition of the matrix and precipitate phases. The matrix appeared to be a homogeneous mixture of the constituent metals in both the ternary (Fig. 4.2) and the quaternary alloys (Fig. 4.3). The main difference between the two types of alloy was in the composition of the precipitates. The ternary precipitates were depleted in Mn and Cr, and also contained large amounts of oxygen. No segregation of other interstitial impurities (namely carbon and nitrogen) was observed. However, the precipitates in the Ti-containing alloys were extremely Ti rich relative to the matrix and were also enriched in all three impurity elements studied. This suggests that the addition of Ti to these alloys acts as a getter for these interstitial impurities, forming Ti-[C,O,N] type precipitates similar to those found in V-4Cr-4Ti.[3, 19, 20]

TEM was used to check for smaller scale elemental segregation as shown in Fig. 4.4. No segregation was found, indicating a homogeneous bcc phase across all length-scales. Diffraction patterns (fig. 4.7) indicated that the precipitates in the ternary

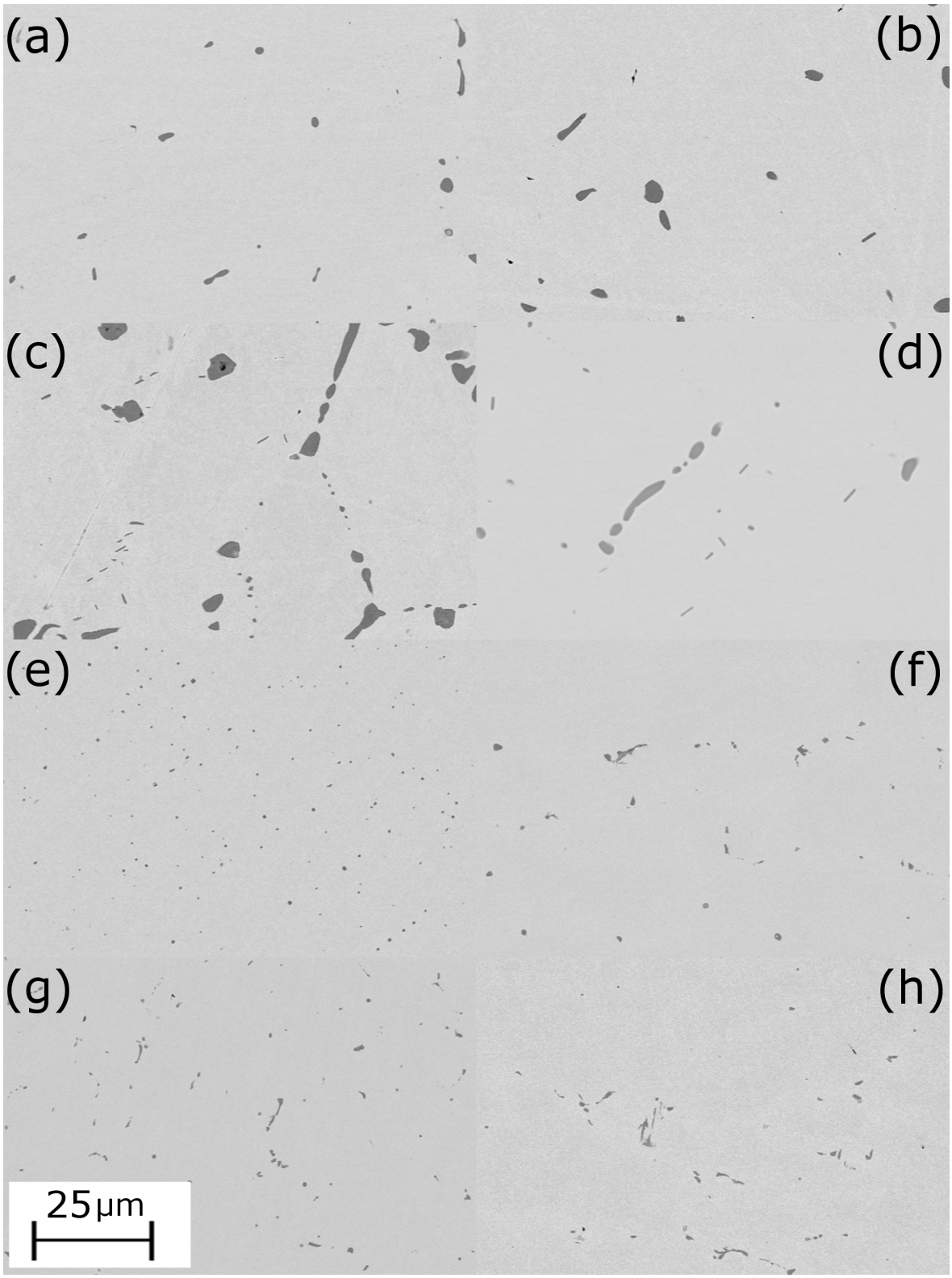

Figure 4.1: Representative BSE images of alloy (a) V-20Cr-20Mn (b) V-20Cr-40Mn (c) V-40Cr-20Mn (d) V-Cr-Mn (e) V-Cr-Mn-1%Ti (f) V-Cr-Mn-2%Ti (g) V-Cr-Mn-4%Ti (h) V-Cr-Mn-8%Ti.

alloys were fcc with a lattice parameter of approximately 8.38 Å. This is a close match with the spinel MnV_2O_4[26] which suggests an similar structure, perhaps with slightly

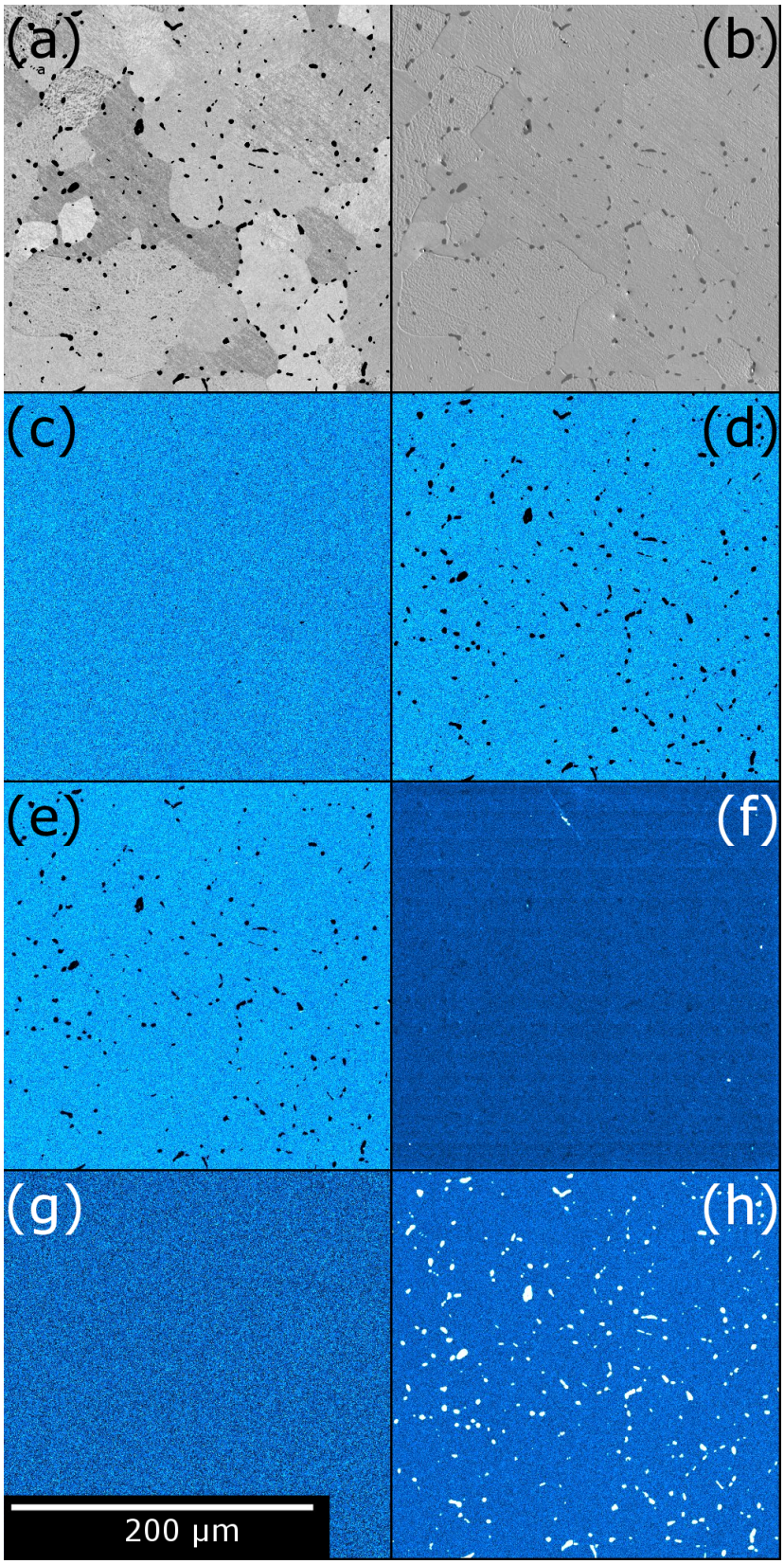

Figure 4.2: WDS map of alloy V-40Cr-20Mn showing: (a) BSE image (b) secondary electron image (c) V (d) Cr (e) Mn (f) C (g) N (h) O.

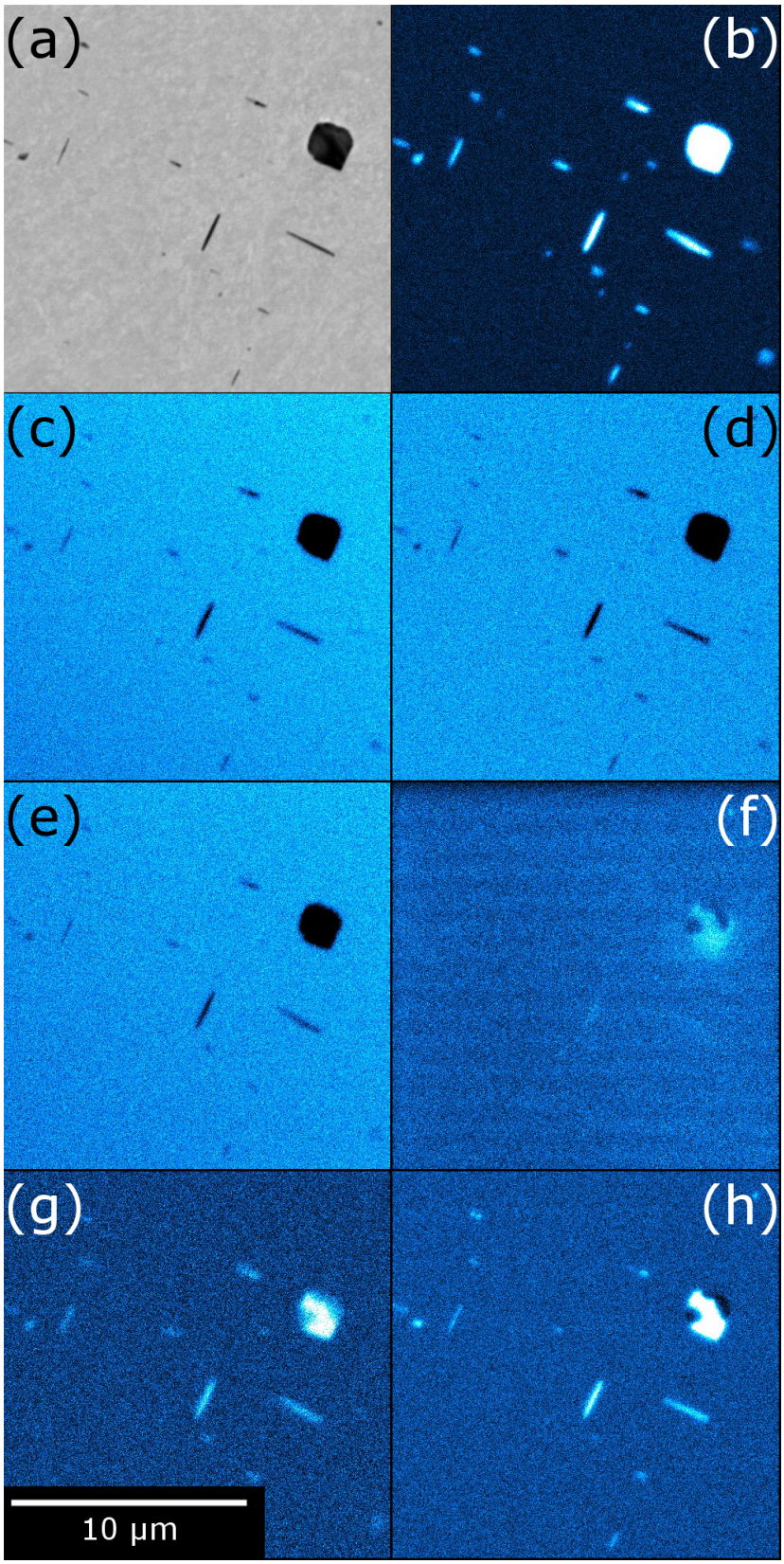

Figure 4.3: WDS map of alloy V-Cr-Mn-8%Ti showing: (a) BSE image (b) Ti (c) V (d) Cr (e) Mn (f) C (g) N (h) O.

altered stoichiometry. Diffraction patterns of the quaternary alloy precipitates (fig. 4.7) indicate an fcc structure with a lattice parameter of approximately 4.16 Å, which is consistent with the Ti-[C,O,N] phase found in V-4Cr-4Ti alloys[19]. As all the precipitates found in this study are formed from impurity elements, there is no indication that these alloys would not form a single bcc phase if interstitial impurity content was lower.

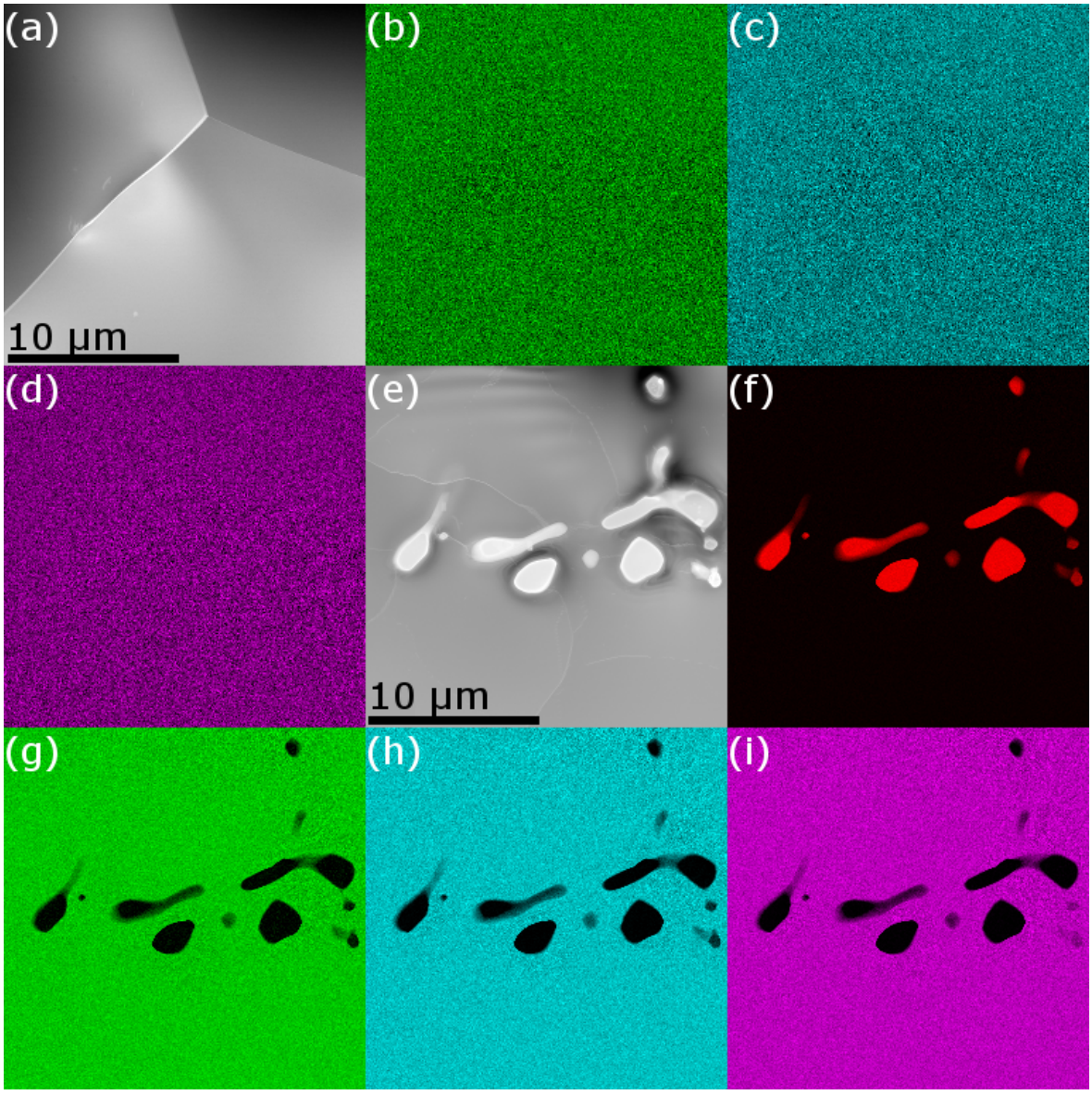

Figure 4.4: Alloy V-Cr-Mn: (a) ADF image (b) V map (c) Cr map (d) Mn map. Alloy V-Cr-Mn-4%Ti precipitate: (e) ADF image (f) Ti map (g) V map (h) Cr map (i) Mn map.

Hardness values were found to range from 348 to 456 HV in the homogenised state (see supplementary information). Hardness decreased slightly after homogenisation for all alloys. The Ti containing alloys were all harder than their equiatomic ternary equivalent, V-Cr-Mn, which may indicate the solute strengthening caused by introducing

Ti[23, 24] is the more dominant effect compared to the softening from gettering interstitial impurities[22]. A high ductile-to-brittle transition temperature and embrittlement by interstitial elements are foreseeable issues with these alloys, as they are with most refractory-based alloys. Hence, in order to assess their suitability for manufacture and service, larger-scale mechanical property and processibility investigations are needed alongside long-term ageing experiments.

To summarise, this study has found that a suite of alloys fabricated from low-activation elements consists of a single bcc phase, with precipitates forming from interstitial impurity elements. The results are promising for the development of high-entropy alloys for use in fusion applications due to the observation of only a single metallic matrix phase after homogenisation. Such microstructures provide an excellent launchpad for the future development of specialist alloys for fusion applications.

Acknowledgements

The authors acknowledge the use of the Department of Materials X-ray Diffraction Suite at the University of Manchester and for the technical support, advice and assistance provided by Dr. John E. Warren. The authors would also like to Dr. Mark Gilbert for fruitful discussions regarding the activation properties of elements. The authors acknowledge funding from the EPSRC Centre for Doctoral Training in Fusion Energy [grant EP/L01663X/1] as well as EPSRC grant EP/R021546/1. This work has been part-funded by the RCUK Energy Programme [grant number EP/T012250/1]. To obtain further information on the data and models underlying this paper please contact PublicationsManager@ukaea.uk.

References

[1] A.R Raffray et al. “Breeding blanket concepts for fusion and materials requirements”. In: *Journal of Nuclear Materials* 307-311 (Dec. 2002), pp. 21–30. ISSN: 00223115. DOI: 10.1016/S0022-3115(02)01174-1.

[2] M.R. Gilbert et al. “Waste implications from minor impurities in European DEMO materials”. In: *Nuclear Fusion* 59.7 (July 2019), p. 076015. ISSN: 0029-5515. DOI: 10.1088/1741-4326/ab154e.

[3] T. Muroga, J.M. Chen, V.M. Chernov, et al. “Present status of vanadium alloys for fusion applications”. In: *Journal of Nuclear Materials* 455.1 (2014), pp. 263–268. ISSN: 00223115. DOI: 10.1016/j.jnucmat.2014.06.025.

[4] S.J. Zinkle, J.-L Boutard, D.T. Hoelzer, et al. “Development of next generation tempered and ODS reduced activation ferritic/martensitic steels for fusion energy applications”. In: *Nuclear Fusion* 57.9 (Sept. 2017), p. 092005. ISSN: 0029-5515. DOI: 10.1088/1741-4326/57/9/092005.

[5] A.F. Rowcliffe et al. “Materials challenges for the fusion nuclear science facility”. In: *Fusion Engineering and Design* 135 (Oct. 2018), pp. 290–301. ISSN: 09203796. DOI: 10.1016/j.fusengdes.2017.07.012.

[6] S. J. Zinkle and N. M. Ghoniem. “Operating temperature windows for fusion reactor structural materials”. In: *Fusion Engineering and Design* 51-52.2000 (2000), pp. 55–71. ISSN: 09203796. DOI: 10.1016/S0920-3796(00)00320-3.

[7] A. Ayyagari et al. “Low activation high entropy alloys for next generation nuclear applications”. In: *Materialia* 4 (Dec. 2018), pp. 99–103. ISSN: 2589-1529. DOI: 10.1016/J.MTLA.2018.09.014.

[8] B. Gludovatz et al. “A fracture-resistant high-entropy alloy for cryogenic applications”. In: *Science* 345.6201 (Sept. 2014), pp. 1153–1158. ISSN: 0036-8075. DOI: 10.1126/science.1254581.

[9] K. Jin et al. “Effects of compositional complexity on the ion-irradiation induced swelling and hardening in Ni-containing equiatomic alloys”. In: *Scripta Materialia* 119 (July 2016), pp. 65–70. ISSN: 13596462. DOI: 10.1016/j.scriptamat.2016.03.030.

[10] O. Carlson and A. Eustice. “Vanadium-chromium alloy system”. In: *Ames Laboratory Technical Reports* (1959).

[11] F.A Garner, M.B Toloczko, and B.H Sencer. “Comparison of swelling and irradiation creep behavior of fcc-austenitic and bcc-ferritic/martensitic alloys at high neutron exposure”. In: *Journal of Nuclear Materials* 276.1-3 (Jan. 2000), pp. 123–142. ISSN: 00223115. DOI: 10.1016/S0022-3115(99)00225-1.

[12] S.J. Zinkle. “Radiation-Induced Effects on Microstructure”. In: *Comprehensive Nuclear Materials* (Jan. 2012), pp. 65–98. DOI: 10.1016/B978-0-08-056033-5.00003-3.

[13] S.J. Zinkle and L.L. Snead. “Designing Radiation Resistance in Materials for Fusion Energy”. In: *Annual Review of Materials Research* 44.1 (July 2014), pp. 241–267. ISSN: 1531-7331. DOI: 10.1146/annurev-matsci-070813-113627.

[14] T.B. Massalski. *Binary alloy phase diagrams*. ASM International, 1986. ISBN: 087170403X.

[15] A. Klopotov et al. "Structure feature of ternary state diagrams of Cr-Ti-V and Cr-Mn-V systems". In: *MATEC Web of Conferences* 243 (Dec. 2018). Ed. by A. Vorozhtsov, p. 00014. ISSN: 2261-236X. DOI: 10.1051/matecconf/201824300014.

[16] E. J. Pickering and N. G. Jones. "High-entropy alloys: a critical assessment of their founding principles and future prospects". In: *International Materials Reviews* 6608.May (2016), pp. 1–20. ISSN: 0950-6608. DOI: 10.1080/09506608.2016.1180020.

[17] D. B. Miracle and O. N. Senkov. "A critical review of high entropy alloys and related concepts". In: *Acta Materialia* 122 (2017), pp. 448–511. ISSN: 13596454. DOI: 10.1016/j.actamat.2016.08.081.

[18] Ortrud Kubaschewski von Goldbeck. "Iron-Chromium Fe-Cr". In: *IRON—Binary Phase Diagrams*. Berlin, Heidelberg: Springer Berlin Heidelberg, 1982, pp. 31–34. ISBN: 978-3-662-08024-5. DOI: 10.1007/978-3-662-08024-5_17.

[19] D.T. Hoelzer. *Structural analysis of Ti-oxycarbonitrides in V-Cr-Ti based alloys*. Tech. rep. Oak Ridge National Laboratory, 1999.

[20] T Nagasaka et al. "Examination of fabrication process parameters for improvement of low-activation vanadium alloys". In: *Fusion Engineering and Design* 61-62 (Nov. 2002), pp. 757–762. ISSN: 09203796. DOI: 10.1016/S0920-3796(02)00258-2.

[21] S Hoile. "Processing and properties of mild interstitial free steels". In: *Materials Science and Technology* 16.10 (Oct. 2000), pp. 1079–1093. ISSN: 0267-0836. DOI: 10.1179/026708300101506902.

[22] J. M. Chen et al. "Overview of the vanadium alloy researches for fusion reactors". In: *Journal of Nuclear Materials* 417.1-3 (2011), pp. 289–294. ISSN: 00223115. DOI: 10.1016/j.jnucmat.2011.02.015.

[23] B.A. Loomis et al. "Effects of neutron irradiation and hydrogen on ductile-brittle transition temperatures of V-Cr-Ti alloys". In: *Journal of Nuclear Materials* 212-215.94 (Sept. 1994), pp. 799–803. ISSN: 00223115. DOI: 10.1016/0022-3115(94)90166-X.

[24] H. M. Chung, B. A. Loomis, and D. L. Smith. "Development and testing of vanadium alloys for fusion applications". In: *Journal of Nuclear Materials* 239.1-3 (1996), pp. 139–156. ISSN: 00223115. DOI: 10.1016/S0022-3115(96)00676-9.

[25] T Fuda et al. "Protium absorption properties of Ti–V–Cr–Mn alloys with a b.c.c. structure". In: *Journal of Alloys and Compounds* 330-332 (Jan. 2002), pp. 522–525. ISSN: 09258388. DOI: 10.1016/s0925-8388(01)01544-4.

[26] R. Plumier. "Etude par diffraction des neutrons du compose spinelle MnV2O4". In: *Comptes Rendus Hebdomadaires des Seances de l'Academie des Sciences* 255 (1962), pp. 2244–2246.

4.2 Supplementary figures

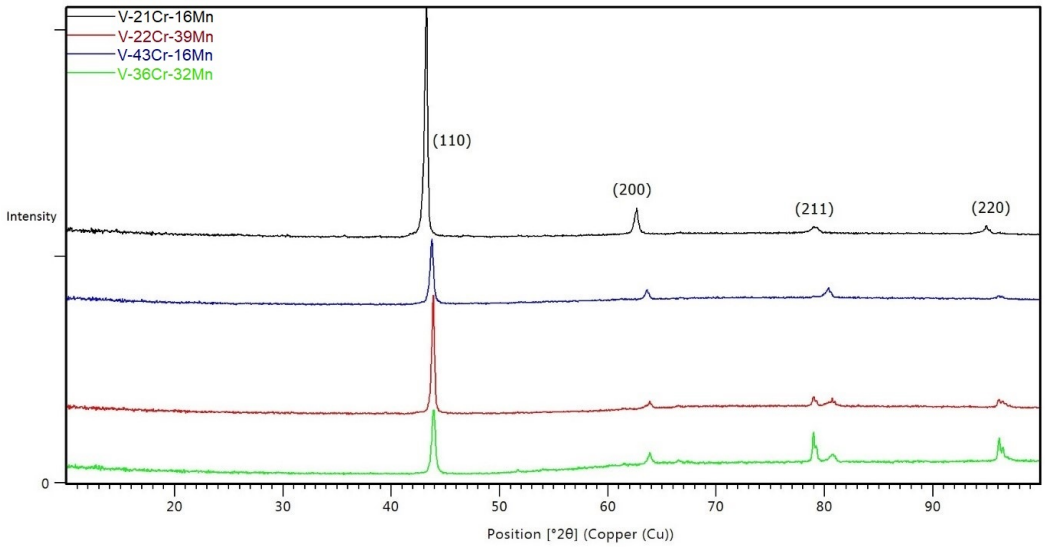

Figure 4.5: XRD patterns of the ternary alloys. Peaks at 79 °were caused by the sample holder.

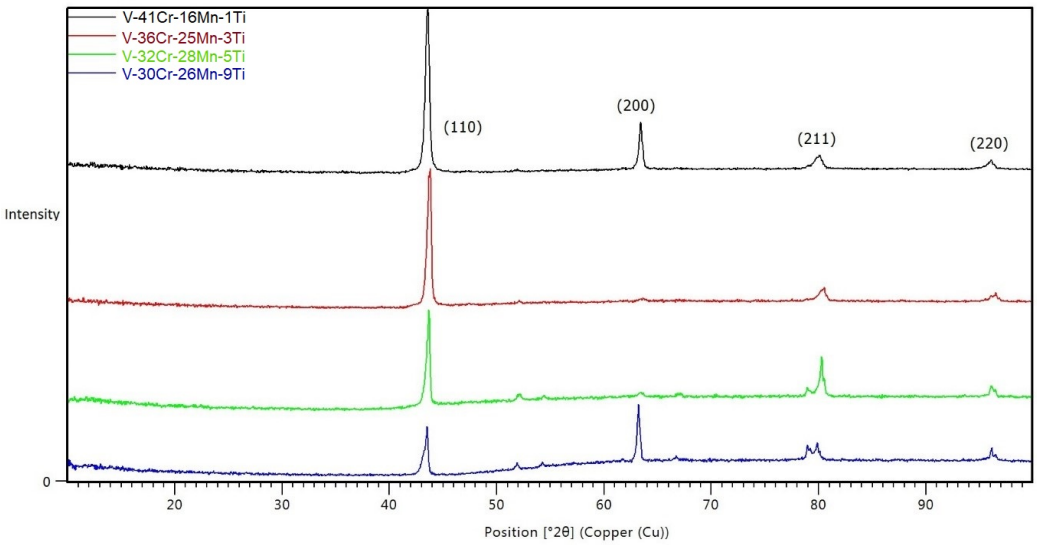

Figure 4.6: XRD patterns of the quaternary alloys. Peaks at 52, 54 and 79 °were caused by the sample holder.

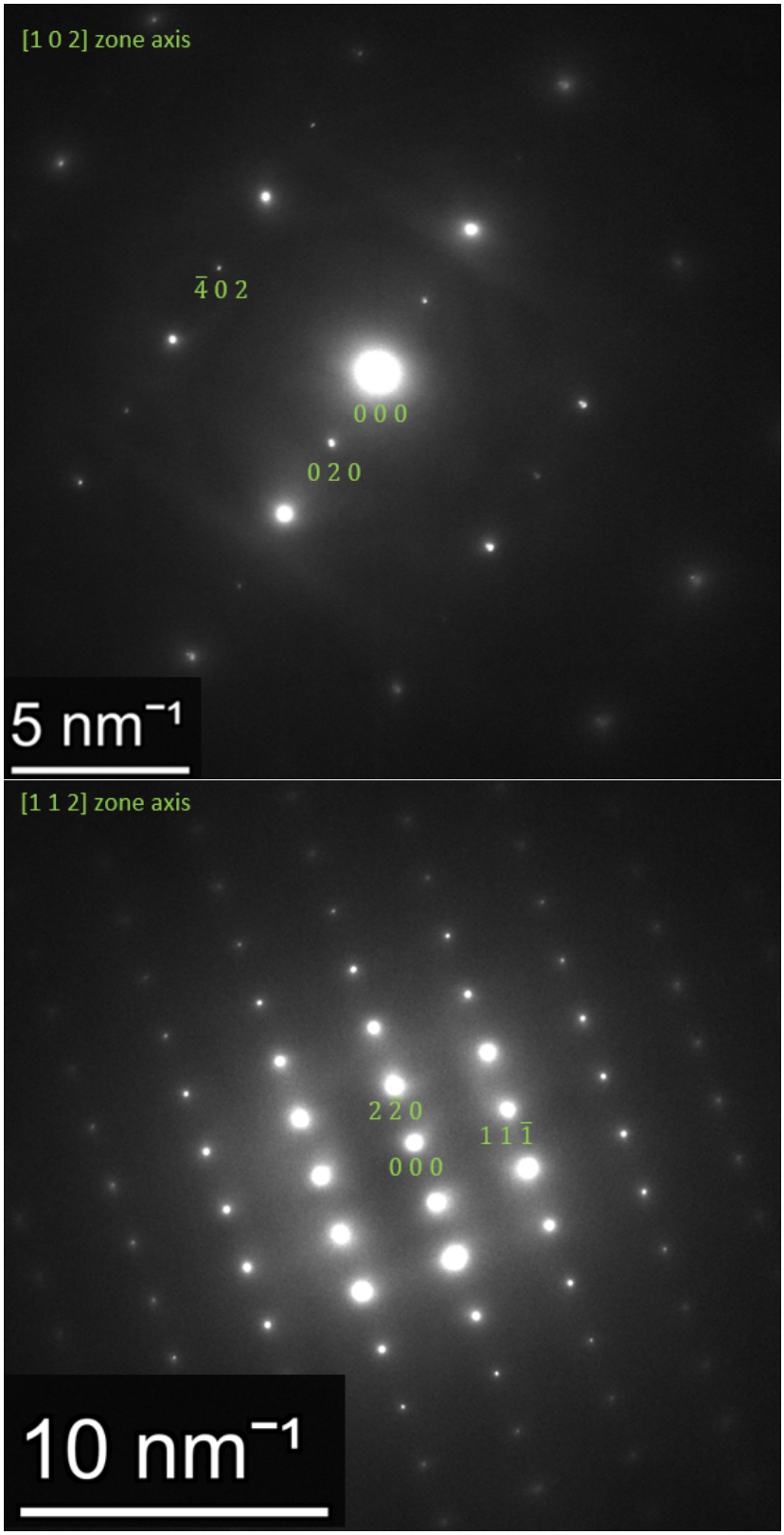

Figure 4.7: Diffraction pattern of a precipitate in V-36Cr-32Mn.

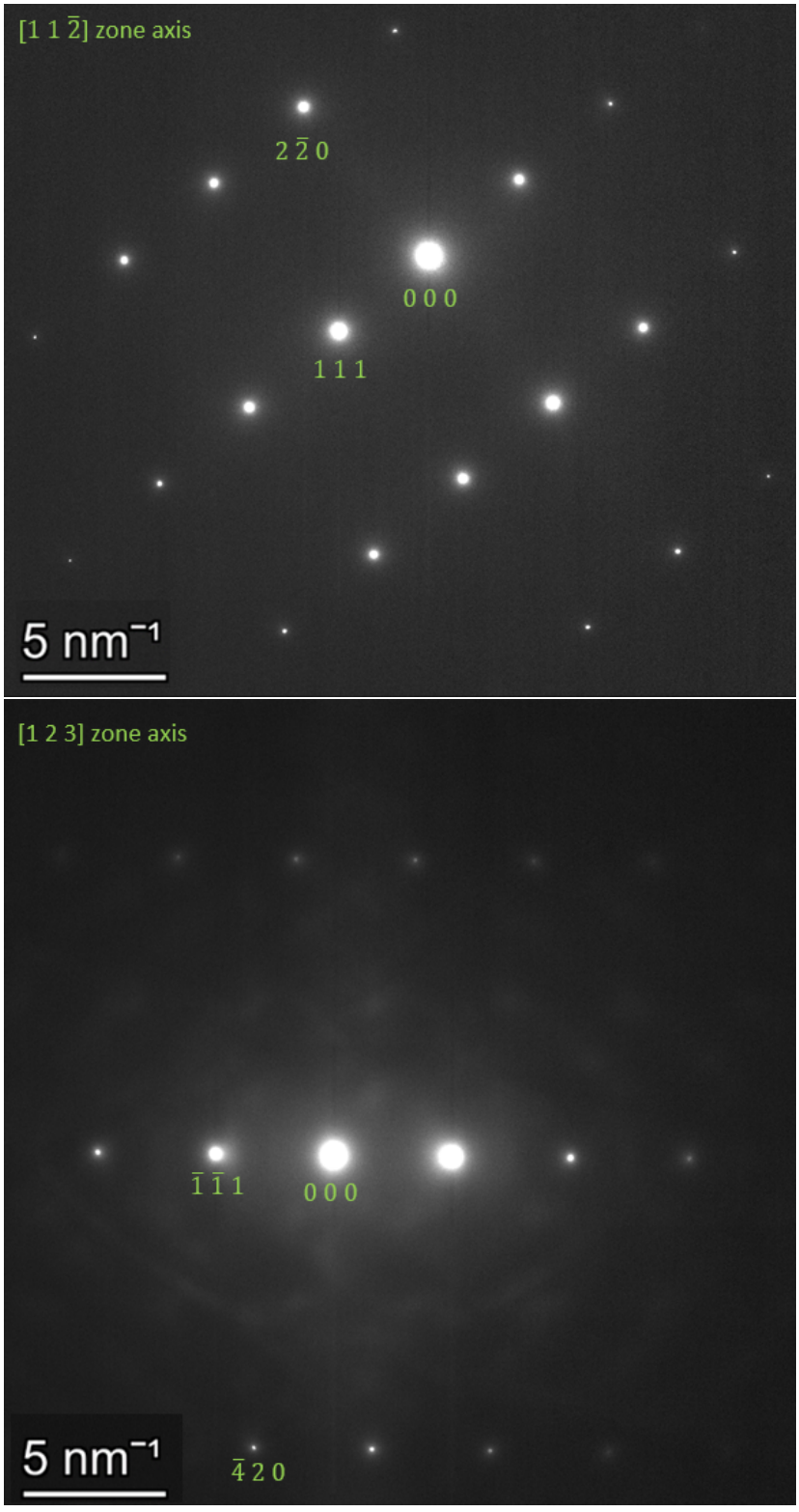

Figure 4.8: Diffraction pattern of a precipitate in V-32Cr-28Mn-5Ti.

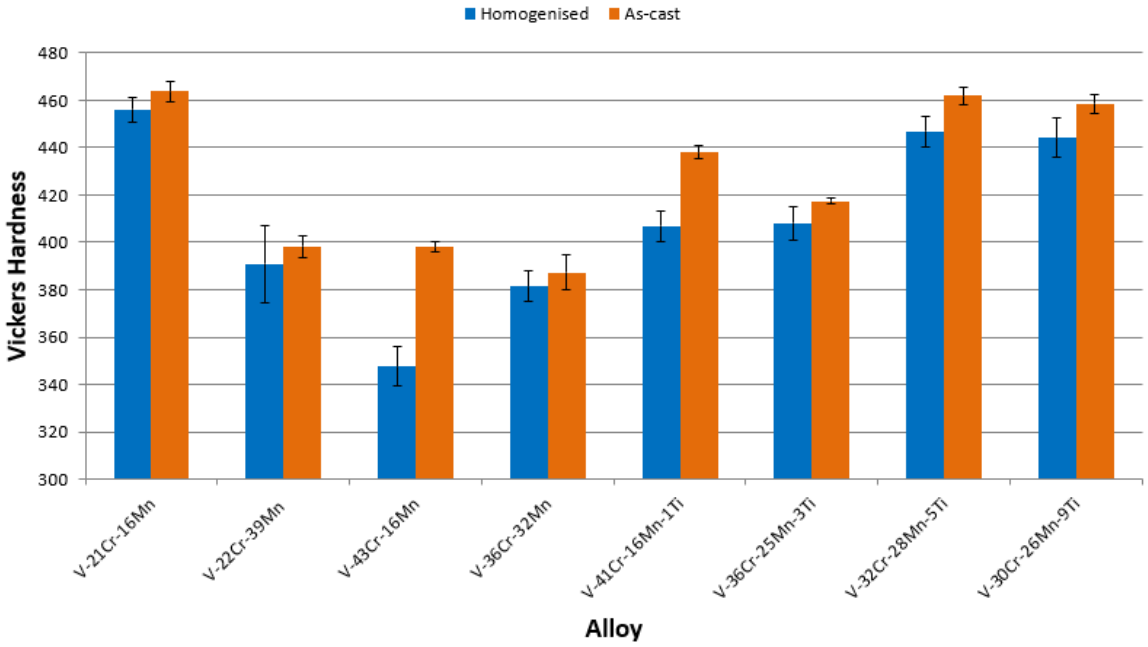

Figure 4.9: Microhardness values of alloys in the as-cast and homogenised states.

4.3 Additional discussion

4.3.1 Activation properties

The activation properties of the elements used in the alloys studied are generally considered low-activation (see Section 2.1.3). In-depth analyses of the activation properties of the elements are presented in Figs. 4.10 and 4.11, which show how the specific activities and decay heat for the elements evolve during cooling after use in various DEMO components. In the long term (>100 years) all four alloys display more favourable activation properties than Fe[1] in all reactor components. In the shorter term, only Mn is more radioactive than Fe, by around an order of magnitude.

Perhaps of greater interest is the decay heat of the elements. If materials in a fusion environment are only accepted for use within a certain temperature range defined by engineering standards, then these temperatures should be not be exceeded, even if the reactor is not operational. Thermal energy generated from radioactivity could continue to heat the reactor even when no plasma is present. In the case of Mn, this decay heat is significantly higher than the other elements and Fe (Fig. 4.11).

To check if these relatively high levels of decay heat would be problematic for a DEMO reactor, a comparison can be made to studies of the decay heat for a proposed DEMO blanket design with an output power of 3 GW operated for two years[1]. Peak decay heat power was calculated to occur immediately after reactor shutdown, with a value of 31 MW in the blanket region. Less than half of this peak value came from the structural material, which was F82H steel. If the steel was replaced with an alloy that contained significant amounts of Mn, as in the alloys studied here, the decay heat may be expected to rise significantly. Although it would require further analysis to more precisely determine how much the decay heat may rise by, this simple example shows that using more Mn in the blanket could result in significant increases in the decay heat.

However, decay heat is not necessarily an issue. If the heat can be managed with cooling to the extent that the materials used stay within an acceptable temperature (as to avoid loss of strength or creep resistance from high temperatures), then the energy generated by radioactive decay can be extracted by the cooling system to provide additional energy from the fusion plant. It may even confer benefits, such as keeping irradiated materials that become brittle at low temperatures above their DBTT, or "smoothing out" the energy release from the pulsed operation of a reactor.

[1]In this case, Fe is being treated as a best case material, i.e. a steel containing elements that are no more active than Fe.

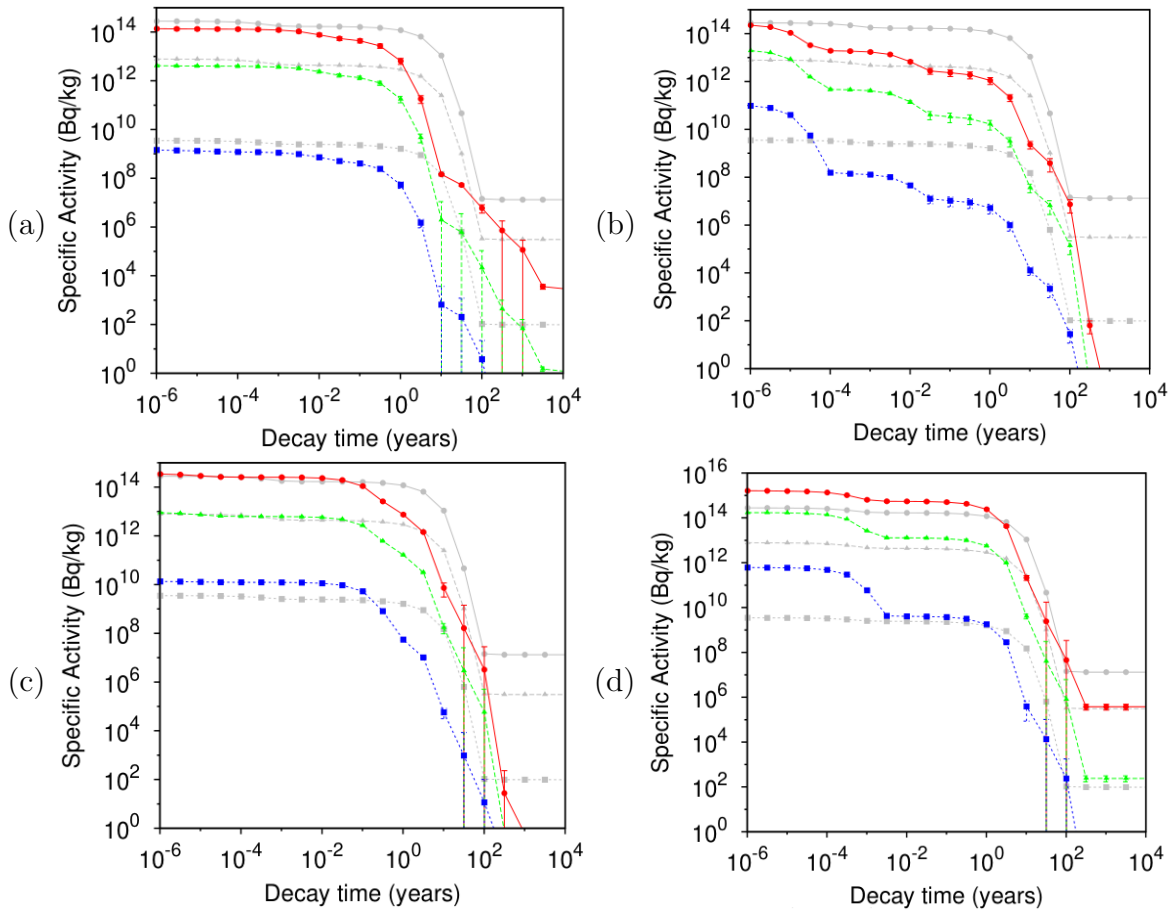

Figure 4.10: Specific activities versus cooling time after exposure to a DEMO-like neutron flux (a) Ti (b) V (c) Cr (d) Mn. Red circles for first wall region, green triangles for blanket region, blue squares for vacuum vessel region, grey lines show equivalent decay curves for pure Fe. Taken from [2].

4.3.1.1 FISPACT analysis

To further examine the activation properties of these alloys, a short analysis was performed using the FISPACT-II nuclear inventory code[3] and the TENDL-2019[4] nuclear data library. The code was used to simulate what the nuclear inventory of the alloys studied would be after being exposed to the neutron flux found in the blanket back plate region (provided by the FISPACT-II Wiki list of reference spectra[5]) for 2 full power years, which is equivalent to the green curves in Figs. 4.10 and 4.11.

Fig. 4.12 shows the specific activity and decay heat that resulted from the FISPACT calculations for V-22Cr-39Mn, the alloy with the highest Mn content. The calculations were also performed with interstitial impurities measured by LECO analysis (see Chapter 5). Overall, the radioactivity profile is dominated by the presence of Mn in the pure alloy, and the plots show very similar values to pure Mn (Figs. 4.10(d) and 4.11(d)).

Also of note are the effects of introducing interstitial impurities into the calculation (blue curves). Impurity elements have been shown to have a major impact on the

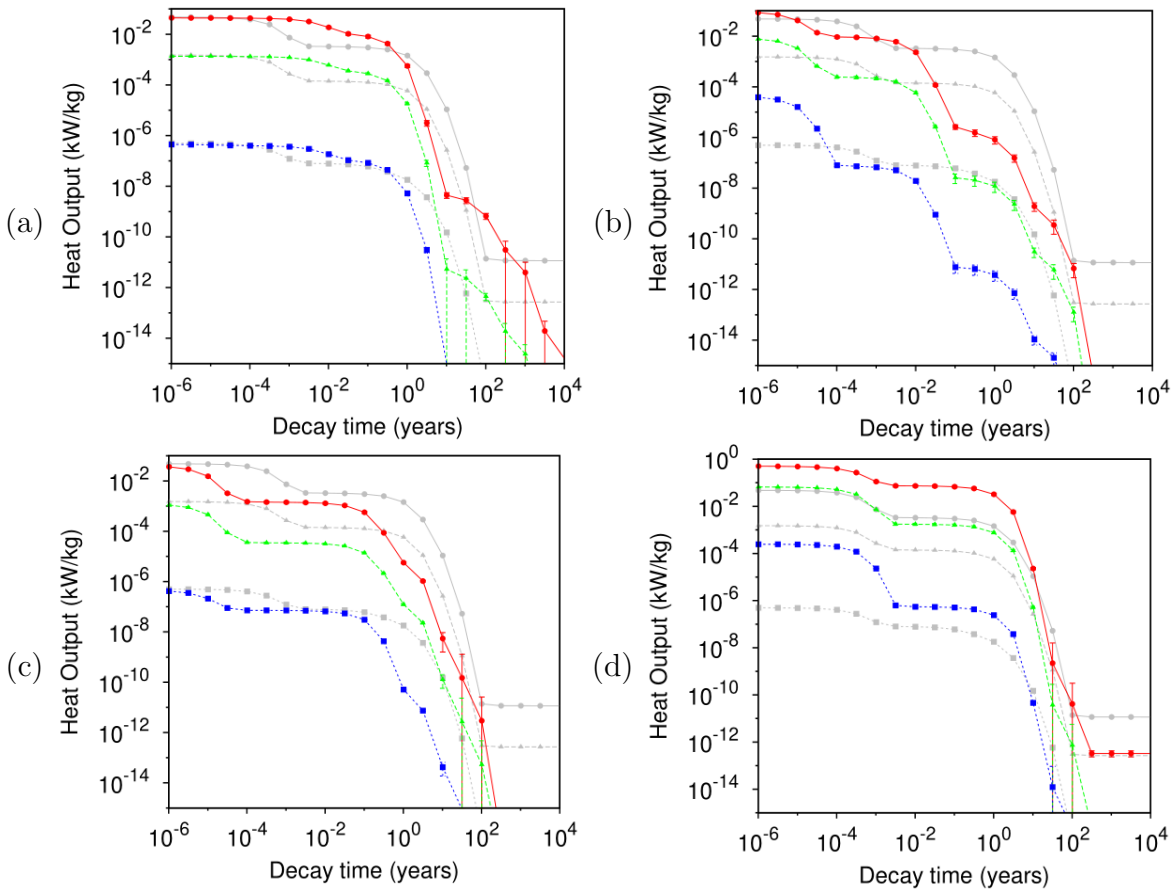

Figure 4.11: Radioactive heat output versus cooling time after exposure to a DEMO-like neutron flux (a) Ti (b) V (c) Cr (d) Mn. Red circles for first wall region, green triangles for blanket region, blue squares for vacuum vessel region, grey lines show equivalent decay curves for pure Fe. Taken from [2].

activation properties of materials. Work by Gilbert et al.[6] showed that steels that are generally considered to be reduced-activation are much more active over large timescales when nitrogen (contained in the steels in the form of nitrides) is added to the calculation. ^{14}N will transmute into ^{14}C, which has a half-life of 5730 years and is the main contributor to the long-term activation properties of otherwise reduced activation alloys. The same behaviour was osberved when interstitials were included in calculations for the alloys studied here. Only after cooling for over a year do the specific activities and decay heat for the pure alloys and the interstitial-containing alloys start to diverge. As the predicted activities are below the acceptable UK LLW limits, the interstitial contents of these alloys are not of immediate concern from an activation standpoint. However, another aspect that was not considered here was the presence of other impurities from the source metal. Similar analysis performed for impure V-4Cr-4Ti that included 66 different elements found that Mo and Nb impurities from the source metal had a large impact on activation properties[7].

Without the use of advanced analytical techniques for measuring impurity content,

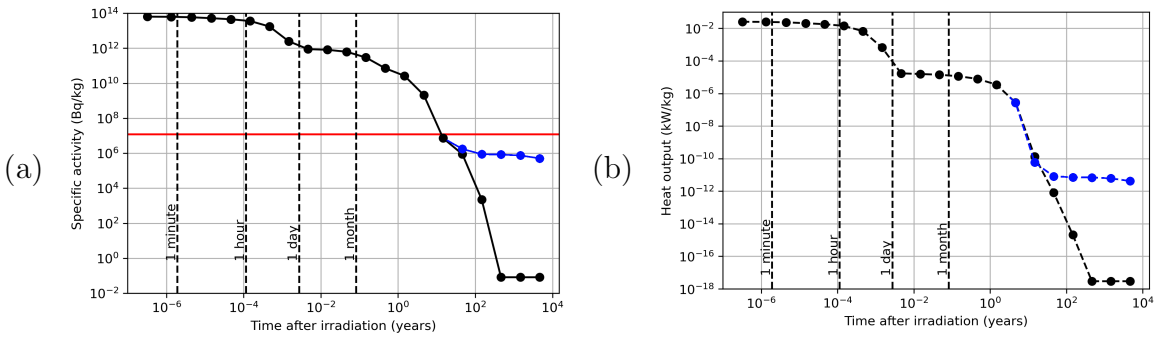

Figure 4.12: FISPACT calculation results for V-22Cr-39Mn (black) and V-22Cr-39Mn-0.003C-0.0002N-0.3O-0.008S (blue) displaying: (a) Specific activity (red line indicates UK LLW limit for beta and gamma radiation) (b) Decay heat output.

it is difficult to make any definitive assessments of the low-activation properties of these alloys. However, it is clear that impurities play a large role in determining the activation profile of a material and any future alloy design process should be cognisant of this fact.

4.3.2 Precipitate distribution

The microstructures reported in the manuscript were accurate for the bulk of the interior the alloys examined. However, some edge effects were present and will briefly be discussed here. Figure 4.13 shows the microstructure of a V-22Cr-39Mn sample that had been cross sectioned in the middle. There is clear change in distribution of precipitates from the sample bulk (upper left of the figure) towards the edge. The density and size of the precipitates near the centre are greater than those near the edge. This change was found to occur in all four V-Cr-Mn ternary alloys. The region that deviated from the bulk was of the order of 100 µm in all four alloys.

Curiously, the opposite behaviour was observed in the quaternary Ti-V-Cr-Mn alloys. Figure 4.14 shows the microstructure of V-41Cr-16Mn-1Ti through the thickness of the sample. A much greater density of precipitates occurs near the surface, although their average size appears to remain roughly constant. This effect is observed in all four quaternary alloys, manifesting in a similar way for each.

No systematic study of these effects was undertaken as they did not seem to influence the microstructure of the bulk material. As the precipitates in this study were found be oxides and carboxynitrides, in the ternary and quaternary alloys respectively, and because the alloys were found to be homogeneous with respect to their principal elements, the anomalous behaviours could perhaps be explained by how interstitial atoms behaved in these alloys. The lack of MnV_2O_4 oxides near the surface of the ternary alloys might suggest a lower O content in the matrix in these regions. Likewise, the increased population of Ti-[C,O,N] precipitates near the edge of the quaternary alloys

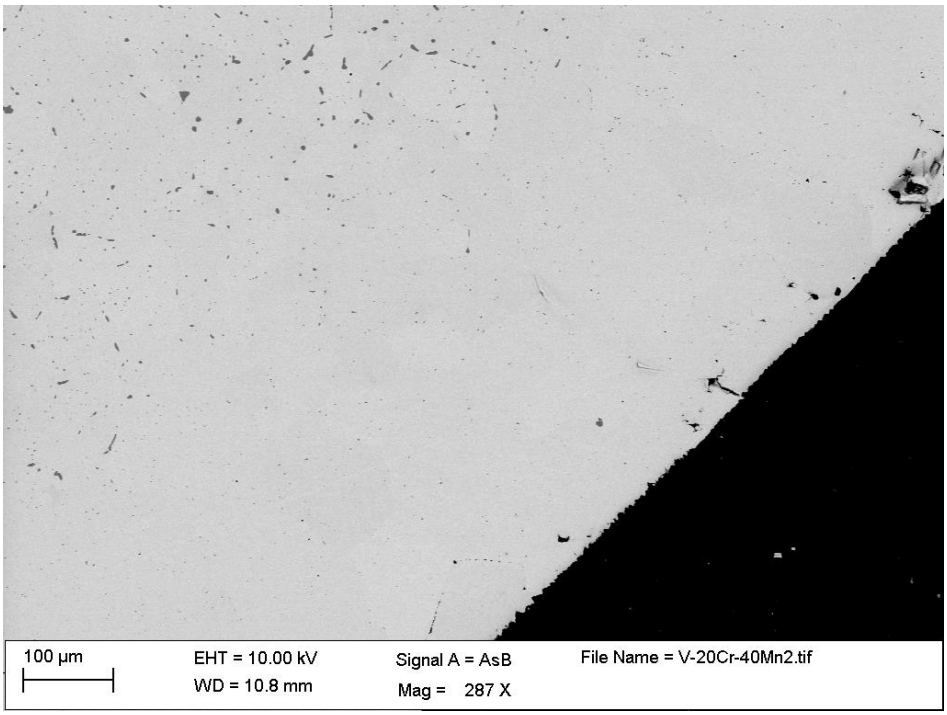

Figure 4.13: BSE image of V-22Cr-39Mn, note the depletion of precipitates near the edge of the sample.

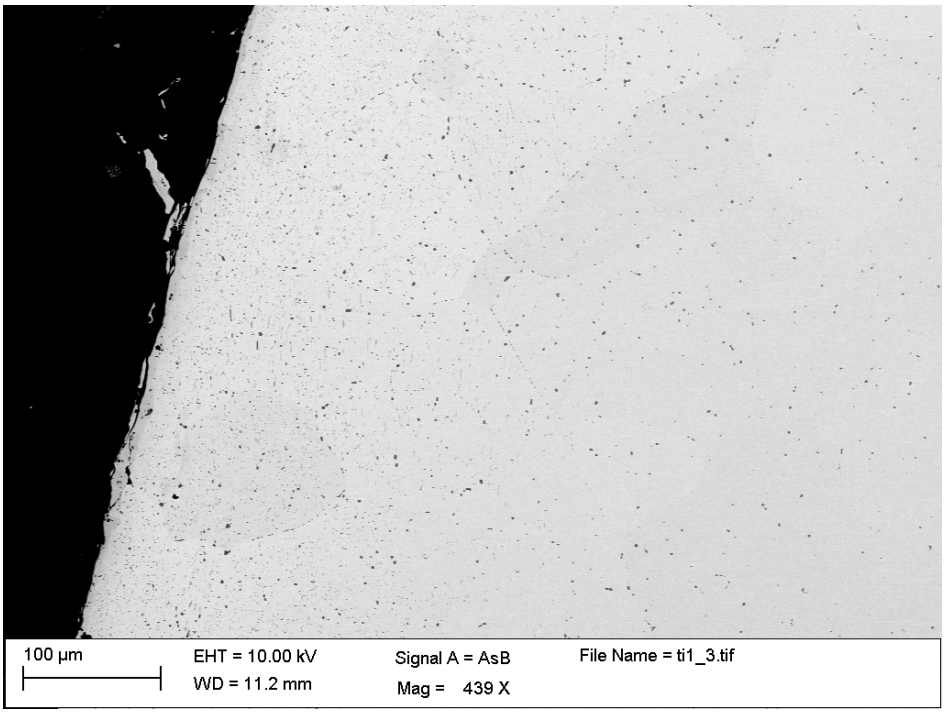

Figure 4.14: BSE image of V-41Cr-16Mn-1Ti, note the abundance of precipitates near the edge of the sample.

Diffusing species	Alloy	D_{1473K} / $m^2\,s^{-1}$	d / mm	Ref
O	Pure V	6.33×10^{-11}	4.78	[8]
O	V-5Cr	1.20×10^{-11}	2.08	[8]
O	V-5Ti	2.51×10^{-10}	9.50	[8]
N	Pure V	1.01×10^{-10}	6.02	[9]
C	Pure V	2.78×10^{-8}	100	[10]
C	V-5.3Ti	1.12×10^{-7}	200	[10]

Table 4.3: Diffusion data at 1473 K and estimated diffusion distances of interstitial atoms in selected alloy systems after annealing for 100 hrs.

might indicate increased C, O, or N content (or any combination of the three) in those regions.

Some diffusion data for interstitials in alloys is presented in Table 4.3. Interstitial diffusion data is scarce for even the binary systems of the elements of interest. O diffusion is of the order of mm in V and adding Cr decreases it further. C diffuses much more easily in the alloys where data is available. Given that the diffusion behaviour of multicomponent alloys is complex (see Section 2.9.1.3), it would not be appropriate to try and extrapolate diffusion behaviour from such limited data.

Given the behaviour of the ternary alloys, one possible explanation might be that there is some process occurring on the surface of the alloy that removes O from the solid solution. Even though the samples were annealed in an Ar atmosphere, it is possible that dissolved O formed an oxide scale that depleted the matrix. However, this explanation would not be satisfactory in the case of the quaternary alloys, as precipitate content increases near the surface.

4.3.3 Hardness testing

Further to the hardness results presented in Fig. 4.9, some observations are added here. Cracks were observed in some microhardness indents (see Fig. 4.15), but they only originated from the indentation corners and propagated small distances relative to the size of the indent. Cracking was almost exclusively observed only in the quaternary alloys (only one instance of cracking was seen in over 50 indents of the ternary alloys), but there was no clear correlation with alloy composition or microstructure near the indent.

Macrohardness measurements were also taken, using a Matsuzawa VMT-X indenter with a load of 196 N. If the alloys were highly brittle, then macrohardness testing would show severe cracking and spalling under the increased load, akin to what is seen in ceramics[11]. The cracking observed was not particularly severe and not observed in all tests. Where cracking did occur, it tended to propagate through precipitates as shown in Fig. 4.16, indicating they are a potential source of embrittlement in the

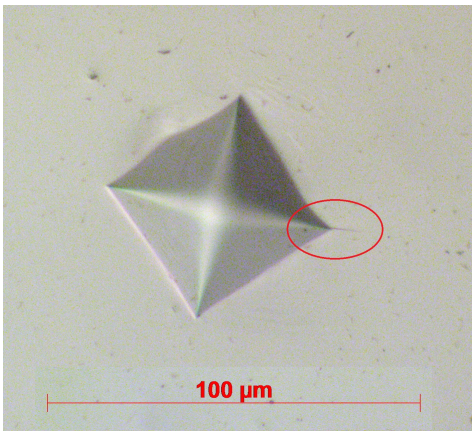

Figure 4.15: Optical micrograph of Vickers microhardness indent of V-32Cr-28Mn-5Ti from 9.8 N of force. Cracking is highlighted.

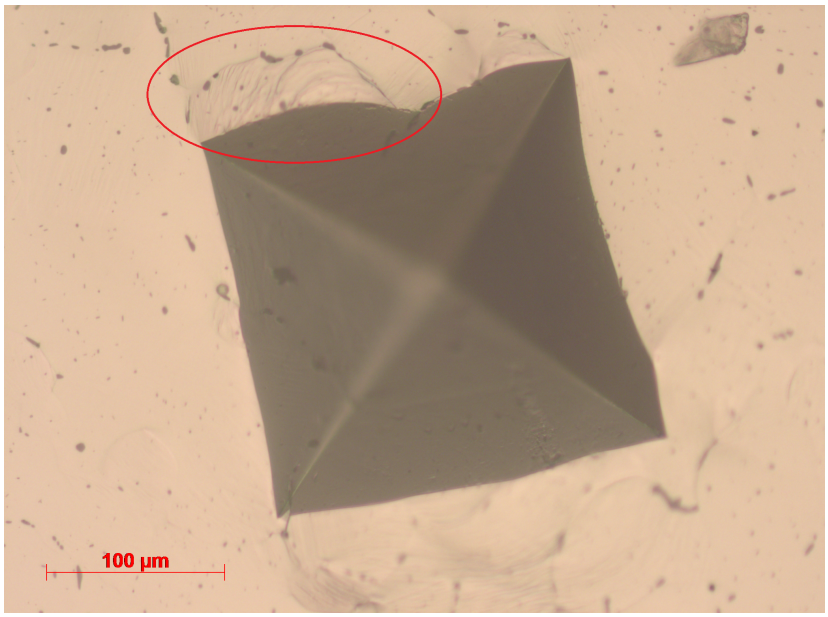

Figure 4.16: Optical micrograph of Vickers macrohardness indent of V-22Cr-39Mn from 196 N of force. Cracking is highlighted.

alloys. Also of note was the "pincushioning" effect observed in the indents, where the sides of the indent appear to bulge inwards slightly. This is indicative of an annealed sample undergoing work hardening and leads an overestimation of the indent size[12]. Measurements from the macrohardness tests are shown in Fig. 4.17. The values are on average slightly lower than the bulk microhardness measurements, possibly as a consequence of the pincushioning effect.

To determine if the anomalous precipitation behaviour had any effect on hardness, microhardness measurements were taken near the edge of the samples for comparison to the bulk (Fig. 4.17). Microhardness was within standard error for all but one of the samples, although the spread of values was generally greater.

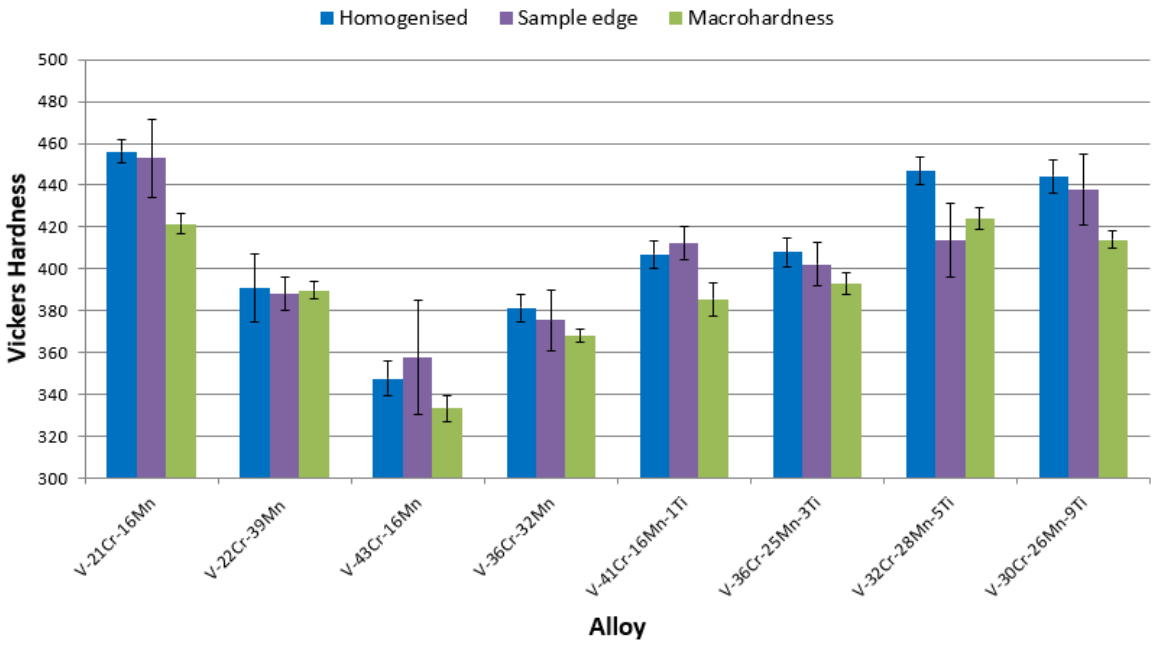

Figure 4.17: Comparison of microhardness and macrohardness values, measured using loads of 9.8 N and 196 N respectively.

Additional references

[1] Youji Someya and Kenji Tobita. "Estimation of Decay Heat in Fusion DEMO Reactor". In: *Plasma and Fusion Research* 7.0 (June 2012), pp. 2405066–2405066. ISSN: 1880-6821. DOI: 10.1585/pfr.7.2405066.

[2] M.R. Gilbert, J.-Ch. Sublet, and R. Forrest. "Handbook of activation, transmutation and radiation dmagae properties of the elements simulated using FISPACT-II and TENDL-2014". In: *UK Atomic Energy Authority* CCFE-R(15) (2015).

[3] J. Ch Sublet et al. "FISPACT-II: An Advanced Simulation System for Activation, Transmutation and Material Modelling". In: *Nuclear Data Sheets* 139 (Jan. 2017), pp. 77–137. ISSN: 00903752. DOI: 10.1016/j.nds.2017.01.002.

[4] A. J. Koning et al. "TENDL: Complete Nuclear Data Library for Innovative Nuclear Science and Technology". In: *Nuclear Data Sheets* 155 (Jan. 2019), pp. 1–55. ISSN: 00903752. DOI: 10.1016/j.nds.2019.01.002.

[5] UK Atomic Energy Agency. *Reference input spectra.*

[6] M.R. Gilbert et al. "Waste implications from minor impurities in European DEMO materials". In: *Nuclear Fusion* 59.7 (July 2019), p. 076015. ISSN: 0029-5515. DOI: 10.1088/1741-4326/ab154e.

[7] M. L. Grossbeck et al. "Analysis of V-Cr-Ti alloys in terms of activation of impurities". In: *Journal of Nuclear Materials* 258-263.PART 2 B (Oct. 1998), pp. 1778–1783. ISSN: 00223115. DOI: 10.1016/S0022-3115(98)00228-1.

[8] H Nakajima et al. "Diffusion of oxygen in vanadium and its alloys". In: *Philosophical Magazine A* 67.3 (Mar. 1993), pp. 557–571. ISSN: 0141-8610. DOI: 10.1080/01418619308207177.

[9] F.J.M. Boratto and R.E. Reed-Hill. "Oxygen and nitrogen diffusion in vanadium". In: *Scripta Metallurgica* 11.12 (Dec. 1977), pp. 1107–1111. ISSN: 00369748. DOI: 10.1016/0036-9748(77)90316-7.

[10] Mehmet Uz and O.N. Carlson. "Thermotransport and diffusion of carbon in vanadium and vanadium-titanium alloys". In: *Journal of the Less Common Metals* 116.2 (Feb. 1986), pp. 317–332. ISSN: 00225088. DOI: 10.1016/0022-5088(86)90665-X.

[11] R.C. Bradt. "Ceramic Crystals and Polycrystals, Hardness of". In: *Encyclopedia of Materials: Science and Technology*. Elsevier, 2001, pp. 1045–1051.

[12] George Ellwood. Dieter. "Applications to materials testing". In: *Mechanical metallurgy*. SI Metric. McGraw Hill, 2011, p. 332. DOI: 10.5962/bhl.title.35895.

Chapter 5

Phase stability of V-based multi-principal component alloys

P. Barron[1], A.W. Carruthers[1], M.T.P Rigby[1], S. Haigh[1], N.G. Jones[2], H. Dawson[3], and E.J. Pickering[1]

[1]Department of Materials, University of Manchester, Oxford Road, Manchester, M13 9PL, UK

[2]Department of Materials Science and Metallurgy, University of Cambridge, 27 Charles Babbage Road, Cambridge, CB3 0FS, UK

[3]Culham Centre for Fusion Energy, Abingdon, OX14 3DB, UK

Foreword

This chapter is presented in journal format. Conceptualisation was done by P.J.B. and E.J.P. As-cast alloys were supplied and fabricated by N.G.J. TEM was performed by A.W.C. FIB was performed by M.T.P.R. LECO analysis was performed externally by AMG Superalloys UK Ltd. All other experimental methods were carried out by P.J.B. Manuscript was written by P.J.B with minor revisions from all authors. Supplementary information submitted alongside the article is presented in Section 5.6. Additional detail is provided in Section 5.7 as it was not deemed sufficiently rigorous for inclusion in the main manuscript and did not add to key conclusions.

Manuscript

Abstract

The environment inside a fusion reactor is exceptionally hostile, subjecting materials to extreme thermal and irradiation conditions. An additional constraint is imposed on alloy design by the activation of elements, as it is desirable that

materials used in fusion applications will generate minimal amounts of radioactive waste. Previous work has demonstrated that it is possible to create a stable metallic body-centred cubic alloy using a combination of highly concentrated, low-activation elements. These initial studies have shown that the multi-principal component alloy systems V-Cr-Mn and Ti-V-Cr-Mn are stable after solution annealing at 1200 °C. For the alloys to be suitable for use in nuclear fusion reactors, they must be stable across a wide range of temperatures relevant to fusion applications. Here, we assess the stabilities of the microstructures of alloys in these systems following heat treatment at 1000 hrs at 600, 800 and 1000 °C. The majority of the alloys studied show no significant change in microstructure across all temperatures studied. Furthermore, significant changes in hardness were observed following the ageing heat treatments. This contrasts with other multi-principal component alloys which develop complex microstructures after ageing at intermediate temperatures. These phases have been assessed using SEM, TEM and XRD, and the results compared to CALPHAD models. Experimental results suggests CALPHAD models are able to provide reasonably accurate predictions for these alloy systems, although some discrepancies are observed in the Ti-V-Cr-Mn system when Ti content is above 5 at%.

5.1 Introduction

As global energy demand continues to grow, the world needs to expand its power output through construction of new sources. However, as the UN's Paris Agreement to reduce greenhouse gas emissions came into effect in late 2016, there is now additional pressure to ensure that these new energy sources are not only able to cope with global demand, but also minimise carbon emissions[1]. Renewable sources such as solar and wind have had significant technological improvements in recent years and are more cost-effective than ever, but they are still beset by problems with supply reliability, which can leave grids short of power if there is less sunshine or wind than expected[2].

Nuclear fusion offers an alternative low-carbon energy source with potentially abundant fuel. However, fusion reactors must minimise the amount of harmful radioactive waste they produce in order to be an attractive alternative to fission power. Even if designing a reactor produces no waste requiring deep geological disposal may not be feasible in the short-term[3, 4], it is still desirable that elements used in reactor materials should produce only intermediate-level waste that is as short-lived as possible. Such a scenario may allow for fusion waste to be recategorised as separate from fission waste (see Nicholas et al.[5] for further discussion).

This criteria necessitates the use of low-activation alloys, made from elements that will not remain radioactive for extended periods of time after exposure to fusion neutrons.

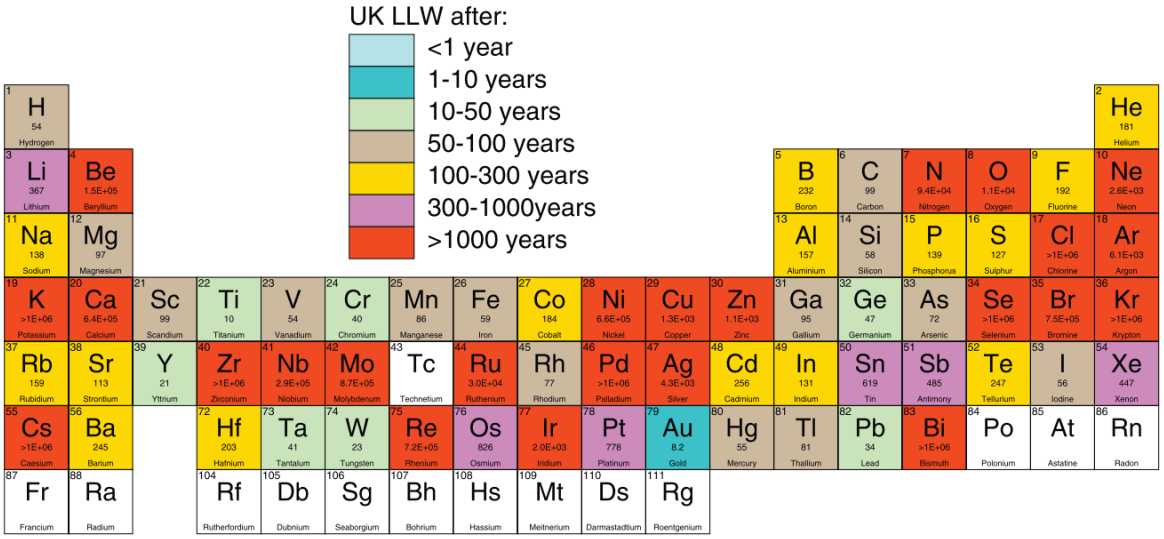

Figure 5.1: Time taken to reach low-level waste after 14 years of pulsed operation in the DEMO divertor. Taken from [3].

Figure 5.1 shows the time taken for elements to reach specific radioactivity levels that can be classified as low-level waste according to UK legislation[1] if the element was used in the divertor of a DEMO (the planned full-power demonstration fusion reactor) reactor design for 14 years of pulsed operation[3]. In order to minimise the long-lived waste produced, it is desirable that any new structural materials for fusion reactors only use elements that generate short-lived waste. Certain elements that are commonly used for nuclear structural applications (e.g. Ni or Zr) may be unacceptable from a waste-management perspective.

Previous work on the V-Cr-Mn and Ti-V-Cr-Mn alloy systems by the authors has confirmed that a range of compositions are capable of forming a single BCC solid solution phase at 1200 °C[6]. A single phase is desirable for irradiation resistance (as opposed to a microstructure comprising significant fractions of two or more phases, since differential irradiation damage across them is likely to cause issues), so any alloy used for fusion applications should exist as a stable single phase across the operating temperature range of a fusion reactor. The operating temperature will be limited by the materials used in the structural components. It is also desirable that the operating temperature is as high as possible to improve thermodynamic efficiency[7]. Any single-phase microstructure must also be shown to be at thermodynamic equilibrium at the desired operating temperature. Many compositionally complex alloys appear stable at a given temperature after short-term ageing (and are reported as such in literature[8, 9]), when longer-term ageing results in a decomposition into a multi-phase microstructure. Many components inside a fusion reactor will remain at elevated temperatures for extended periods of time (although the exact length will depend on reactor design and

[1] <4 MBq/kg alpha activity or <12 MBq/kg beta + gamma activity.

operation), so it is important that any materials used remain microstructurally stable across these timescales.

This study aims to investigate the long-term phase stability of the alloys presented in the previous work[6] by heat treating the alloys for periods of time up to several weeks at fusion relevant temperatures: 600, 800 and 1000 °C. The resulting microstructures will then be characterised using secondary electron microscopy (SEM), transmission electron microscopy (TEM), and X-ray diffraction (XRD) to assess thermodynamic stability. Microhardness will also be assessed and correlated with microstructure. The relationship between interstitial content and alloy properties will be investigated. Some conclusions will be drawn regarding the relationship between interstitial content and alloy properties.

5.2 Method

Eight alloys were fabricated as ingots weighing approximately 25 g using an arc melting process in an argon atmosphere (see Table 4.2). The ingots were inverted and remelted three times to ensure homogeneity. Sections of each ingot were cut off, wrapped in tantalum foil, and then encapsulated in quartz ampoules backfilled with low pressure argon. These samples then underwent a homogenisation heat treatment at 1200 °C for 100 hours, before quenching in water. From these homogenised samples, further sections of the ternary and quaternary alloys were cut for ageing at 600, 800 and 1000 °C. Three samples were held at each ageing temperature for 1000 hours. A V-4Cr-4Ti reference sample was also heat treated using the same procedure at 1200 °C for 100 hours.

Nominal				**Measured (EPMA)**			
V	**Cr**	**Mn**	**Ti**	**V**	**Cr**	**Mn**	**Ti**
60	20	20	-	63.04 ± 0.07	20.58 ± 0.03	16.39 ± 0.09	-
40	20	40	-	39.40 ± 0.24	21.60 ± 0.17	39.01 ± 0.08	-
40	40	20	-	41.08 ± 0.22	43.20 ± 0.35	15.73 ± 0.14	-
33.33	33.33	33.33	-	32.80 ± 0.28	35.53 ± 0.29	31.68 ± 0.04	-
33	33	33	1	42.03 ± 0.03	40.89 ± 0.05	15.69 ± 0.07	1.38 ± 0.01
32.67	32.67	32.67	2	35.82 ± 0.16	36.08 ± 0.15	25.10 ± 0.11	3.00 ± 0.42
32	32	32	4	34.53 ± 0.02	32.09 ± 0.02	27.92 ± 0.02	5.45 ± 0.05
30.67	30.67	30.67	8	35.84 ± 0.18	29.95 ± 0.12	25.52 ± 0.03	8.68 ± 0.32

Table 5.1: Measured alloy compositions (determined using wavelength dispersive spectroscopy) compared with their nominal values. Values are in at.% with absolute standard errors shown[6].

CALPHAD results were obtained by using Thermocalc 2021a with a high-entropy alloy database (TCHEA4) and a ferrous alloy database (TCFE10). The ferrous database,

although not strictly appropriate for performing calculations on alloys not containing Fe, was used as it was capable of assessing O and S interstitial impurities. All ternary and quaternary alloys were evaluated using both databases between temperatures of 200 and 2000 °C. Measured compositions were assessed, with and without interstitial impurities (C, N, O and S in the TCFE10 database; C and N in the TCHEA4 database) as the presence of interstitial elements is known to be the cause of certain microstructural features in this suite of alloys[6]. Interstitial impurity contents were known for some alloys (see below). For the alloys where interstitial content was not known, an average of the measured values was used as an estimate.

Secondary electron microscopy (SEM) specimens were prepared using standard metallographic techniques. The final polish was performed with a 0.04 µm oxide polishing suspension. Back scattered electron (BSE) images and energy dispersive X-ray (EDX) spectra were obtained using a Zeiss Ultra55 microscope at 10 kV with an Oxford Instruments EDX detector. SEM-EDX quantification was performed using the AZTEC software. Electron back-scattered diffraction (EBSD) was performed using a Zeiss Sigma electron microscope with Oxford Instruments EDX and EBSD detectors. Vickers hardness measurements were taken with a load of 9.8 N and dwell time of 10 s using a Matsuzawa MMT-X indenter. Nine microhardness measurements were made spaced 0.5 mm apart in a three by three grid formation. Thin foils were prepared via the focused ion beam (FIB) in-situ lift-out method[10] using an FEI Nova Nanolab 600 dual beam SEM/FIB, operated at 30 kV and with a Ga^+ beam current of 10 pA – 9 nA. A FEI Talos F200 TEM with a 200 kV X-FEG was used to produce annular dark field (ADF) images, EDX maps (using Super X EDX with four silicon drift detectors), and selected area electron diffraction (SAED) patterns. TEM-EDX quantification was performed using the Velox software.

A selection of samples in the homogenised state were sent for external analysis to determine C, N, O and S content using LECO infrared combustion analysers. The surface of the samples was ground away to ensure no oxide film was present before analysis. Two reference samples of V-4Cr-4Ti have also been included for comparison. One was a highly purified sample in its as-received state from the Culham Centre for Fusion Energy, having undergone refinement processes described in Ref. [11]. The other sample was the as-received V-4Cr-4Ti which was subject to the same homogenisation process as the other alloys.

5.3 Results

5.3.1 CALPHAD

Using the TCHEA4 database, CALPHAD results predicted the formation of a single BCC phase at high temperatures for all the ternary alloys, as seen in fig. 5.2. Some sigma phase is predicted to form below 600 °C for the higher Mn ternary alloys. In the quaternary alloys some Laves and sigma phases are predicted for temperatures as high as around 600 °C for V-30Cr-26Mn-9Ti. None of the alloys, in their interstitial-free states, are predicted to form anything other than a BCC phase in the range of temperatures studied in this work, with the exception of V-30Cr-26Mn-9Ti.

Fig. 5.3 shows how the predicted phases change when including C and N interstitial impurity atoms (O was not included in the database) in the calculation performed using TCHEA4. A wide variety of new phases are predicted in both the ternary and quaternary alloys containing the impurities. When C and N impurities (the concentrations of which were determined by LECO analysis) are included in the calculation, the phases present in the ternary alloys increase in number to include vanadium carbides and nitrides, which were not observed in the samples. A zeta phase is also predicted at lower temperatures, but again outside the range of study. For the quaternary alloys, titanium carbonitrides are predicted in lieu of their vanadium counterparts. Carbides and carbonitrides are predicted in all alloys between 600 and 1000 °C in sub-percent quantities. Sigma and Laves phases are expected in the same fractions and temperature ranges as their interstitial-free equivalents.

The same calculations were also run using TCFE10, a ferrous alloys database (shown in Supp. Figs. 5.15 and 5.16). The Laves and Sigma phases were still predicted to form at roughly the same temperatures and fractions for all alloys, with the only difference in predictions caused by O and S being added to the assessed elements. Including O led to the prediction of VO in the ternary alloys, whereas including S led to very small proportions of MnS and $Ti_4C_2S_2$ phases being predicted.

5.3.2 Microstructure

Figs. 5.4 to 5.7 show BSE images of the four ternary V-Cr-Mn alloys after heat treatment. Most of the alloys showed limited microstructural changes from the homogenised state (Figs. 5.4,5.6, and 5.7(a)), which was previously identified to be a single-phase BCC matrix with MnV_2O_4 precipitates formed from oxygen impurities[6]. Fig. 5.5 indicated some slight microstructural changes in V-22Cr-39Mn with long, thin precipitates appearing in the aged samples (b) to (d). EDX and EBSD indicated that these morphologically distinct precipitates had the same crystal structure and chemistry as the precipitates in the other ternary alloys (see Supp. Fig. 5.18).

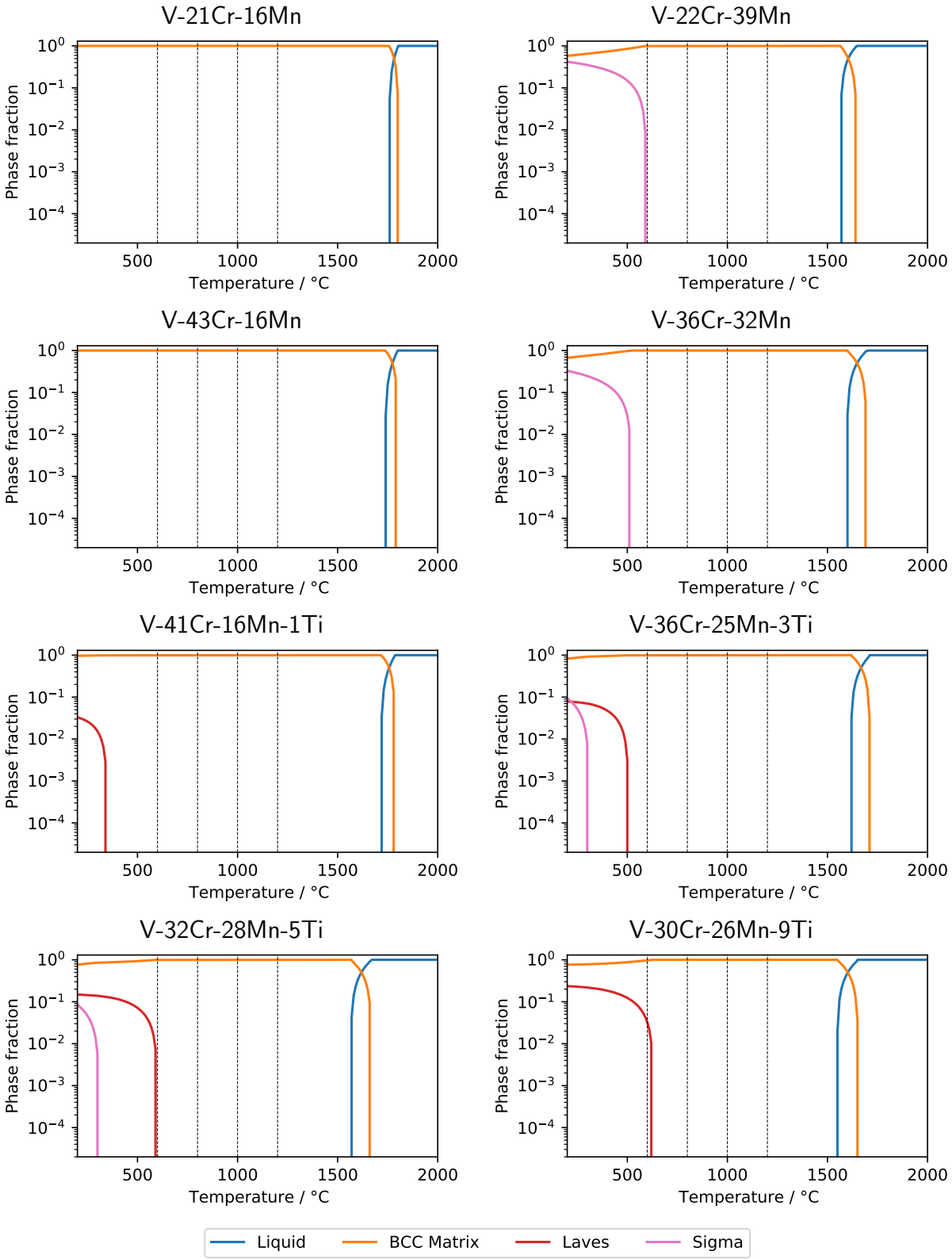

Figure 5.2: Phase proportions of alloys with no interstitial impurities, determined by CALPHAD using the TCHEA4 database. Temperatures of study are marked with dashed lines.

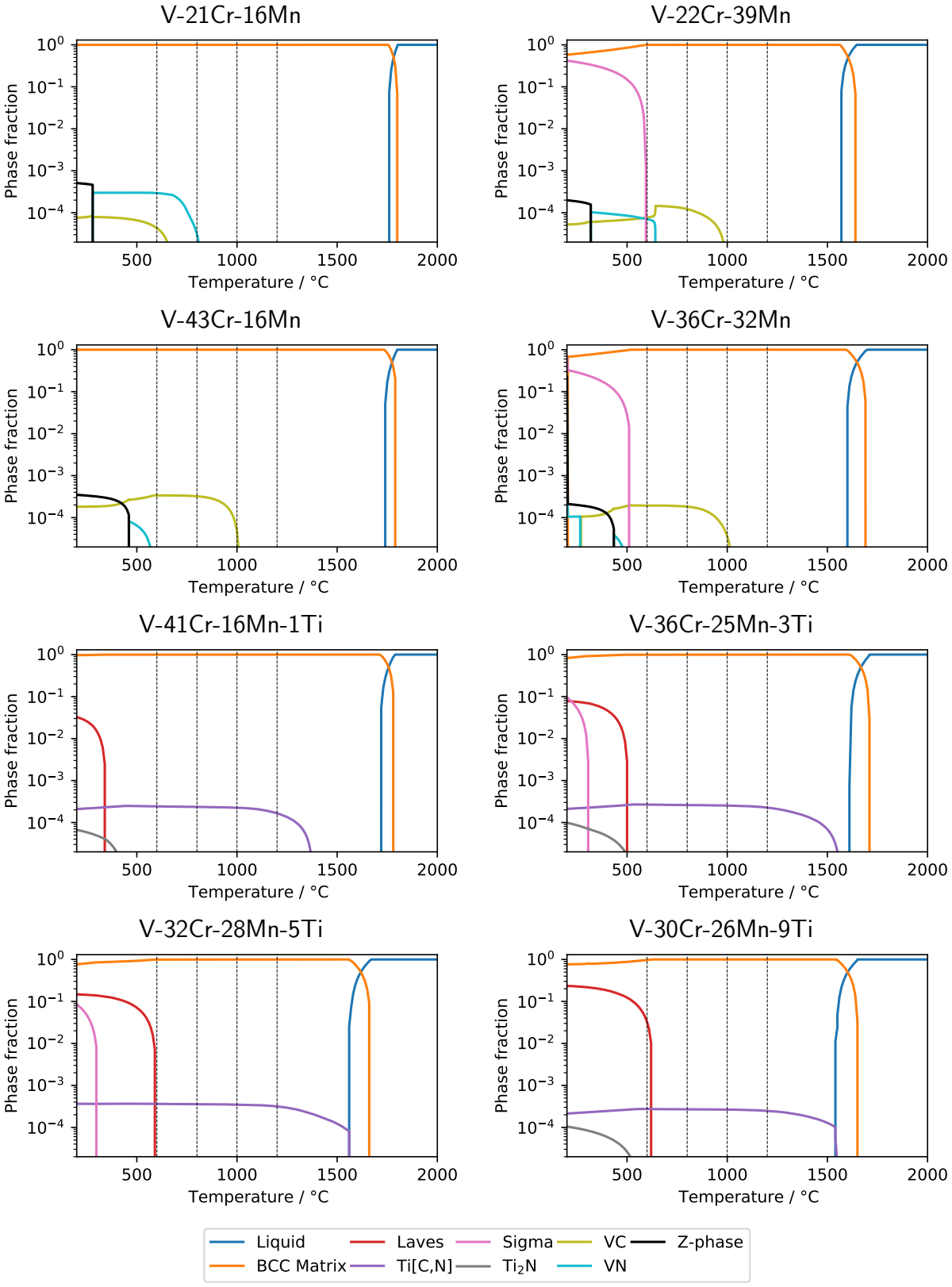

Figure 5.3: Phase proportions of alloys containing both C and N impurities, determined by CALPHAD using the TCHEA4 database. Temperatures of study are marked with dashed lines.

Figs. 5.8 to 5.11 show BSE images of the quaternary alloys heat treated in the same manner as the ternary alloys. Alloys V-41Cr-16Mn-1Ti and V-36Cr-25Mn-3Ti again show a single-phase matrix with small precipitates in all four heats. The only change in microstructure appears to be a slight coarsening of the precipitates in V-41Cr-16Mn-1Ti. EDX indicated that these precipitates were rich in Ti and presumably the same Ti[C,O,N] precipitates observed in the homogenised state[6].

Alloys V-32Cr-28Mn-5Ti and V-30Cr-26Mn-9Ti showed more significant microstructural changes with respect to ageing temperature. Three different precipitates are observed: one denoted white (W), which only appears in the 1000 °C heats, and two other types, denoted dark grey (DG) and light grey (LG), which appear at all three ageing temperatures (Figs. 5.10 and 5.11). Tables 5.2 and 5.2 show the results of SEM and TEM EDX quantification of the precipitates. Some discrepancies between SEM and TEM results were noted, possibly due to the SEM interaction volume overlapping into regions that contained a different phase. SEM-EDX indicated the white precipitates were enriched in Ti and Mn relative to the matrix. The dark grey precipitates were chemically similar to those observed in the lower at%Ti alloys. The light grey precipitates were also enriched in Ti, but also showed an increase in Mn, N and S relative to the matrix.

SAED were utilised to identify these new precipitates. Fig. 5.12 shows TEM-EDX maps of a FIB foil taken from a region of alloy V-30Cr-26Mn-9Ti treated for 1000 hours at 1000 °C that contained all three precipitates, for the purpose of characterising them. TEM-EDX was used to match regions of the foil to their respective precipitates. (Fig. 5.12(a)-(f)). Electron diffraction patterns for W and DG precipitates and the matrix, are shown in Fig. 5.12. The matrix was BCC (a = 3.0±0.1 Å), dark grey was FCC (a = 4.1±0.1 Å)), and white was hexagonal (a = 4.8±0.1 Å and c = 7.0±0.1 Å). The diffraction pattern for the light grey precipitate could not be indexed. EBSD results showed that the W precipitates were hexagonal, but the other precipitates were not able to be indexed (see Supp. Fig. 5.17).

A FIB foil taken from V-32Cr-28Mn-5Ti aged for 1000 hours at 1000 °C used the same approach to identify the precipitates and found similar chemistries and lattice parameters. Furthermore, the diffraction pattern of a light grey precipitate was indexed as FCC with a lattice parameter of approximately 11.8±0.5 Å. Difficulty obtaining good diffraction patterns contributed to the low precision of this measurement.

FIB foils of alloys V-32Cr-28Mn-5Ti and V-30Cr-26Mn-9Ti aged at 600 and 800 °C were also investigated. Both light grey and dark grey precipitates had similar compositions and identical lattice parameters to their counterparts in the 1000 °C aged samples. Interestingly, the white phase was observed in the V-30Cr-26Mn-9Ti samples in the form of sub-micron precipitates that were found adjacent to light grey particles, despite not being observed under SEM.

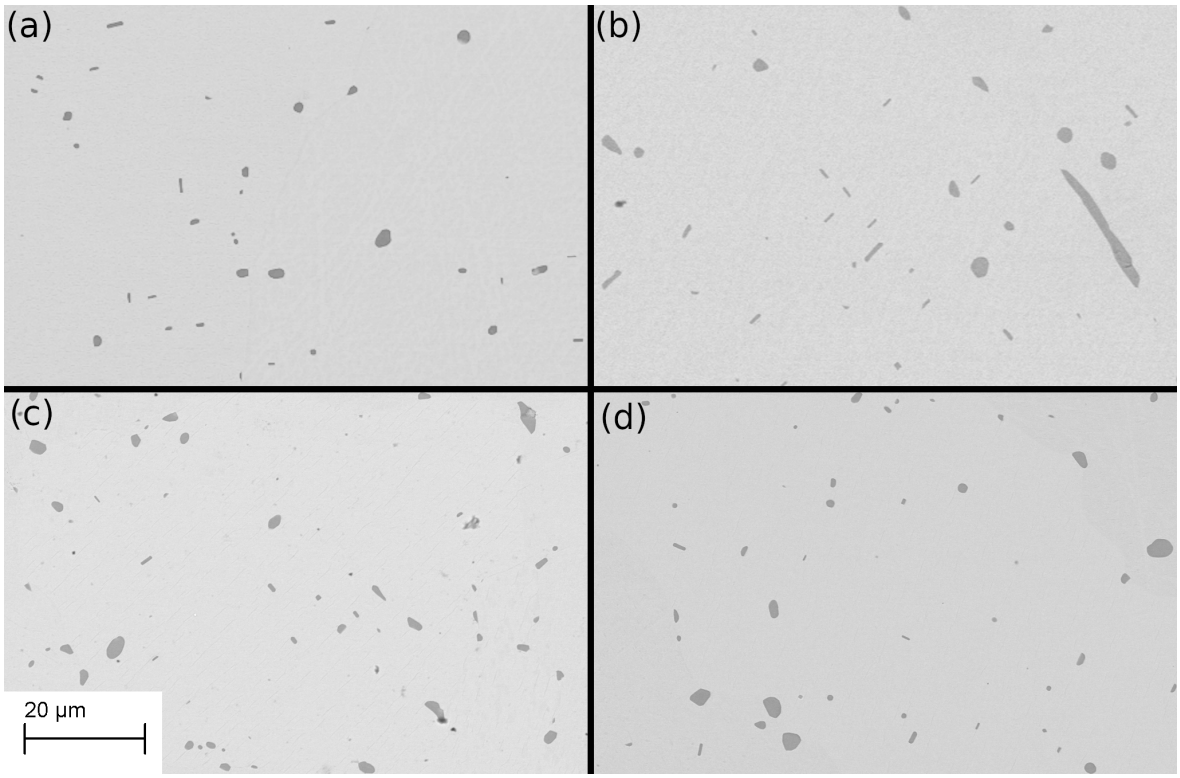

Figure 5.4: BSE images of V-21Cr-16Mn (a) homogenised at 1200 °C for 1000 hrs (b) aged at 600 °C for 1000 hrs (c) aged at 800 °C for 1000 hrs (b) aged at 1000 °C for 1000 hrs.

Overall, the lattice parameters of the white precipitates suggested a C14-Laves phase, and the chemistries implied it was $TiMn_2$ with significant deviations from ideal stoichiometry. The dark grey phase comprised mostly of Ti and also showed high quantities of N and O which were not included in the quantification due to large errors in fitting the X-ray peak data (see Supp. Fig 5.20), and had a lattice parameter consistent with Ti-[C,O,N] precipitates observed in the homogenised alloys[6]. The light grey phase contained high amounts of Ti, N (not quantified) and S, with an FCC lattice (a = 11.8 Å). The relatively high proportions of Ti and N and the lattice parameter were similar to nitrides found in the Ti-Ni-Al-N system[12].

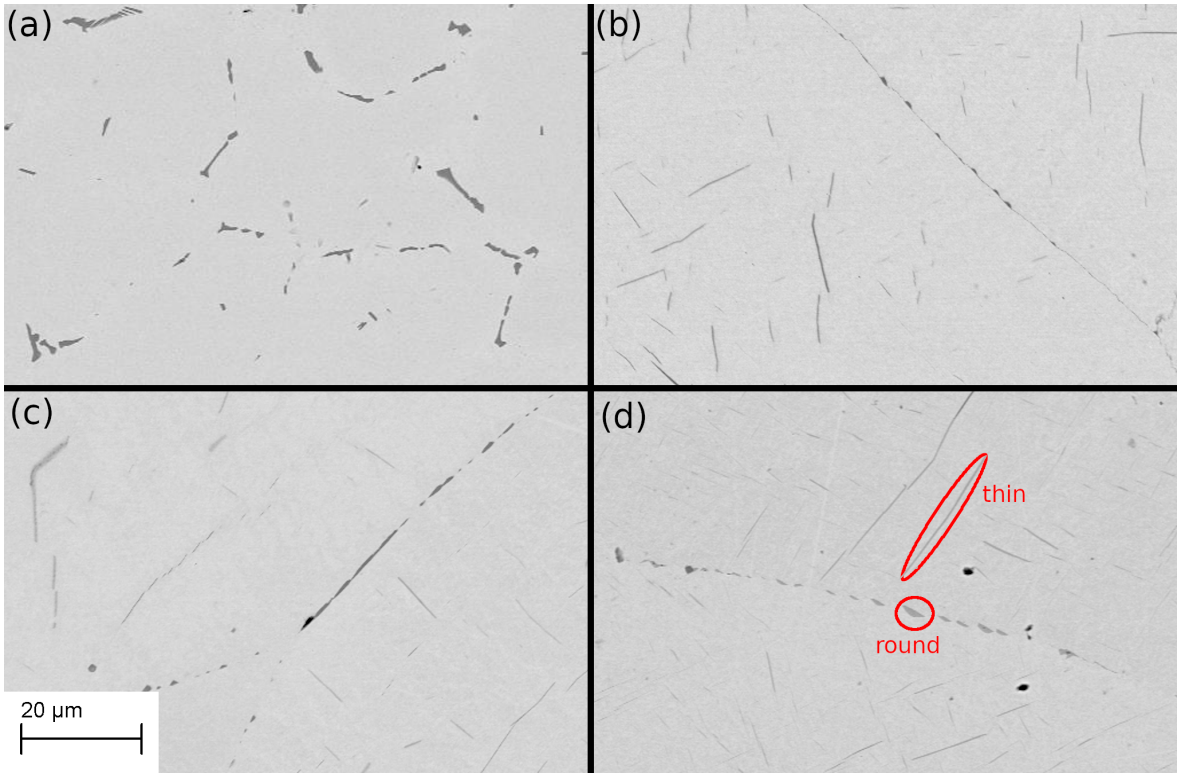

Figure 5.5: BSE images of V-22Cr-39Mn (a) homogenised at 1200 °C for 100 hrs (b) aged at 600 °C for 1000 hrs (c) aged at 800 °C for 1000 hrs (b) aged at 1000 °C for 1000 hrs.

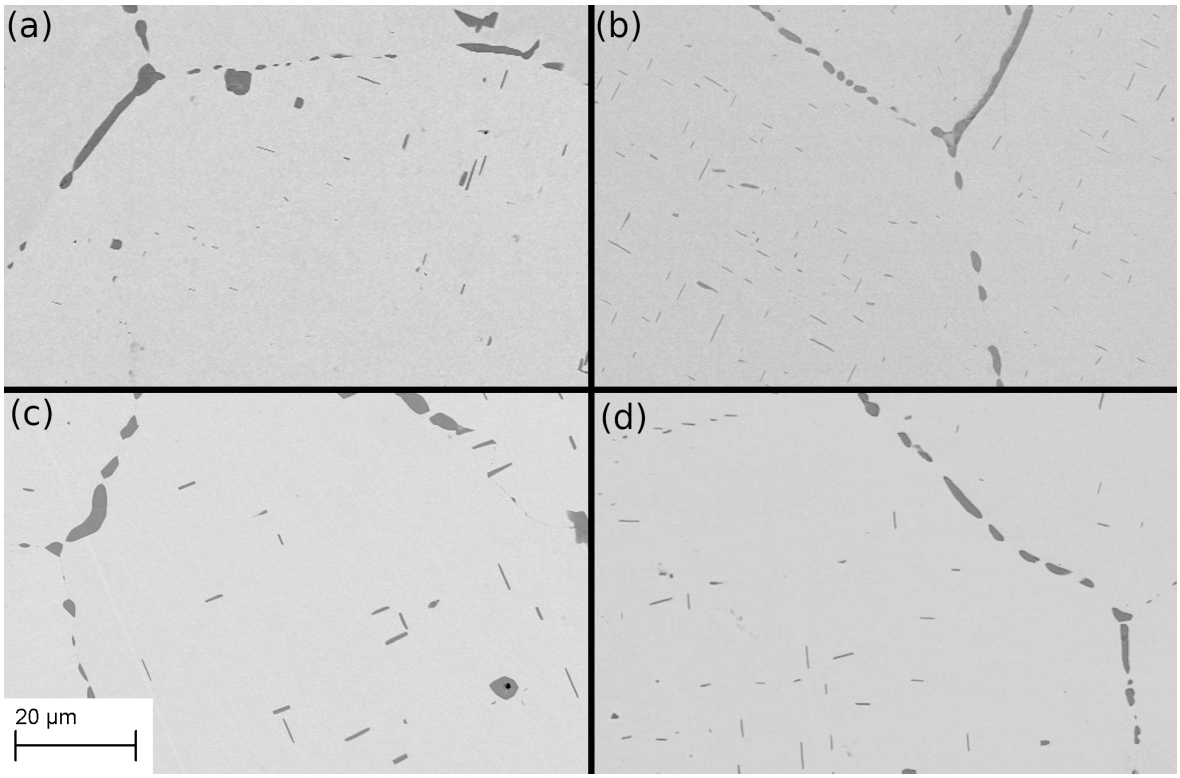

Figure 5.6: BSE images of V-43Cr-16Mn (a) homogenised at 1200 °C for 100 hrs (b) aged at 600 °C for 1000 hrs (c) aged at 800 °C for 1000 hrs (b) aged at 1000 °C for 1000 hrs.

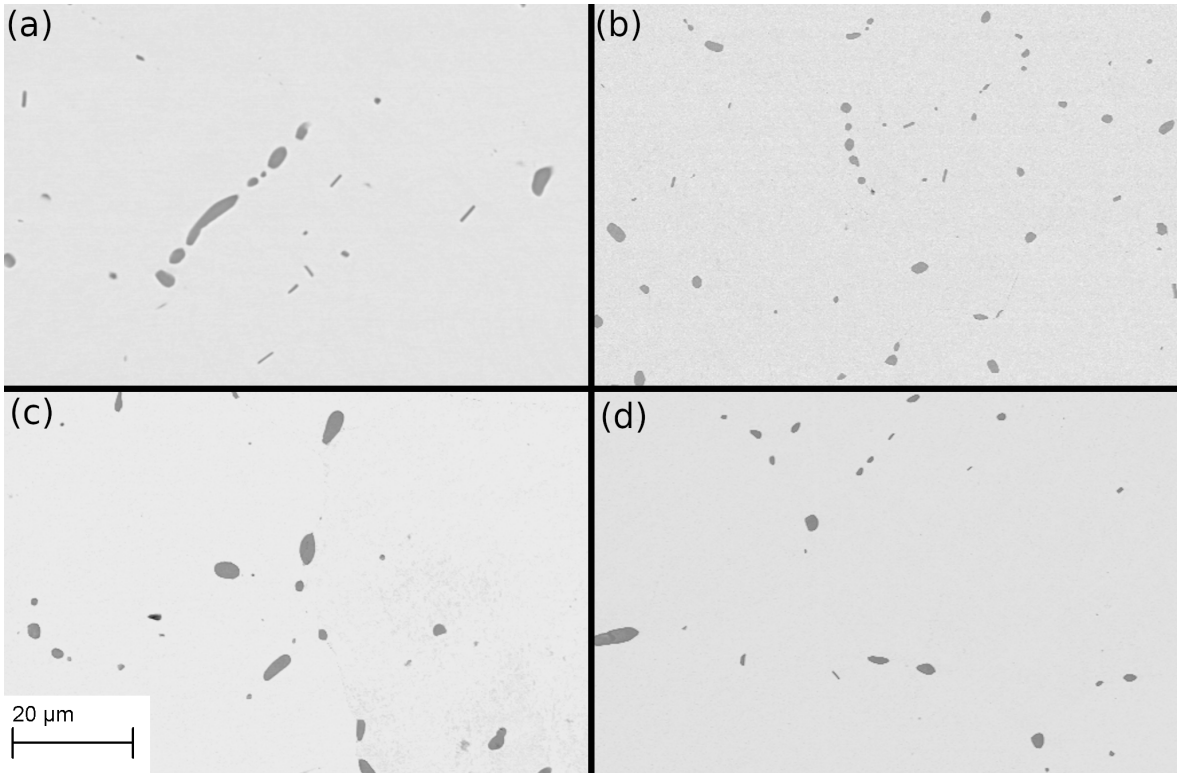

Figure 5.7: BSE images of V-36Cr-32Mn (a) homogenised at 1200 °C for 100 hrs (b) aged at 600 °C for 1000 hrs (c) aged at 800 °C for 1000 hrs (b) aged at 1000 °C for 1000 hrs.

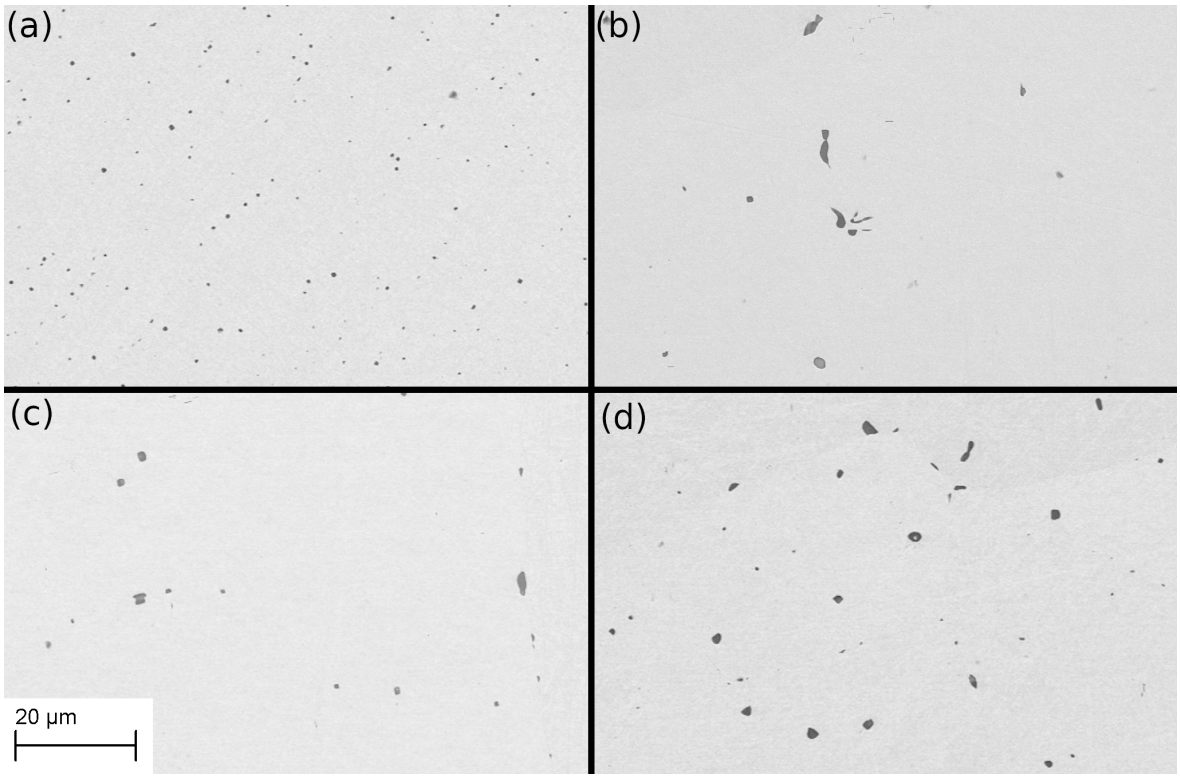

Figure 5.8: BSE images of V-41Cr-16Mn-1Ti (a) homogenised at 1200 °C for 100 hrs (b) aged at 600 °C for 1000 hrs (c) aged at 800 °C for 1000 hrs (b) aged at 1000 °C for 1000 hrs.

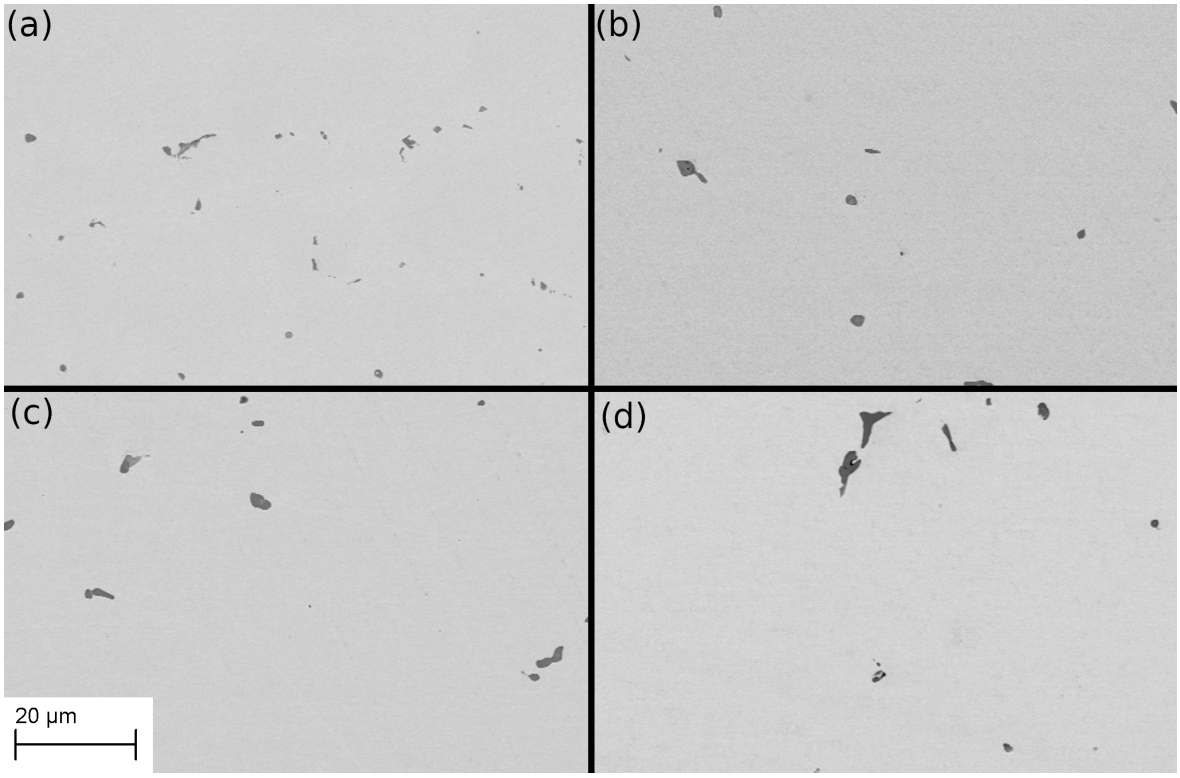

Figure 5.9: BSE images of V-36Cr-25Mn-3Ti (a) homogenised at 1200 °C for 100 hrs (b) aged at 600 °C for 1000 hrs (c) aged at 800 °C for 1000 hrs (b) aged at 1000 °C for 1000 hrs.

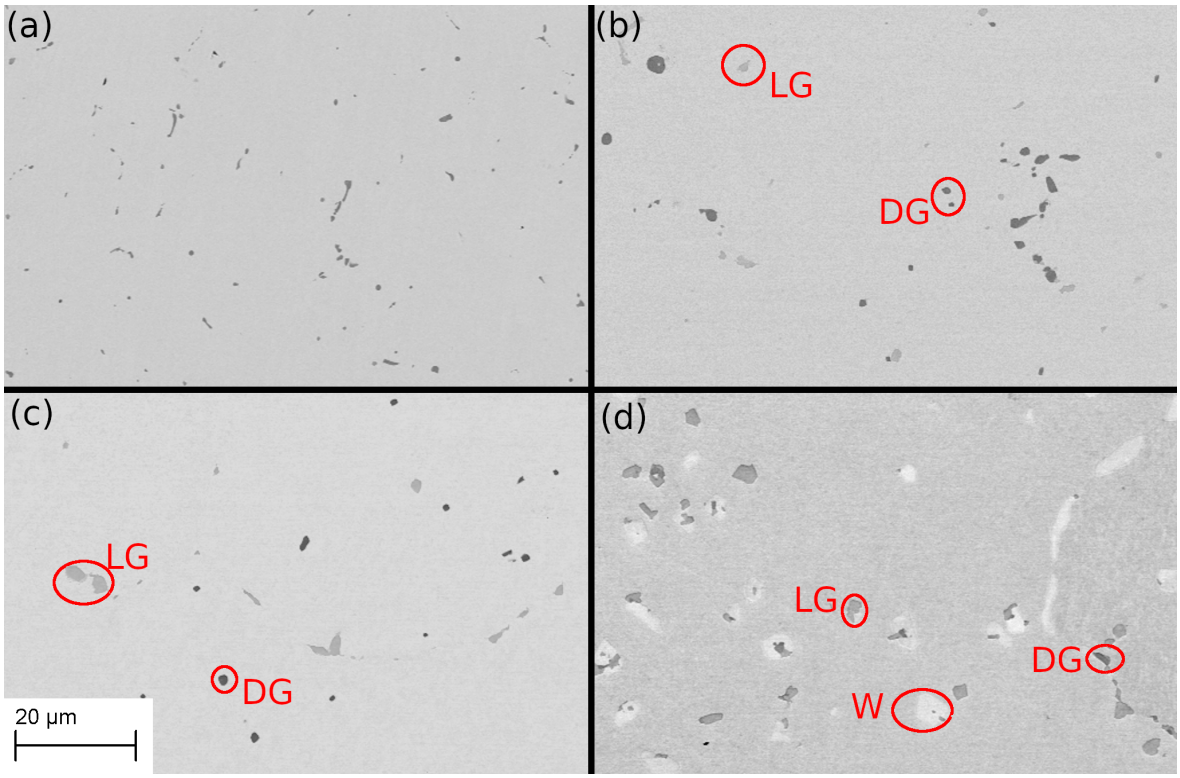

Figure 5.10: BSE images of V-32Cr-28Mn-5Ti (a) homogenised at 1200 °C for 100 hrs (b) aged at 600 °C for 1000 hrs (c) aged at 800 °C for 1000 hrs (b) aged at 1000 °C for 1000 hrs.

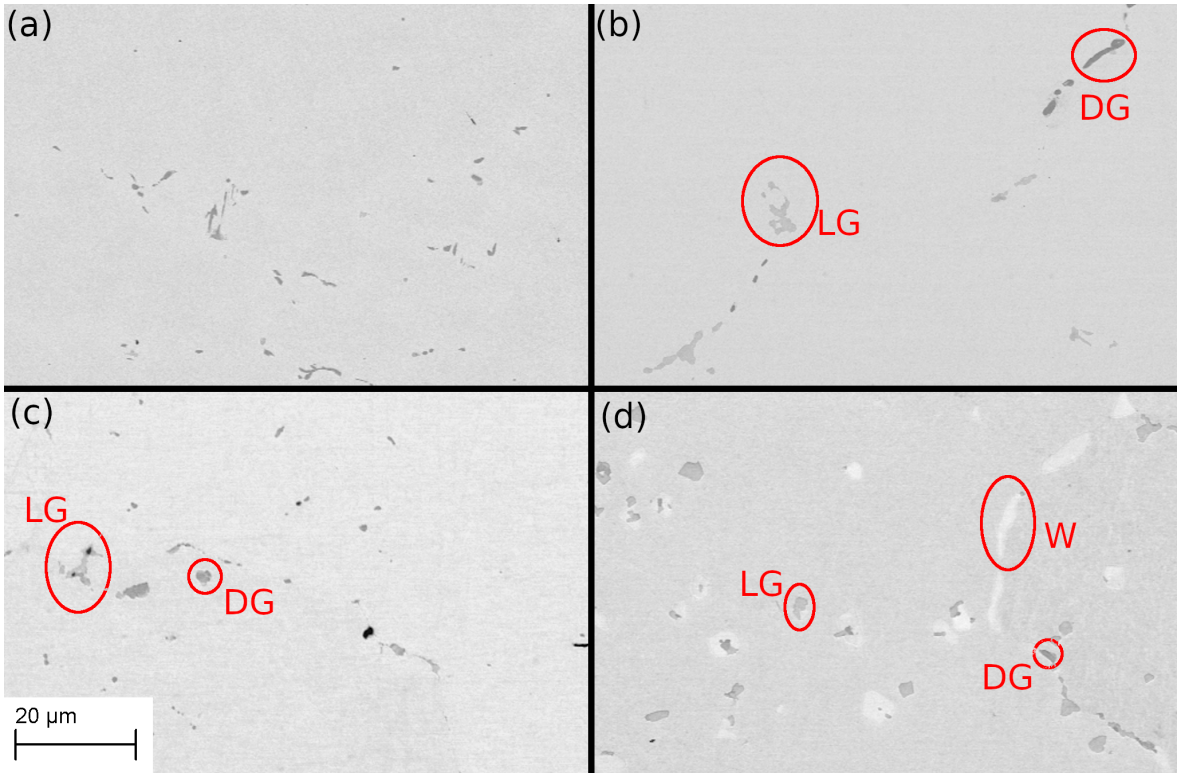

Figure 5.11: BSE images of V-30Cr-26Mn-9Ti (a) homogenised at 1200 °C for 100 hrs (b) aged at 600 °C for 1000 hrs (c) aged at 800 °C for 1000 hrs (b) aged at 1000 °C for 1000 hrs.

		Precipitate composition / at%				
ppt	**Method**	**S**	**Ti**	**V**	**Cr**	**Mn**
W	SEM	0.08±0.02	29.4±0.1	10.4±0.1	18.3±0.1	41.9±0.1
W	TEM	0.12±0.01	29.5±5.3	18.7±3.3	20.4±3.6	31.4±5.6
LG	SEM	1.9±0.1	43.7±0.6	6.5±0.4	15.3±3.9	32.5±2.3
LG	TEM	1.53±0.2	49.5±9.4	7.5±1.4	11.6±2.2	29.9±5.7
DG	SEM	0	79.4±0.7	0.6±0.4	20.0±3.8	0
DG	TEM	0	74.6±16.2	10.5±2.3	8.1±1.8	6.8±1.5

Table 5.2: Precipitate compositions for V-32Cr-28Mn-5Tiaged at 1000 °C. C, N, and O X-ray peaks were not included in the quantification.

		Precipitate composition / at%				
ppt	**Method**	**S**	**Ti**	**V**	**Cr**	**Mn**
W	SEM	0±0.04	26.0±0.1	16.1±0.1	21.0±0.2	37.0±0.2
W	TEM	0.03±0.03	29.6±0.1	12.4±0.1	19.7±0.1	38.3±0.1
LG	SEM	2.2±0.4	44.9±3.2	11.7±2.2	14.8±1.7	26.4±3.1
LG	TEM	4.8±0.7	61±12.3	3.9±0.8	8.3±1.7	21.6±4.4
DG	SEM	0.1±0.1	62.8±0.5	4.2±0.4	10.2±3.6	22.8±1.9
DG	TEM	0.8±0.4	66.2±13.6	14.9±3.1	10.9±2.3	7.3±1.5

Table 5.3: Precipitate compositions for V-30Cr-26Mn-9Tiaged at 1000 °C. C, N, and O X-ray peaks were not included in the quantification.

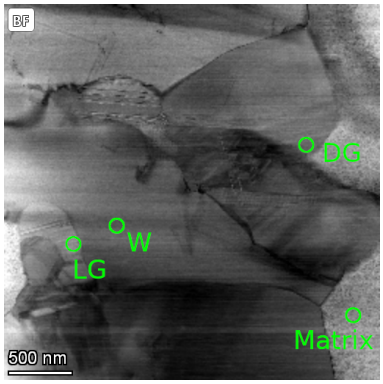

(a) Bright field image

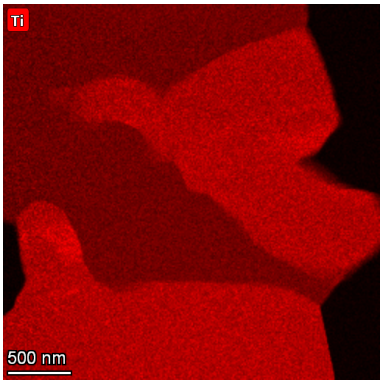

(b) Ti map

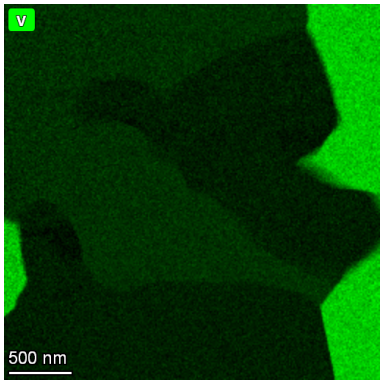

(c) V map

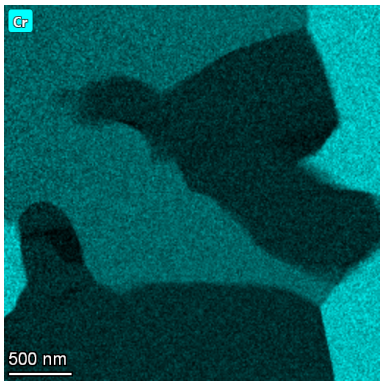

(d) Cr map

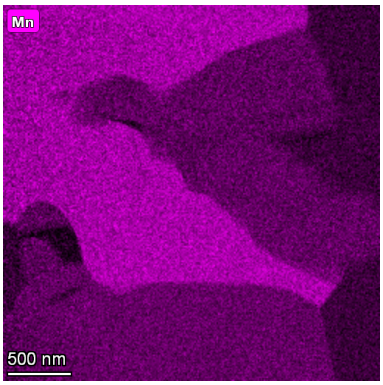

(e) Mn map

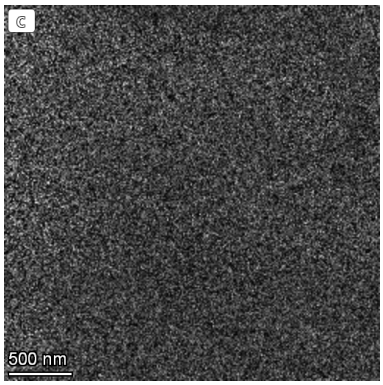

(f) C map

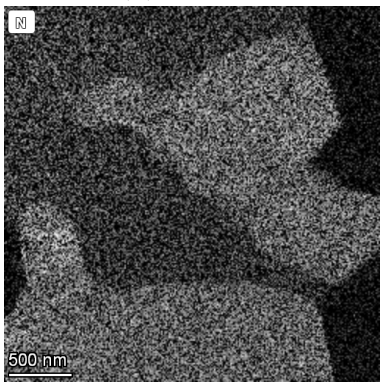

(g) N map

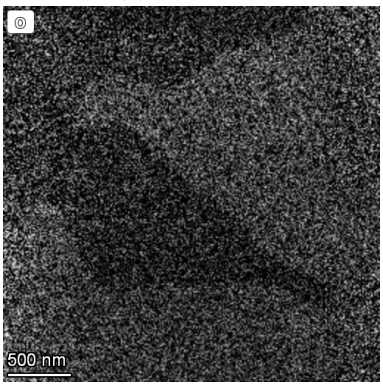

(h) O map

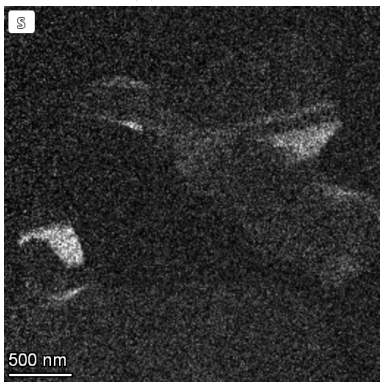

(i) S map

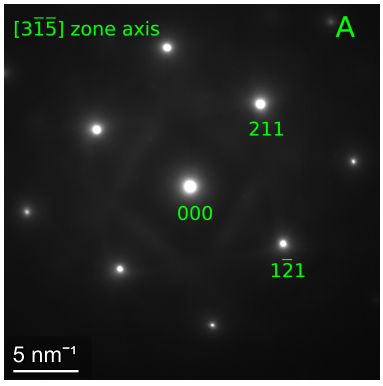

(j) Diffraction pattern of matrix

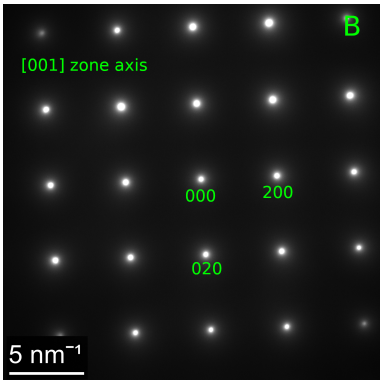

(k) Diffraction pattern of region DG

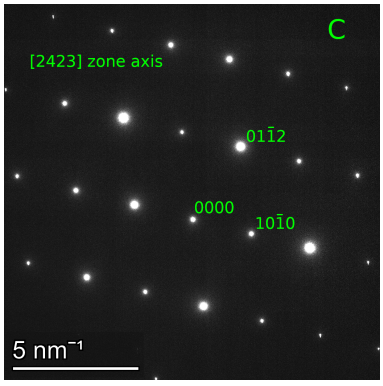

(l) Diffraction pattern of region W

Figure 5.12: TEM-EDX map and diffraction patterns from V-30Cr-26Mn-9Ti aged for 1000 °C for 1000 hours.

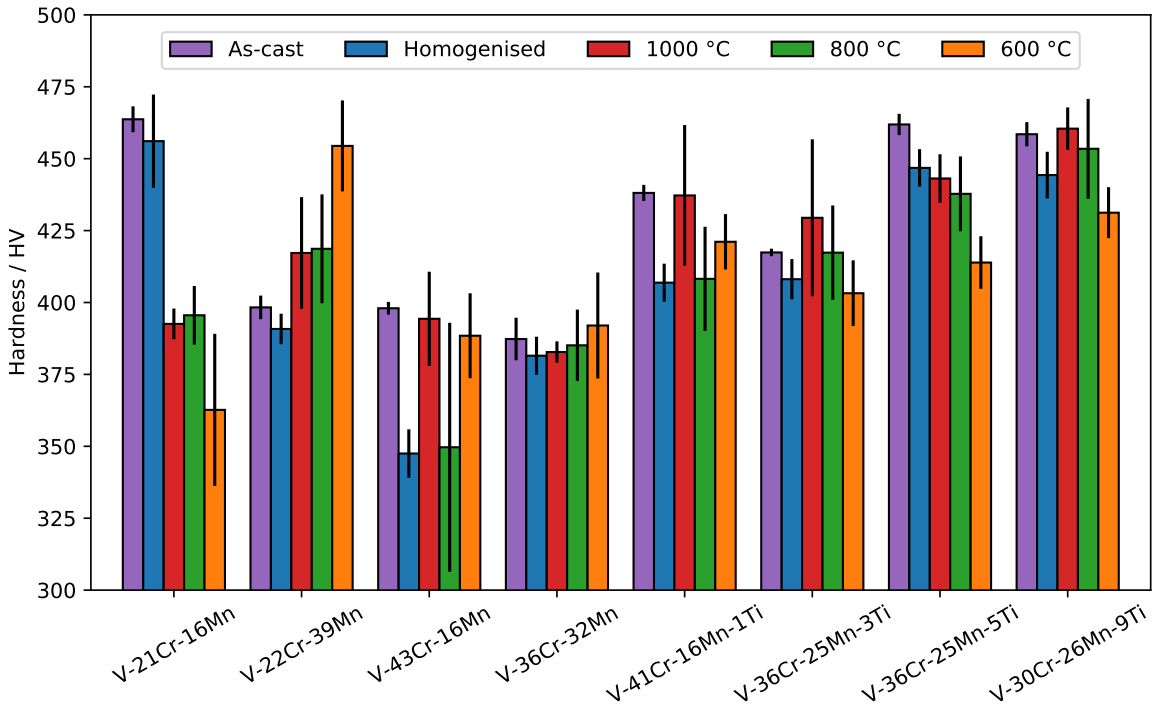

Figure 5.13: Vickers hardness variation for each heat treatment of the alloys. Error bars show the standard deviation in the measurements taken.

5.3.3 Microhardness

Microhardness data are presented in Fig. 5.13, which shows no apparent relation between heat treatment conditions and hardness. There are significant variations between the various heat treatments of a single alloy, which may be explained by differences in interstitial content, which is known to have a noticeable effect on the mechanical properties of vanadium alloys[13] (see Section 4.3.2).

5.3.4 Impurity analysis

Results of the elemental analysis are shown in Table 5.4. Oxygen is by far the most prevalent impurity element in all of the alloys, and appears to be correlated with alloy vanadium content (Fig. 5.14) in the homogenised alloys. Vanadium has a high solubility of oxygen relative to other metals[14, 15], which may explain the relationship.

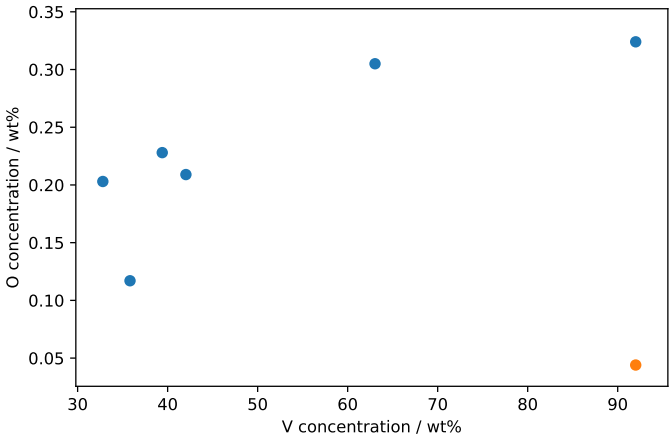

Figure 5.14: Variation of oxygen concentration with vanadium content. As-received V-4Cr-4Ti sample in orange.

	Impurity content / wt%			
Alloy	**C**	**N**	**O**	**S**
V-21Cr-16Mn	0.003	0.008	0.305	0.008
V-22Cr-39Mn	0.002	0.003	0.228	0.006
V-36Cr-32Mn	0.004	0.003	0.203	0.009
V-41Cr-16Mn-1Ti	0.007	0.004	0.209	0.012
V-36Cr-25Mn-5Ti	0.012	0.004	0.117	0.015
V-4Cr-4Ti (as-received)	0.009	0.005	0.324	0.001
V-4Cr-4Ti (homogenised)	0.009	0.007	0.044	0.002

Table 5.4: Impurity content of alloys measured by LECO analysis.

5.4 Discussion

5.4.1 Microstructure & CALPHAD predictions

5.4.1.1 Ternary alloys

The results indicate that no significant microstructural evolution of the alloys occurred during thermal ageing at the temperatures studied for times of up to 1000 hours in five of the eight compositions studied. Out of ternary alloys, only V-22Cr-39Mn showed a noticeable change in microstructure. The more round particles in this alloy appear at grain boundaries, whereas the long, thin precipitates seem to appear inside grains. However, these morphologically distinct precipitates do not appear to change in character between ageing treatments and appeared to be the same phase as the more round precipitates in the same alloy and the other ternary alloys. Any precipitate evolution might be problematic from a fusion perspective, rendering V-22Cr-39Mn unsuitable for such applications. However, as the precipitates are caused by interstitial impurities, control of these elements may prevent the observed microstructural changes from occurring.

In the case of interstitial-free ternary alloys, CALPHAD successfully predicts that a single BCC phase will be present across all temperature ranges (Fig. 5.2). Although sigma phase is predicted to precipitate at lower temperatures ($< 600\,^{\circ}C$) in alloys with higher Mn content, these temperatures are outside the range of this study. The main discrepancy between the CALPHAD predictions and observed microstructures are the MnV_2O_4 precipitates, but as the TCHEA4 database does not include oxygen, it clearly could not have been predicted.

5.4.1.2 Quaternary alloys

The two alloys with lower Ti content (V-41Cr-16Mn-1Ti and V-36Cr-25Mn-3Ti) displayed good thermal stability. The only microstructural change observed was a coarsening of the Ti-[C,O,N] precipitates in V-41Cr-16Mn-1Ti. The fact that these precipitates are still present at 1200 and $1000\,^{\circ}C$ in all Ti-containing alloys is somewhat notable as equivalent precipitates in V-4Cr-4Ti alloys will dissolve at these temperatures[16]. CALPHAD predictions indicate this may be due to Mn acting as a stabiliser for these particles, as dissolution temperature seems to increase with Mn content (Fig. 5.3). CALPHAD results for V-4Cr-4Ti predicted a much lower dissolution temperature of around $800\,^{\circ}C$ for the Ti-[C,N] precipitates (see Supp. Fig. 5.19) relative to the alloys studied here.

The two alloys with the higher Ti (V-32Cr-28Mn-5Ti and V-30Cr-26Mn-9Ti) content did exhibit evidence of new phases, such as the $TiMn_2$ Laves phase and possibly a nitride, forming after heat treatment at fusion relevant temperatures, potentially

rendering them unsuitable for use in a fusion environment. Another study examining the TiVCrMnFe system found that increased Ti content promoted the formation of the Laves phase, with 20 at.% Ti leading to a Laves phase fraction of greater then 50%[17]. The appearance of these phases only at higher Ti concentrations is not necessarily an issue from an alloy design perspective. Low Ti content (<1wt%) is sufficient for suppressing void swelling in vanadium fusion alloys[18]. Due to variations in the alloy composition from the arc-melting process, the Mn content of the Laves-forming quaternaries is higher than those that don't form Laves. As the Laves phase appears to be Mn_2Ti, it is likely that this increased Mn content is an additional driver for the formation of the Laves phase. For V-30Cr-26Mn-9Ti aged at 600 and 800 °C, a probable reason for the observation of the Laves phase in the TEM and not in the SEM is that the particles that were detected in the FIB foil were less than a micron in size and were either adjacent to or partially surrounded by larger light-grey type precipitates. There appears to be some sort of connection between the Laves phase and the unknown nitrides. They are compositionally similar (showing high Ti and N content relative to the matrix) and often appear adjacent to each other if present in the same alloy.

This alloy system also shows reasonable agreement with CALPHAD predictions without interstitials (Fig. 5.2). Alloys V-41Cr-16Mn-1Ti and V-36Cr-25Mn-3Ti show complete agreement across the range of temperatures studied (i.e. a single BCC phase). Ti-[C,O,N] type precipitates do appear in the microstructures but are not predicted due to these calculations not including C or N. A deviation from prediction does occur for alloys V-32Cr-28Mn-5Ti and V-30Cr-26Mn-9Ti. CALPHAD predicts a single BCC phase across almost the entire temperature range (with the exception of a few % of Laves forming at 600 degree C in V-30Cr-26Mn-9Ti). However, in practice, the Laves phase forms at 1000 °C for both V-32Cr-28Mn-5Ti and V-30Cr-26Mn-9Ti. It also forms in very small quantities at 600 and 800 °C in V-30Cr-26Mn-9Ti. Given that O is not included in this database, it is fair to say that the predictions of the CALPHAD calculations with interstitials are generally accurate if the predicted Ti[C,N] phase is treated analogously to the Ti[C,O,N] phase seen in practice.

5.4.2 Microhardness & impurities

As discussed in a previous work[6], the solid solution strengthening from introducing Ti may outweigh the softening effect of gettering interstitials in the Ti-containing alloys, leading to an overall hardening of these alloys relative to the ternary system. V-21Cr-16Mn is an exception, which is harder than all of the quaternary alloys in the as-cast state. It also has the highest concentration of interstitials, shown in Table 5.4. Interstitial impurities are known to harden vanadium alloys[13], so this is a possible source of the anomalous hardness. The presence of new phases in alloys V-32Cr-28Mn-

5Ti and V-30Cr-26Mn-9Ti does not appear to have had any systematic effect on the microhardness properties of these alloys.

The source of these interstitial impurities present in these alloys was investigated using the V-4Cr-4Ti reference sample. Comparing the highly purified V-4Cr-4Ti sample to one that had been homogenised under the same conditions as the alloys studied here reveals a greatly increased oxygen content. Therefore, as might be expected, the homogenisation procedure and subsequent heat treatments (which used the same method) are likely to have introduced additional impurities to the alloys, potentially altering their properties despite best efforts to mitigate against this.

5.4.3 Fusion applications

As seen in Section 5.4.1, the alloy systems seem to possess good thermal stability at a range of fusion relevant temperatures. Only when Ti is present above a few at% or Mn is present above equiatomic proportions is any sort of microstructural evolution observed. Even still, many of the changes seen occur in phases that arise as a consequence of the alloys interstitial content rather than their principal constituents. Of course, phases that are produced by interstitials are not inconsequential and are utilised in most candidate fusion structural materials, but their presence is well controlled through processing routes.

However, there are many other factors that must be considered before a serious justification is made for using these alloys in a fusion context. Foremost of which will be the structural properties of these alloys. Although not quantitatively determined, the brittleness observed when handling and preparing these alloys would limit their usefulness in structural applications. It is not yet known if this brittleness is inherent to such a highly alloyed refractory BCC material, or if interstitials play a significant role. Furthermore, the effects of radiation on these alloys must be assessed. Some V-based alloys have exhibited significant (and undesirable) irradiation swelling, but this seems to be mitigated by the addition of Ti[19, 20].

As previously mentioned, the neutronic properties of the majority elements of these alloys render them acceptable from a long-term recycling and disposal standpoint. However, there other safety issues pertaining to element choice in fusion reactors that shall be touched upon here. Analyses by Piet et al.[21, 22] gave an overall score for each element in the periodic table based on structural and biological safety considerations in the event of an accident. According to those studies, Mn is the element contained in these alloys that is of greatest concern. This is due to its particularly high short term decay properties, which could pose a radiological hazard from the dose released if an accident were to occur. Furthermore, the large temperature rises accompanying the decay heat could lead to further exposure to harmful materials. However, the same

analysis reveals that elements such as W score equally as poorly, so such findings do not necessarily preclude the use of an element in a reactor.

5.5 Conclusions

1. V-Cr-Mn alloys were found to possess thermal phase stability across a range of fusion-relevant temperatures, from 600 to 1000 °C.

2. CALPHAD predictions were generally accurate for most compositions, predicting a predominantly BCC microstructure across the range of temperatures investigated. It also correctly predicted the higher temperature of dissolution for Ti-[C,N] precipitates in these alloys relative to V-4Cr-4Ti.

3. Laves phase appears in some Ti-V-Cr-Mn alloys after ageing at 1000 °C, which is not predicted by Thermocalc CALPHAD databses. This behaviour is suppressed in alloys with reduced Ti content.

4. Another phase appeared at all three ageing temperatures studied in the higher Ti concentration alloys that is enriched in N, S, and Ti.

5. No significant changes in hardness measurements were observed after ageing treatments.

6. Impurity content varied considerably between samples. This is thought to be introduced in the homogenisation and heat treat processes, and may have an effect on alloy properties.

7. Most alloys were stable in fusion relevant temperature regimes, with no microstructural evolution observed.

Acknowledgements

The authors acknowledge the use of the Department of Materials X-ray Diffraction Suite at the University of Manchester and for the technical support, advice and assistance provided by Dr. John E. Warren and Gary Harrison. The authors would also like to Dr. Mark Gilbert for fruitful discussions regarding the activation properties of elements. The authors acknowledge funding from the EPSRC Centre for Doctoral Training in Fusion Energy [grant EP/L01663X/1] as well as EPSRC grant EP/R021546/1. This work has been part-funded by the RCUK Energy Programme [grant number EP/T012250/1]. We also wish to acknowledge the support of the Henry Royce Institute for Advanced Materials for access to the FEI Talos electron microscope

at Royce@Manchester, funded through EPSRC grants EP/R00661X/1, EP/S019367/1, EP/P025021/1 and EP/P025498/1. E. Pickering wishes to acknowledge the same funds for supporting his Research Lead role within Royce. The raw data associated with this work can be accessed via the following link: `https://zenodo.org/record/4643803`

References

[1] United Nations. *The Paris Agreement*. 2016.

[2] B.P. Heard et al. *Burden of proof: A comprehensive review of the feasibility of 100% renewable-electricity systems*. Tech. rep. Sept. 2017, pp. 1122–1133. DOI: 10.1016/j.rser.2017.03.114.

[3] M.R. Gilbert et al. "Waste implications from minor impurities in European DEMO materials". In: *Nuclear Fusion* 59.7 (July 2019), p. 076015. ISSN: 0029-5515. DOI: 10.1088/1741-4326/ab154e.

[4] G W Bailey, O V Vilkhivskaya, and M R Gilbert. "Waste expectations of fusion steels under current waste repository criteria". In: (2021). DOI: 10.1088/1741-4326/abc933.

[5] T.E.G. Nicholas et al. "Re-examining the role of nuclear fusion in a renewables-based energy mix". In: *Energy Policy* 149 (Feb. 2021), p. 112043. ISSN: 03014215. DOI: 10.1016/j.enpol.2020.112043. arXiv: 2101.05727.

[6] P.J. Barron et al. "Towards V-based high-entropy alloys for nuclear fusion applications". In: *Scripta Materialia* 176 (Feb. 2020), pp. 12–16. ISSN: 13596462. DOI: 10.1016/j.scriptamat.2019.09.028.

[7] M Kovari et al. "Converting energy from fusion into useful forms". In: *Proceedings of the Institution of Mechanical Engineers, Part A: Journal of Power and Energy* 228.3 (May 2014), pp. 234–240. ISSN: 0957-6509. DOI: 10.1177/0957650913514230.

[8] E. J. Pickering and N. G. Jones. "High-entropy alloys: a critical assessment of their founding principles and future prospects". In: *International Materials Reviews* 6608.May (2016), pp. 1–20. ISSN: 0950-6608. DOI: 10.1080/09506608.2016.1180020.

[9] D. B. Miracle and O. N. Senkov. "A critical review of high entropy alloys and related concepts". In: *Acta Materialia* 122 (2017), pp. 448–511. ISSN: 13596454. DOI: 10.1016/j.actamat.2016.08.081.

[10] F. A. Stevie et al. "Application of focused ion beam lift-out specimen preparation to TEM, SEM, STEM, AES and SIMS analysis". In: *Surface and Interface Analysis* 31.5 (May 2001), pp. 345–351. ISSN: 0142-2421. DOI: 10.1002/sia.1063.

[11] Jiming Chen, Zengyu Xu, and Lin Yang. "The influence of hydrogen on tensile properties of V-base alloys developed in China". In: *Journal of Nuclear Materials* 307-311.1 SUPPL. (Dec. 2002), pp. 566–570. ISSN: 00223115. DOI: 10.1016/S0022-3115(02)01214-X.

[12] B. Huneau et al. "Experimental Investigation in the Quaternary Systems Ti-Ni-Al-N and Ti-Ni-Al-O". In: *Journal of Solid State Chemistry* 155.1 (Nov. 2000), pp. 71–77. ISSN: 00224596. DOI: 10.1006/jssc.2000.8893.

[13] J. M. Chen et al. "Overview of the vanadium alloy researches for fusion reactors". In: *Journal of Nuclear Materials* 417.1-3 (2011), pp. 289–294. ISSN: 00223115. DOI: 10.1016/j.jnucmat.2011.02.015.

[14] H. J. Goldschmidt. *Interstitial Alloys*. 1967. ISBN: 9781489958822. DOI: 10.1007/978-1-4899-5880-8.

[15] M. G. Ulitchny and R. Gibala. "The effects of interstitial solute additions on the mechanical properties of niobium and tantalum single crystals". In: *Journal of The Less-Common Metals* 33.1 (1973), pp. 105–116. ISSN: 00225088. DOI: 10.1016/0022-5088(73)90061-1.

[16] Takeo Muroga, Takuya Nagasaka, A Nishimura, et al. "Improvement of Vanadium Alloys by Precipitate Control for Structural Components of Fusion Reactors". In: *Materials Science Forum* 475-479 (2005), pp. 1449–1454. ISSN: 1662-9752. DOI: 10.4028/www.scientific.net/MSF.475-479.1449.

[17] A. W. Carruthers et al. "Novel reduced-activation TiVCrFe based high entropy alloys". In: *Journal of Alloys and Compounds* 856 (Mar. 2021), p. 157399. ISSN: 09258388. DOI: 10.1016/j.jallcom.2020.157399.

[18] K. Fukumoto et al. "Effect of Ti addition on microstructural evolution of V-Cr-Ti alloys to balance irradiation hardening with swelling suppression". In: *Nuclear Materials and Energy* 15 (May 2018), pp. 122–127. ISSN: 23521791. DOI: 10.1016/j.nme.2018.03.008.

[19] H. Matsui et al. "Effects of temperature history during neutron irradiation on the microstructure of vanadium alloys". In: *Journal of Nuclear Materials* 212-215.PART 1 (Sept. 1994), pp. 784–789. ISSN: 00223115. DOI: 10.1016/0022-3115(94)90163-5.

[20] B.A. Loomis, D.L. Smith, and F.A. Garner. "Swelling of neutron-irradiated vanadium alloys". In: *Journal of Nuclear Materials* 179-181.PART 2 (Mar. 1991), pp. 1166–1167. ISSN: 00223115. DOI: 10.1016/0022-3115(91)90306-R.

[21] Steven J. Piet, Edward T. Cheng, and Lisa J. Porter. "Accident safety comparison of elements to define low-activation materials". In: *Fusion Technology* 17.4 (1990), pp. 636–657. ISSN: 07481896. DOI: 10.13182/FST17-4-636.

[22] Steven J. Piet et al. "Initial integration of accident safety, waste management, recycling, effluent, and maintenance considerations for low-activation materials". In: *Fusion Technology* 19.1 (1991), pp. 146–161. ISSN: 07481896. DOI: 10.13182/FST19-1-146.

5.6 Supplementary figures

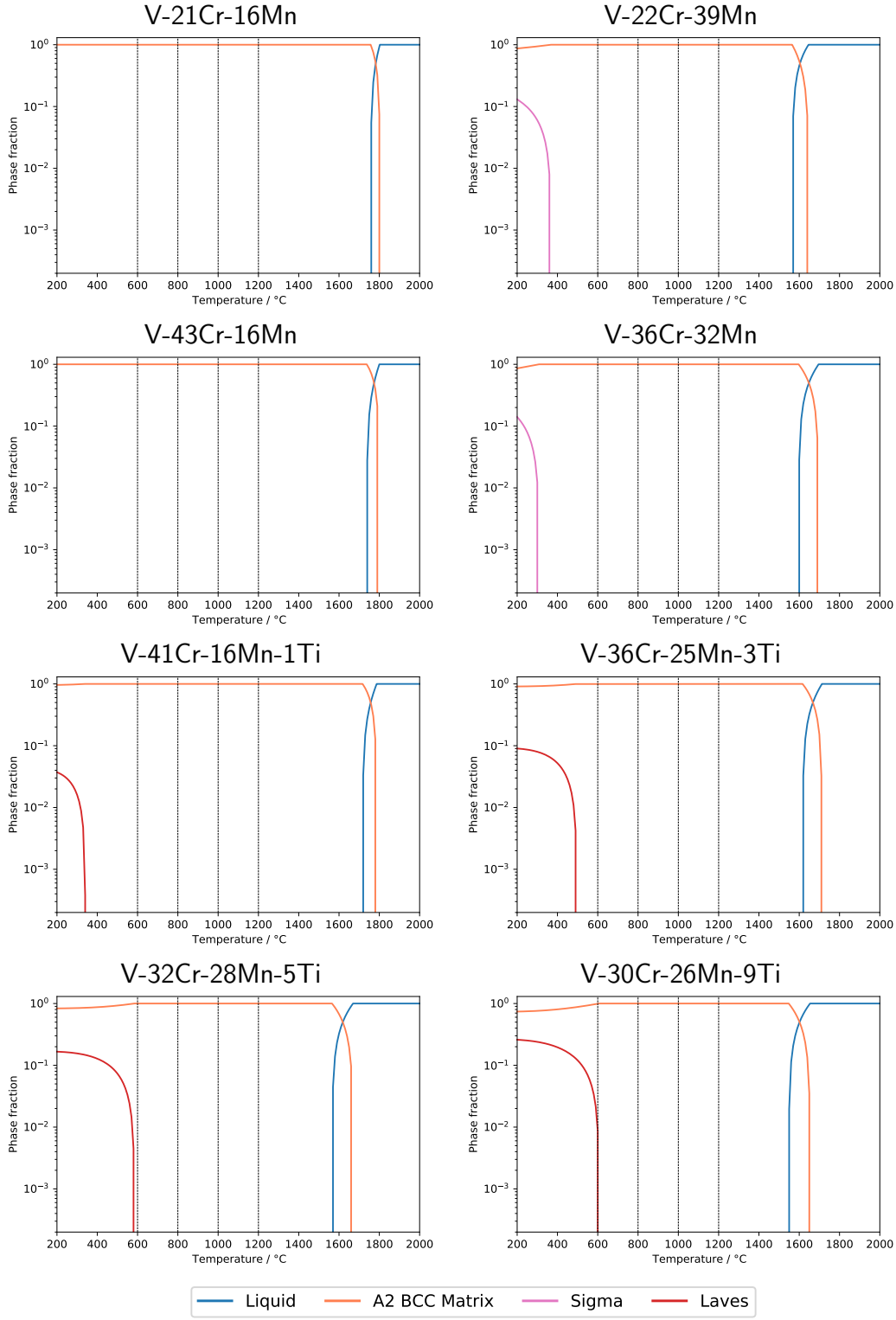

Figure 5.15: Phase proportions of alloys containing both C and N impurities, determined by CALPHAD using the TCFE10 database. Temperatures of study are marked with dashed lines.

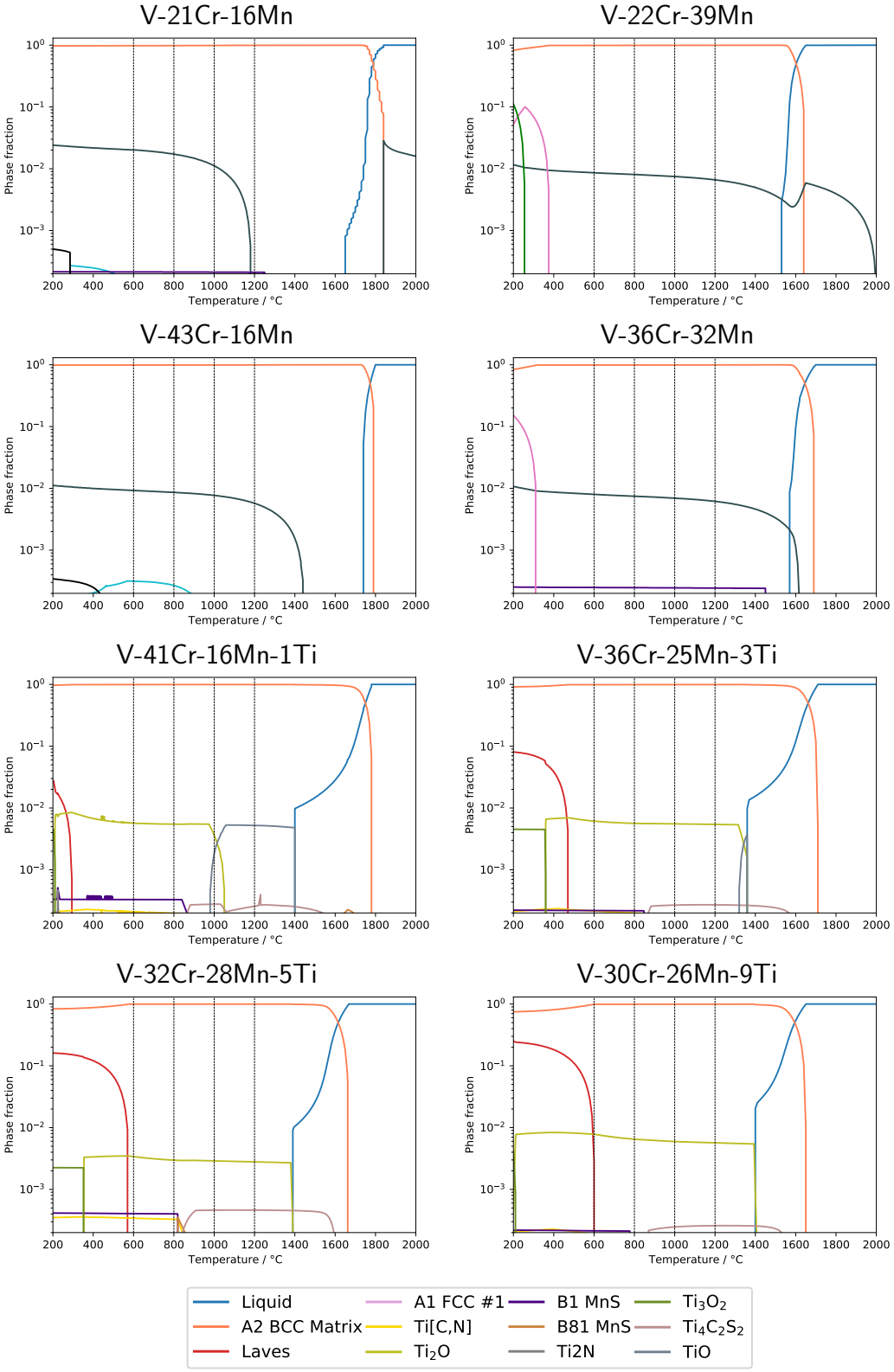

Figure 5.16: Phase proportions of alloys containing both C and N impurities, determined by CALPHAD using the TCFE10 database. Temperatures of study are marked with dashed lines.

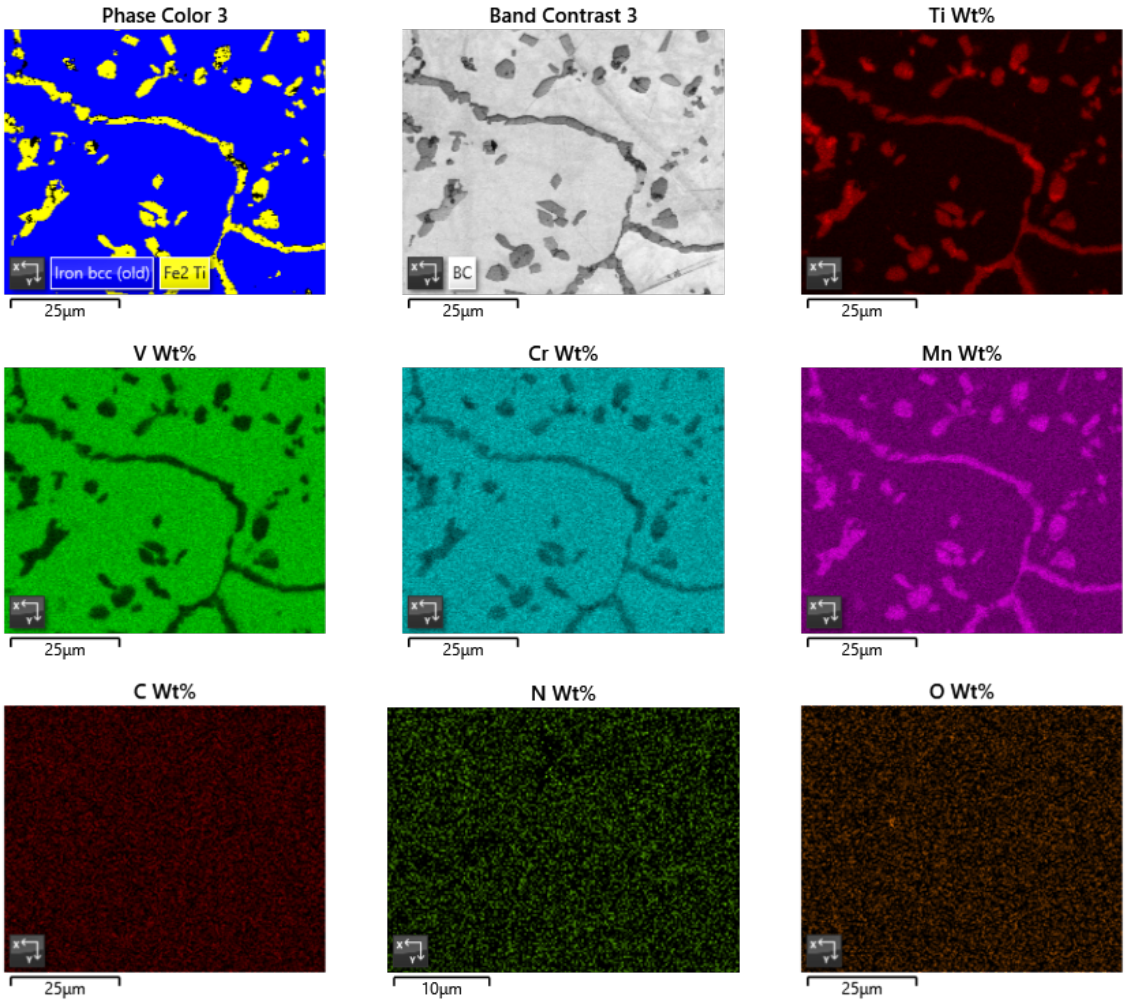

Figure 5.17: EBSD and EDX maps of V-30Cr-26Mn-9Ti heat treated at 1000 °C for 1000 hours. Note: BCC matrix and C14 Laves have been indexed by the software as Iron BCC and Fe2Ti respectively.

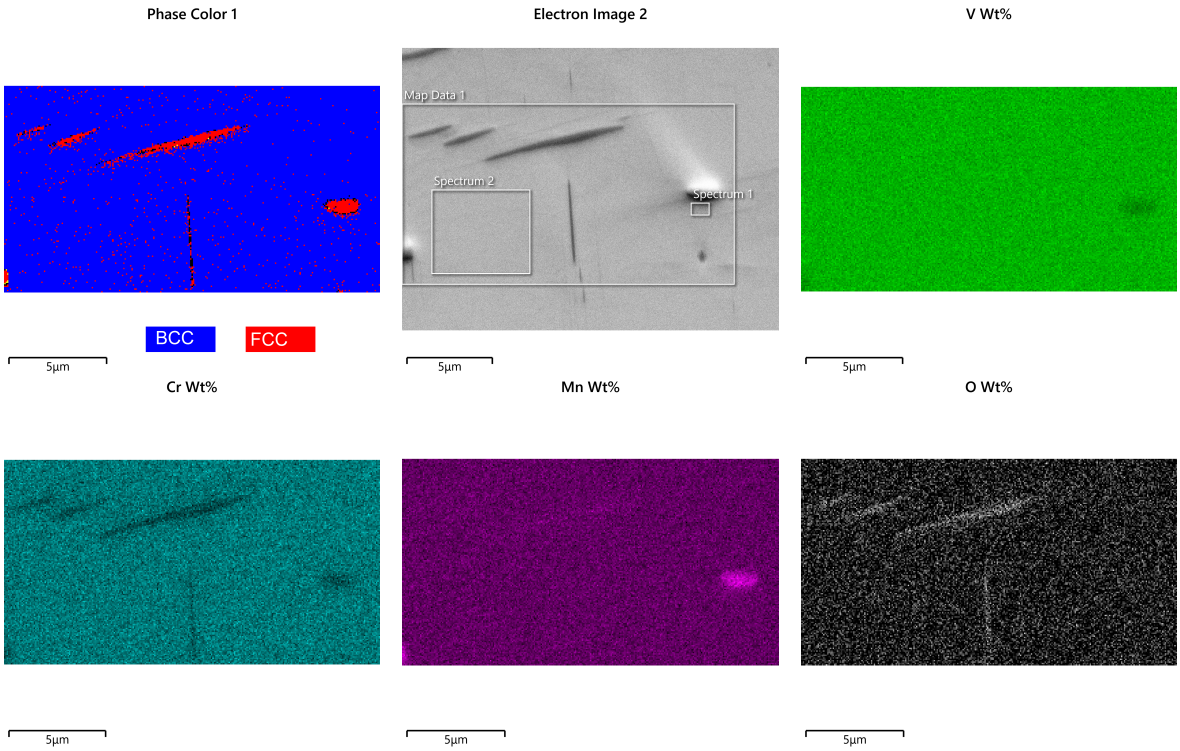

Figure 5.18: EBSD and EDX maps of V-22Cr-39Mn heat treated at 800 °C for 1000 hours.

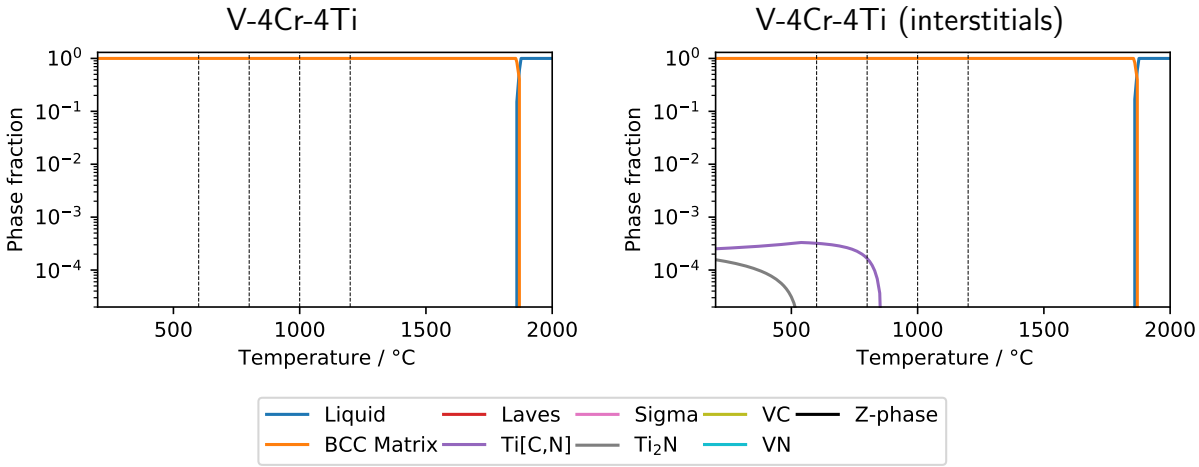

Figure 5.19: Phase proportions of V-4Cr-4Ti alloys with and without interstitial impurities, determined by CALPHAD using the TCHEA4 database. Temperatures of study are marked with dashed lines.

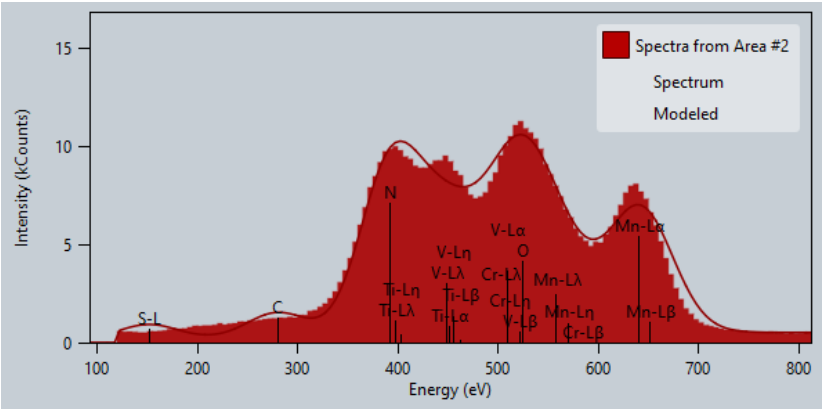

Figure 5.20: Low-energy TEM-EDX spectrum from V-30Cr-26Mn-9Ti N-rich region. Note the poor adherence of the peak model to the peak data.

5.7 Additional discussion

5.7.1 XRD

To check if there were any changes or evolution of the BCC phase, XRD measurements for each heat treatment were taken with a PANalytical X'Pert Pro diffractometer. Lattice parameter measurements were obtained by refining a BCC lattice to fit an XRD diffraction pattern using the HighScore Plus software. No significant changes between heat treatments were observed outside what would be considered experimental scatter (Fig. 5.22).

XRD data showed no evolution in lattice parameter for any of the alloys across the heat treatments performed. However, a consistent lattice parameter is not, in itself, evidence of a stable microstructure in the alloys studied here. Given how lattice parameter changes very little with ageing (see Fig. 5.22), depletion of a metallic element (or elements) from the matrix phase into a new phase would not significantly affect the lattice parameter. Observed variations in lattice parameter could perhaps be explained by the introduction of interstitial impurities into the matrix during the heat treatment process, with a 0.1 wt% increase in interstitial O and N corresponding to a 0.01 Å increase in lattice parameter[1]. The lattice parameters also appear to be approximately proportional to the average atomic radii of the alloy (Fig. 5.21). The exception is V-21Cr-16Mn, which has a lattice parameter significantly higher than would be expected for its atomic radius. This may be explained by a higher O content. However, lattice parameters for concentrated multi-component alloys do not obey Vegard's law, so it is possible that this deviation would occur without interstitials. Furthermore, the apparently reduced volume fraction of O-containing precipitates suggests that a greater proportion of the O contained in the alloy is in the form of interstitials, rather than in a separate phase, leading to a larger lattice parameter. Figure 5.23 shows the result of wide-area (1×1 mm) EDX scans performed on the XRD samples (also including additional, shorter heat treatments that were not included in this study). There is little variation in the composition of the samples subjected to each heat treatment (i.e., there was not much through-ingot segregation).

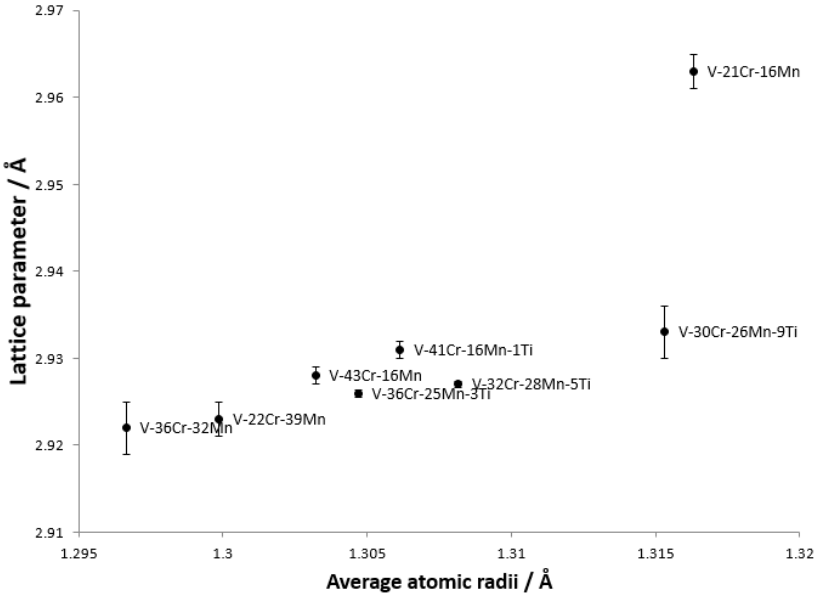

Figure 5.21: Lattice parameter variation with average atomic radius.

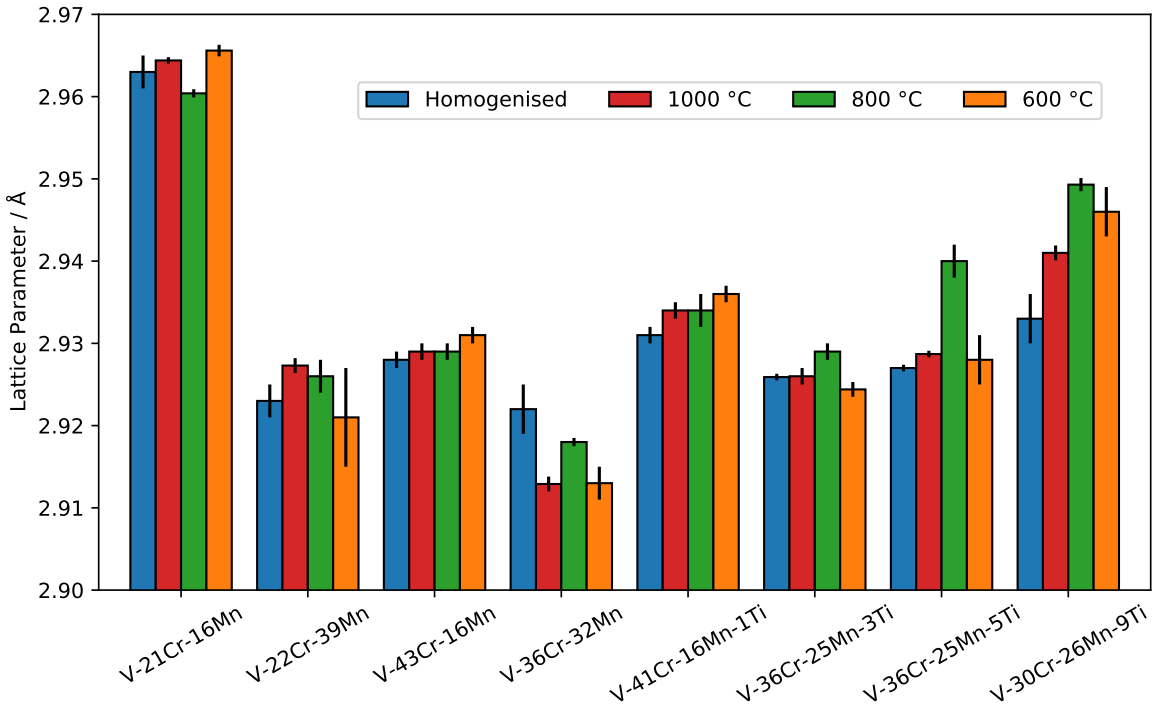

Figure 5.22: Vickers hardness variation for each heat treatment of the alloys. Error bars were determined by fitting the lattice parameter in HiScore software.

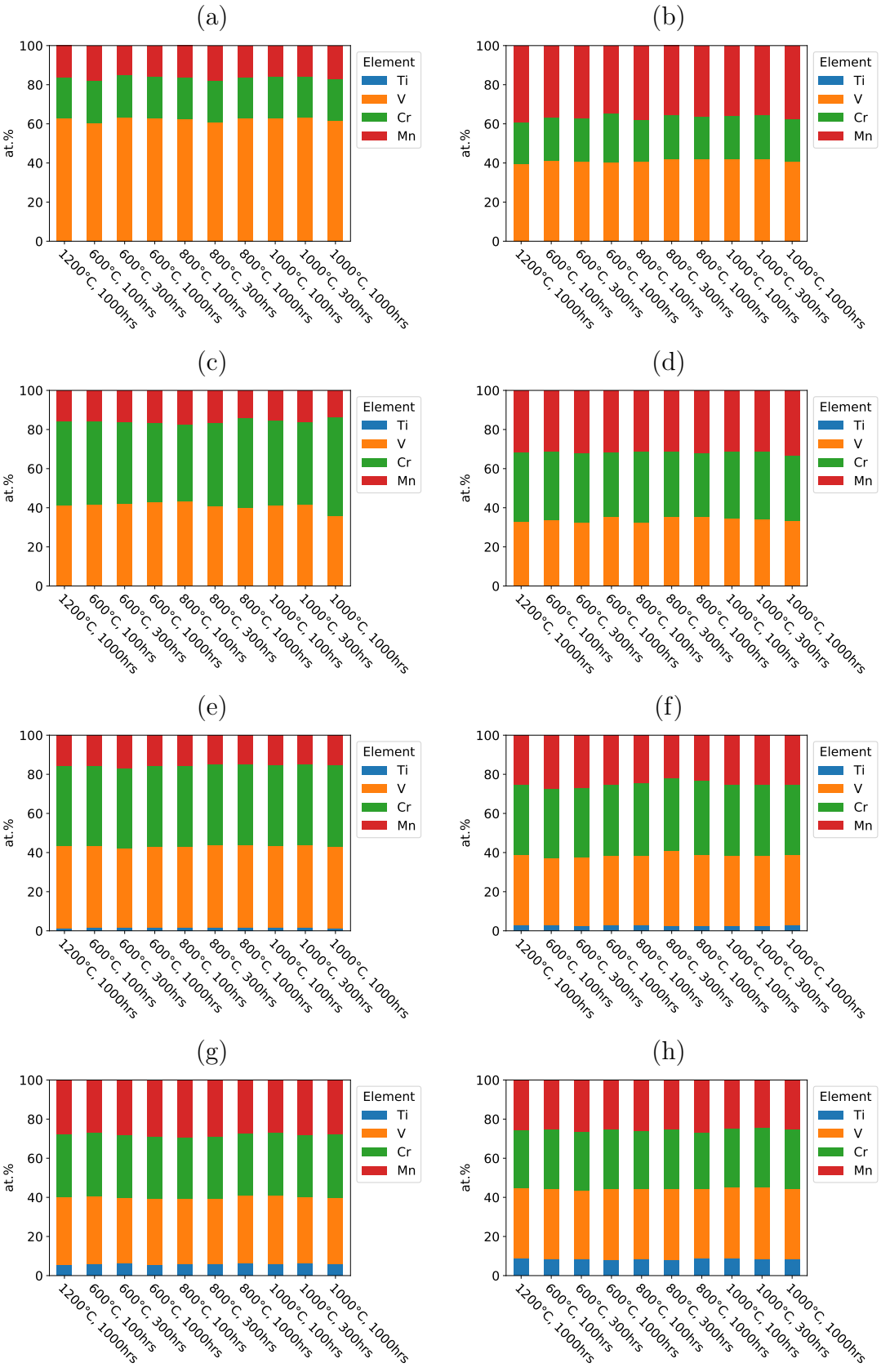

Figure 5.23: Chemical compositions of the heat treated alloys determined by EDX (a) V-21Cr-16Mn (b) V-22Cr-39Mn (c) V-43Cr-16Mn (d) V-36Cr-32Mn (e) V-41Cr-16Mn-1Ti (f) V-36Cr-25Mn-3Ti (g) V-32Cr-28Mn-5Ti (h) V-30Cr-26Mn-9Ti.

5.7.2 Ordered phase

Also of note is the discovery of an ordered CsCl-type phase in V-Mn and V-Cr-Mn alloys by Suzuki and Hagiwara[2, 3] in the 1970s. Studies of the binary V-Mn system showed that the transition temperature, below which the ordered phase is stable, drops parabolically with deviation from the equiatomic composition. The transition temperature also drops in a similar manner with increasing Cr content. As the ternary alloys studied here have V:Mn ratios that deviate significantly from the equiatomic composition, as well as significant concentrations of Cr, the transition temperature will be suppressed, possibly below the range of this study. To verify this ordered phase was not present, anomalous scattering XRD was utilised (as in Suzuki et al.[2] and Hagiwara et al.[3]) to check for the existence of ordered phase reflections, which would ordinarily be imperceptible using normal XRD due to the small differences in atomic scattering factor between V, Cr and Mn. However, due to the very small size of the sample (V-22Cr-39Mn chosen due to its relatively high Mn and low Cr content, making it the most likely to form the ordered phase) and the limited diffractometer time, the patterns obtained were not conclusive and contained substantial amounts noise and fluorescence effects.

Additional references

[1] Paluri Bhimeswara Rao. "The lattice constants of chromium and vanadium containing dissolved gases dissolved gases". PhD thesis. Missouri University of Science and Technology, 1960.

[2] Tomoo Suzuki and Masuo Hagiwara. "CsCl-Type Order-Disorder Transition in δ-VMn Solid Solution". In: *Transactions of the Japan Institute of Metals* 16.8 (1975), pp. 473–479. ISSN: 0021-4434. DOI: 10.2320/matertrans1960.16.473.

[3] Masuo Hagiwara, Jun-ichi Seki, and Tomoo Suzuki. "CsCl-Type Superlattice Formation in V-Mn-Fe, Fe-V-Cr and V-Mn-Cr Ternary Alloys". In: *Journal of the Japan Institute of Metals* 39.4 (1975), pp. 402–408. ISSN: 0021-4876. DOI: 10.2320/jinstmet1952.39.4_402.

Chapter 6

Oxidation behaviour of V-Cr-Mn and Ti-V-Cr-Mn alloys

P. Barron[1], N.G. Jones[2], H. Dawson[3], B.J. Connolly[1], and E.J. Pickering[1]

[1]Department of Materials, University of Manchester, Oxford Road, Manchester, M13 9PL, UK

[2]Department of Materials Science and Metallurgy, University of Cambridge, 27 Charles Babbage Road, Cambridge, CB3 0FS, UK

[3]Culham Centre for Fusion Energy, Abingdon, OX14 3DB, UK

Foreword

This chapter is presented in the format of a journal article. Conceptualisation was done by P.J.B., E.J.P., and B.J.C. As-cast alloys were supplied and fabricated by N.G.J. Furnace operation and calibration was performed by B.J.C. All other experimental methods listed were carried out by P.J.B. Manuscript was written by P.J.B with minor revisions from all authors. Additional information not directly related to the main conclusions is presented in Section 6.6.

Manuscript

Abstract

Under normal operating conditions, the structural materials in a fusion reactor will not be exposed to oxygen at high temperatures. However, in the event of an accident, high temperature oxidation could occur. It is therefore desirable that alloys used in fusion environments are able to adequately resist high temperature oxidation in the interests of safety. A suite of low-activation, multi-principal component alloys have been oxidised at temperatures of 600, 650 and 700 °C for

times of 10, 100 and 1000 hours. Weight and thickness gain measurements show improved oxidation performance in this temperature range relative to V-4Cr-4Ti, another candidate alloy. Oxidation behaviour is modelled and qualitatively assessed. Increased Cr content was found to positively impact oxidation resistance, as was the introduction of Ti.

6.1 Introduction

Nuclear fusion offers the prospect of generating large amounts of energy by using abundant resources as fuel while producing no carbon emissions. It would also generate a constant amount of power, unlike less predictable renewable sources. It also has advantages over conventional nuclear fission plants in that it produces much shorter lived and less radioactive waste.

However, for the advantages of less active waste to be realised, the materials used in a fusion reactor must themselves consist of elements that produce short-lived isotopes when exposed to a fusion neutron spectrum. It is for this reason that considerable effort has been devoted to developing reduced activation materials, composing wholly of elements with favourable activation properties. These materials include ferritic-martensitic steels, oxide-dispersion strengthened steels, vanadium alloys, tungsten alloys; and more recently, multi-principal component alloys.

Aside from being low-activation, materials must also be microstructurally stable in the extreme thermal and neutronic environments found within a fusion reactor. Additional constraints on mechanical properties are imposed on structural materials, and likewise with corrosion properties and coolant-facing materials in the blanket (the exact nature of which will depend on blanket design).

So far, these are all requirements borne from the expected conditions inside a fusion reactor throughout normal operation. However, the conditions experienced during unexpected accidents must also be considered. A loss-of-coolant accident (LOCA) could lead to high temperatures persisting in the reactor structure for weeks[1]. If a LOCA occurred in conjunction with a vacuum leak, the ingress of air exposed to high temperature alloys could result in severe oxidation.

Oxidation of materials could lead to several new hazards that would be severely detrimental to the safety case of a fusion reactor. If an oxide with a melting point lower than the temperature of components during an accident were to form, this could lead to a runaway reaction where melted oxide melts away, exposing fresh material to react with oxygen. Not only would this lead to damage of the structural components, but it could also cause volatilisation of the oxide species. Given these species would contain radioactive material due to neutron activation, their release into the atmosphere could be potentially disastrous.

There is a growing body of literature dedicated to investigating and mitigating the effects of a LOCA and air ingress event in tungsten, the plasma-facing material of choice for ITER (the largest fusion reactor to date). Early research found that radiation release for oxidised tungsten from a LOCA would be unacceptably high and suggested avoiding the use of tungsten[2]. More recently, effort has been devoted to developing new alloys that can mitigate the undesirable oxidation behaviour[3, 4, 5].

So-called "self-passivating" or "smart" tungsten alloys allow the desirable functional properties of tungsten, such as high melting point and low sputtering rate, to be retained while inhibiting oxidation in the event of an accident. By alloying with elements such as Cr, Ti and Y to W, the alloy will form a protective oxide film that grows far more slowly and is more strongly adhering to the bulk under accident conditions. During normal reactor operation, the lighter elements will sputter away, leaving a thin layer that is mostly W and possesses the desirable functionality that pure W gives. Under accident conditions, this thin layer will rapidly oxidise and spall away, exposing the alloyed bulk which will then produce a much more adhesive oxide[4, 6].

Note that this responsive behaviour is only necessary in plasma-facing components. For non-plasma-facing components within the reactor that have a surface that may be exposed to oxygen in a leak, it would be sufficient to simply have a strong and stable oxide that forms under accident conditions. For reduced activaton ferritic-martensitic (RAFM) steels, which are considered the leading candidate structural materials for fusion reactors, limited work has been done on their oxidation behaviour at accident relevant temperatures, although there exists some research on their atmospheric oxidation[7]. There is a larger body of work on the oxidation of fission relevant ferritic-martensitic steels, although this is mostly focused on steam environments[7, 8, 9], with limited research on oxidation in air[10, 11].

Vanadium alloys are arguably the second most advanced class of materials considered for fusion structural applications. In an early study, the oxidation of V-4Cr-4Ti and V-5Cr-5Ti in air or pure O_2 had to be investigated at temperatures of 620 °C or less to avoid the melting of the oxide V_2O_5 (T_m = 670 °C)[12]. A later study using a different methodology was able to quantify oxidation in air at higher temperatures, and also found a much increased reaction rate between 600 and 700 °C for the same alloys[13]. For most alloys, weight gain did not alter significantly between 700 and 900 °C, with the exception of V-4Cr-10Ti and V-4Cr-4Ti, which could not be measured due to melting of the surface oxide.

Another consequence of the oxidation of vanadium alloys is the potential for embrittlement. Specimens that were oxidised to form a scale, then annealed under vacuum were found to undergo significant loss in ductility due to the oxide films acting as a source for interstitial O, which causes embrittlement in vanadium alloys[14]. A more chemically stable and adherent oxide film may be able to prevent this ingress of oxygen,

thus preserving the mechanical properties of the alloy in the event of an accident.

However, it is not just the accident-tolerance that may benefit from improved oxidation behaviour. Vanadium alloys require intensive refinement processes to remove impurities for optimum properties[15, 16, 17, 18, 19]. Once these alloys have been refined, they are either canned inside or thermally sprayed with a protective barrier of stainless steel[17, 19]. This layer is to prevent oxidation and impurity pickup during forging. For final annealing, the protective layers are removed, but annealing is still performed under high vacuum ($\sim 5 \times 10^{-4}$ Pa). Such processing is economically intensive and may limit the size of the ingots that can be fabricated. A more protective oxide scale, while perhaps not entirely eliminating the need for impurity control measures, may reduce the magnitude of mitigating processes require (e.g. annealing that can be performed under low vacuum, or hot rolling in air at reduced temperatures).

A suite of V-Cr-Mn and V-Cr-Mn-Ti alloys possessing good thermal stability have recently been investigated as candidate fusion materials[20]. They generally possess good thermal stability across a wide range of fusion relevant temperatures (see Chapter 5), with a single BCC phase comprising of the bulk of the microstructure between 600 and 1200 °C. Their high Cr content compared to other, less alloyed vanadium alloys may offer improved oxidation resistance during accident scenarios, as Cr is known to dramatically lower high-temperature oxidation rates in the V-Cr binary[21]. The approach of using concentrated alloys is similar to that adopted in high entropy alloys (HEAs). HEAs have recently garnered attention as potentially attractive prospects for fusion structural materials and many candidate alloy system have emerged[22, 23, 24, 25, 26]. However, to the authors' knowledge, there exists very limited work on the oxidation of fusion HEAs, only focused on the Ti_xWTaVCr system[27].

The range of temperatures studied here is in the range of 600 to 700 °C. This range was chosen in part due to the rapid acceleration of oxidation behaviour observed within this temperature range by Fujiwara et al[13]. From this perspective, this work will inform whether the alloys studied offer improved performance near this apparent threshold region for rapid oxidation. Another motivation for selecting this temperature range is its applicability to predicted fusion reactor accident scenarios. Fig. 6.1 shows how the temperature will evolve for components of a potential blanket design for a DEMO reactor after a LOCA. The cooling plates, one of the main structural components, are predicted to remain at temperatures between 600 and 700 °C for several hours[28]. Another analysis of a LOCA scenario in a power plant reactor concept found that the first wall of the reactor would remain at a temperature of between 600 and 900 °C for several weeks, although an estimate was not given for the blanket structural materials[1].

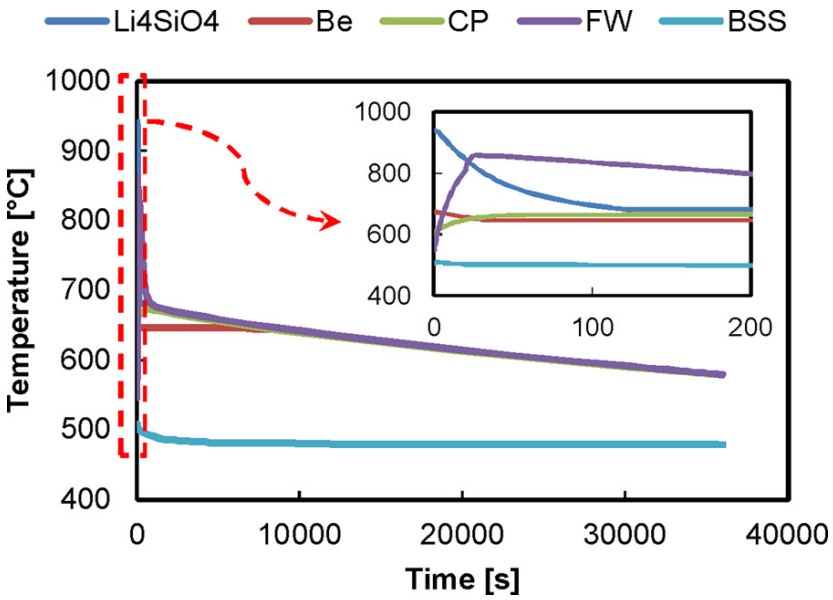

Figure 6.1: Temperature evolution of a helium-cooled pebble breeder blanket in the European DEMO design after a LOCA. Li_4SiO_4 is the tritium breeding material, Be is the beryllium neutron multiplier, CP is the cooling plates supporting the breeding material, FW is the first wall, and BSS is back-supporting structure. Taken from Ref. [28].

6.2 Method

Eight alloys were fabricated as ingots weighing approximately 25 g using an arc melting process in an argon atmosphere (see Table 6.1). The ingots were inverted and remelted three times to ensure homogeneity. Sections of each ingot were cut off, wrapped in tantalum foil, and then encapsulated in quartz ampoules backfilled with low pressure argon. These samples then underwent a homogenisation heat treatment at 1200 °C for 100 hours, before quenching in water. As a comparison, the oxidation experiments will also be performed using a sample of V-4Cr-4Ti provided by the Culham Centre for Fusion Energy, which has undergone thermomechanical processing as described in Ref. [17], followed by the same homogenisation treatment as the other alloys.

After homogenisation, the alloys were sectioned off into thin slices approximately 5×5 mm in size and 0.3 mm in thickness, although exact shape and size of the samples differed due to the shape of the original ingots. In the interests of maximising surface area and thereby improving the precision of weight gain measurements, as well as to conserve material, slices with irregular shapes were not cut to a standard size. The thin edges of the samples were roughly ground away to remove any surface oxidation present from previous heat treatments. Both sides of the samples were ground and polished to a 0.25 µm finish using standard metallographic preparation techniques. Before oxidation all samples were weighed using 0.1 mg precision scales. A photograph of the samples was taken and the polished surface areas were measured using ImageJ software.

	Composition / wt%							
Alloy	**V**	**Cr**	**Mn**	**Ti**	**C**	**N**	**O**	**S**
V-21Cr-16Mn	balance	20.7	17.4	0.0	0.003	0.002	0.305	0.008
V-22Cr-39Mn	balance	21.3	40.6	0.0	0.002	0.003	0.228	0.002
V-43Cr-16Mn	balance	43.2	16.6	0.0	not measured			
V-36Cr-32Mn	balance	35.1	33.1	0.0	0.004	0.003	0.203	0.009
V-41Cr-16Mn-1Ti	balance	40.9	16.6	1.3	0.007	0.004	0.209	0.012
V-36Cr-25Mn-3Ti	balance	35.9	26.4	2.7	0.012	0.004	0.117	0.015
V-32Cr-28Mn-5Ti	balance	32.0	29.4	5.0	not measured			
V-30Cr-26Mn-9Ti	balance	29.9	27.0	8.0	not measured			
V-4Cr-4Ti	balance	4.1	0.0	4.2	0.009	0.005	0.324	0.001

Table 6.1: List of alloys studied in this work. Primary component compositions determined using wavelength dispersive spectroscopy (WDS)[20] (except V-4Cr-4Ti, which was measured using EDX), impurity compositions measured using LECO analysis (see Chapter 5. Note: alloys are labelled by at% in the results for consistency with previous work.

Oxidation was performed using a standard tube furnace exposed to atmospheric air inside a fume hood. The samples were placed into ceramic boats and then moved inside the tube to within the region where temperatures did not deviate from the target temperature by more than 10 °C. The hot zone of the tube was determined using a thermocouple. A silica wool bung was placed inside each end of the tube for insulation but air flow into the tube was otherwise unimpeded and samples were left to oxidise. When the experiment was complete, the hot samples were removed from the furnace and left to cool in air.

Oxidation behaviour with respect to time was assessed by oxidising three sets of samples at 650 °C for 10, 100, and 1000 hours. To assess the effect of temperature, a further two experiments were performed at 600 and 700 °C for 10 hours.

Samples were then re-weighed using the same scales and cross-sectioned for analysis. The cut samples were mounted in resin and the cross-sections were ground and polished to a 0.04 µm finish. The other half of the samples were retained to examine the oxide surface in its as-oxidised state. The cross-sections were examined using a Zeiss Ultra55 secondary electron microscopy (SEM) at 10 kV with an Oxford Instruments energy dispersive X-ray (EDX) detector and a TESCAN Mira3 SEM at 10 kV with an Oxford Instruments EDX detector. EDX quantification and analysis was performed using the INCA and AZTEC software packages.

Fitting the weight gain and thickness data was done using the SciPy package from the Python programming language. Thickness measurements were taken at three different regions in the each sample, where the oxide scale appeared to be representative of the sample's behaviour.

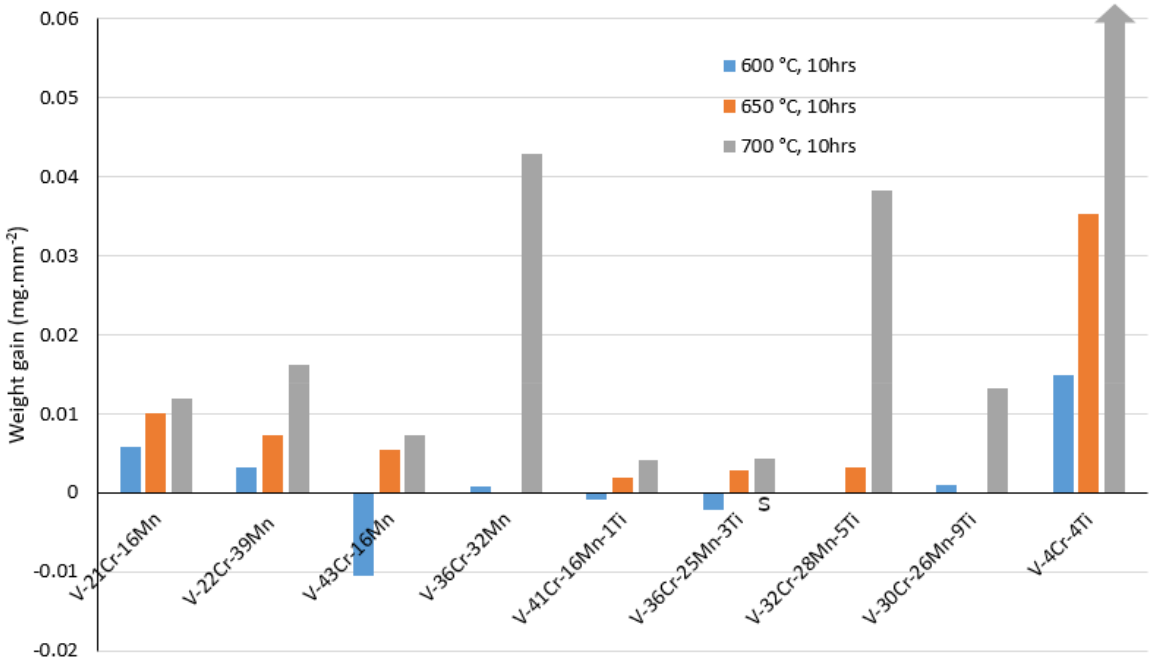

Figure 6.2: Weight gain variation with temperature. Arrows on top of bars indicate volatilisation. An S under the bar indicates that the sample visibly spalled during handling

6.3 Results

6.3.1 Weight gain

The weight gain for the samples, varying with temperature at constant time (10 hours), is shown in Fig. 6.2. The oxide films of certain samples did undergo minor spallation during handling, which is noted in the figure. Looking at the data, a few general trends can be observed. Raising temperature increased oxidation rate. The quaternary alloys tended to gain less mass than the ternaries. All of the alloys studied survived oxidation at 700 °C, unlike the V-4Cr-4Ti reference which underwent volatilisation and oxide melting. However, some data points are irregular, including weight loss for V-43Cr-16Mn and V-32Cr-28Mn-5Ti. This is most likely a consequence of the extremely small absolute weight changes measured at short timescales (fractions of a mg in some alloys). Although the alloys that suffered *visible* spallation are marked on the figure, it is possible that some minor spallation in the samples went unnoticed.

The results of oxidation at 650 °C for varying times (10, 100, and 1000 hours) are shown in Fig. 6.3. As is expected, longer oxidation times led to increased weight gain. The quaternary alloys generally performed better at longer exposure times, with the exception of V-30Cr-26Mn-9Ti. However, these alloys all exhibited visible spallation, so the weight gains may be slightly below their true values. V-21Cr-16Mn underwent volatilisation (partially melting into the weighing boat) and V-4Cr-4Ti oxidised very

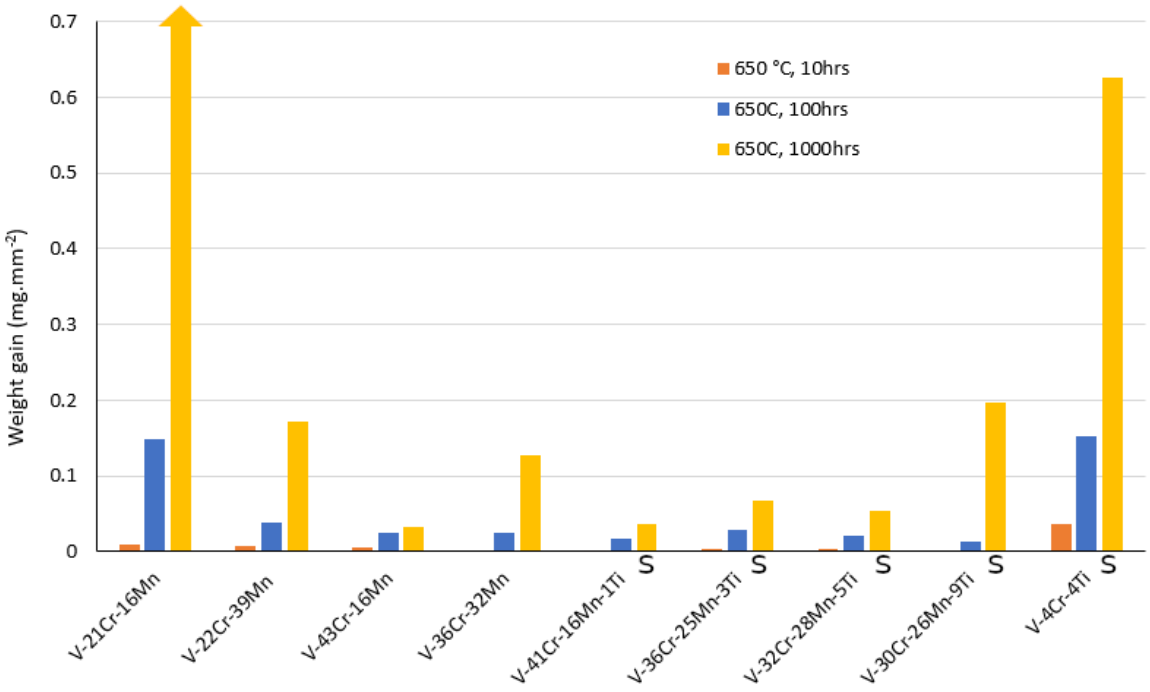

Figure 6.3: Weight gain variation with time. Arrows on top of bars indicate volatilisation. An S under the bar indicates that the sample visibly spalled during handling.

heavily after 1000 hours, producing a very thick and delicate oxide scale.

The weight gain measurements of samples oxidised at 650 °C were fitted to a simple parabolic oxidation model (see Fig. 6.4) alongside a model of growth kinetics using parameters for V-5Cr-5Ti obtained from Ref. [29]. Parabolic growth is described by the equation (where W is weight gain per unit area, k is a constant, and t is time):

$$W = \sqrt{k_1 t} \tag{6.1}$$

Both figures show that the parabolic fits for these data are poor, with residuals that are often of a similar magnitude to the measured values, especially for the data points at 10 and 100 hours.

6.3.2 Thickness measurements

Oxide thickness measurements are shown fitted to an equivalent parabolic growth model in Fig. 6.5. Again, the parabolic model is a poor fit for almost all of the data, with the exception of V-22Cr-39Mn, for which the model falls within the margin of errors. The errors themselves are generally very large as a consequence of the oxide thickness varying considerably along the length of the sample cross-section.

6.3.3 Layer characterisation

Most samples studied showed multiple layers of oxide species, either distinguishable by chemistry, morphology, or both. Four were observed in V-36Cr-32Mn oxidised at for 1000 hrs at 650 °C, shown in Fig. 6.6 for demonstration purposes. Going from left to right: (i) Mn-rich oxide (ii) V,Mn-rich oxide (iii) Cr-rich oxide (iv) V,Cr-rich oxide (v) substrate break-off layer (vi) V-36Cr-32Mn substrate. Equivalent oxides were identified in the quaternary Ti-V-Cr-Mn alloys, with the Ti tending to remain within the Cr-rich oxides. Fig. 6.7 shows the equivalent map for V-36Cr-25Mn-3Ti. The layers for this figure are (going left to right): (i) V-36Cr-25Mn-3Ti substrate (ii) spalled region where mounting resin has penetrated (iii) Cr-rich oxide (iv) V, Mn-rich oxide (v) Mn-rich oxide.

All of the V-Cr-Mn and Ti-V-Cr-Mn alloys exhibited multiphasic oxides. Only V-4Cr-4Ti produced a single oxide in all experiments. The oxide was most likely V_2O_5 due to the orange colour that appeared on these samples and also from previous work confirming that this was the predominant oxide in the temperature regimes studied here[29].

The thicknesses of each individual oxide layer are presented in Fig. 6.6. Note it was often difficult to distinguish certain layers, such as the [V,Cr] and Cr rich regions, as well as the [V,Mn] rich and V rich regions. It is possible these layers may simply represent a concentration gradient within a single phase. Some other features were observed in isolated areas, discussed in Section 6.6.

Some general trends are apparent from observing the graphs. The internal oxidation layer is always a Cr-rich or V, Cr-rich oxide, with Ti also appearing in these region for the quaternary alloys. This layer is underneath either one or two Mn containing oxides (although as mentioned distinguishing these can be difficult). Some alloys, more commonly the ones oxidised for 1000 hours, show a final, thin Mn oxide scale at the very surface.

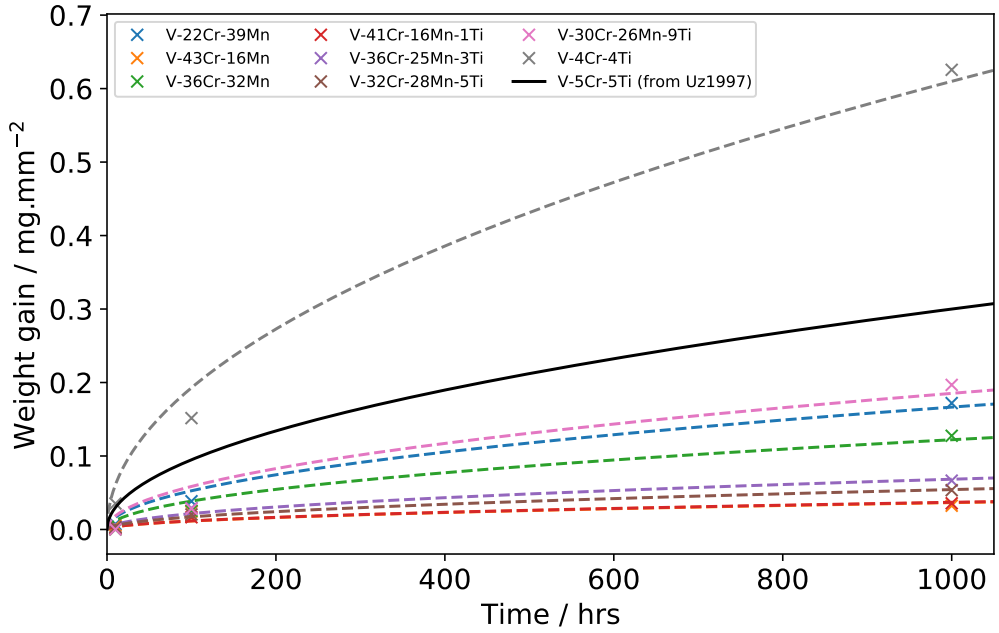

(a) Full data (t = 0 to 1000 hours).

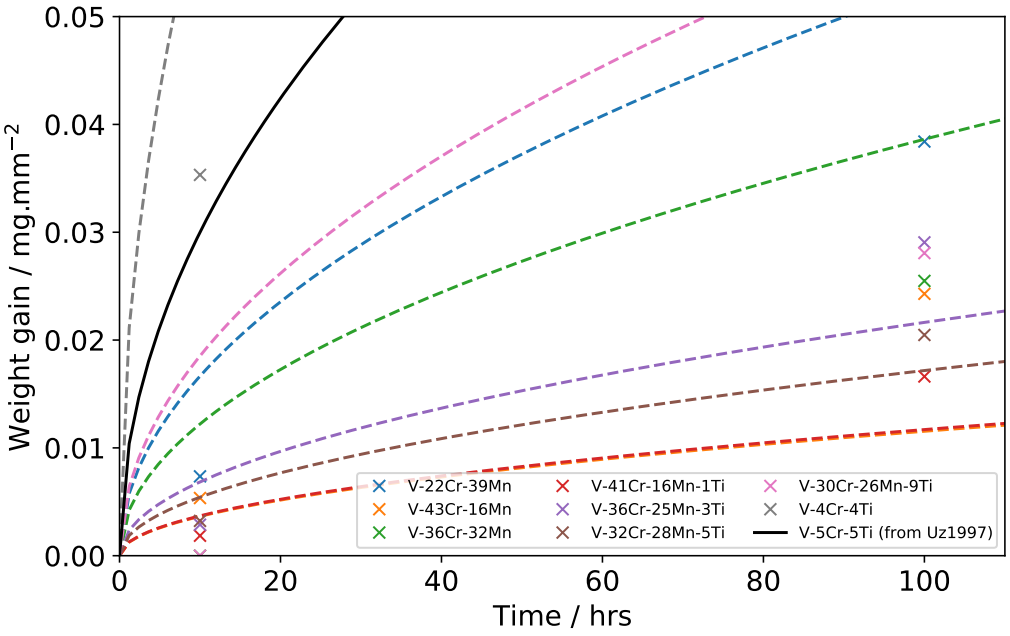

(b) Zoomed in to show short term behaviour (t = 0 to 100 hours).

Figure 6.4: Weight gain against time with parabolic models fitted for samples at 650 °C.

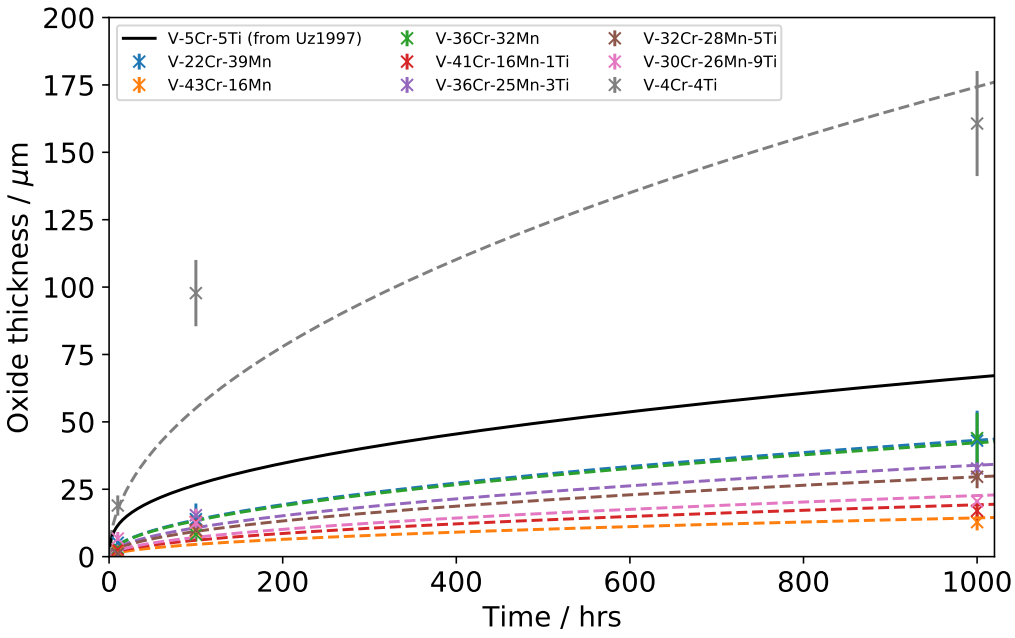

(a) Full data (t = 0 to 1000 hours).

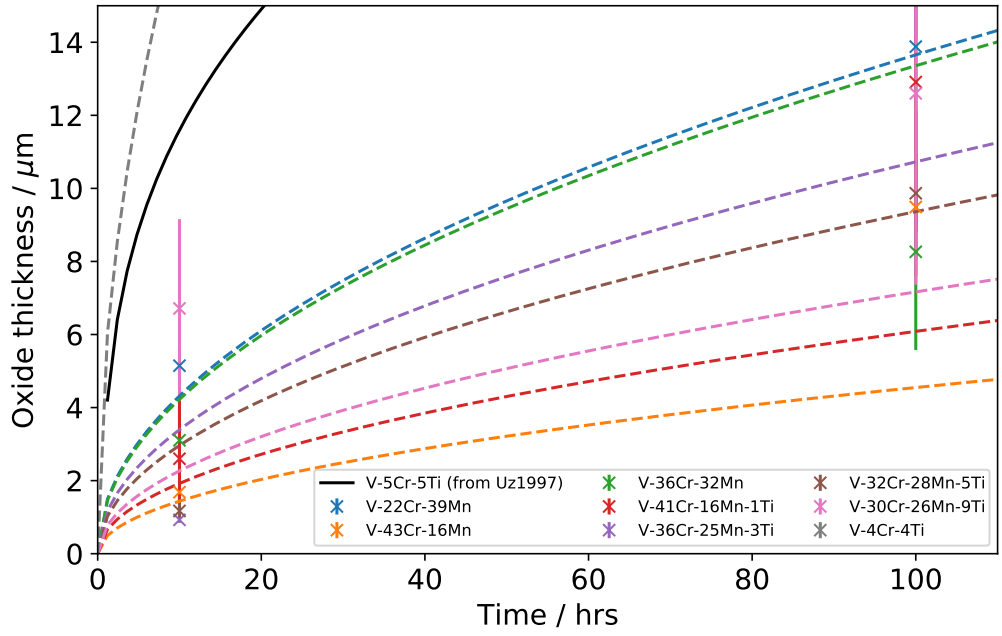

(b) Zoomed in to show short term behaviour (t = 0 to 100 hours).

Figure 6.5: Oxide thickness against time with parabolic models fitted for samples at 650 °C. Error bars determined by standard deviation of multiple measurements along the alloy.

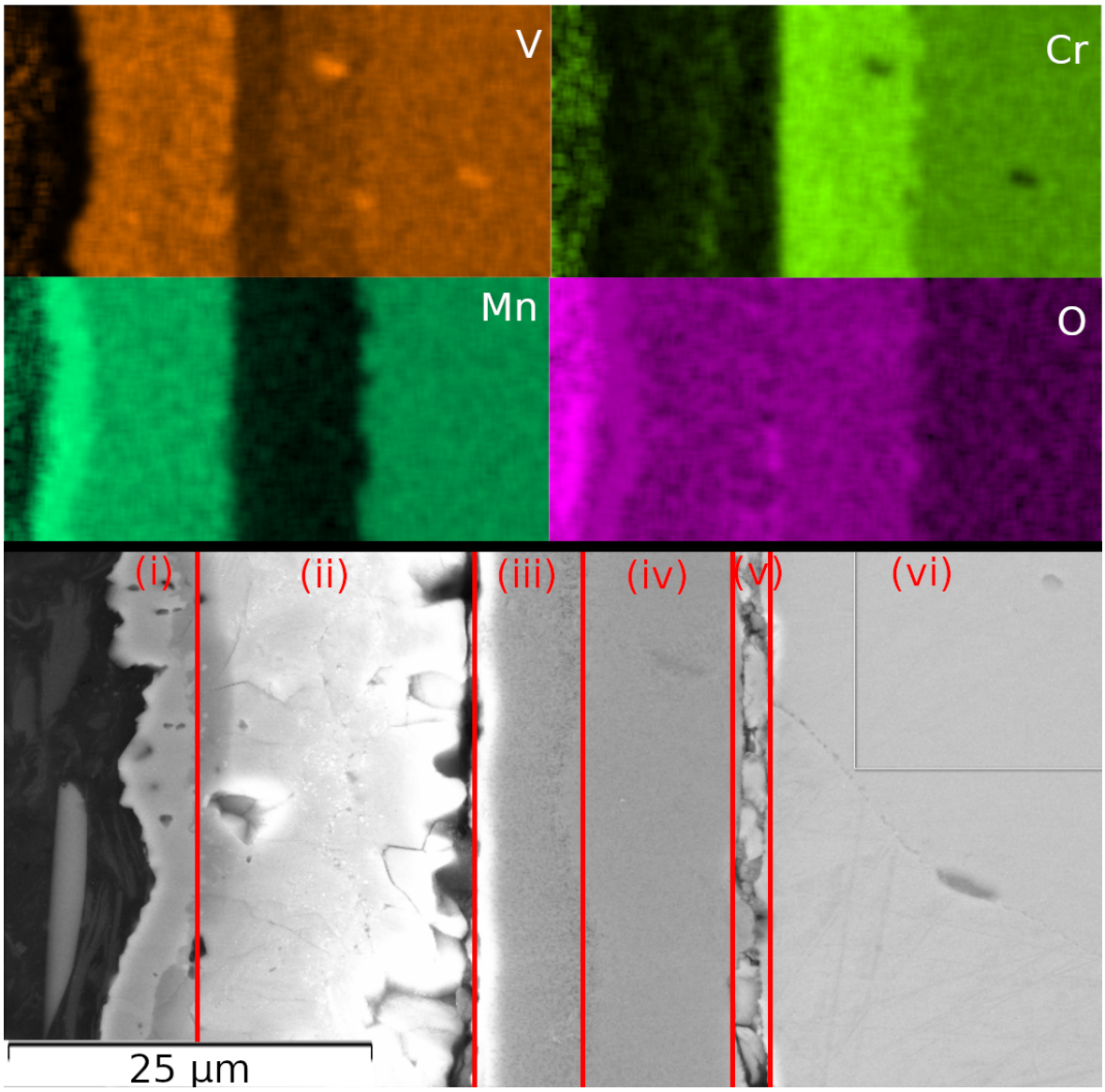

Figure 6.6: SEM-EDX maps and secondary electron image of V-36Cr-32Mn oxidised for 1000 hrs at 650 °C. (i) Mn-rich oxide (ii) V,Mn-rich oxide (iii) Cr-rich oxide (iv) V,Cr-rich oxide (v) substrate break-off layer (vi) V-36Cr-32Mn substrate.

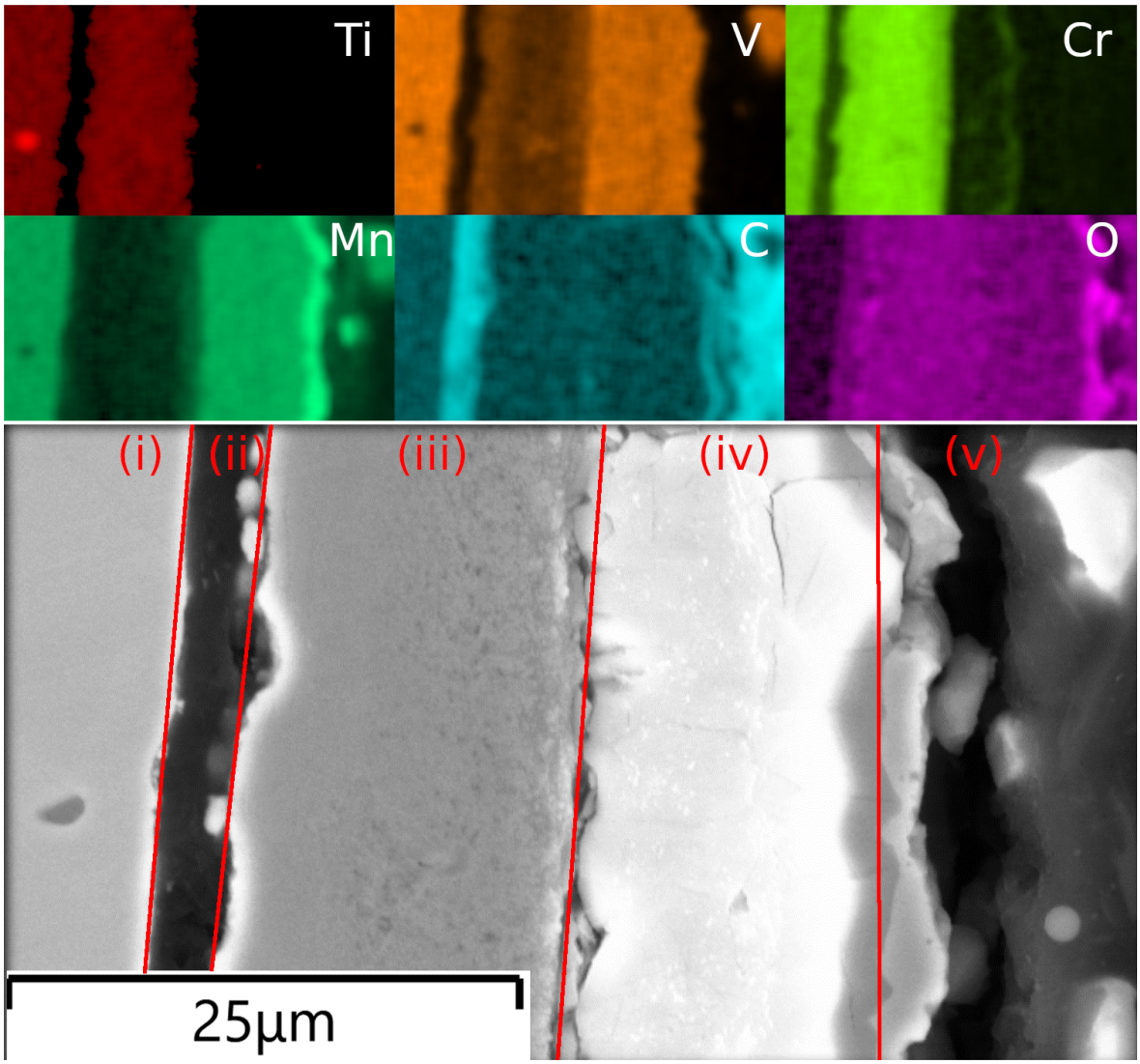

Figure 6.7: SEM-EDX maps and secondary electron image of V-36Cr-25Mn-3Ti oxidised for 1000 hrs at 650 °C. (i) V-36Cr-25Mn-3Ti substrate (ii) spalled region where mounting resin has penetrated (iii) Cr-rich oxide (iv) V, Mn-rich oxide (v) Mn-rich oxide.

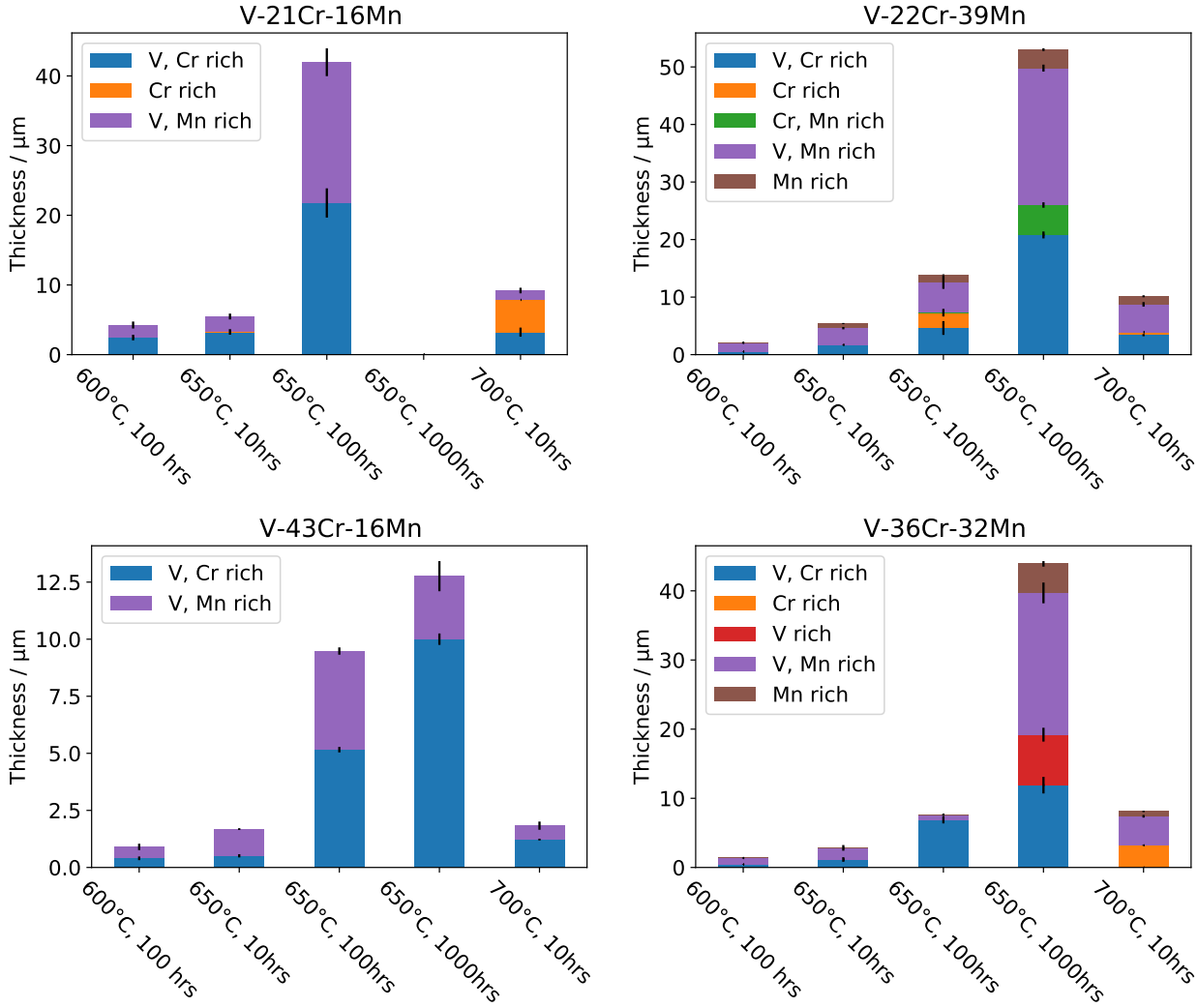

Figure 6.8: Growth of oxide species in the alloys studied. Error bars from standard deviations in measurements.

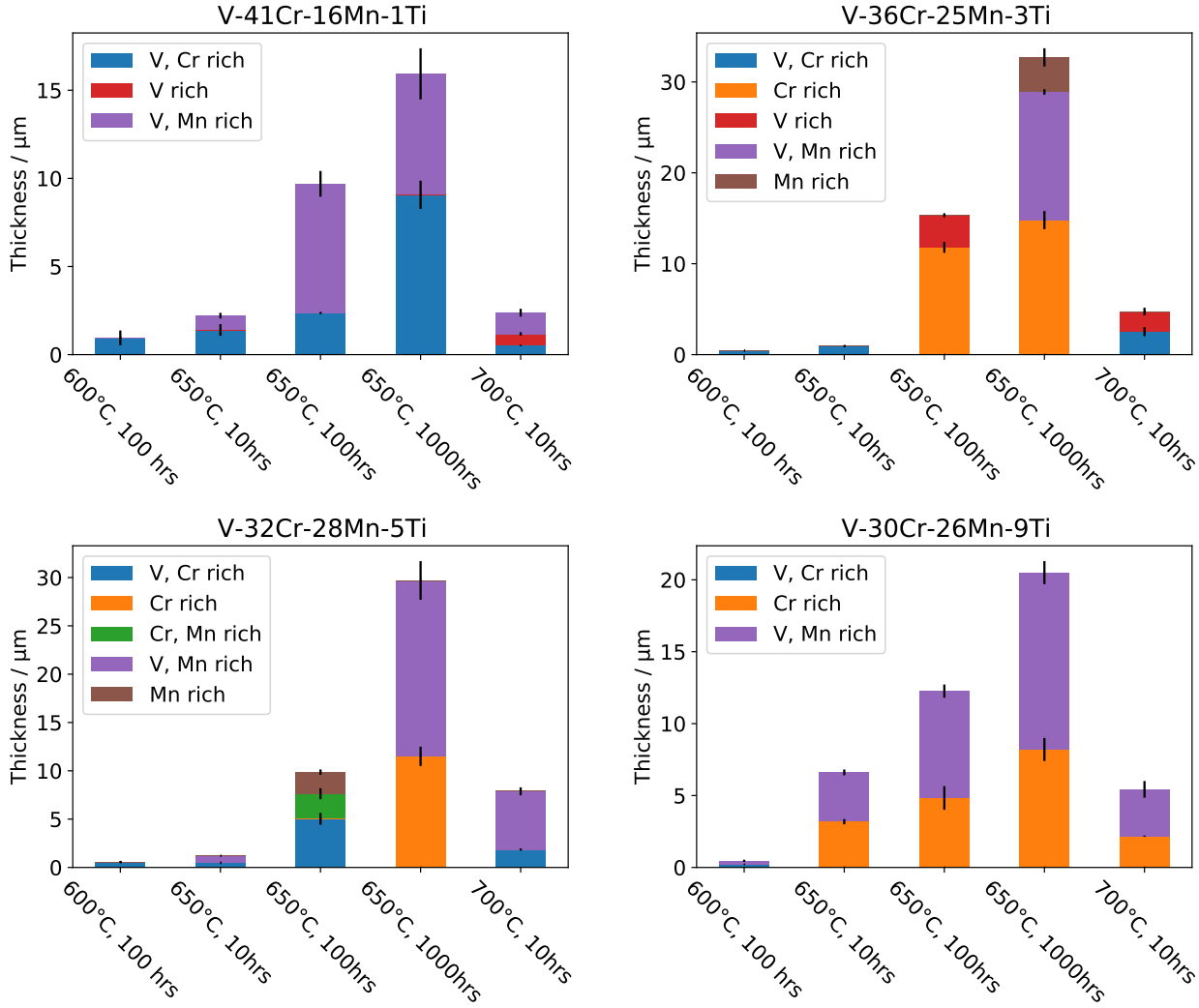

Figure 6.8: Growth of oxide species in the alloys studied (cont). Error bars from standard deviations in measurements.

6.4 Discussion

Parabolic growth is associated with oxidation that is governed by the diffusional behaviour of one species through the oxide[30]. The poor quality fitting observed in the models is evidence that such a simple mechanism is likely not a sufficient explanation. The actual mechanisms at play will probably be described by equations with a more complex form. Section 6.3.3 shows that there are multiple oxide species present, which will each have their own diffusion and growth behaviour, and the oxidation rate will be governed by a combination of these parameters. Analysing weight gain continuously for a single sample as it is oxidised, e.g. via thermogravimetric analysis[1], would allow for a more detailed model to be proposed and tested.

The alloy studied that exhibited the simplest oxidation behaviour was the V-4Cr-4Ti reference sample. It is also the alloy that is most accurately described by the parabolic model, with a k_1 value of 3.7×10^{-4} $\mathrm{mg^2\,mm^{-4}\,s^{-1}}$. This is slightly higher than the rate constants predicted by Uz et al.[29] which are 8.99×10^{-5} and 2.48×10^{-5} $\mathrm{mg^2\,mm^{-4}\,s^{-1}}$ for V-5Cr-5Ti at 650 °C and V-4Cr-4Ti at 620 °C respectively[2]. The results here are consistent with that study as V-4Cr-4Ti oxidises more rapidly at a given temperature than V-5Cr-5Ti, an effect that is attributed by the authors to the fact that Ti is known to trap oxygen and impair its diffusion in the matrix (other studies have found that increasing Cr also reduces oxidation [13]). Also of note is the vastly increased interstitial oxygen content in of the V-4Cr-4Ti (0.324 wt% vs. 0.047 wt% in Uz et al.) which may also play a role in accelerating the oxidation kinetics.

Without knowledge of the oxidations mechanisms at play, it is difficult to make any firm assessments as to the reason why these alloys performed better than V-4Cr-4Ti. Increased Cr is known to reduce oxidation rates in this temperatures range, as per Fujiwara et al.[13], but a mechanistic explanation was not offered as there was no evidence of Cr oxide layers forming. In steels, high Cr content leads to the formation of a protective layer of Cr_2O_3 which inhibits further oxidation[30]. This is caused by oxygen diffusing into the metal and reacting with Cr to form Cr_2O_3. This protective layer inhibits the inwards diffusion of O and the outwards diffusion of metal atoms, thereby hindering further oxidation. Similar behaviour is observed in the alloys studied here, with Cr-rich phases appearing adjacent to the substrate. Some similarities between steels (under certain conditions) and these alloys are seen in the oxide scales that form on top of this Cr-rich region. Breakout layers of MCr_2O_4 spinel structures can appear on the outside of Cr_2O_3 films in cast steels[30]. It is possible that the V,Mn-rich oxides on the surface are spinels formed in a similar manner, via metal species diffusing outwards through the Cr-rich layer, potentially even the same VMn_2O_4

[1] Use of thermogravimetry was planned, but COVID-19 restrictions on equipment training and lab access made this impossible.

[2] V-4Cr-4Ti was never tested at 650 °C in this study.

spinel observed as precipitates in the ternary alloy microstructure[20]. Examining the effects of composition, alloys with higher Cr content tended to form an oxide that was thinner, and more significantly comprised of a Cr-rich layer, than the lower Cr counterparts (see Fig. 6.8 comparing V-43Cr-16Mn with V-21Cr-16Mn, and V-41Cr-16Mn-1Ti with V-32Cr-28Mn-5Ti). No clear trend was observed with respect to Mn content. Work done at similar temperatures on RAFM steels has shown that the addition of Mn can produce a more compact and homogeneous oxide scale with higher oxidisation resistance[31]. This is attributed to the larger free energy of formation of Mn oxides, as well as its enhanced diffusivity in the surface layer.

The quaternary alloys generally performed better than their ternary counterparts. As mentioned earlier, work by Uz et al.[29] cited Ti inhibiting the diffusion of O as an explanation for the improved performance of higher-Ti alloys. Comparing the oxide film thicknesses in Fig. 6.8 of V-43Cr-16Mn and V-41Cr-16Mn-1Ti (which are chemically similar aside from the inclusion of Ti) it is observed that the Cr-rich regions of V-41Cr-16Mn-1Ti are thinner at longer exposure times. This may be due to the presence of Ti inhibiting the diffusion of O through the pre-existing Cr-rich film, and consequently slowing growth. However, the external V, Mn-rich oxides appear to grow at similar or even faster rates, suggesting that Ti does not inhibit the outwards diffusion of the metal species. Mn is known to diffuse relatively rapidly through the Cr_2O_3 scale in steel[32], so a similar process may be at play here. Work by Lu et al.[31] also found that Mn tended to form Mn and Mn,Cr oxides towards the surface of oxidised RAFM steels.

To probe if the growth of the Cr-rich layers were governed by a simple parabolic law, the results of fitting a parabolic model to the combined thickness of the Cr-rich and V, Cr-rich layers is shown in Fig. 6.9. Again, the model fits are quite poor, so even the growth of this layer is likely to be affected by the growth of the other layers on top.

Curiously, the quaternary alloys exhibited a greater propensity for spallation during handling. Although the data is not nearly complete enough to establish any firm conclusions, it is interesting to note that the S content of the quaternary alloys (where measured) is higher than the ternaries. S is known to segregate to the scale-alloy boundary, where it can nucleate voids and weaken the interfacial adherence[30].

6.5 Conclusions

1. V-Cr-Mn and Ti-V-Cr-Mn were found to oxidise at a lower rate in fusion accident-relevant temperatures compared to V-4Cr-4Ti and V-5Cr-5Ti candidate fusion materials.

2. At 700 °C, oxidation was accelerated (relative to 650 and 600 °C) but the alloys did not volatilise.

3. Evolution of both weight gain and oxide thickness did not fit well to a parabolic model, indicating more complex oxidation behaviour.

4. Higher Cr content appeared to be beneficial to oxidation performance.

5. The oxides formed were generally complex, consisting of multiple scales with distinct chemistries.

6. The addition of Ti appeared to slow the growth of the innermost Cr-rich layer, possibly by inhibiting the diffusion of O. However, this layer did not appear to affect the formation of other V,Mn-rich oxides nearer the sample surface.

7. Mechanical adherence of the oxides to the substrate was poor, with spallation frequently occurring with thicker scales.

Acknowledgements

The authors acknowledge funding from the EPSRC Centre for Doctoral Training in Fusion Energy [grant EP/L01663X/1] as well as EPSRC grant EP/R021546/1. This work has been part-funded by the RCUK Energy Programme [grant number EP/T012250/1]. The raw data associated with this work can be accessed via the following link: `https://zenodo.org/record/4643803`

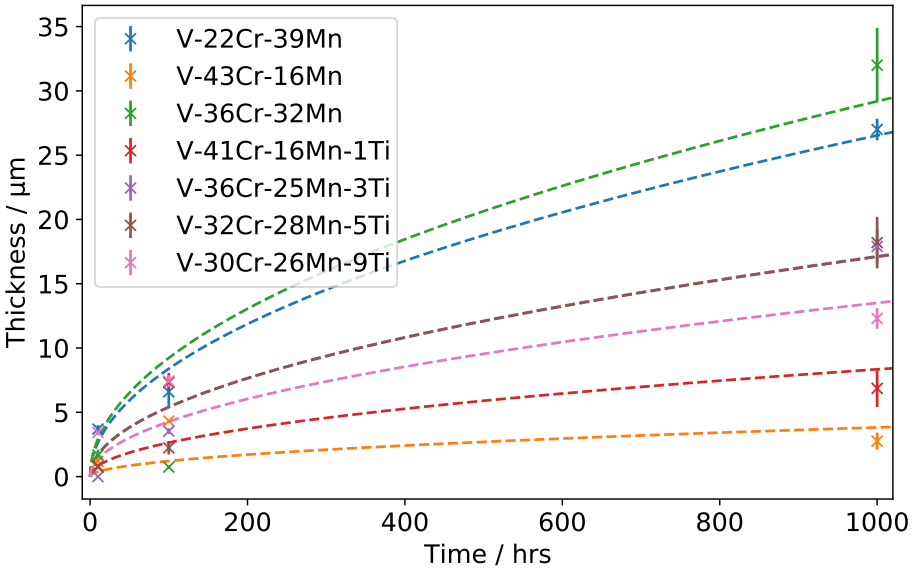

(a) Full data (t = 0 to 1000 hours).

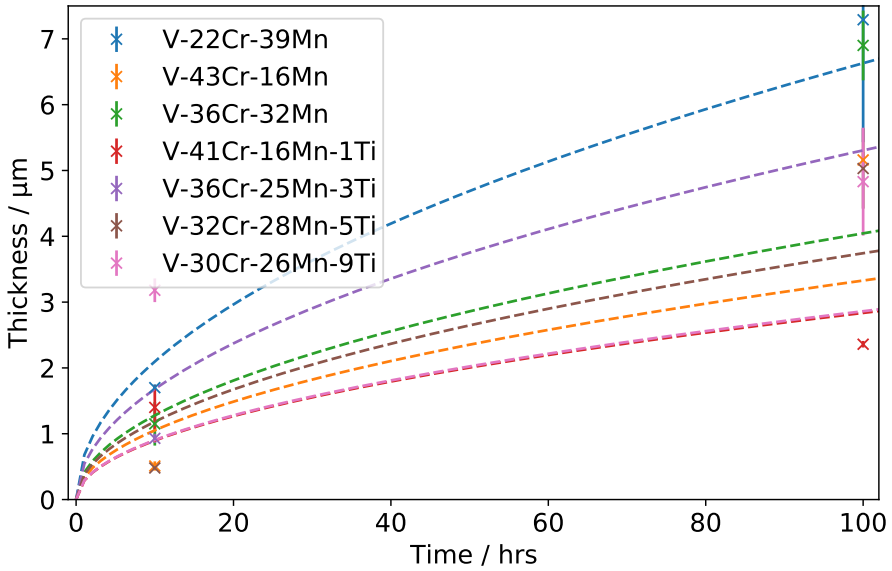

(b) Zoomed in to show short term behaviour (t = 0 to 100 hours).

Figure 6.9: Cr-rich and V,Cr-rich oxide thickness against time with parabolic models fitted for samples at 650 °C.

References

[1] D. Maisonnier et al. "The European power plant conceptual study". In: *Fusion Engineering and Design* 75-79.SUPPL. (Nov. 2005), pp. 1173–1179. ISSN: 09203796. DOI: 10.1016/j.fusengdes.2005.06.095.

[2] G. R. Smolik, S. J. Piet, and R. M. Neilson. "Predictions of Radioactive Tungsten Release for Hypothetical ITER Accidents". In: *Fusion Technology* 19.3P2B (1991), pp. 1398–1402. ISSN: 0748-1896. DOI: 10.13182/fst91-a29538.

[3] T. Wegener et al. "Development of yttrium-containing self-passivating tungsten alloys for future fusion power plants". In: *Nuclear Materials and Energy* 9 (Dec. 2016), pp. 394–398. ISSN: 23521791. DOI: 10.1016/j.nme.2016.07.011.

[4] A. Litnovsky et al. "Smart tungsten alloys as a material for the first wall of a future fusion power plant". In: *Nuclear Fusion* 57.6 (2017). ISSN: 17414326. DOI: 10.1088/1741-4326/aa6816.

[5] Tobias Wegener et al. "Development and analyses of self-passivating tungsten alloys for DEMO accidental conditions". In: *Fusion Engineering and Design* 124 (Nov. 2017), pp. 183–186. ISSN: 09203796. DOI: 10.1016/j.fusengdes.2017.03.072.

[6] Felix Klein et al. "Sublimation of advanced tungsten alloys under DEMO relevant accidental conditions". In: *Fusion Engineering and Design* 146.February (2019), pp. 1198–1202. ISSN: 09203796. DOI: 10.1016/j.fusengdes.2019.02.039.

[7] N. Sreevidya et al. "A comparative study on atmospheric oxidation of reduced activation ferritic martensitic steel and grade 91 steel". In: *Fusion Engineering and Design* 135 (Oct. 2018), pp. 204–215. ISSN: 09203796. DOI: 10.1016/j.fusengdes.2018.07.024.

[8] E. O. Mogire et al. "Microstructural characterization of oxide scales formed on steels P91 and P92". In: *Materials at High Temperatures* 28.4 (Nov. 2011), pp. 361–368. ISSN: 09603409. DOI: 10.3184/096034011X13193830650089.

[9] Yanhong Lu et al. "Effect of Nanostructured Surface on the Corrosion Behavior of RAFM Steels". In: *Oxidation of Metals* 91.3-4 (Apr. 2019), pp. 495–510. ISSN: 0030770X. DOI: 10.1007/s11085-019-09895-0.

[10] T. Kaito et al. "High temperature oxidation behavior of ODS steels". In: *Journal of Nuclear Materials* 329-333.1-3 PART B (Aug. 2004), pp. 1388–1392. ISSN: 00223115. DOI: 10.1016/j.jnucmat.2004.04.203.

[11] Keisuke Kimura et al. "Oxide layer formation in reduced activation ferritic steel F82H under DEMO reactor blanket condition". In: *Fusion Engineering and Design* 146 (Sept. 2019), pp. 1564–1568. ISSN: 09203796. DOI: 10.1016/j.fusengdes.2019.02.129.

[12] K Natesan and M Uz. "Oxidation performance of V-Cr-Ti alloys". In: *Fusion Engineering and Design* 51-52.52 (Nov. 2000), pp. 145–152. ISSN: 09203796. DOI: 10.1016/S0920-3796(00)00308-2.

[13] M Fujiwara et al. "Influence of Cr, Ti concentrations on oxidation and corrosion resistance of V–Cr–Ti type alloys". In: *Journal of Nuclear Materials* 329-333 (Aug. 2004), pp. 452–456. ISSN: 0022-3115. DOI: 10.1016/J.JNUCMAT.2004.04.090.

[14] B. A. Pint and J. R. DiStefano. "The Role of Oxygen Uptake and Scale Formation on the Embrittlement of Vanadium Alloys". In: *Oxidation of Metals* 63.1-2 (Feb. 2005), pp. 33–55. ISSN: 0030-770X. DOI: 10.1007/s11085-005-1950-7.

[15] W.R Johnson and J.P Smith. "Fabrication of a 1200 kg ingot of V-4Cr-4Ti alloy for the DIII-D radiative divertor program". In: *Journal of Nuclear Materials* 258-263 (Oct. 1998), pp. 1425–1430. ISSN: 00223115. DOI: 10.1016/S0022-3115(98)00209-8.

[16] T Muroga et al. "NIFS program for large ingot production of a V-Cr-Ti alloy". In: *Journal of Nuclear Materials* 283-287 (Dec. 2000), pp. 711–715. ISSN: 00223115. DOI: 10.1016/S0022-3115(00)00281-6.

[17] H.Y. Fu et al. "Fabrication using electron beam melting of a V-4Cr-4Ti alloy and its thermo-mechanical strengthening study". In: *Journal of Nuclear Materials* 442.1-3 (Nov. 2013), S336–S340. ISSN: 00223115. DOI: 10.1016/j.jnucmat.2013.01.337.

[18] V. Chernov et al. "Low Activation Vanadium Alloys for Fusion Power Reactors - the RF Results". In: *24th IAEA Fusion Energy Conference*. San Diego, USA, 2012.

[19] Vincent Duquesnes, Thomas Guilbert, and Marion Le Flem. "French investigation of a new V-4Cr-4Ti grade: CEA-J57 - Fabrication and microstructure". In: *Journal of Nuclear Materials* 426.1-3 (July 2012), pp. 96–101. ISSN: 00223115. DOI: 10.1016/j.jnucmat.2012.03.029.

[20] P.J. Barron et al. "Towards V-based high-entropy alloys for nuclear fusion applications". In: *Scripta Materialia* 176 (Feb. 2020), pp. 12–16. ISSN: 13596462. DOI: 10.1016/j.scriptamat.2019.09.028.

[21] O. Carlson and A. Eustice. "Vanadium-chromium alloy system". In: *Ames Laboratory Technical Reports* (1959).

[22] Owais Ahmed Waseem and Ho Jin Ryu. "Powder Metallurgy Processing of a WxTaTiVCr High-Entropy Alloy and Its Derivative Alloys for Fusion Material Applications". In: *Scientific Reports* 7.1 (Dec. 2017), p. 1926. ISSN: 2045-2322. DOI: 10.1038/s41598-017-02168-3.

[23] A. Ayyagari et al. "Low activation high entropy alloys for next generation nuclear applications". In: *Materialia* 4 (Dec. 2018), pp. 99–103. ISSN: 2589-1529. DOI: 10.1016/J.MTLA.2018.09.014.

[24] O. El-Atwani et al. "Outstanding radiation resistance of tungsten-based high-entropy alloys". In: *Science Advances* 5.3 (Mar. 2019), eaav2002. ISSN: 23752548. DOI: 10.1126/sciadv.aav2002.

[25] A. Kareer et al. "Short communication: 'Low activation, refractory, high entropy alloys for nuclear applications'". In: *Journal of Nuclear Materials* 526 (Dec. 2019), p. 151744. ISSN: 00223115. DOI: 10.1016/j.jnucmat.2019.151744.

[26] A. W. Carruthers et al. "Novel reduced-activation TiVCrFe based high entropy alloys". In: *Journal of Alloys and Compounds* 856 (Mar. 2021), p. 157399. ISSN: 09258388. DOI: 10.1016/j.jallcom.2020.157399.

[27] Owais Ahmed Waseem et al. "The effect of Ti on the sintering and mechanical properties of refractory high-entropy alloy TixWTaVCr fabricated via spark plasma sintering for fusion plasma-facing materials". In: *Materials Chemistry and Physics* 210 (May 2018), pp. 87–94. ISSN: 02540584. DOI: 10.1016/j.matchemphys.2017.06.054.

[28] Guangming Zhou et al. "Transient thermal analysis and structural assessment of an ex-vessel LOCA event on the EU DEMO HCPB breeding blanket and the attachment system". In: *Fusion Engineering and Design* 136.November (Nov. 2018), pp. 34–41. ISSN: 09203796. DOI: 10.1016/j.fusengdes.2017.12.017.

[29] M. Uz, K. Natesan, and V.B. Hang. "Oxidation kinetics and microstructure of V-(4-5) wt% Cr-(4-5) wt% Ti alloys exposed to air at 300–650°C". In: *Journal of Nuclear Materials* 245.2-3 (June 1997), pp. 191–200. ISSN: 00223115. DOI: 10.1016/S0022-3115(97)00008-1.

[30] David J. Young. *High Temperature Oxidation and Corrosion of Metals*. Elsevier, 2016. ISBN: 9780081001011. DOI: 10.1016/C2014-0-00259-6.

[31] Y. H. Lu et al. "Effects of pre-formed nanostructured surface layer on oxidation behaviour of 9Cr2WVTa steel in air and liquid Pb-Bi eutectic alloy". In: *Corrosion Science* 102 (Jan. 2016), pp. 301–309. ISSN: 0010938X. DOI: 10.1016/j.corsci.2015.10.021.

[32] R. E. Lobnig et al. "Diffusion of cations in chromia layers grown on iron-base alloys". In: *Oxidation of Metals* 37.1-2 (Feb. 1992), pp. 81–93. ISSN: 0030770X. DOI: 10.1007/BF00665632.

6.6 Additional discussion

As seen in the previous two chapters, precipitates of some form are present in all of the alloys studied. When these precipitates were observed at the oxide surface of samples, some anomalous behaviour was observed. Figs. 6.10 and 6.11 show how the precipitates found in the ternary alloys influenced oxidation behaviour at 650 °C for 1000 hours. In Fig. 6.10, looking to the left of the precipitates, the Cr-rich layer appears to split in two, with a Mn-rich phase appearing between it. Fig. 6.11 appears to show a similar situation, except the Cr-rich region has split across the length of the micrograph, effectively introducing a new layer into the oxide film. Such behaviour is likely to complicate the modelling of oxide growth even further and suggests that the presence of precipitates may lead to the formation of structures that would not be expected in the bulk.

Even the shorter oxidations at 650 °C show the influence of precipitates. Fig. 6.12 shows how a significantly thicker oxide scale has developed on top of a precipitate region in V-43Cr-16Mn. It is also rich in V and Mn as oppose to the Cr-rich film

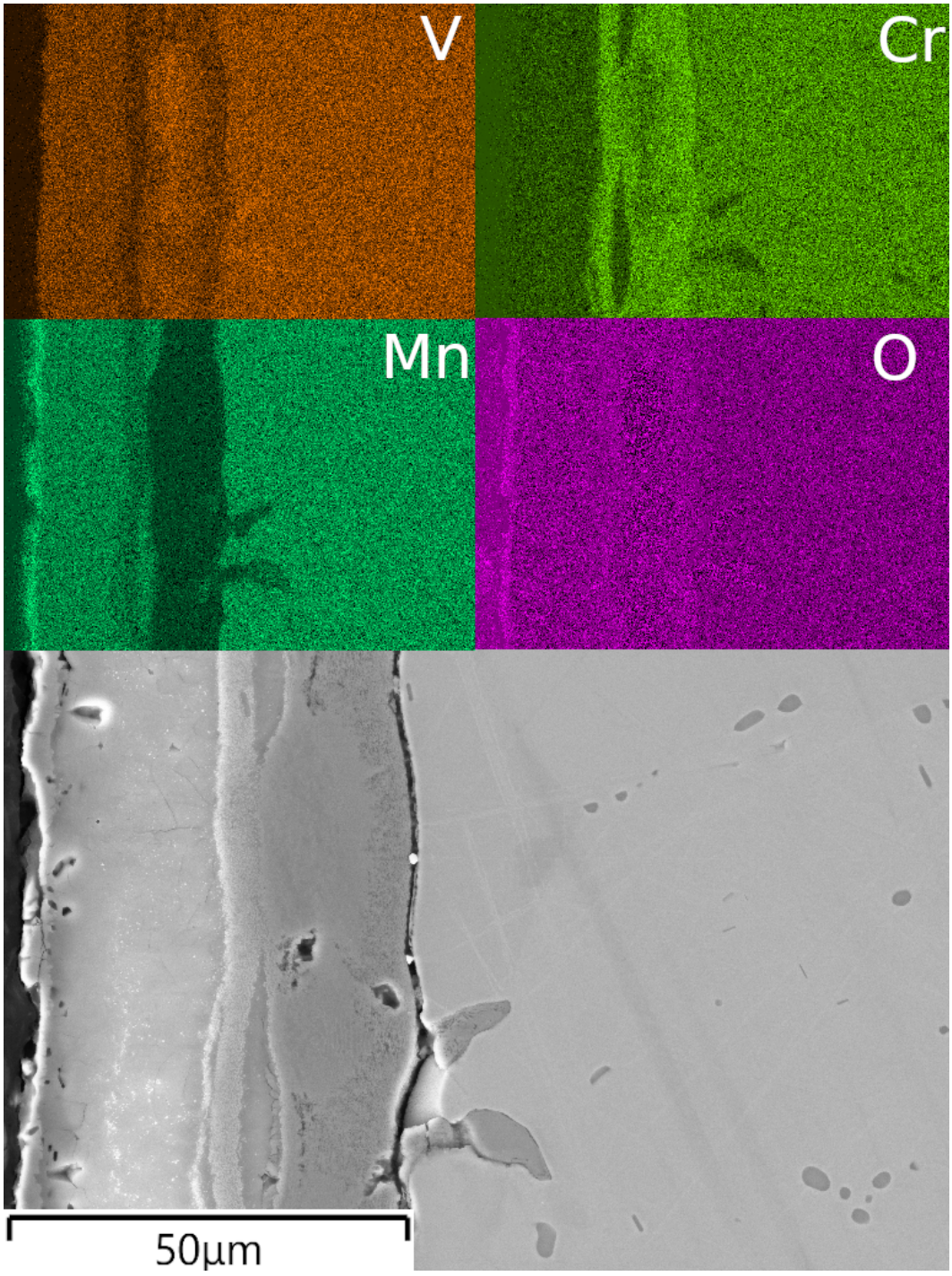

Figure 6.10: Cross-section of V-22Cr-39Mn oxidised at 650 °C for 1000 hrs.

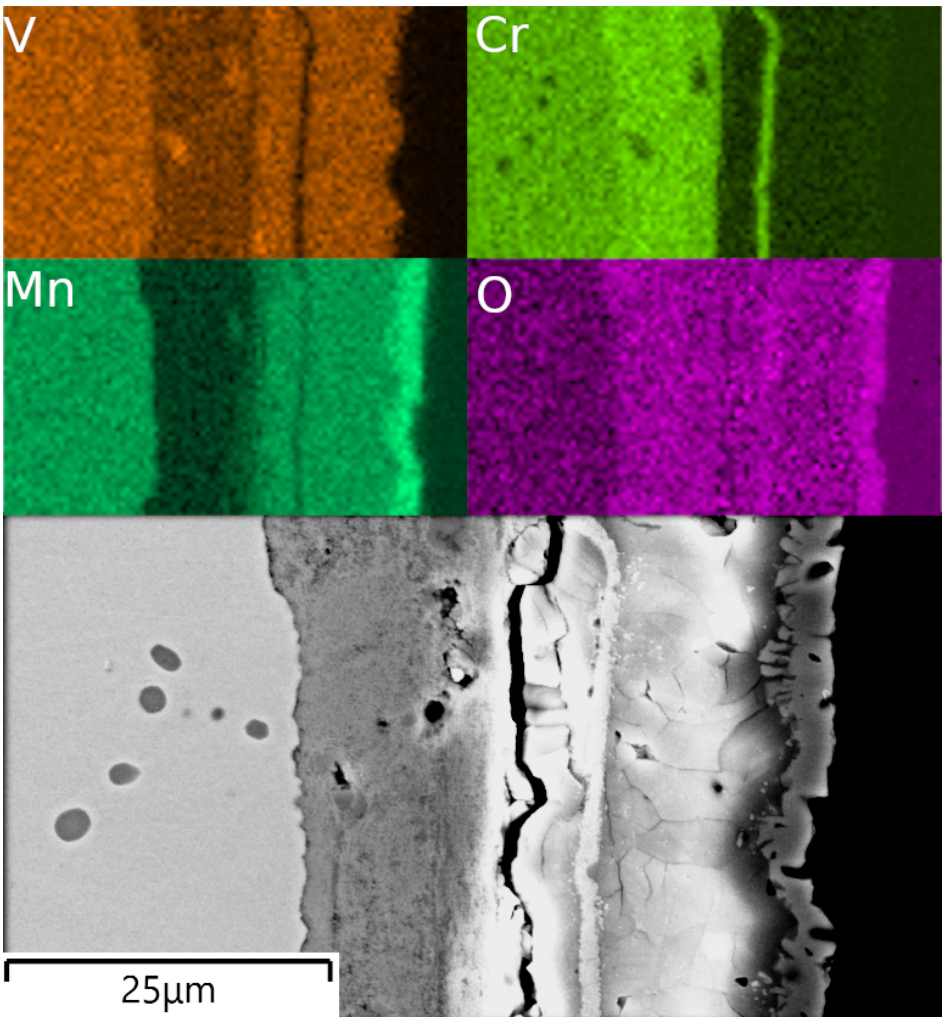

Figure 6.11: Cross-section of V-36Cr-32Mn oxidised at 650 °C for 1000 hrs.

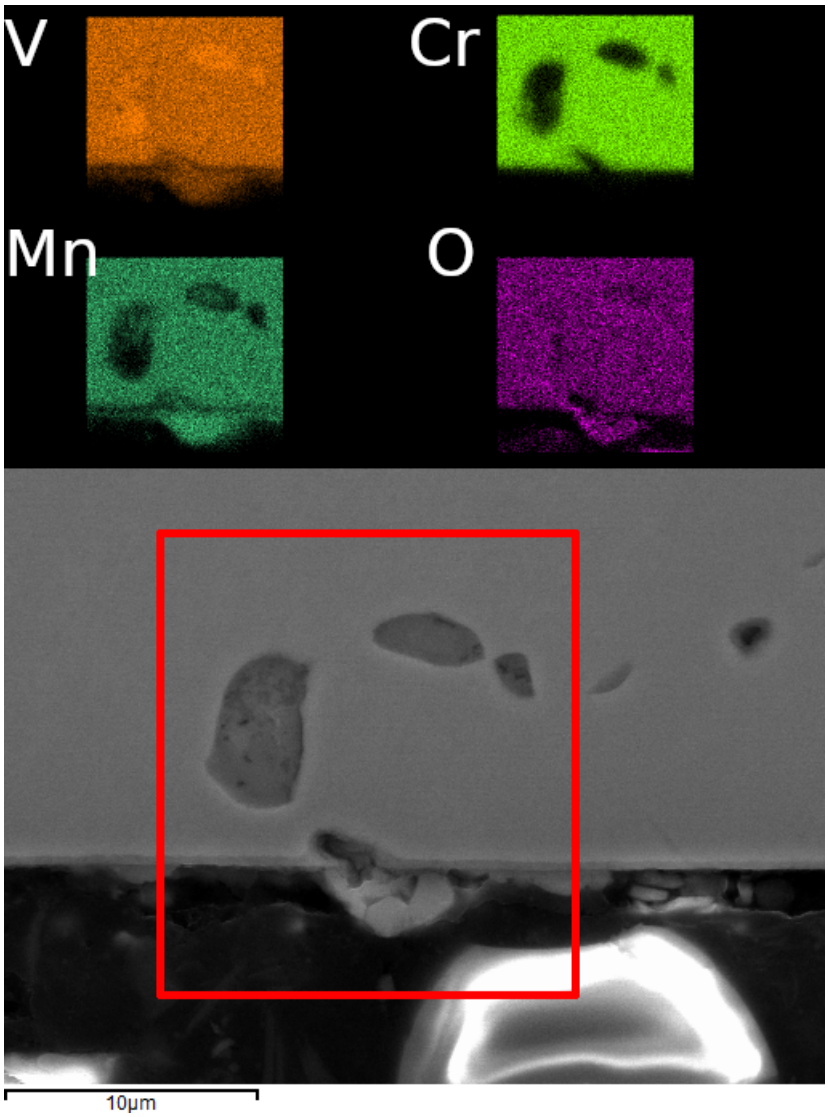

Figure 6.12: Cross-section of V-43Cr-16Mn oxidised at 650 °C for 10 hrs.

seen along the rest of the sample. A similar picture is observed in V-32Cr-28Mn-5Ti, shown in Fig. 6.13. The region just above the Ti-[C,O,N] precipitate shows a slightly thicker oxide. It is also the only time that Ti has been observed near the surface of the alloy and not remaining primarily in the Cr-rich region. Precipitates seem to influence the oxidation behaviour and in a way that seems to promote accelerated oxidation. Improved interstitial impurity control may reduce precipitate content, in turn improving oxidation performance.

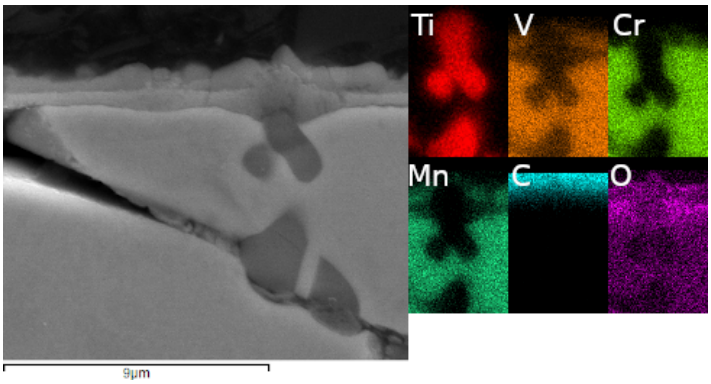

Figure 6.13: Cross-section of V-32Cr-28Mn-5Ti oxidised at 650 °C for 10 hrs.

Chapter 7

Conclusions

The aim of this work was to assess the suitability of adopting a HEA-like alloy design rationale to fusion materials and determine whether the resultant alloys had the potential to either be used in a fusion environment or show a route through which a different novel alloy system may be developed. This was to be achieved through characterising the resultant microstructure of the alloys in their homogenised state, which formed the basis of Chapter 4, characterising their thermal stability at fusion relevant temperatures, shown in Chapter 5, and finally assessing one of their potential advantages over other candidate alloys, namely oxidation resistance, which was presented in Chapter 6. The key conclusions of the work are brought together in following paragraphs.

- Two multi-principal component alloy systems (V-Cr-Mn and Ti-V-Cr-Mn) were designed and fabricated using only low-activation elements. These elements, when combined in their pure state, were shown to produce a material that has activation properties that could be classed as reduced-activation. The intention of mixing these elements was to produce BCC alloys that would be stable under fusion relevant conditions. The alloys formed BCC microstructures in the homogenised state.

- Subsequent study found that the BCC microstructure was generally retained during ageing at fusion relevant temperatures. CALPHAD calculations were also able to predict the phases present with a good degree of success, which may aid in further alloy exploration. Any deviations from this microstructure that were observed were due to specific compositional variations within the systems, and methods for controlling these microstructural features were suggested. The usually undesirable Laves phase was only found to form in Ti-V-Cr-Mn with Ti content greater than 5 at%. The only other precipitates observed were found to be a result of interstitial impurity atoms, most likely introduced from either the source metal or the heat treating process.

- Impurity elements had a considerable effect on the properties of these alloys and varied a lot between samples. They formed precipitates in all of the alloys at every homogenisation and heat treatment temperature studied, and it is likely that they have an impact on mechanical properties too. Furthermore, their presence would fundamentally alter the activation properties of these alloys for the worse, potentially to an extent where they could no longer be considered low-activation.

- Studying the oxidation properties of these alloys revealed an area where they may confer an advantage over other candidate fusion structural materials. Most compositions studied had improved high temperature oxidation properties compared to a V-4Cr-4Ti reference sample, believed to be caused by increased Cr content and improved by the presence of Ti (in the case of the quaternary alloys). The oxidation behaviour was found to be complex, with multiple layers forming on the surface after long exposures. However, this complexity is not necessarily a problem as protective oxide layers can be utilised to improve both the accident tolerance and processability of these alloys.

7.1 Suitability for fusion

Overall, none of the conclusions presented in this work preclude either of the alloy systems from being used in a fusion environment. Specific alloy compositions may be unsuitable (e.g. V-30Cr-26Mn-9Tifor its microstructural evolutions during ageing or V-21Cr-16Mn for its propensity to volatilise at accident relevant temperatures), but generally speaking *the systems of alloys developed show promise for use in fusion applications, or for development with further alloying additions and/or modifications.*

There are other, secondary conclusions to be drawn from this work as well. The first of which is the importance of interstitial and impurity elements in these alloys. These elements played a part in the conclusions of every section in this work as they were fundamental to the microstructures seen in all of the alloys. It is regrettable that it was not possible to quantify their presence more accurately for most of the samples studied, as this information would strengthen many of the arguments presented.

Some remarks can also be made about the compositions of the systems studied. In the quaternary system, it seems that a Ti content of around 3 at% or less is desirable, as any more than this leads to the evolution of a Laves phase which would most likely be detrimental to materials performance. In the ternary system, V-22Cr-39Mn (i.e. high V and Mn, low Cr) showed some microstructural evolution which may make it unsuitable for fusion applications and is perhaps a composition to be avoided. However, beyond these general guidelines it is difficult to make any firmer statements about an ideal composition.

Chapter 8

Future work

As the alloy systems presented in this work are relatively uncharacterised (in comparison to other fusion candidate alloys such as RAFM steels and V-Cr-Ti alloys) the scope for discovery and future work is enormous. Unfortunately, the time and resources available for this project (and the impact of COVID-19 restrictions) meant that there are still many unanswered questions which could easily form the basis for future work. The most immediate issues are discussed here.

8.1 Irradiation resistance

As discussed in Section 2.9.3, one of the potential advantages of HEAs (for some systems) was their resistance to radiation damage. An unavoidable fact of fusion materials is that they will be exposed to significant doses of neutron irradiation. While the predominantly BCC microstructure exhibited in the alloys studied here is generally a favourable one for resistance to irradiation, the only way this could be definitively assessed would be to conduct irradiation studies, either with ions or neutrons. Even a relatively short radiation campaign would be very illuminating for these alloys. For example, if they displayed a reduced density of radiation induced damage features (e.g. voids and dislocation loops) then such findings would enormously strengthen the case for using these alloys in a fusion environment. Likewise, evidence of increased radiation damage or phase instability would likely render these alloys unsuitable. In the absence of a physical radiation experiment, molecular dynamics studies may also be useful in predicting some of the behaviour of these alloys under irradiation.

8.2 Mechanical properties

Any candidate fusion structural material must be sufficiently strong and tough to withstand the large loads (both static and transient) present in the reactor structure.

Further to this, they must also retain their properties to an adequate degree under irradiation. Only a very preliminary assessment of the materials' mechanical properties was performed in this work, through the use of hardness testing. Direct measurements of strength and toughness (e.g. uniaxial tensile and Charpy impact tests) in the unirradiated would highlight issues such as poor ductility or embrittlement. Such assessments would combine well with irradiation resistance studies to give a more well-rounded view of how these materials may perform in fusion conditions. Even further study might involve examining the high temperature creep behaviour of these alloys, as thermal creep is one of the limiting factors on the upper operating temperature limit of fusion structural materials, alongside thermal stability, which has been demonstrated.

8.3 Interstitial measurements

As alluded to in the previous chapter, interstitial and impurity elements played a large role in the behaviour of these alloys. A better understanding of how interstitials interact with these alloys and potential mitigation strategies would only serve to improve their performance. Ideally, any future assessment of this alloy system would include a quantification of elements such as C, N, O, and possibly S. Techniques such as WDS, LECO analysis, and secondary ion mass spectroscopy should be employed where possible. More generally speaking, such analyses would be useful for the assessment of any refractory BCC alloy, as they are known to be embrittled by significant interstitial content.

If a conclusive link can be made between interstitial content and some undesirable property (e.g. loss of ductility), then efforts should also be made to reduce the amount of interstitials present in alloys. The prior work done on vanadium alloys serves as a good example of how this might be possible, by utilising techniques such as electron beam welding and vacuum arc remelting. Furthermore, care must be taken not to reintroduce these elements during experiments (as noted for the heat treatments in Chapter 5), or failing that, quantifying any such impurification. Impurity elements are also important (and detrimental) from the standpoint of activation properties, as discussed in Section 4.3 .

8.4 Optimising alloys

Although a variety of alloy compositions were studied here, it was for the purpose of more fully exploring the alloy phase space rather than trying to optimise any properties. However, once a more complete picture of these alloy systems' behaviour has been built up, it will be possible to optimise the properties through changing the mixture of metals. In the absence of any definitive data on the effects of varying individual

elements, I would tentatively suggest any work on the V-Cr-Mn system focus on the equiatomic composition, for no other reason than for drawing easier comparisons with the growing body of work on other ternary alloy systems. An equiatomic Ti-V-Cr-Mn would likely result in large amounts of the Laves phase, and as such I would follow this work in keeping Ti content to less than 10 %.

Further changes to composition can be achieved by introducing another element (or more). This would lead to an alloy system that will better fit the conventional definition of a HEA, but as seen in Section 2.9 there is nothing inherently advantageous in adding more elements to fit the HEA definition just its own sake. Instead, any new alloy systems should follow the rationale outlined in this work. That is, use low-activation elements and also use elements that likely produce a single solid phase. Alternatively, minor mechanical alloying additions such as those seen in ODS steels could also deliver improved behaviour, if an appropriate manufacturing route can be found.